

AD-A059 988

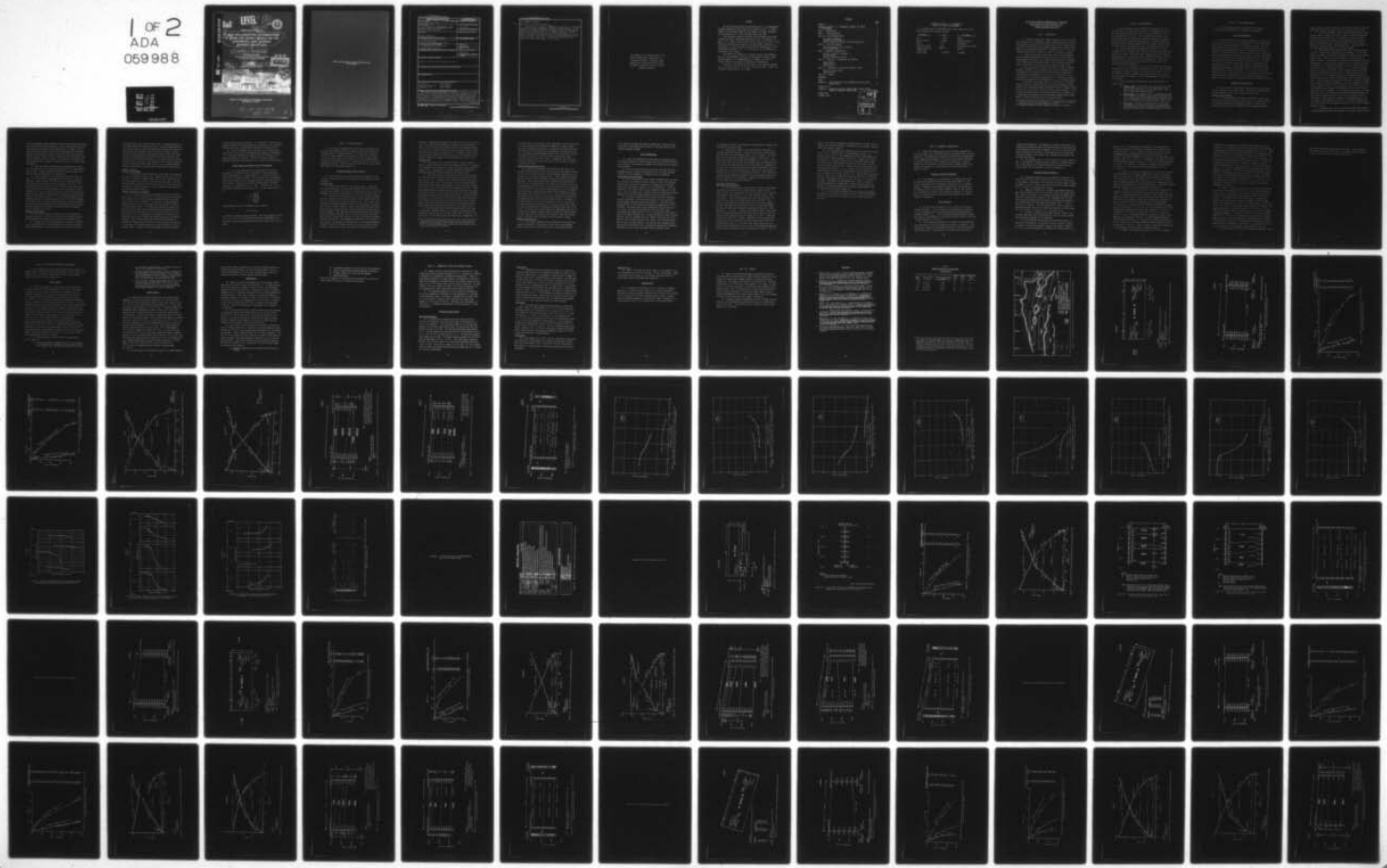
ARMY ENGINEER WATERWAYS EXPERIMENT STATION VICKSBURG MISS F/G 13/13
IN SITU AND LABORATORY DETERMINATIONS OF SHEAR AND YOUNG'S MODU--ETC(U)
AUG 78 J R CURRO, W F MARCUSON

UNCLASSIFIED

WES-MP-S-78-12

NL

1 OF 2
ADA
069988



ADA059988

DDC FILE COPY



LEVEL

14
WES-MP-

MISCELLANEOUS PAPER S-78-12



IN SITU AND LABORATORY DETERMINATIONS
OF SHEAR AND YOUNG'S MODULI FOR THE
PORTSMOUTH, OHIO, GASEOUS
DIFFUSION ADD-ON SITE

by

1D

Joseph R. Curro, Jr. William F. Marcuson, III

Geotechnical Laboratory

U. S. Army Engineer Waterways Experiment Station
P. O. Box 631, Vicksburg, Miss. 39180

12

192 p.

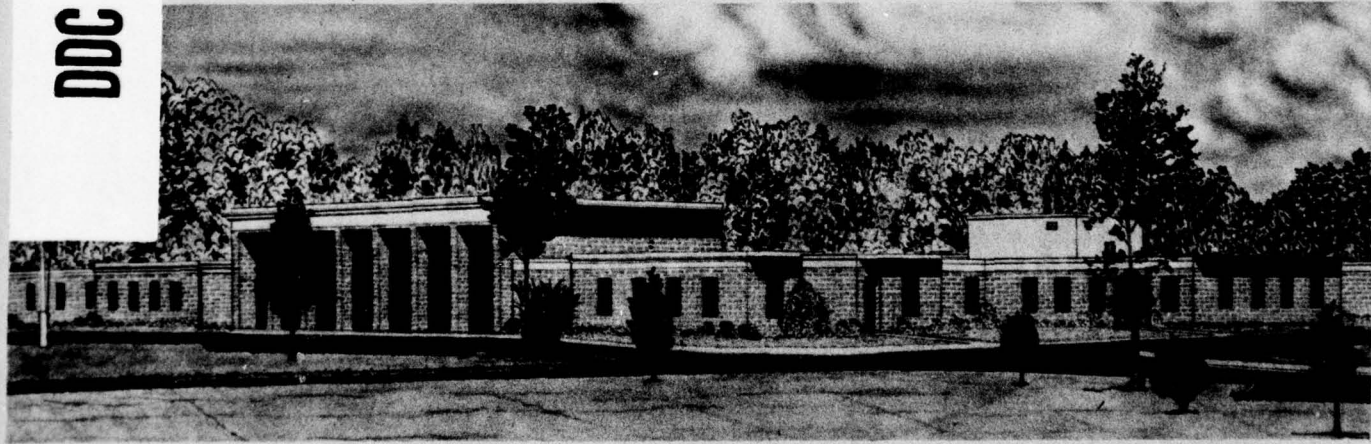
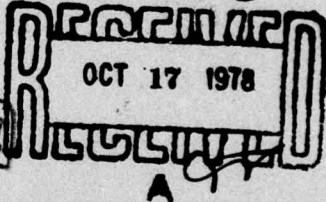
11 Aug 78

Final Report, Nov 76 - Dec 77

Approved for Public Release; Distribution Unlimited

D D C

OCT 17 1978



Prepared for U. S. Energy Research and Development Administration
Oak Ridge, Tenn. 37830

78 10 16 054
038 100

AK

**Destroy this report when no longer needed. Do not return
it to the originator.**

Unclassified

SECURITY CLASSIFICATION OF THIS PAGE (When Data Entered)

REPORT DOCUMENTATION PAGE		READ INSTRUCTIONS BEFORE COMPLETING FORM
1. REPORT NUMBER Miscellaneous Paper S-78-12	2. GOVT ACCESSION NO.	3. RECIPIENT'S CATALOG NUMBER
4. TITLE (and Subtitle) IN SITU AND LABORATORY DETERMINATIONS OF SHEAR AND YOUNG'S MODULI FOR THE PORTSMOUTH, OHIO, GASEOUS DIFFUSION ADD-ON SITE		5. TYPE OF REPORT & PERIOD COVERED Final report
7. AUTHOR(s) Joseph R. Curro, Jr. William F. Marcuson III		6. PERFORMING ORG. REPORT NUMBER
9. PERFORMING ORGANIZATION NAME AND ADDRESS U. S. Army Engineer Waterways Experiment Station Geotechnical Laboratory P. O. Box 631, Vicksburg, Miss. 39180		10. PROGRAM ELEMENT, PROJECT, TASK AREA & WORK UNIT NUMBERS
11. CONTROLLING OFFICE NAME AND ADDRESS U. S. Energy Research and Development Administration, P. O. Box E Oak Ridge, Tenn. 37830		12. REPORT DATE August 1978
14. MONITORING AGENCY NAME & ADDRESS (if different from Controlling Office)		13. NUMBER OF PAGES 99
		15. SECURITY CLASS. (of this report). Unclassified
		15a. DECLASSIFICATION/DOWNGRADING SCHEDULE
16. DISTRIBUTION STATEMENT (of this Report) Approved for public release; distribution unlimited.		
17. DISTRIBUTION STATEMENT (of the abstract entered in Block 20, if different from Report)		
18. SUPPLEMENTARY NOTES		
19. KEY WORDS (Continue on reverse side if necessary and identify by block number) Field tests Shear properties Geophysical exploration Soil strength Laboratory tests Young's modulus		
20. ABSTRACT (Continue on reverse side if necessary and identify by block number) A field geophysical investigation was performed to determine the shear and Young's moduli as a function of depth for a site near Portsmouth, Ohio. This investigation included crosshole, downhole, and surface refraction investigation techniques. A supplementary set of laboratory resonant column tests was performed with the Drnevich resonant column device. Laboratory undisturbed specimens were excited in both the longitudinal and torsional modes to obtain both Young's and shear moduli as a function of strain. Both laboratory and		

DD FORM 1 JAN 73 1473 EDITION OF 1 NOV 65 IS OBSOLETE

Unclassified

SECURITY CLASSIFICATION OF THIS PAGE (When Data Entered)

Unclassified

SECURITY CLASSIFICATION OF THIS PAGE(When Data Entered)

20. ABSTRACT (Continued).

CONT field data are presented and compared.

An idealized soil profile for boring 821-UD is presented. At this boring location, bedrock lies approximately 36 ft below the ground surface. The 36-ft-thick soil deposit has been subdivided into four layers whose shear moduli range from 3.4×10^3 to 86×10^3 psi. The moduli increase as a function of depth. The Young's moduli for this soil profile range from 10×10^3 to 225×10^3 psi and also increase with depth. The internal damping of the soil deposit was found to range from 3 to 5 percent for low dynamic strain amplitudes and is constant with depth. The bedrock has a shear modulus of 125×10^3 psi and a Young's modulus of 370×10^3 psi.

Unclassified

SECURITY CLASSIFICATION OF THIS PAGE(When Data Entered)

THE CONTENTS OF THIS REPORT ARE NOT TO BE
USED FOR ADVERTISING, PUBLICATION, OR
PROMOTIONAL PURPOSES. CITATION OF TRADE
NAMES DOES NOT CONSTITUTE AN OFFICIAL EN-
DORSEMENT OR APPROVAL OF THE USE OF SUCH
COMMERCIAL PRODUCTS.

PREFACE

The study reported herein was performed by the U. S. Army Engineer Waterways Experiment Station (WES) at the request of the U. S. Energy Research and Development Administration (ERDA), Oak Ridge, Tennessee, and was authorized in a letter from ERDA dated 6 Nov 1976.

This study was conducted during the period November 1976 through December 1977 under the general supervision of Mr. R. F. Ballard, Jr., and Dr. P. F. Hadala, former Acting Chief and Chief, respectively, of the Earthquake Engineering and Vibrations Division (EE&VD) and Messrs. R. G. Ahlvin and J. P. Sale, Assistant Chief and Chief, respectively, of the Geotechnical Laboratory. Mr. J. R. Curro and Dr. W. F. Marcuson are the authors of this report.

The authors are indebted to Dr. James W. Spotts, Soils Research Facility, Soils Mechanics Division, who performed the resonant column tests, and Messrs. W. A. Bieganousky, E. S. Stewart, Jr., and D. H. Douglas, EE&VD, who conducted the geophysical investigation.

Directors of the WES during the conduct of the study and preparation of the report were COL G. H. Hilt, CE, and COL John L. Cannon, CE. Technical Director was Mr. F. R. Brown.

CONTENTS

	<u>Page</u>
PREFACE	2
CONVERSION FACTORS, U. S. CUSTOMARY TO METRIC (SI) UNITS OF MEASUREMENT	4
PART I: INTRODUCTION	5
PART II: SITE DESCRIPTION	6
PART III: FIELD INVESTIGATION	7
Drilling and Sampling	7
Geophysical Investigation	7
Elastic Moduli and Poisson's Ratio Determinations	11
PART IV: FIELD TEST RESULTS	12
Proposed Building X-340-4 Location	12
Data Interpretation	15
PART V: LABORATORY INVESTIGATION	18
Resonant Column Test Equipment	18
Test Procedures	18
Resonant Column Test Results	19
PART VI: DISCUSSION OF LABORATORY TEST RESULTS	23
Shear Modulus	23
Young's Modulus	24
Damping Ratio	25
PART VII: COMPARISON OF FIELD AND LABORATORY VALUES	27
Shear and Young's Moduli	27
Damping Values	29
PART VIII: SUMMARY	30
REFERENCES	31
TABLE 1	
APPENDIX A: TEST RESULTS AND DATA INTERPRETATION FROM IN SITU SEISMIC TESTS	A1
FIGURES A1-A35	
APPENDIX B: DYNAMIC MODULUS AND DAMPING VERSUS DYNAMIC STRAIN AMPLITUDE, RESONANT COLUMN TESTS	B1
TABLES B1-B7	
FIGURES B1-B62	

REF ID:	White Section <input checked="" type="checkbox"/>	Black Section <input type="checkbox"/>
DOC	<input type="checkbox"/>	<input checked="" type="checkbox"/>
UNARMED		
JUSTIFICATION.....		
DT.....		
DISTRIBUTOR/AVAILABILITY CODES		
DIGL	AVAIL.	DOC/W SPECIAL
A		

CONVERSION FACTORS, U. S. CUSTOMARY TO
METRIC (SI) UNITS OF MEASUREMENT

U. S. customary units of measurement used in this report can be converted to metric (SI) units as follows:

<u>Multiply</u>	<u>By</u>	<u>To Obtain</u>
feet	0.3048	metres
feet per second	0.3048	metres per second
inches	25.4	millimetres
inches per second	25.4	millimetres per second
pounds (force) per square inch	6894.757	pascals
pounds (mass)	0.4535924	kilograms

IN SITU AND LABORATORY DETERMINATIONS OF SHEAR AND
YOUNG'S MODULI FOR THE PORTSMOUTH, OHIO,
GASEOUS DIFFUSION ADD-ON SITE

PART I: INTRODUCTION

1. In order to evaluate the dynamic response of soil or a structure founded on soil, knowledge of stress-strain properties of the foundation material is required. When using current finite element static and dynamic foundation analysis computer techniques, the initial elastic moduli (very low strains, generally 10^{-4} cm/cm (in./in.)* or less) are required along with the variation in moduli as a function of strain.

2. These initial moduli (shear and Young's) can be determined in situ using various geophysical techniques such as the crosshole or uphole/downhole technique. Or, resonant column tests can be conducted in the laboratory on undisturbed samples of the foundation material to obtain initial moduli and variation as a function of strain level.

3. Since the moduli discussed above would be needed for dynamic foundation design** of four buildings and a test loop structure to be constructed at the Portsmouth, Ohio, Gaseous Diffusion Add-On Site, a test program was formulated that consisted of field and laboratory investigations to provide the required moduli. In addition, Poisson's ratios were determined from investigations to aid in the dynamic design.

4. Therefore, the primary purpose of this report is to present values of shear and Young's moduli for the foundation materials underlying the four proposed buildings (designated as X-340-1 through X-340-4) and the test loop structure (X-774), located as shown in Figure 1. Additionally, building X-340-4 was arbitrarily selected as an example case to illustrate the procedure used for determining dynamic design values. Results of these calculations are also presented herein.

* A table of factors for converting U. S. customary units of measurement to metric (SI) units is presented on page 4.

** Foundation design for static loading is reported in Reference 1.

PART II: SITE DESCRIPTION

5. The construction site is located in southeastern Ohio near the confluence of the Ohio and Scioto Rivers. Overburden soils at the site were primarily Pleistocene river- and lake-bed deposits. Figure 1 is a geologic map of the site.¹ The map shows the east bank of the Scioto River valley and outlines the areal distribution of the glacial lake-bed deposits and early alluvial deposits. The lake-bed deposits, consisting of fat, thinly laminated clays, are largely confined to the old Scioto River channel that lies under a large portion of the site.

6. The area outlined as lake deposits in Figure 1 shows the occurrence of fat, laminated clay either at the surface or at some depth beneath the surface. Lean clays, silts (alluvium), and fill material placed during the period 1953 to 1955 lie above the fat clay in various thicknesses over a large portion of the outlined area. Early river alluvial silty clay and silt occupy that portion of the valley fill outside the fat clay boundaries.

7. Up to 60 ft (average of 35 to 40 ft) of early river- and lake-bed deposits in the old valley still remain at the site. These deposits are mostly fat, laminated clays, lean clays, and fine silts, with a 2- to 10-ft-thick layer of weathered clayey gravel at the base. A 1- to 10-ft-thick layer of residual soil and colluvium mantles a large part of the valley.

8. The rock formations underlying the surficial soils are described below:

- a. Cuyahoga shale. The Cuyahoga shale forms the hills along the east side of the site. It is a medium gray, hard, thinly bedded shale with occasional thin (1/2 in. to 1 ft thick) fine-grained sandstone lenses.
- b. Sunbury shale. The Sunbury shale lies immediately beneath the Cuyahoga; the interface is just above the valley floor. It is a black, hard, highly carbonaceous fissile shale that contains occasional thin veinlets and small nodules of pyrite. The thickness of the Sunbury shale is about 19 ft.
- c. Deep strata. Beneath the Sunbury shale lies the Berea sandstone, with a thickness of about 30 ft; then follows the Bedford shale, with a thickness of about 98 ft; and then the Ohio shale, with an estimated thickness of 300 ft.

PART III: FIELD INVESTIGATION

9. The field investigation was comprised of two phases:
(a) drilling and sampling and (b) geophysical investigation.

Drilling and Sampling

10. During this phase of the field investigation, 27 holes were drilled at the site for use in the performance of in situ seismic tests and to obtain undisturbed samples for laboratory testing. The holes were drilled in sets of three with one set being near each end of the four proposed building locations and one set made at the test loop location. The three holes were oriented to form an L-type configuration with the distance from the boring at the vertex of the L to the borings at the end of each leg of the L being approximately 20 ft. Undisturbed samples were obtained from the boring at the vertex of the L for each set with a 5-in. Hvorslev fixed piston sampler. The remaining holes were drilled with a U. S. Army Engineer Waterways Experiment Station (WES) modified fishtail bit with upward baffles. After the holes had been drilled to the desired depth (2 to 5 ft in rock), 3-in. ID PVC (polyvinyl chloride) pipe was installed in the boreholes, and the annular space between the casing and walls of the borings was grouted with a mixture of cement, bentonite, and water that had the consistency of soil.

Geophysical Investigation

11. The geophysical investigation conducted at the site consisted of nine series of in situ seismic tests. Each series was comprised of crosshole, downhole, and surface refraction seismic tests.

Crosshole test procedure

12. In most instances, the crosshole technique is used in conjunction with surface refraction seismic surveys. The crosshole method is a straightforward way of determining horizontal velocities and layering, and has a distinct advantage over the conventional surface

refraction method in that low-velocity zones can be detected if they are sufficiently thick with respect to the source and receiver spacing.

13. Crosshole surveys are normally conducted by using two or more borings, cased or uncased, into which a seismic source and transducers are placed at known elevations. The spacing of borings and source elevations may be varied according to site-dependent conditions and sources, and geophones may be of various types in order to enhance shear-wave (S-wave) arrival time determinations. Compression wave (P) and S-wave measurements may be made by this procedure.

14. The crosshole tests discussed herein were conducted using a portable 24-channel refraction/reflection seismograph. A strip chart recorder displayed the data while operating at a paper speed of approximately 35 ips. Timing lines were displayed on the oscillogram at 10-msec intervals. The procedure was a modified technique that used the same vibratory source and control package as that described by Ballard in Reference 2. The primary difference in the two procedures was concerned with the data acquisition package, i.e., no signal enhancement was used. Rather, the vibratory source was swept through a frequency range while monitoring the output of the two geophones placed at the same elevation in the receiver boreholes (the vibrator was producing vertical oscillations, thereby transmitting a vertically polarized shear wave). When an acceptable response was received at a specific frequency, this frequency was then interrupted by a tone burst generator to send a specific number of cycles of that frequency to the receiver units. The source geophone was displayed simultaneously along with both receiver geophones on the oscillograph. In this manner, the origin of the source pulse could easily be recognized, and the time difference between that pulse and the signal arrival at each of the two receivers could be determined. In most cases the frequency that propagated well at the site appeared to be between 100 and 200 hz. Accuracy associated with this test procedure and instrumentation would be on the order of approximately 0.5 msec.

15. In practice, the tests to obtain S-wave data were conducted by first placing the source and receivers at the same elevation near the

top of the boreholes, then pulsing the source unit several times recording both transmitted and received signals. After a satisfactory record had been obtained, the units were then repositioned 5 ft deeper. The procedure above was repeated at this and each succeeding 5-ft depth until reaching the bottom of the boring. Since these holes were relatively shallow, their verticality could be checked by visual observation using either flashlight or mirror sources. In all cases, the boreholes were vertical within ± 3 in., thereby eliminating the need for a formal deviation survey.

16. The P-wave data were obtained in a similar manner, except that the vibrator and its associated instrumentation as a signal source were not used. Instead, exploding bridgewire detonators (EBW's) were used at each 5-ft increment as the P-wave source.

17. Data obtained from the crosshole tests were the times required for P- and S-waves to propagate from the source to a point of detection. These times were then divided into the distance between source and receiver geophones to provide apparent velocities. If a nearby higher velocity layer exists, the wave will refract and travel along that layer, thus traveling along a faster path than the direct distance path. When this occurs, calculations based on Snell's law of refraction were invoked to determine true velocities by accounting for zones of high velocity contrast. Due to the nature and number of calculations involved in a typical application of the crosshole technique to a layered site, a computer program for crosshole seismic interpretation was used for data reduction. This program applies Snell's law to develop a plausible true velocity interpretation from the apparent velocity obtained in the field.

Downhole test procedure

18. This test, designed to provide data for determination of vertically oriented P- and S-wave velocities, was conducted using the same seismograph and recorder as those used for the crosshole tests.

19. In practice, the receiver geophone was placed at a depth of 5 ft in a borehole, and a vertical hammer blow to a steel plate positioned approximately 1 ft from the mouth of the boring on the ground

surface was used as the vertical P-wave source. A geophone adjacent to the hammer impact point provided zero time. S-wave determinations were then made by placing a large wood plank on the ground surface and striking the plank with successive blows at each end in order to reverse polarity of the horizontally polarized shear wave to facilitate identification. The procedures for obtaining P- and S-wave data were then repeated with the receiver geophone at 5-ft increments until the bottom of the borehole was reached. Data obtained from the downhole tests were plotted as time versus depth from the source to the receiver geophone. Average and incremental velocities were determined from this type plot.

Surface refraction
seismic test procedure

20. Conventional surface refraction seismic tests were conducted at the site using the 24-channel unit. Refraction lines run at the site were 240 ft in length. Geophones were spaced at 10-ft intervals with the first geophone positioned 5 ft from an explosive source. Both forward and reverse traverses were shot at the site so that true velocities, in addition to apparent velocities, could be determined and depths to refracting interfaces computed.

Surface vibratory test procedure

21. In order to provide greater confidence in the data obtained at the site, surface vibratory tests³ were conducted near each crosshole set. Surface Rayleigh (R) waves may be generated using a controlled energy source such as a vibrator. In this case, the electromagnetic vibrator used to conduct the crosshole tests was also used to provide the surface R-wave source. The vibrator was operated at several frequencies, and the surface wave was monitored by the geophones used for the surface refraction seismic tests, which were placed in a line at intervals of 1 ft. In this manner, the velocity of the R-wave can be determined from a plot of R-wave time versus distance for each specific frequency. Then, a corresponding wave length can be calculated by dividing the frequency into the velocity. Wave velocities thus derived are considered to be average values for an effective depth of one half the wave length. S-waves, for practical purposes, can be considered

to have the same velocity as R-waves. For the range of Poisson's ratios commonly found in soil and rock materials, errors due to the assumption above are less than 10 percent and are generally 5 percent or less.

22. Since the vibrator used at this site was of limited force output (50 lb), the depth of investigation was limited to approximately 5 ft. These data could then be compared with those obtained for the shallow crosshole test position. Further, the surface velocity is provided--a necessary input parameter to the crosshole computer program.

Elastic Moduli and Poisson's Ratio Determination

23. The P- and S-wave velocities determined from the above-mentioned test procedures should be converted to elastic parameters such as shear modulus G , Young's modulus E , and Poisson's ratio ν for use in the foundation design. This conversion can be accomplished using elastic theories of wave propagation and the total mass density ρ of the medium. Therefore, the relation of shear modulus to S-wave velocity V_s and mass density is $G = V_s^2 \rho$. Poisson's ratio of the medium can be determined by the relation of V_s and P-wave velocity V_c as

$$\nu = \frac{1 - 2 \left(\frac{V_s}{V_c} \right)^2}{2 + 2 \left(\frac{V_s}{V_c} \right)^2}$$

Young's modulus can then be determined by the relation

$$E = 2(1 + \nu)G$$

for isotropic, linearly elastic materials. With these equations, values of G , E , and ν can be determined through the measurement of P- and S-wave velocities, provided that the wet unit weight of the soil is known.

PART IV: FIELD TEST RESULTS

24. The results determined from the in situ seismic tests conducted at the proposed location of building X-340-4 are presented and discussed below. It appeared feasible to the authors to select one location as being "typical" and to discuss the test results obtained there, since discussions of the results at the other locations would be virtually a repetition with only the numerical values of the in situ parameters different. Therefore, the test results for the other building locations are presented in Appendix A.

Proposed Building X-340-4 Location

25. Two series of in situ seismic tests were conducted at this location, one near each end of the proposed building location as shown in Figure 2.

Crosshole tests

26. These tests consisted of two crosshole sets. Borings 821, 822, and 823 comprised one set that was near the south end of the proposed building, whereas the second set, located near the north end of the building, was made up of borings 824, 825, and 826 as shown in Figure 2.

27. Borings 821 and 824 were used as the seismic source boreholes for their respective sets, and borings 822, 823, 825, and 826 were employed as receiver holes for their respective sets. The seismic source and receiver (geophone) placements used in the performance of the cross-hole tests are shown in Figure 3. True P- and S-wave velocities determined from the crosshole data are presented alongside the receiver and source locations. Note that only one P- and S-wave velocity is shown for each test elevation although true P- and S-wave velocities were determined from the seismic source borehole to each of the receiver boreholes for each crosshole set. In comparing the velocities from the source to each receiver, the spread was so narrow that it was thought advantageous to average the two true P-wave velocities at each test elevation and, likewise, average the two true S-wave velocities determined at each

elevation. Maximum error encountered in doing this was less than 10 percent. The S-wave velocities appear to generally increase with depth from a low of 235 fps near the surface to 2175 fps at a depth of about 45 ft (el 629).* P-wave velocities, as shown, range from 1250 fps near the surface to 8240 fps at a depth of 45 ft. However, it will be noted that the P-wave velocities determined from the tests conducted in borings 824 through 826 indicate a decreasing trend from el 664 to 639.

Downhole tests

28. Two downhole tests located as shown in Figure 2 were conducted, one using boring 821 and the other using boring 824. The results of the downhole tests conducted in borings 821 and 824 are presented in Figures 4 and 5, respectively. As shown, average and incremental P- and S-wave velocities were determined from the downhole data.

29. Data from boring 821 indicated three P-wave velocity zones: 1540 fps from el 671 to 665, 4450 fps from el 665 to 641, and 2500 fps from el 641 to 636. It should be noted that the 2500-fps layer underlies a high velocity zone. The presence of the 2500-fps layer was not indicated from the crosshole data (Figure 3), which is entirely possible if the zone is only 5 ft thick and borehole spacings were 20 ft. Incremental P-wave velocities ranged from a low of 1540 fps near the surface to a high of 5000 fps at el 641 where the 2500-fps zone was encountered. Four S-wave velocity zones were noted from the data. Average vertical velocities were 415 fps from el 671 to 666, 520 fps from el 666 to 651, 770 fps from el 651 to 641, and 1665 fps from el 641 to 636. Incremental S-wave velocities generally exhibited an increasing trend with depth, ranging from 415 fps near the surface to 1665 fps at el 636.

30. Downhole data from boring 824 indicated four P- and S-wave velocity zones. Average vertical P- and S-wave velocities were 1820 and 310 fps, respectively, for the near surface zone; 5715 and 515 fps, respectively, for the second zone; 2220 and 625 fps, respectively, for

* Depth and elevation (referenced to mean sea level) are used interchangeably in this report. The elevation (top) of boring 821 was 671 ft. With this information the reader can convert depth to elevation and vice versa, as required.

the third zone; and 7335 and 1835 fps, respectively, for the fourth zone. It will be noted that the 2220-fps zone underlies a higher velocity zone, and the downhole P-wave value is consistent with the lower velocity value (3710 fps) noted from the crosshole data between el 649 and 639. Incremental P-wave velocities varied from a low of 1820 fps near the surface to 8000 fps at el 629, with the lower velocity zone (2220 fps) ranging from el 649 to 639. Incremental S-wave velocities generally increased with depth from a low of 310 fps near the surface to 2000 fps at el 629.

Surface refraction seismic tests

31. These tests consisted of four traverses (two lines), the orientation and location of which are shown in the test layout, Figure 2. The time versus distance plots for these traverses, designated as S-15 through S-18, are shown in Figures 6 and 7. These figures also present apparent velocities, true velocities, and associated depths to refracting layers. Three velocity zones were indicated from the surface refraction data. The near-surface zone exhibited a velocity of 1,340 fps to depths ranging from 4 to 11 ft. The true velocity of the second zone varied from 4,700 to 5,070 fps and ranged from 30 to 56 ft in thickness. Data from borings located near the seismic lines indicated the ground water table to be at a depth of about 11 ft. True velocities of 9,675 and 12,350 fps were noted for the third zone and would be indicative of the underlying rock (shale) at this building location. The depths to the third velocity zone and the thickness of the second zone should be suspect because of the presence of the lower velocity zones (2,220 to 3,710 fps) detected by the crosshole and downhole tests from el 649 to 636. The effect that a lower velocity zone underlying a high velocity zone has on surface refraction data is to make the computed depths to zones below the lower velocity zone too great. Thus, the computed depths to the 9,675- and 12,350-fps zones are probably too deep.

Surface vibratory tests

32. One surface vibratory test was conducted at boring 821 and another at boring 824. The results of these tests yielded average R-wave velocities of 375 and 235 fps for the near-surface material

(<5 ft depth) at borings 821 and 824, respectively. These velocities were used as true S-wave velocity inputs for the near surface to the crosshole computer program.

Data Interpretation

33. Since data interpretation procedures and discussions would be virtually identical for each building location, the X-340-4 location will continue to be discussed as regards data interpretation and associated procedures.

34. It will be noted that the test results near each end of the building were used to make an interpretation for the entire building location to aid the engineers in designing the full foundation.

P- and S-wave velocity zoning

35. The P- and S-wave velocity results determined from the cross-hole, downhole, and surface refraction seismic tests at this building location were analyzed and interpreted to produce the P- and S-wave velocity profiles shown in Figures 8 and 9, respectively. It will be noted that P- and S-wave zones will not necessarily align with one another. This is primarily due to P-wave velocities increasing as percent saturation of the soil increases, whereas S-wave velocities do not.

36. Referring to Figure 8, five velocity zones were delineated from the P-wave data. The velocities presented for the zones were usually weighted averages based on data quality. A 1400-fps velocity was established for the near-surface zone, which averaged about 7 ft in thickness. The second velocity zone averaged 4900 fps and was about 20 ft thick. This zone was underlain by a lower velocity layer (2800 fps), which ranged from 5 to 13 ft in thickness and is best delineated by the uphole seismic data. The next two velocity zones (7100 and 9400 fps) could be collapsed into one. However, since the top of the 9400-fps zone coincides with the top of shale, it was believed advantageous to keep the zones separate. The 7100-fps zone interpreted from the crosshole and downhole tests in borings 824 through 826 is probably indicative of a silt, sand, and gravel mixture cemented to form

the conglomerate noted in the laboratory classifications of samples from boring 824 in this depth range.

37. Referring to Figure 9, five S-wave velocity zones were interpreted from the S-wave data. A 350-fps velocity was established for the near-surface zone and averaged about 7 ft in thickness. The underlying zone had a 500-fps average and a thickness of about 15 ft. The third zone averaged 700 fps and was approximately 12 ft thick. The two deeper zones (1750 and 2000 fps) could probably have been combined; however, for the same reason given for the P-wave zoning (to separate top of shale and its associated velocity from material immediately above it), they were not. It will be noted that the value of wet unit weight applicable for each zone is also presented in Figure 9. These values were obtained from the undisturbed samples used in the resonant column tests and from laboratory tests conducted on samples from borings near the in situ seismic test locations (Reference 1).

Shear and Young's moduli
and Poisson's ratio (G, E, v)

38. The interpretation of the data was continued by establishing zones from the velocity profiles and determining values of shear (G), Young's modulus (E), and Poisson's ratio (v) for these zones. This was accomplished by overlaying the P- and S-wave velocity profiles (Figures 8 and 9). This overlay produced some seven zones because P- and S-wave velocity zones do not always align with one another. Then, values of shear and Young's moduli and Poisson's ratio were computed for each zone using the P- and S-wave velocities and wet unit weights that fell into each zone obtained by overlaying the profiles. After analyzing G , E , and v values for the various zones, it was evident that the controlling factor was the S-wave velocity zoning because the P-wave velocity variations had little effect on E and v values and of course, no effect on G values. Therefore, the seven newly established zones could be reduced to the five original zones shown on the S-wave profile (Figure 9). The final field interpretation for this building location showing the five zones with their associated shear and Young's moduli and Poisson's ratios is presented in Figure 10. Also

shown in the figure are laboratory classifications of the soil and rock samples from borings 821 and 824. Explanations of the graphic classifications are shown in Figure A1.

39. The near-surface zone exhibited values of 3,300 and 9,700 psi for G and E, respectively, to a maximum depth of about 7 ft. Poisson's ratio was 0.47. The underlying zone had a shear modulus of 6,600 psi and a Young's modulus of 19,700 psi. Thickness of this zone was about 15 ft. Poisson's ratio was 0.49. Shear and Young's moduli for the third zone were 12,600 and 37,100 psi, respectively, and extended from about el 652 to 639. Poisson's ratio in this zone was 0.48. The fourth zone exhibited G and E values of 85,900 and 225,000 psi (range 200,000 to 250,000 psi), respectively, with a thickness of 5 to 9 ft. Poisson's ratio of this zone was 0.47. However, near boring 821, Poisson's ratio was 0.18 based on P- and S-wave velocities of 2800 and 1750 fps, respectively, which accounts for the range in E values for this zone. The deepest zone encountered had G and E values of 125,100 and 369,800 psi, respectively. Poisson's ratio in this zone was 0.48. Boring and piezometer data indicated the groundwater table to be about 11 ft as shown in Figure 10.

40. It will be noted that the soil profile varies considerably from one end of the proposed building location to the other; therefore, no attempt has been made to correlate velocity or moduli zones with soil type.

PART V: LABORATORY INVESTIGATION

41. Undisturbed samples taken in the field were transported by truck to the WES. Once in the WES laboratory, the samples were opened and classified. The samples were evaluated to see which were representative of field conditions according to the boring logs and general knowledge of the site¹ and which could be tested in the laboratory. Resonant column tests were performed on the representative samples found to be suitable for testing, i.e. those which did not contain particles of gravel, or roots.

Resonant Column Test Equipment

42. The equipment used in this series of resonant column tests is known as the Drnevich torsional resonant column apparatus. This device is manufactured by Soil Dynamics Instruments, Inc., Lexington, Kentucky. Resonant column apparatus normally excite the specimen only torsionally; however, this equipment differs in that it also includes an electromagnetic oscillator for longitudinal vibration of the specimen. For a more detailed description of this equipment, the reader is referred to Reference 4.

Test Procedures

43. All tests were performed on 2.8-in.-diam by 7-in.-long undisturbed specimens. These specimens were isotropically consolidated so as to correspond to the in situ mean principle effective stress or octahedral stress, $\bar{\sigma}_{oct}$. The in situ mean principle effective stress was computed assuming normally consolidated conditions¹ and a coefficient of earth pressure at rest of 0.5.

44. After primary consolidation was complete, the drainage valve was closed and the B valve was checked and reported in Appendix B. The specimen was subjected to sinusoidal excitation in both the longitudinal and torsional modes. Longitudinal and torsional vibrations were not

conducted simultaneously. The frequency of vibration was varied until resonance was obtained and data were recorded such that the modulus and strain amplitude values could be computed. In order to obtain the variation of modulus as a function of strain amplitude, the driving force (current delivered to the vibrator) was increased and the general test procedure was repeated.

45. The procedure above is a brief description of that used by the WES. A more detailed testing procedure, along with a complete discussion of the analysis and calculations required to obtain shear and Young's moduli from the raw data, is given in Reference 4.

Resonant Column Test Results

46. Undisturbed samples from various depths in borings 800 UD, 803 UD, 806 UD, 809 UD, 812 UD, 815 UD, 818 UD, and 821 UD were tested in the resonant column device. The locations of these borings are shown in Figures 2, A2, A9, A18, and A27, and test results are shown in Appendix B. A total of 37 specimens were tested.

47. Appendix B contains plots of modulus and damping versus dynamic strain amplitudes for all the resonant column tests conducted by WES. Shown on the plots are the compression modulus and damping values obtained by vibrating the specimen in the longitudinal mode and the shear modulus and damping values obtained by vibrating the specimen in the torsional mode for strain amplitudes ranging from 10^{-7} to about 10^3 in./in. or rad/rad. For each building site, a table is given indicating the depth from which the sample was obtained, the depth range that it is thought to represent, and its Atterberg limits.

48. In order to familiarize the reader with the format of the resonant column data and its interpretation, the test results obtained from boring 821 UD samples will be discussed.

49. Four specimens were selected from undisturbed samples obtained from boring 821 UD. As indicated in Table 1 (which is similar in format to those described above), sample 2 was taken at a depth of 2.7 to 4.2 ft and was considered to represent the surficial layer to a

depth of 14 ft. This material was classified in the laboratory as a CH clay and tested in the resonant column device at a mean effective principle stress of 1.7 psi. Figure 11 presents the results in terms of dynamic modulus versus dynamic 0-peak strain amplitude for the resonant column tests conducted on this specimen. The shear modulus has a maximum value of 5.6×10^3 psi at a torsional strain amplitude of about 10^{-5} rad/rad and decreases to about 2.4×10^3 psi at a strain amplitude of about 5×10^{-4} rad/rad. The compression modulus varies from about 26×10^3 to 16×10^3 psi over the axial strain range of 10^{-6} to 5×10^{-4} in./in.

50. Figure 12 presents the damping ratio as a function of dynamic strain amplitude for the resonant column tests conducted on sample 2 taken from boring 821 UD. The damping ratio varies from approximately 5 to 10 percent over the strain range of 10^{-6} to 10^{-3} in./in. In general, the damping determined in the torsional mode is approximately two thirds of that determined in the longitudinal mode. As expected, damping generally increases with increasing strain (References 5-8).

51. Sample 9 was taken at a depth of 20 to 21.8 ft and was considered to be typical and represent a clay layer from a depth of 14 to 22 ft. A resonant column test was performed on the specimen taken from sample 9 and consolidated to a mean effective principle stress of 6 psi. The results of this resonant column test are presented in Figures 13 and 14. Figure 13 shows that the shear modulus is approximately 2.8×10^3 psi at a strain range of 10^{-5} rad/rad and decreases to about one half of that value (1.4×10^3 psi) at a strain range of 10^{-3} rad/rad. The compression modulus varies from a high of about 26×10^3 psi at a strain of 3×10^{-6} in./in. to about 10.4×10^3 psi at a strain of about 10^{-4} in./in. The damping values as a function of dynamic strain amplitude are presented in Figure 14. The shear damping (torsional mode) increases from about 3 to 9 percent with increasing strain as expected. However, the longitudinal damping remains relatively constant as indicated in Figure 14. Since the trend in longitudinal damping data is very atypical, the data should be considered suspect.

52. Sample 11 was taken at a depth of 24.5 to 26.6 ft and was

considered to be typical of the 5-ft-thick layer between a depth of 22 and 27 ft. This material was a silt and was tested in the resonant column apparatus at a mean effective principle stress of 9.5 psi. Shear and compression moduli as a function of dynamic strain amplitudes are presented in Figure 15. The shear modulus varies from about 17×10^3 to 5.6×10^3 psi over the strain range of 10^{-6} up to 10^{-4} rad/rad. The compression modulus is more or less constant at about 56×10^3 psi for straining less than 10^{-6} in./in. However, it decreases sharply as strains increase above 10^{-6} and drops to 20.1×10^3 psi at a strain of about 3×10^{-5} in./in. The damping data obtained during this test are presented in Figure 16. One sees that the torsional damping or shear damping is approximately constant at 3 percent over the strain range considered. The longitudinal damping appears to increase from about 4 to 13 percent as the strains increase from 10^{-7} to 10^{-5} in./in. The last point that was obtained at a strain of about 3×10^{-5} in./in. is considered erroneous because it does not fit the trend of the other longitudinal test data.

53. Sample 13 taken at a depth of 29.2 to 30.5 ft was considered to be typical and representative of the soil layer between a depth of 27 and 31 ft. This sample was classified a CL clay and tested in the resonant column device under a mean principle effective stress of 10.75 psi. The dynamic modulus and damping ratio as a function of dynamic strain amplitude are presented in Figures 17 and 18, respectively. The shear modulus is shown to vary from about 4.2×10^3 psi to 2.1×10^3 psi over the strain range of about 10^{-5} to 10^{-3} rad/rad. The compression modulus is constant at about 43×10^3 psi up to a strain range of 10^{-6} in./in. Above a strain of about 10^{-6} in./in. the compression modulus decreases to a value of about 16.0×10^3 psi at a strain range of 5×10^{-5} in./in. The damping values obtained in the longitudinal mode are more or less independent of strain and are in the range of 5 or 6 percent (Figure 18). The damping ratio obtained in the torsional mode varies from about 2.5 percent at a strain range of 10^{-5} in./in. to 12 percent at a strain range of approximately 10^{-3} in./in.

54. Below a depth of 31 ft the soil is extremely gravelly. This

means that undisturbed samples could not be taken. Samples obtained were disturbed to such an extent as to be considered unsatisfactory for testing. Rock was found at a depth of about 36 ft.

PART VI: DISCUSSION OF LABORATORY TEST RESULTS

55. The resonant column data obtained from specimens trimmed from samples taken in boring 821 UD have been presented. In this part a soil profile will be developed for boring 821 in terms of shear modulus, Young's modulus, and internal damping ratio.

Shear Modulus

56. Figure 19 summarizes the shear modulus data obtained from testing four specimens taken from samples of boring 821. Also shown in Figure 19 is a soil profile depicting the four layers that were observed in boring 821 UD. Note that the near-surface clay layer is 14 ft thick and has a shear modulus at low strain levels of about 3.5×10^3 psi. As the strain is increased to a dynamic strain level of about 10^{-3} rad/rad, this shear modulus decreases to about 1.7×10^3 psi. Immediately below this 14-ft-thick surficial layer is an 8-ft-thick layer of clay. From the resonant column test results, it appears that this material has a shear modulus of about 2.8×10^3 psi at very low strains. This modulus decreases to about 1.0×10^3 psi as the strain level increases to 10^{-3} rad/rad. Below a depth of 22 ft there exists a 4-ft-thick silt layer. This material exhibits a shear modulus of 17×10^3 psi at low strain levels. As the strain increases to a dynamic strain amplitude of about 10^{-4} rad/rad, dynamic shear modulus decreases to a value of 5.6×10^3 psi. Below the 4-ft-thick silt layer there exists a 5-ft-thick clay layer between a depth of 26 and 31 ft. This layer exhibits a shear modulus of about 5.6×10^3 psi at low strain levels. This modulus decreases to about 2.8×10^3 psi as the strain level becomes greater than 10^{-4} rad/rad.

57. In reviewing Figure 19 several specific items should be noted. These are:

- a. As the strain level increases from 10^{-5} to 10^{-3} rad/rad, the shear modulus is generally reduced by about 50 percent, except in the silt layer at a depth of 22 to 26 ft.

In this layer the shear modulus is reduced to about one third of its original low strain value.

- b. One would expect that the modulus would be a function of the mean principle effective stress. Thus, the modulus should increase as a function of depth. This is not the case in boring 821 UD. The clay layer at a depth of 14 to 22 ft is not stiffer than the surficial clay.
- c. The 5-ft-thick clay layer immediately below the silt has a modulus that is significantly lower than the silt layer at a depth of 22 to 26 ft. This is not unusual but should be noted because it may be important in any future dynamic analyses or dynamic calculations.

Young's Modulus

58. Figure 20 shows Young's modulus (E) versus dynamic strain amplitude as a function of depth in boring 821 UD. The 14-ft-thick surficial layer has a compression modulus at low strain levels of about 26×10^3 psi. This value decreases to approximately 15×10^3 psi when the strain level increases to 5×10^{-5} in./in. It should be noted that groundwater table is located at a depth of about 12 ft. Since this should not have a significant effect on the shear and Young's moduli, it was ignored. The clay layer between a depth of 14 and 22 ft is very similar to the surficial layer. This 8-ft-thick clay layer has a Young's modulus of about 26×10^3 psi at a strain level of 4×10^{-7} in./in. As the strain increases to a level of approximately 10^{-4} in./in., the compression modulus decreases to 9.7×10^3 psi. The Young's modulus in the silt layer that lies at a depth of 22 to 26 ft is approximately 56×10^3 psi at strain levels below 10^{-6} in./in. As the strain level increases above 10^{-6} in./in., this Young's modulus decreases to approximately 20×10^3 psi when the strain level is about 4×10^{-5} in./in. The 5-ft-thick clay layer located at a depth of 26 to 31 ft in boring 821 UD has a compression modulus at low strain levels of about 43×10^3 psi. Again, as the strain increases from a level of around 10^{-6} to 10^{-4} in./in., the compression moduli decreases to approximately 16×10^3 psi.

59. As one looks at this collection of data, it is again apparent

that the silt layer at a depth of 22 to 26 ft is relatively stiff compared with the other layers. The two clay layers above 22 ft have similar characteristics, with the layer located between 14 and 22 ft being more sensitive to strain than the surficial layer.

Damping Ratio

60. Figure 21 presents the damping ratio versus dynamic strain amplitude as a function of depth for boring 821 UD. In dynamic analyses and in the calculation of dynamic response of soils, the predominant energy input comes from shear waves. Consequently, shear or torsional damping is the most important consideration, and only shear damping will be discussed here. Close study of Figure 21 reveals that damping is relatively constant as a function of depth for boring 821. For strains less than 10^{-4} in./in., the damping ratio is on the order of 3 percent. As the strains increase above 10^{-4} , then the damping ratio approaches 12 percent. Based on WES experience, this appears to be reasonable and consistent.

61. As mentioned previously, resonant column tests were performed on undisturbed samples from borings 800 UD, 803 UD, 806 UD, 809 UD, 812 UD, 815 UD, 818 UD, and 821 UD. These data are presented in Appendix B. The data from boring 821 UD have been discussed in detail. The data obtained from the samples from the other borings should be treated in a similar manner as those from boring 821.

62. The collection of data presented in Appendix B was obtained from 35 resonant column tests. In general, shear and compression moduli decrease as a function of increasing strain (References 3-6) while damping increases. These trends are evident in the data in Appendix B. However, it is not unusual for some of the data to exhibit a fair amount of scatter, and some of the data presented in Appendix B do not follow the expected trends. This merely indicates that these data are suspicious and should be treated as such. Explanations for why these data might be erroneous are as follows:

- a. Equipment problems such as increased piston friction or binding.

- b. A variable calibration of one or more of the instruments.
- c. Operator inadvertently measuring apparatus resonances.
- d. Slippage between the top cap and the specimen.
- e. Sample disturbance.

Note that in Appendix B the data points are plotted but no curves are drawn through the points if the data look suspicious.

PART VII: COMPARISON OF FIELD AND LABORATORY VALUES

63. Figure 22 shows a field boring log for boring 821 UD. This boring log was taken directly from Taylor et al.¹ The reader is referred to Appendix A for explanation of symbols and nomenclature. Values of shear modulus (Figure A1), Young's modulus, and damping as a function of depth were determined in the laboratory by the resonant column test technique at low ($\sim 10^{-6}$) strain levels, and are shown in Figure 22. The subdivision of the soil profile was based on soil type and laboratory visual classification. These values have been discussed previously.

64. For comparison purposes, the values that were determined in the field by geophysical techniques are shown immediately to the right of the laboratory values. The reader is reminded that the subdivision of the soil profile is based on field techniques and results from changes in P- and S-wave velocities. Generally, this development of a soil profile is accomplished independently of material types or visual classification.

Shear and Young's Moduli

Near-surface material

65. In comparing the laboratory and field values, one first notices that thickness of the near-surface layer was determined to be 14 ft in the laboratory. This was based primarily on the boring logs; however, in the field, using velocity data, the near-surface layer was chosen to be only 8 ft thick. The laboratory-determined shear modulus of 3.5×10^3 psi compares very favorably with the field-determined value of 3.3×10^3 psi for locations above the 6 or 7. For practical purposes, these numbers are the same. The Young's modulus computed from the field data was determined to be 9.7×10^3 psi. This value seems reasonable; however, it is about one third of the laboratory-determined value, which is 26×10^3 psi. This value is judged to be too high. For the top layer, values of shear and Young's moduli selected for design were 3.4×10^3 and 10×10^3 psi, respectively.

Second layer

66. Immediately below the near-surface layer is a second clay layer that ends at 20 to 22 ft depending on whether you accept as valid the field seismic data or the laboratory classifications of samples obtained in the boring. The shear modulus as determined in the laboratory for this layer is 2.8×10^3 psi. This value is slightly less than half of the shear modulus (6.6×10^3 psi) that was determined in the field. Because the soil is predominantly clay to a depth of 20 ft, and because the shear modulus should increase with increasing depth, a design shear modulus of about 5×10^3 psi was selected. The values of Young's modulus range from 19.7 to 24.4×10^3 psi depending on whether you choose to use field or laboratory values. These values are relatively close (within about 20 percent of each other), and this is considered good agreement. A value of 20×10^3 psi has been selected for design purposes.

Third layer

67. The third layer selected for design purposes combines the two layers within the depth interval of 22 to 31 ft in the laboratory-determined values and is assumed to be at a depth of 20 to 30 ft. If one averages the shear modulus values of 16.7×10^3 and 5.56×10^3 psi, one obtains 11.1×10^3 psi. This value is in close agreement with 12.6×10^3 psi that was obtained in the field, and consequently a value of 12×10^3 psi was assigned for design purposes. In the laboratory, averaging the Young's moduli for the two layers between 22 and 31 ft yields a value of about 50×10^3 psi. This is considerably higher than Young's modulus of 37.1×10^3 psi as determined by geophysical methods. Based on WES experience and engineering judgment, a value of 40×10^3 psi has been selected for design purposes.

Fourth layer

68. From a depth of 30 to 36 ft, the soil consisted of sandy silts with gravels and consequently was not suitable for laboratory testing. Shear and Young's moduli of 86×10^3 and 225×10^3 psi, respectively, were assumed for design purposes. These values are based on the field information.

Foundation rock

69. Finally, the shear and Young's moduli of the foundation rock were determined to be 125×10^3 and 370×10^3 psi, respectively. Again, this material was not tested in the laboratory and these values are based solely on WES field geophysical evaluations.

Damping Values

70. If analytical calculations are to be conducted, a damping value of 3 to 5 percent should be used for low strain calculations. This value is based on resonant column data and is valid only to a depth of 31 ft because the soil below that depth was not tested. However, because the damping appears to be uniform with depth, extrapolation to the bottom layer (30 to 36 ft in depth) does not seem unreasonable.

PART VIII: SUMMARY

71. Based on the data and the analysis presented, the soil at boring 821 UD can be subdivided and zoned as shown in Figure 22 for the purpose of design loads or dynamic analysis of building on machine foundations. This figure shows four soil layers above rock. The near-surface layer is 8 ft thick, the second layer is 12 ft thick, the third layer is 10 ft thick, and there is a 6-ft-thick layer immediately overlying the rock. This is an idealized soil profile that would be suitable for design calculations. The values of shear modulus, Young's modulus, and damping ratio for each of these layers to be used in design are listed in the right hand three columns of Figure 22.

72. If dynamic response calculations for other building sites are required, then an idealized soil profile will have to be developed for each of these sites. This should be done in a manner similar to that presented in this report.

REFERENCES

1. Taylor, H. M., Jr., et al., "Title I Design Foundation Investigation for Static Loading, Gaseous Diffusion Add-On Plant, Portsmouth, Ohio," Miscellaneous Paper S-77-20, Nov 1977, U. S. Army Engineer Waterways Experiment Station, CE, Vicksburg, Miss.
2. Ballard, R. F., Jr., "A Method for Crosshole Seismic Testing," Journal, Geotechnical Engineering Division, American Society of Civil Engineers, Vol 102, No. GT12, Dec 1976, pp 1261-1273.
3. Fry, Z. B., "A Procedure for Determining Elastic Moduli of Soils by Field Vibratory Techniques," Miscellaneous Paper No. 4-577, Jun 1963, U. S. Army Engineer Waterways Experiment Station, CE, Vicksburg, Miss.
4. Drnevich, V. P., Hardin, B. O., and Shippy, D. J., "Modulus and Damping of Soils by the Resonant Column Method," Symposium on Dynamic Soil and Rock Testing in the Field and Laboratory for Seismic Studies, American Society of Testing Materials, Jun 1977, Denver, Colo.
5. Hardin, B. O. and Drnevich, V. P., "Shear Modulus and Damping in Soils: Measurement and Parameter Effects," Journal, Soil Mechanics and Foundations Division, American Society of Civil Engineers, Vol 98, No. SM6, Jun 1972, pp 603-624.
6. _____, "Shear Modulus and Damping in Soils: Design Equations and Curves," Journal, Soil Mechanics and Foundations Division, American Society of Civil Engineers, Vol 98, No. SM7, Jul 1972, pp 667-692.
7. Marcuson, W. F., III, and Wahls, H. E., "Effects of Time on the Damping Ratio of Clays," Symposium on Dynamic Soil and Rock Testing in the Field and Laboratory for Seismic Studies, American Society of Testing Materials, June 1977, Denver, Colo.
8. Seed, H. B. and Idriss, I. M., "Soil Moduli and Damping Factors for Dynamic Response Analyses," Report No. EERC 70-10, Dec 1970, Earthquake Engineering Research Center, University of California, Berkeley.

Table 1
Samples Tested in the Laboratory
Boring 821 UD

Sample No.	Sample Depth ft	Interval Represented by Sample, ft	Liquid Limit %	Plastic Limit %	Plasticity Index %
2-1*	2.7-4.2	0-14	53	22	31
9-1	20.0-21.8	14-22	--	--	--
11-1	24.5-26.6	22-28	--	--	--
13-1	29.2-30.5	28-31	49	24	25

* Note that the Atterberg limits for sample 2 do not agree with those presented in Figure 22. The limits presented in this table and in Appendix B were obtained from tests conducted at the WES. Those reported in Reference 1 were obtained from tests conducted at the Corps of Engineers South Atlantic Division Laboratory, Marietta, Ga. This discrepancy indicates a significant variation in soil profile, which is not otherwise apparent.

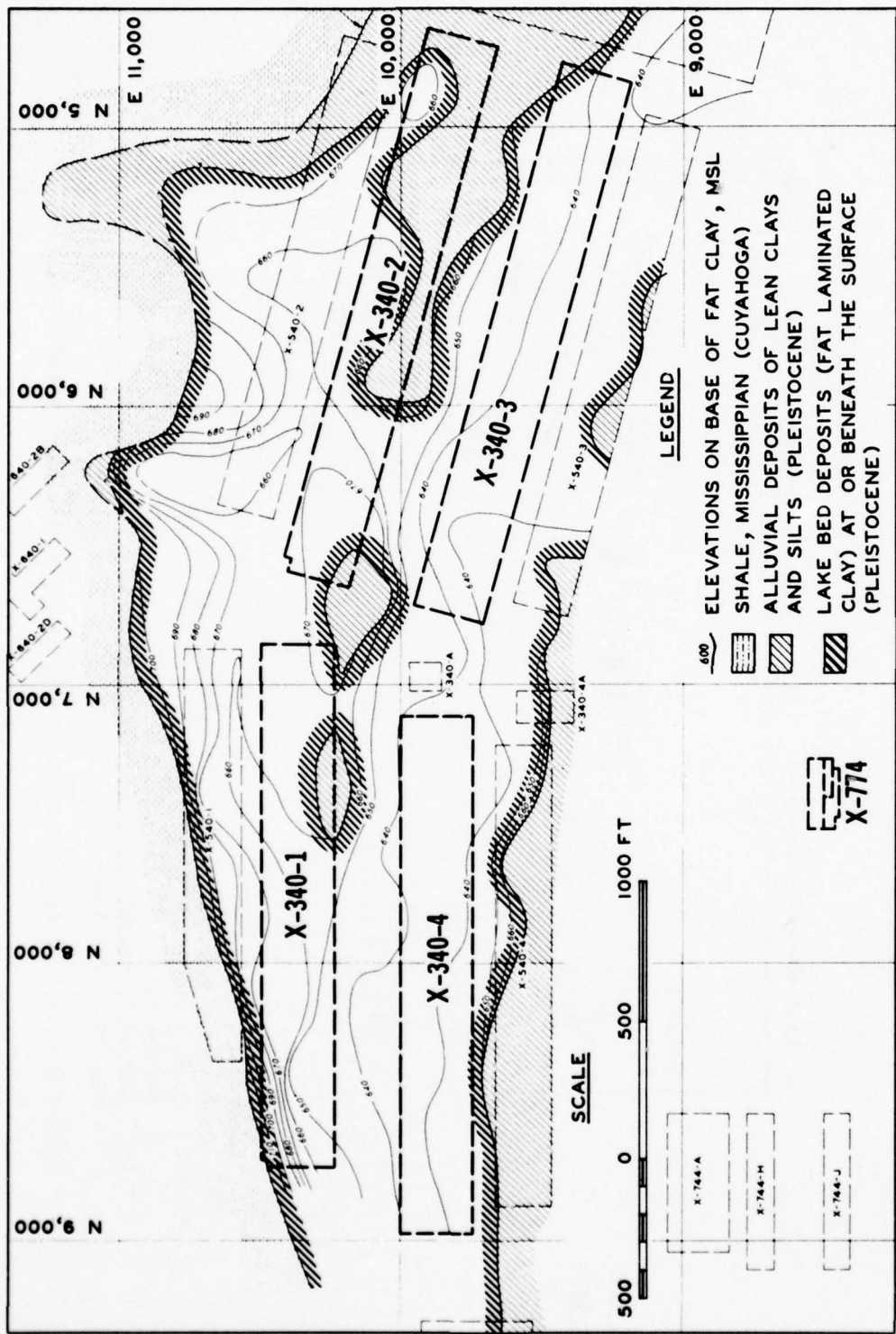


Figure 1. Proposed building and test loop locations and geologic map of the site

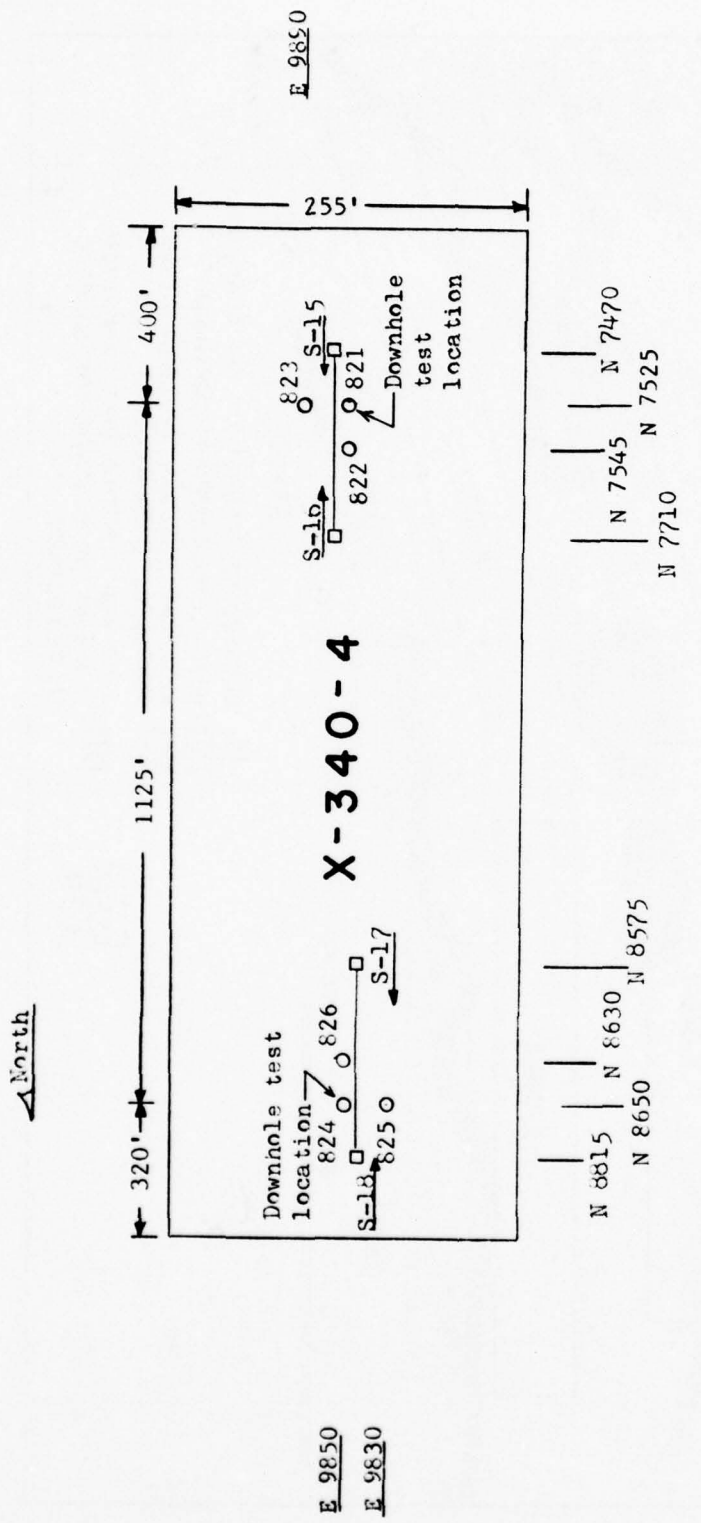


Figure 2. In situ seismic test layout, proposed building X-340-4 location

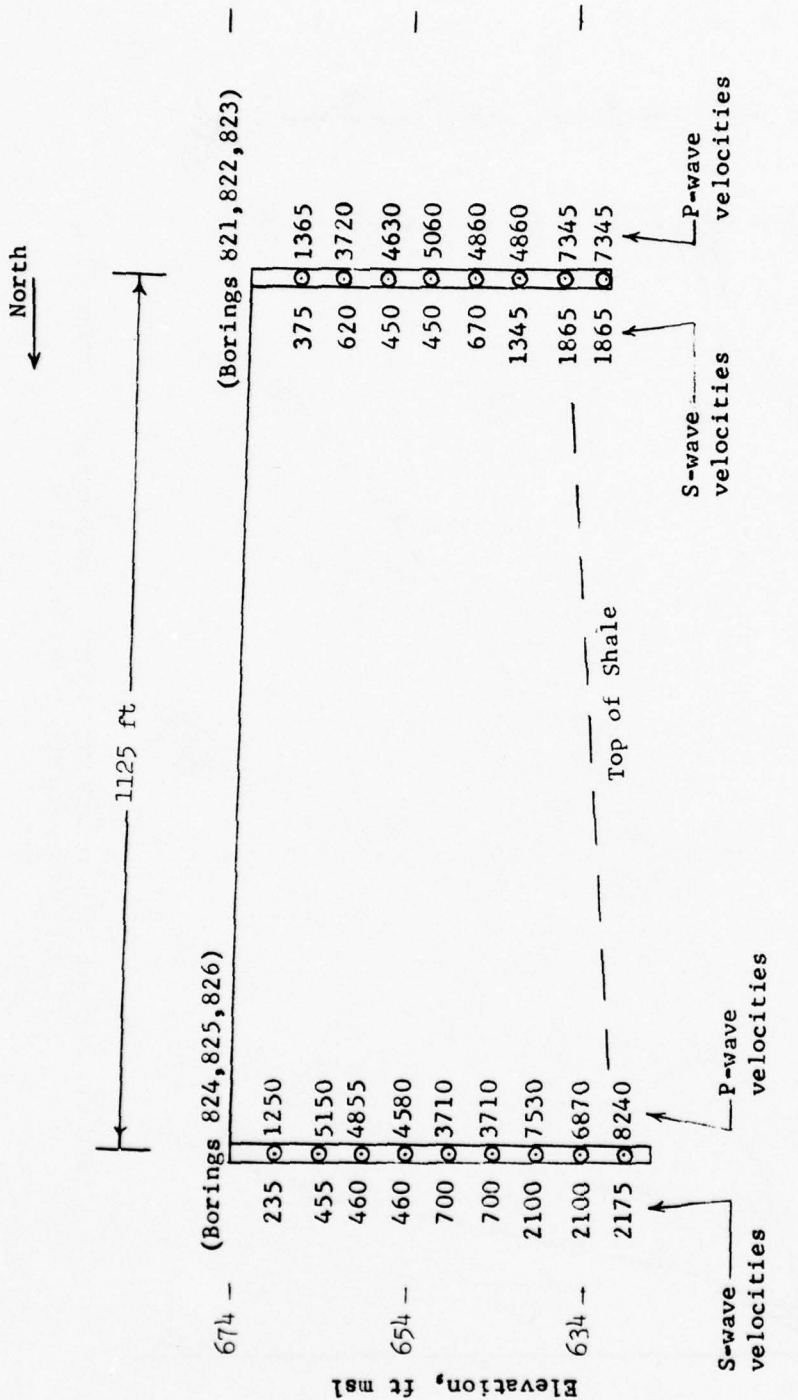


Figure 3. P- and S-wave velocities determined from crosshole tests, proposed building X-340-4 location

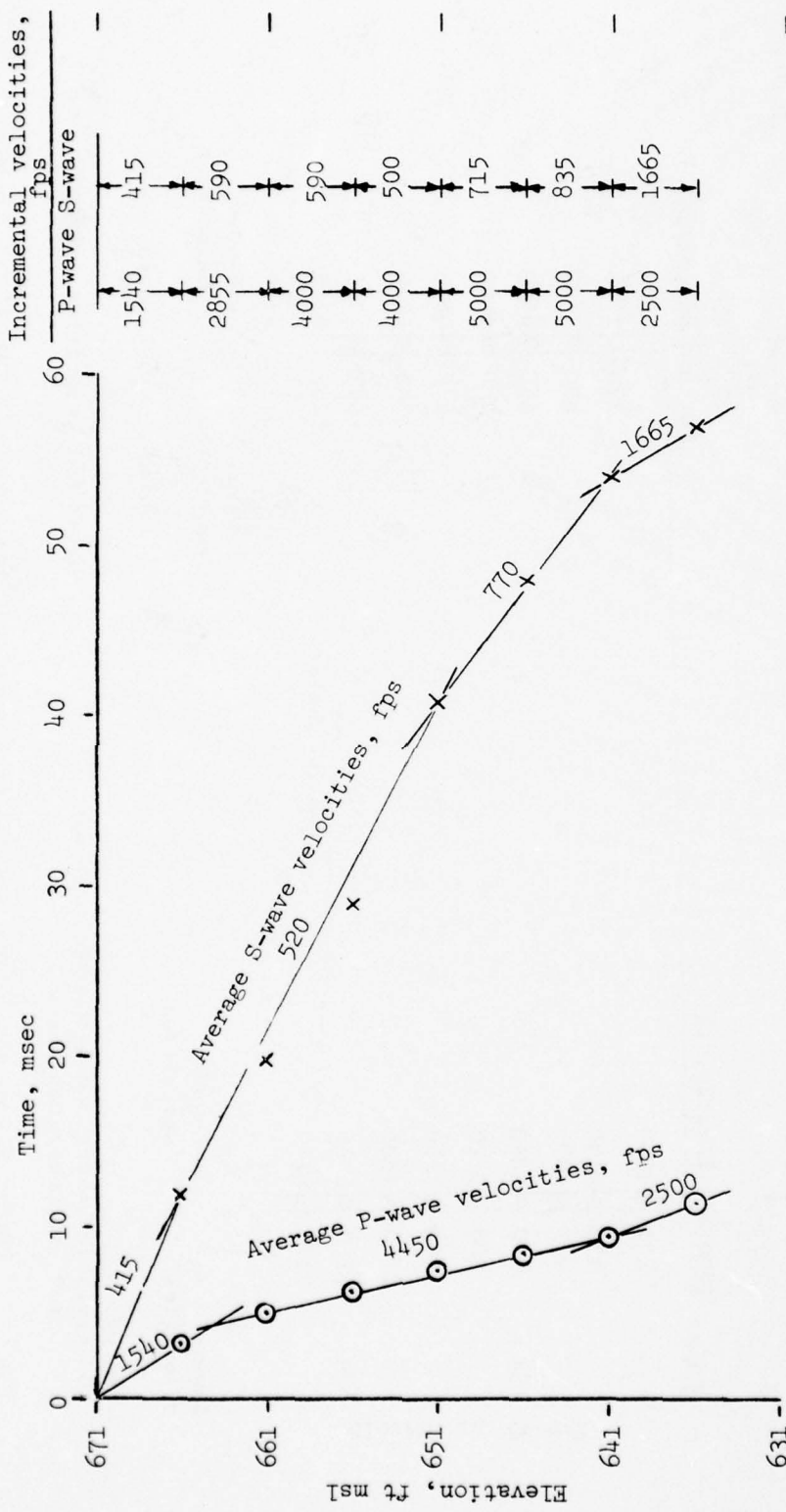


Figure 4. Arrival time versus depth from downhole test, boring 821, proposed building X-340-4 location

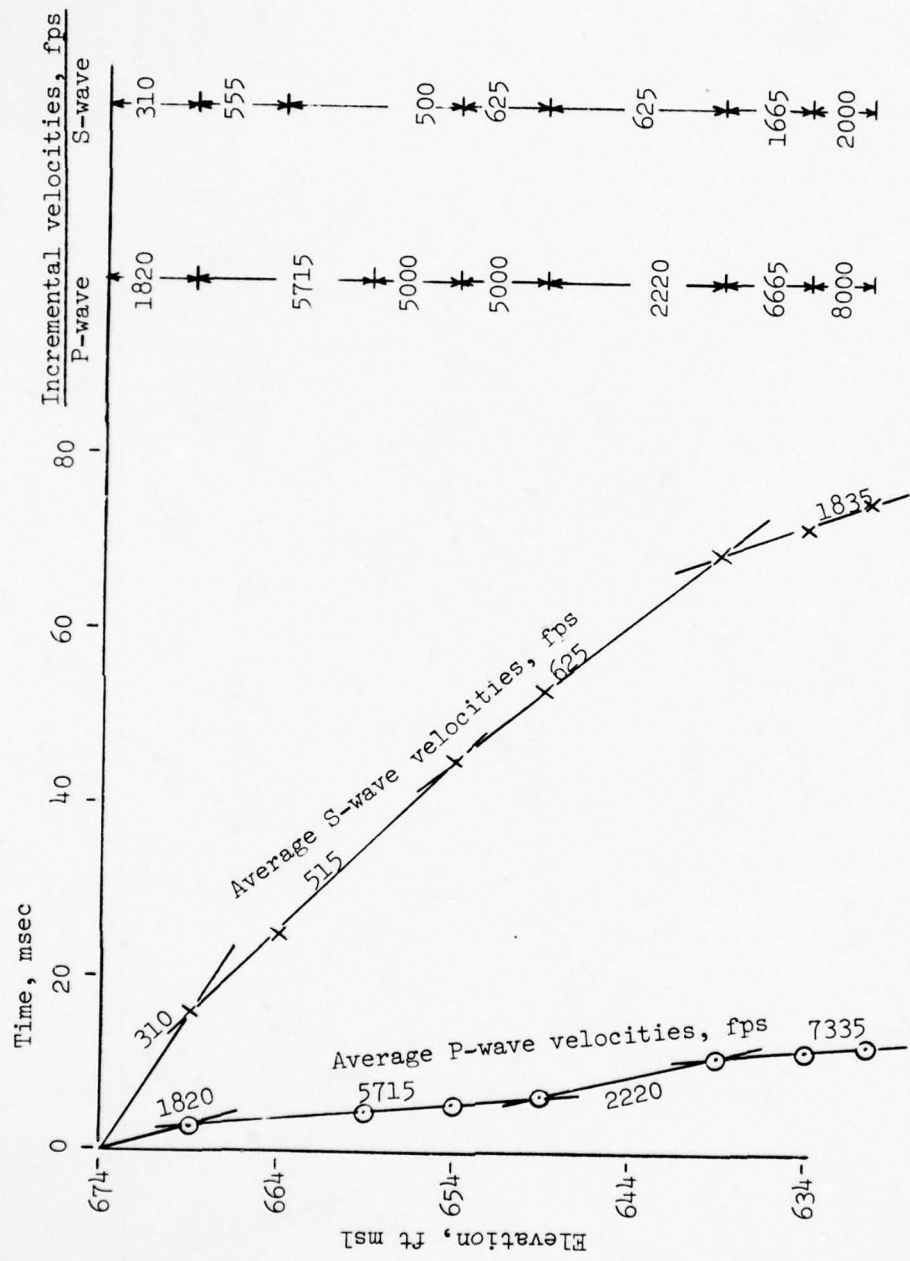


Figure 5. Arrival time versus depth from downhole test, boring 824,
proposed building X-340-4 location

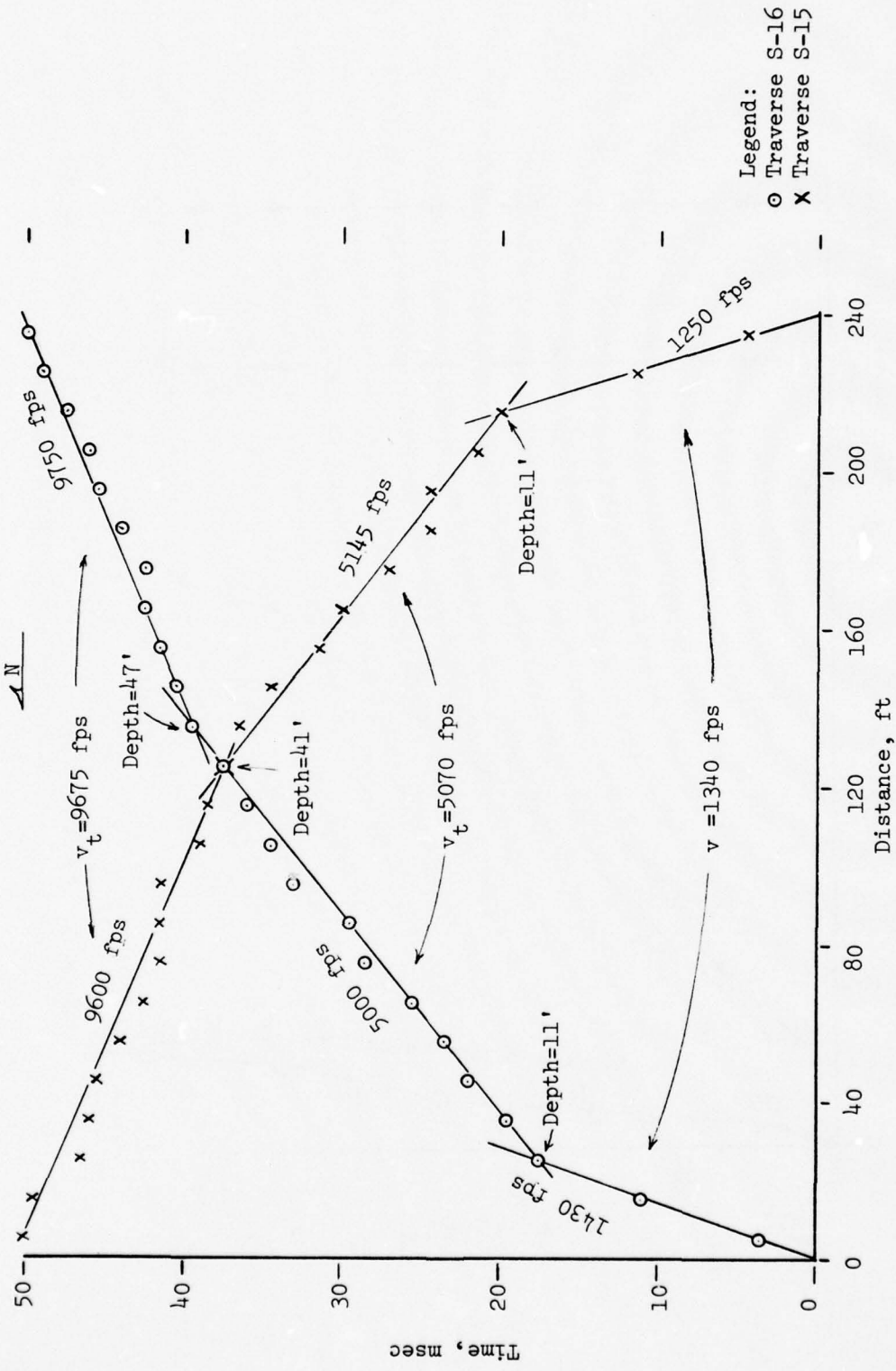


Figure 6. P-wave arrival time versus distance, proposed building X-340-4 location, S-15 and S-16

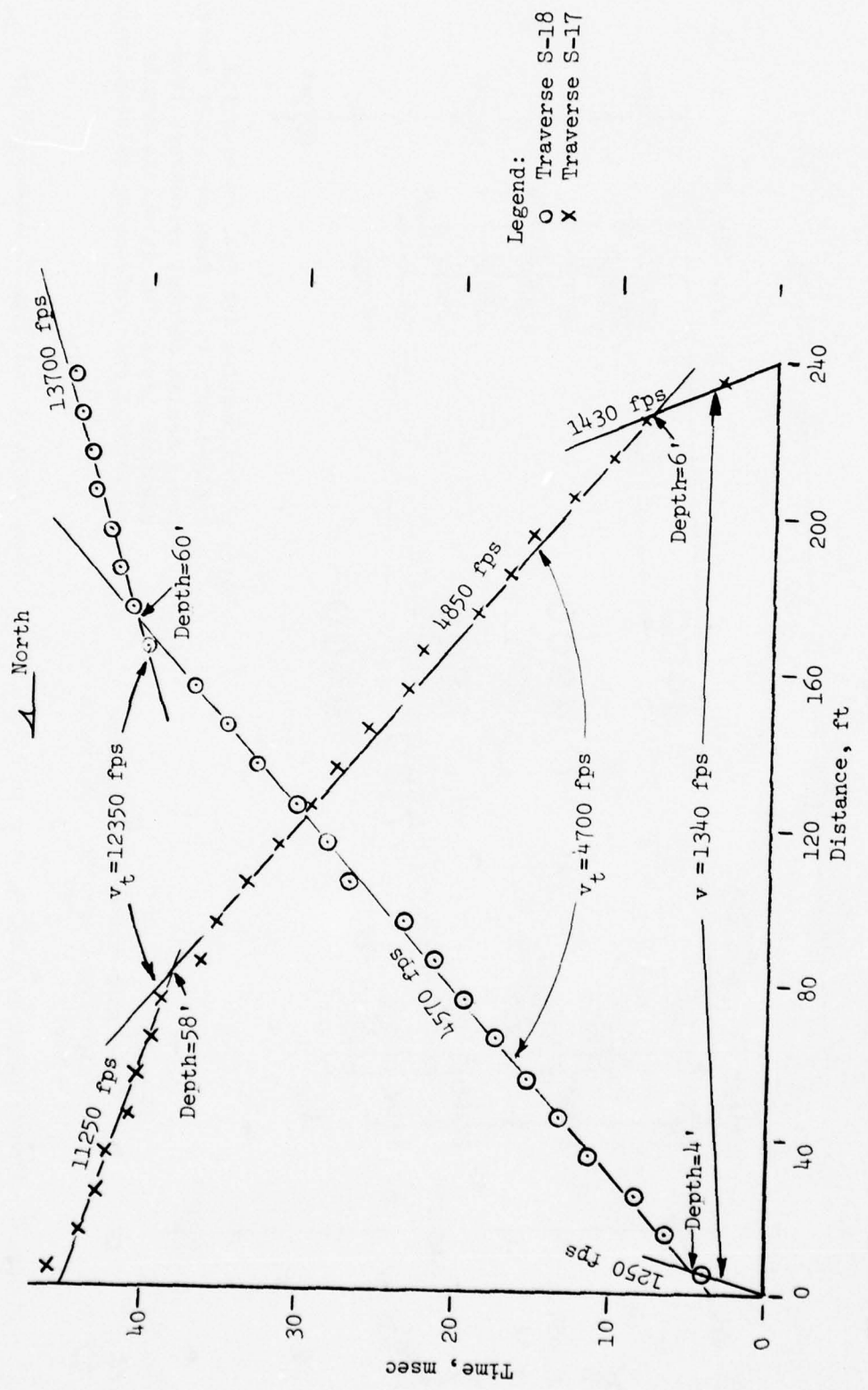


Figure 7. P-wave arrival time versus distance, proposed building X-340-4 location, S-17 and S-18

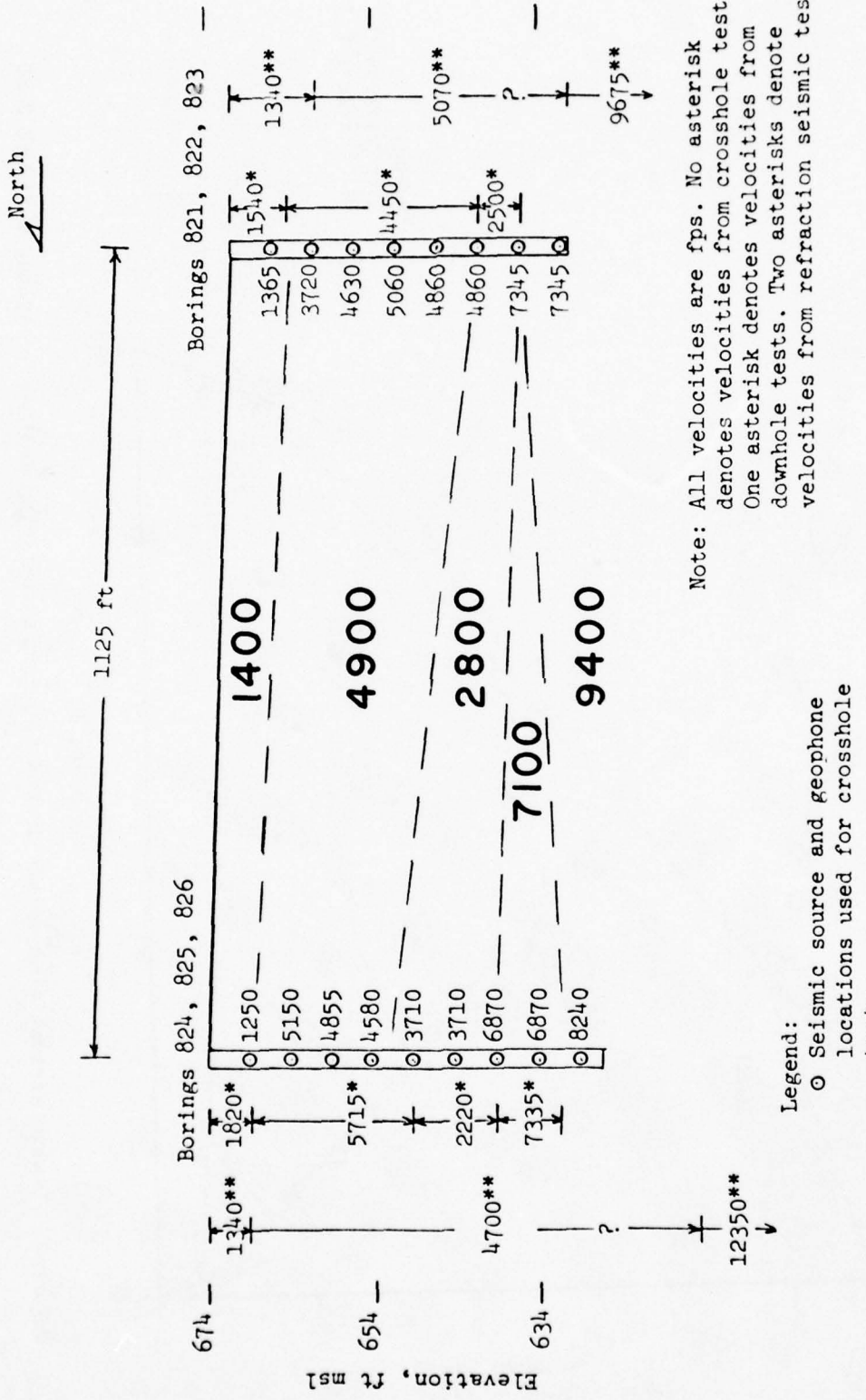


Figure 8. P-wave velocity profile from in situ seismic tests, proposed building X-340-4 location

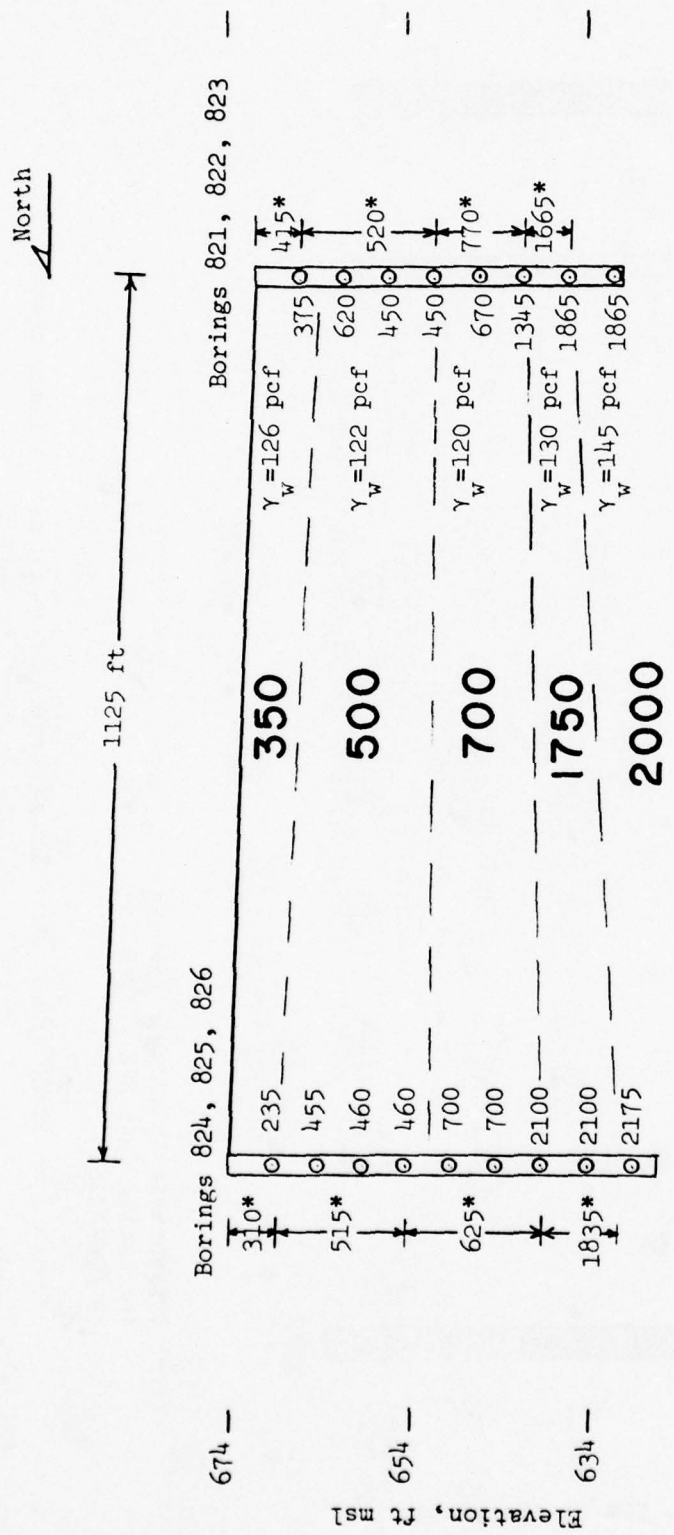
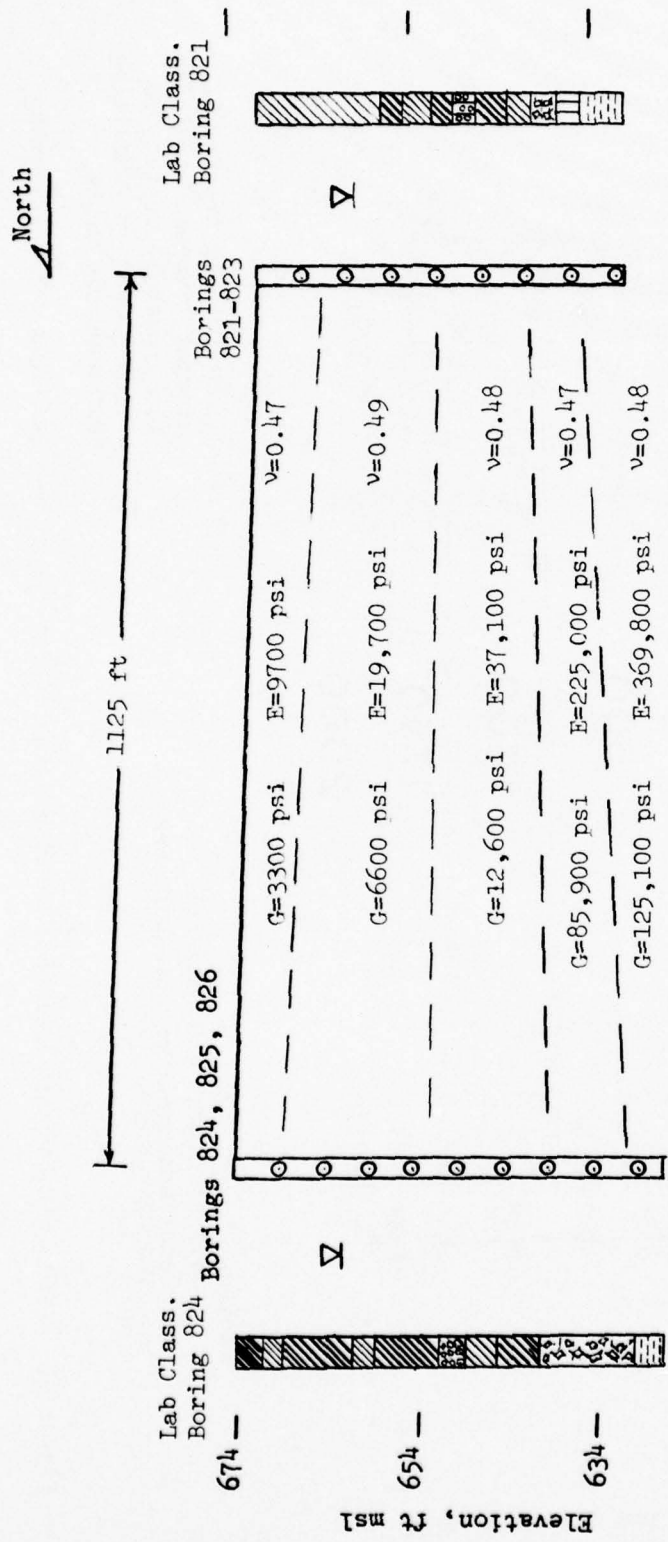


Figure 9. S-wave velocity profile from in situ seismic tests, proposed building X-340-4 location



Note: Explanation of graphic symbols
for boring data are presented
in Figure A1.

Figure 10. Shear and Young's moduli profile from in situ seismic tests,
proposed building X-340-4 location

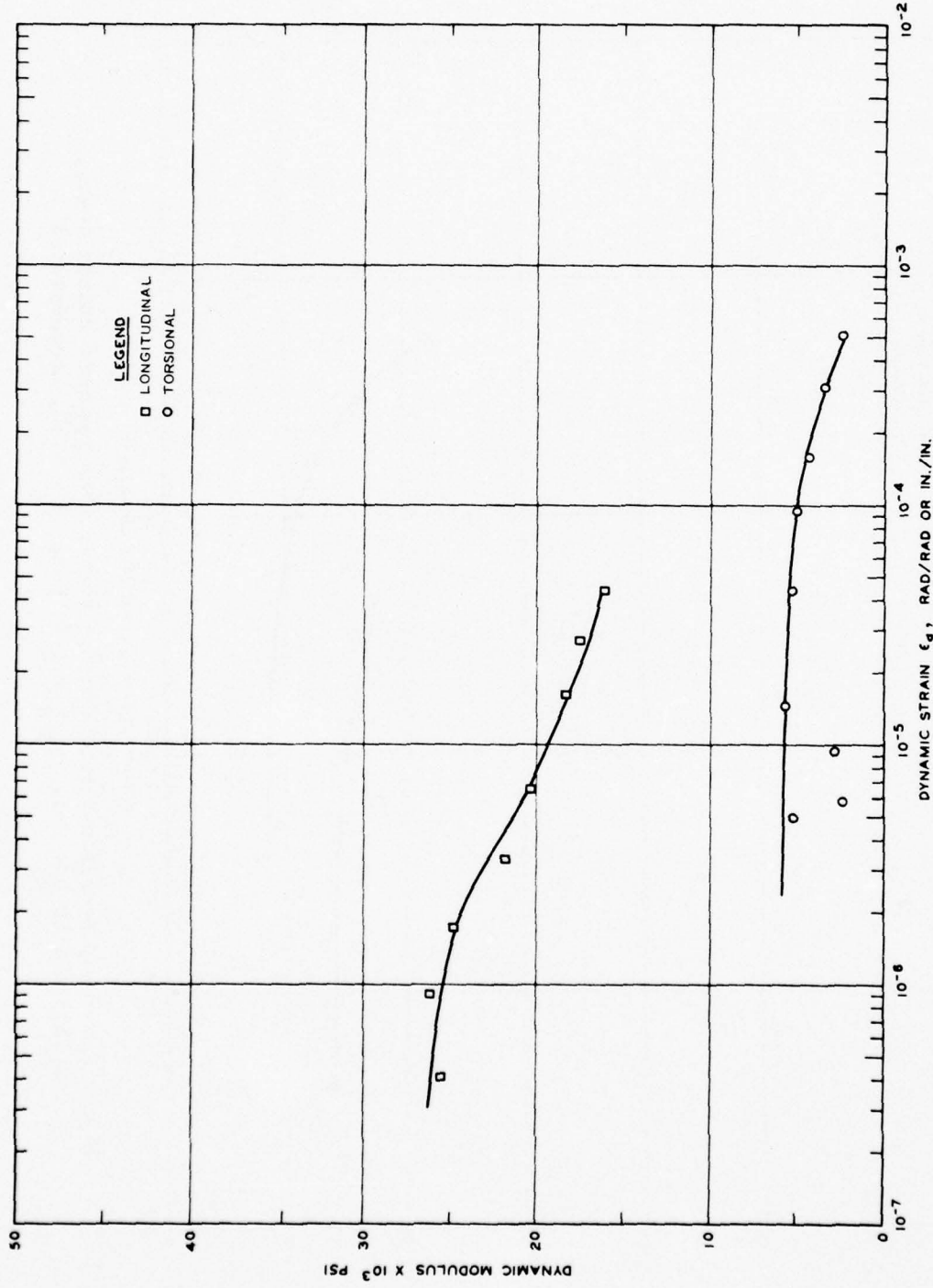


Figure 11. Dynamic modulus versus dynamic strain from resonant column tests, sample: 821 UD No. 2-1, $\bar{\sigma}_{oct} = 1.75$ psi, $B = 0.18$, nonsaturated

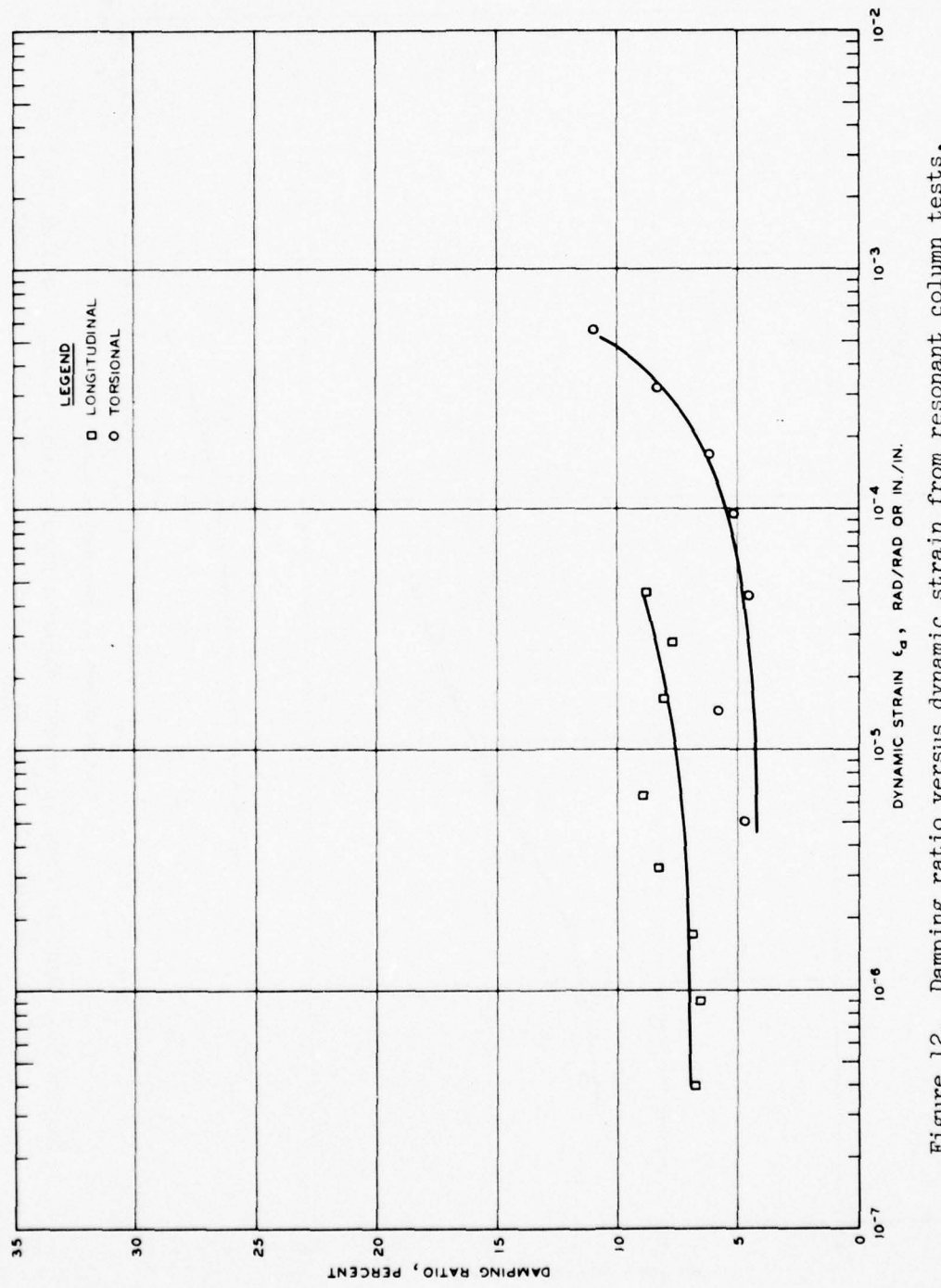


Figure 12. Damping ratio versus dynamic strain from resonant column tests,
sample: 821 UD No. 2-1, $\bar{\sigma}_{oct} = 1.75$ psi, $B = 0.18$, nonsaturated

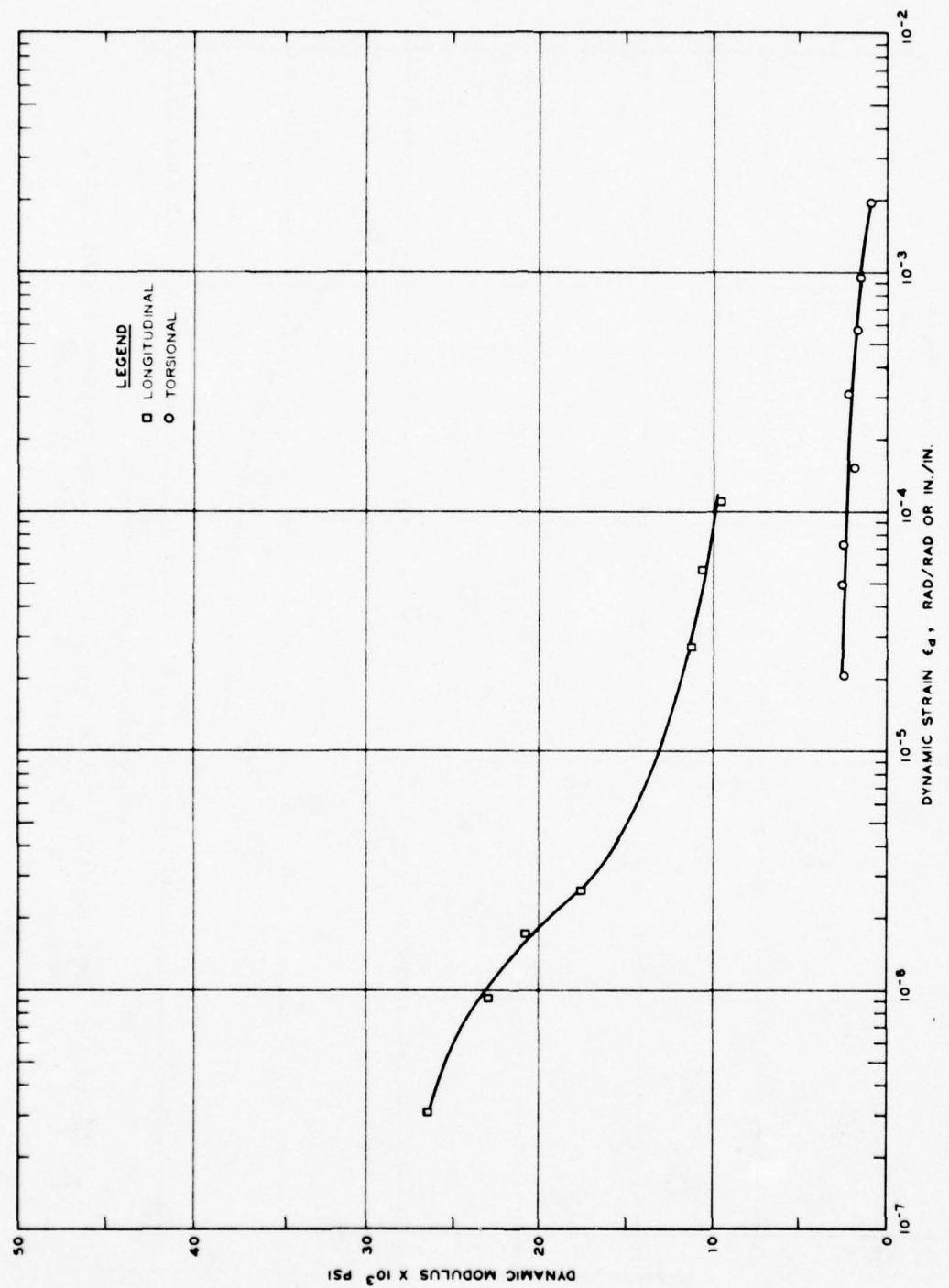


Figure 13. Dynamic modulus versus dynamic strain from resonant column tests,
sample: 821 UD No. 9-1, $\bar{\sigma}_{oct} = 6$ psi, $B = 0.68$

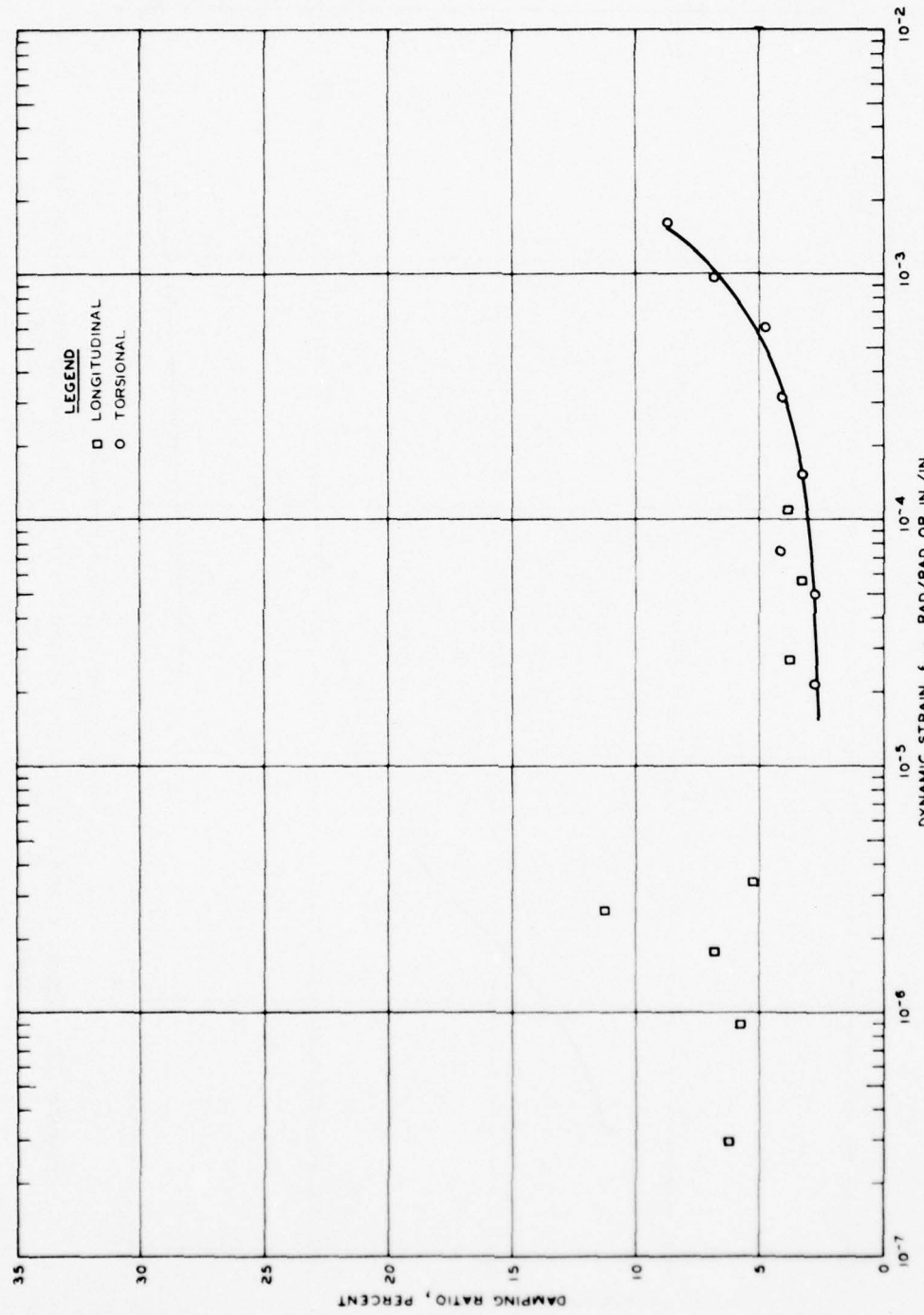


Figure 14. Damping ratio versus dynamic strain from resonant column tests,
sample: 821 UD No. 9-1, $\bar{\sigma}_{oct} = 6$ psi, $B = 0.68$

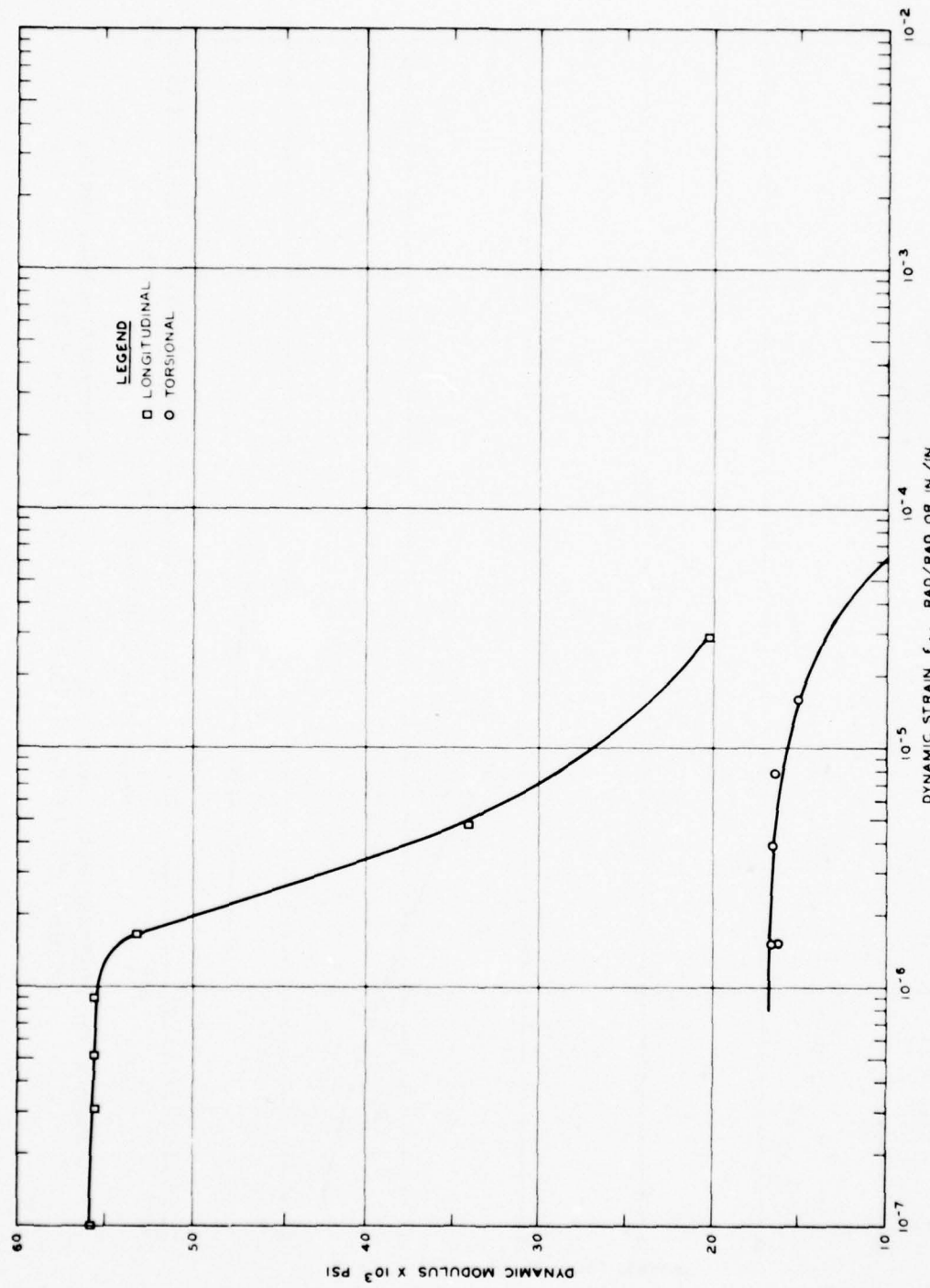


Figure 15. Dynamic modulus versus dynamic strain from resonant column tests,
sample: 821 UD No. 11-1, $\bar{\sigma}_{oct} = 9.5$ psi, $B = 0.83$

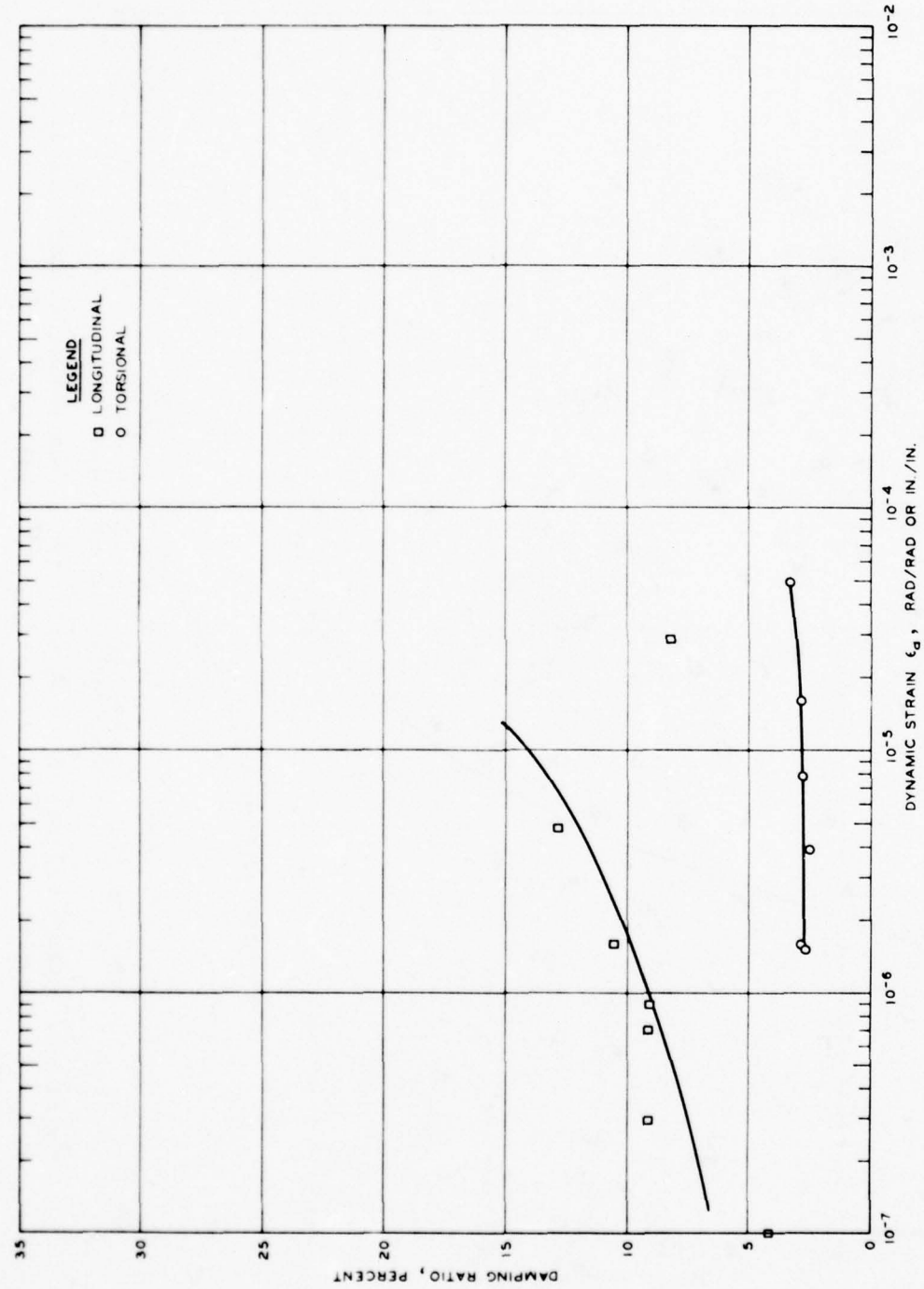


Figure 16. Damping ratio versus dynamic strain from resonant column tests,
sample: 821 UD No. 11-1, $\bar{\sigma}_{oct} = 9.5$ psi, $B = 0.83$

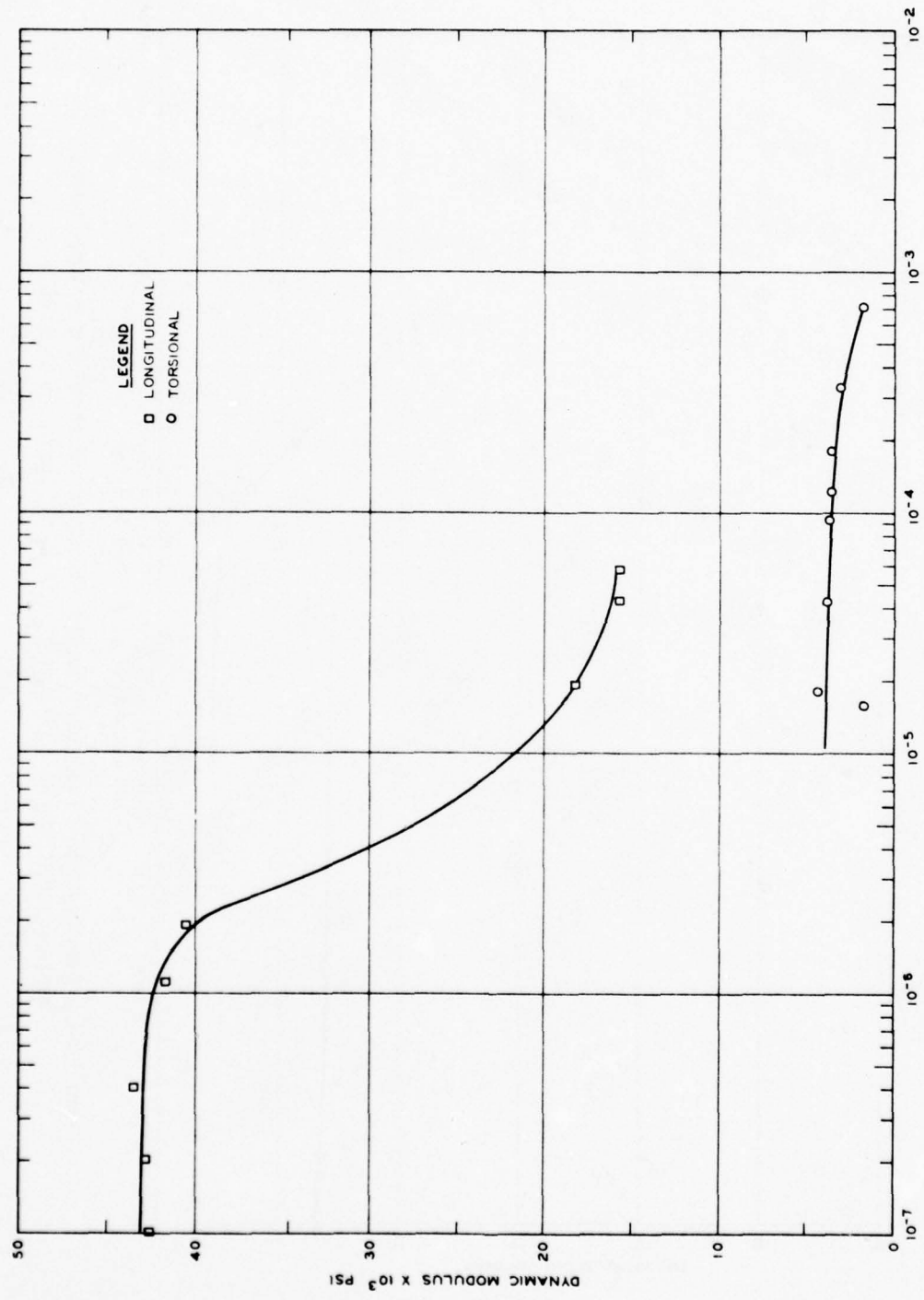


Figure 17. Dynamic modulus versus dynamic strain from resonant column tests,
sample: 821 UD No. 13-1, $\bar{\sigma}_{oct} = 10.75$ psi, $B = 0.91$

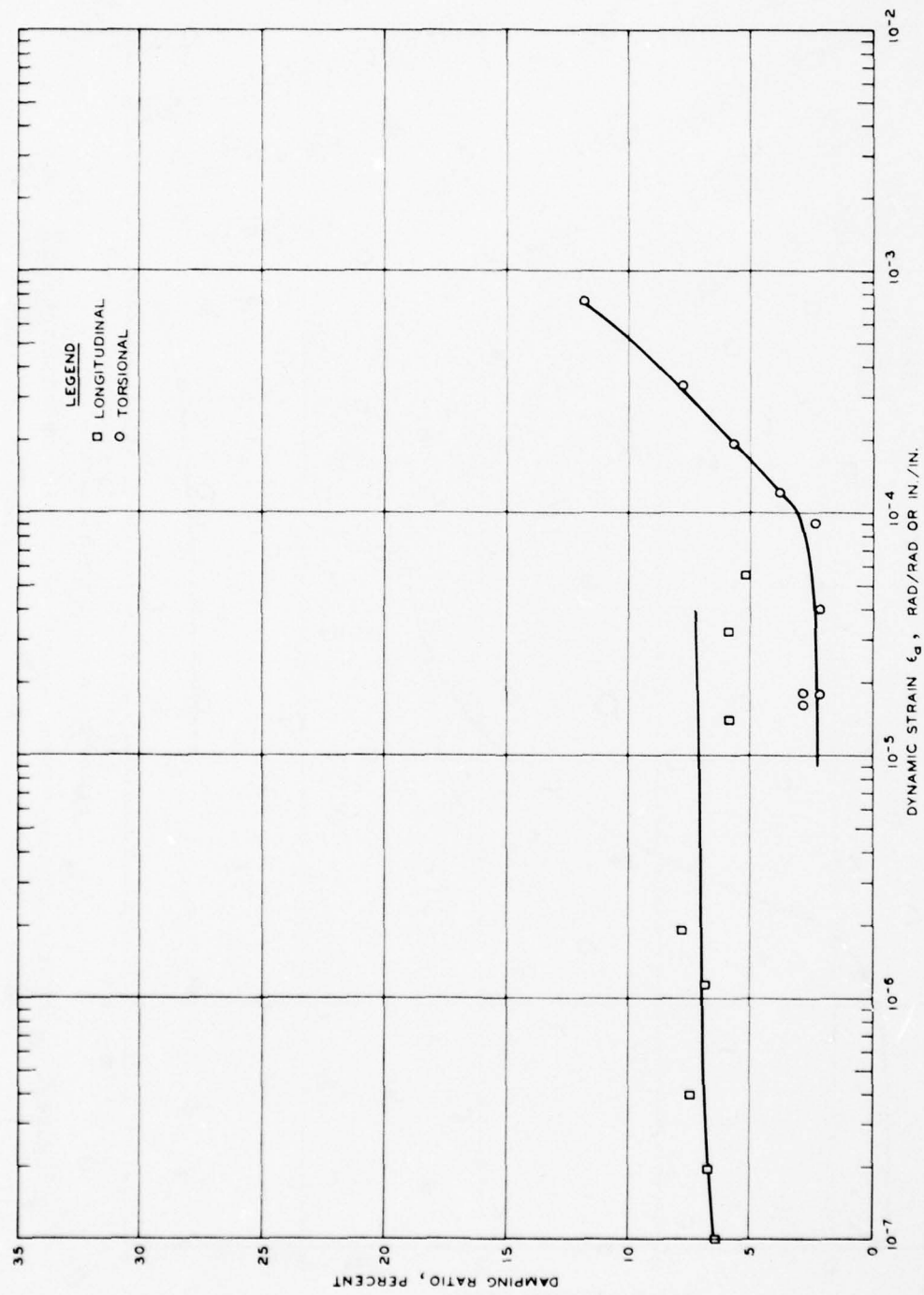


Figure 18. Damping ratio versus dynamic strain from resonant column tests,
sample: 821 UD No. 13-1, $\bar{\sigma}_{Oct} = 10.75$ psi, $B = 0.91$

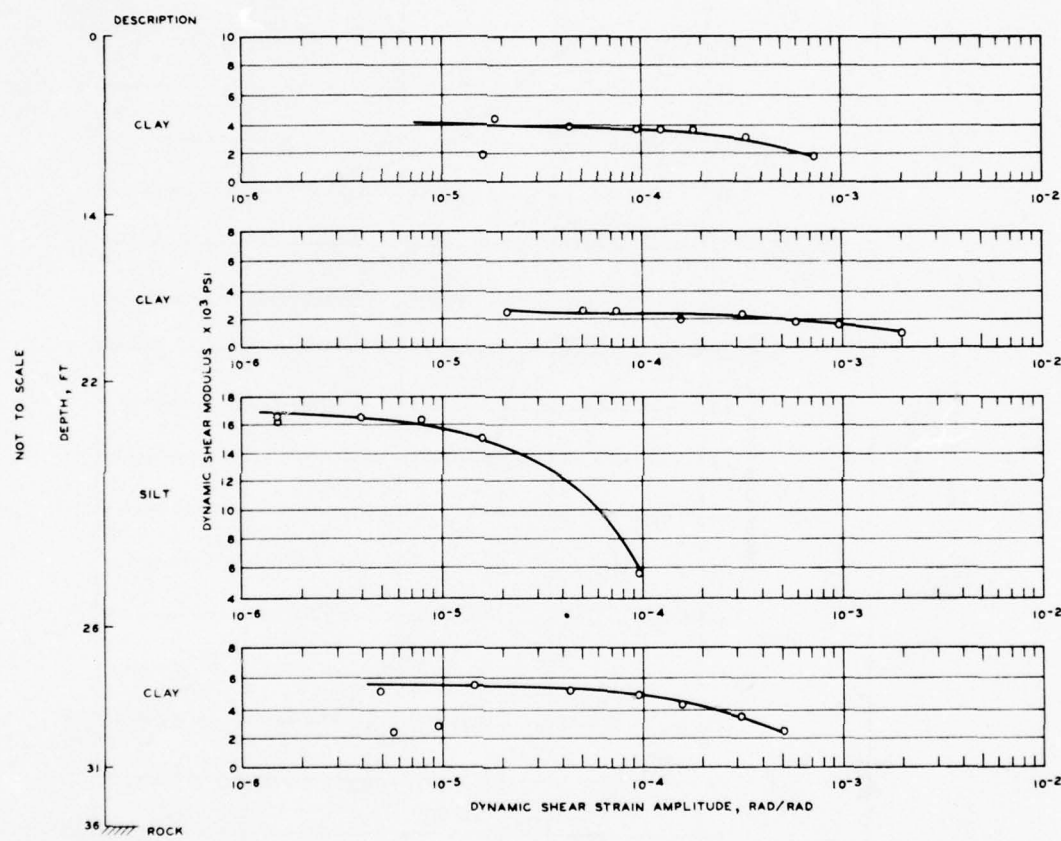


Figure 19. Dynamic shear modulus versus dynamic shear strain amplitude from resonant column tests, boring 821 UD

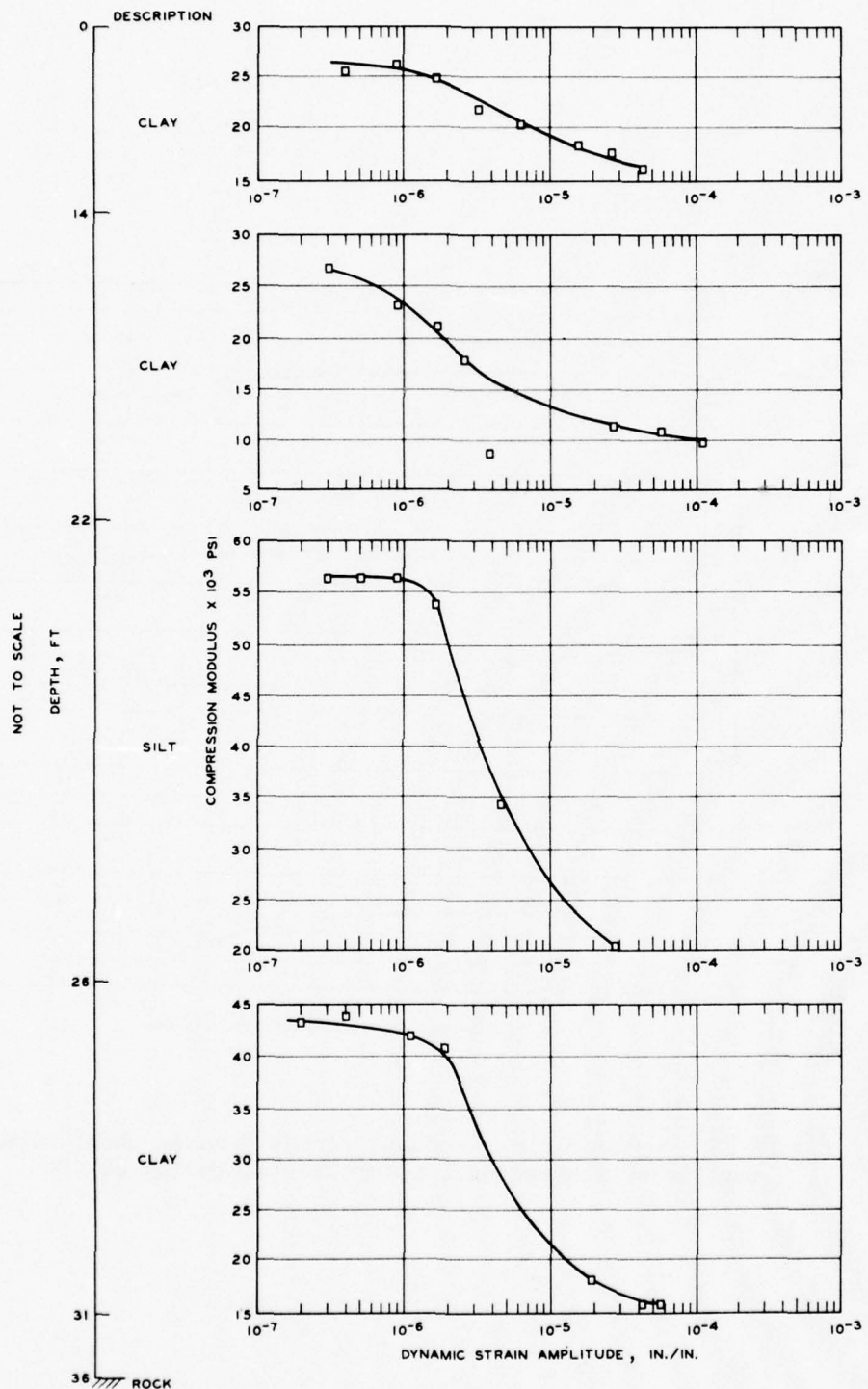


Figure 20. Dynamic compression modulus versus dynamic strain amplitude from resonant column tests, boring 821 UD

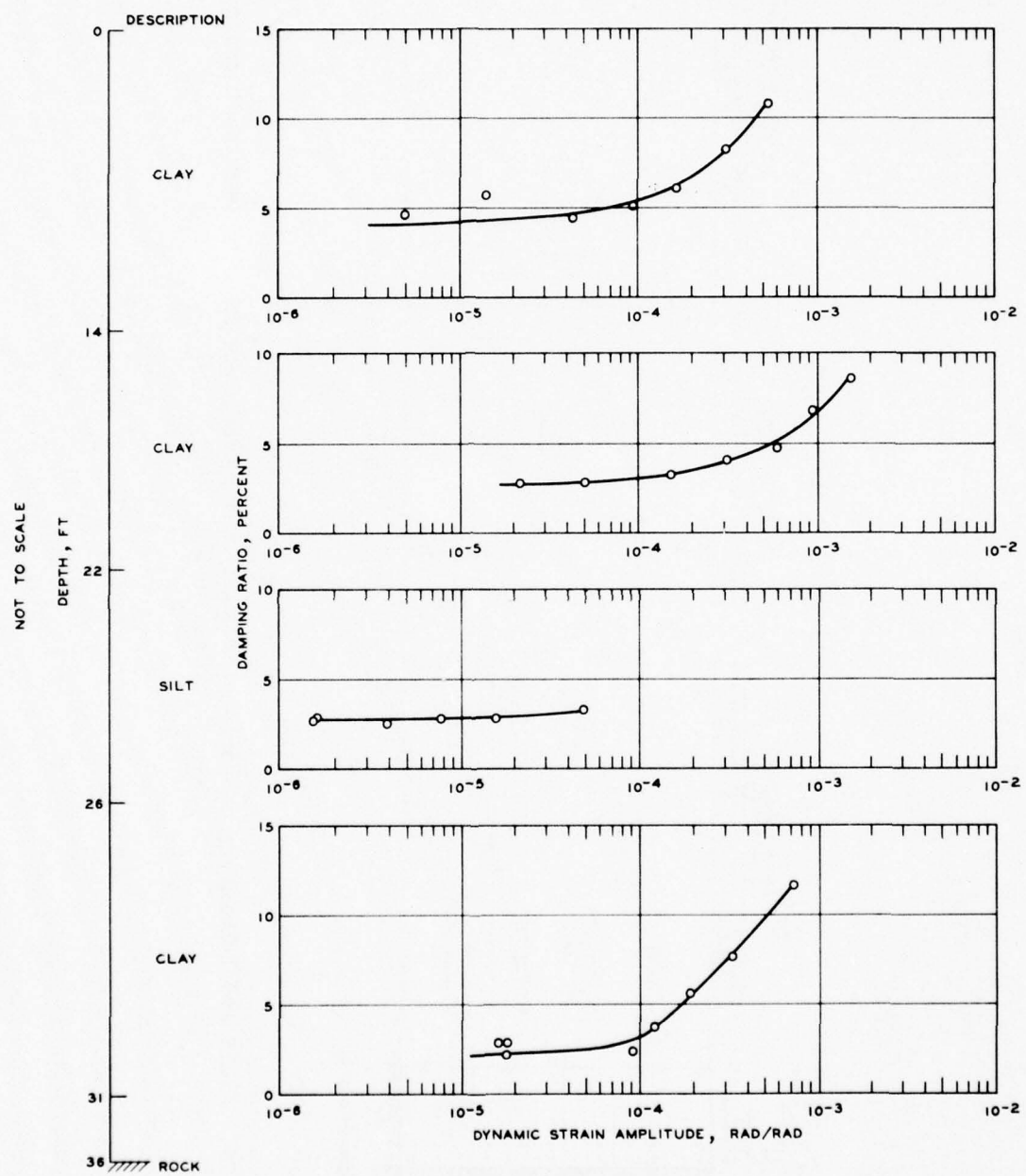


Figure 21. Damping ratio versus dynamic strain amplitude from resonant column tests, boring 821 UD

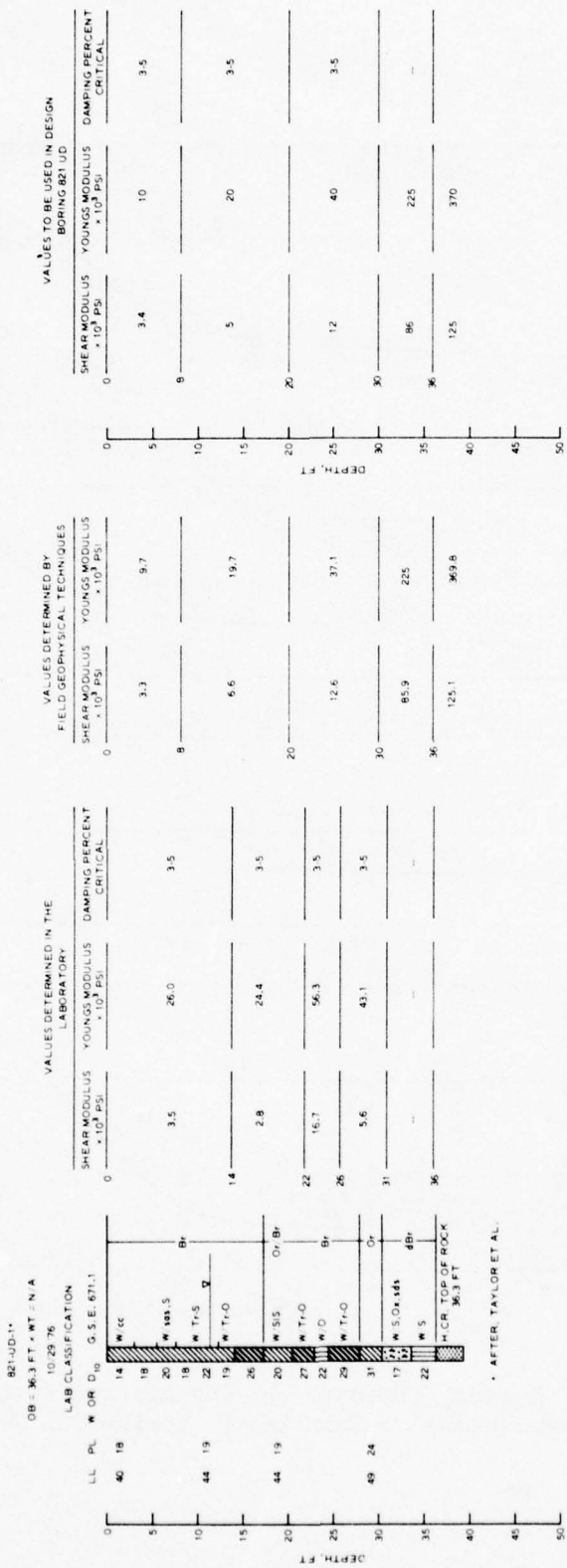


Figure 22. Field and laboratory comparison of shear and Young's moduli with resultant design values for boring 821 UD-1

APPENDIX A: TEST RESULTS AND DATA INTERPRETATION
FROM IN SITU SEISMIC TESTS

UNIFIED SOIL CLASSIFICATION

MAJOR DIVISION	TYPE	LETTER SYMBOL	TYPICAL NAMES
CARBO - GRAINED SOILS	GRAVELS	GW	Well graded gravels, gravel-sand mixtures, little or no fines
	CLEAN GRAVEL (Little or No Fines)	GP	Poorly graded gravels, gravel-sand mixtures, little or no fines
	GRAVEL WITH FINES (Irreducible Amount of Fines)	GM	Silty gravels, poorly graded gravel-sand-silt mixtures
	GRAVEL WITH FINES (Irreducible Amount of Fines)	GC	Clayey gravels, poorly graded gravel-sand-clay mixtures
	CLEAN SAND (Little or No Fines)	SW	Well graded sands, gravelly sands, little or no fines
	SANDS WITH FINES (Irreducible Amount of Fines)	SP	Poorly graded sands, gravelly sands, little or no fines
	SANDS WITH FINES (Irreducible Amount of Fines)	SM	Silty sands, poorly graded sand-silt mixtures
	SANDS WITH FINES (Irreducible Amount of Fines)	SC	Clayey sands, poorly graded sand-clay mixtures
FINE - GRAINED SOILS	SILTS AND CLAYS (Liquid Limit < 30)	ML	Inorganic silts and very fine sands, mock flour, silty or clayey fine sands with slight plasticity
	SILTS AND CLAYS (Liquid Limit > 30)	CL	Inorganic clays of low to medium plasticity, gravelly clays, sandy clays, silty clays, lean clays
		OL	Organic silts and organic silt-clays of low plasticity
		MH	Inorganic silts, micaceous or diatomaceous fine sandy or silty soils, elastic silts
		CH	Inorganic clays of high plasticity, fat clays
	HIGHLY ORGANIC SOILS	OH	Organic clays of medium to high plasticity
	WOOD	P†	Peat and other highly organic soils
	NO SAMPLE	Wd	WOOD

ROCK CLASSIFICATION

CON	CONGLOMERATE
SAN	SANDSTONE
SIL	SILTSTONE
CLA	INDURATED CLAY OR CLAYSTONE
COM	COMPACTED SHALE

Figure A1. Unified Soil and Rock Classification System used for boring data.

Figures A2-A8, Test Loop Location, X-77⁴

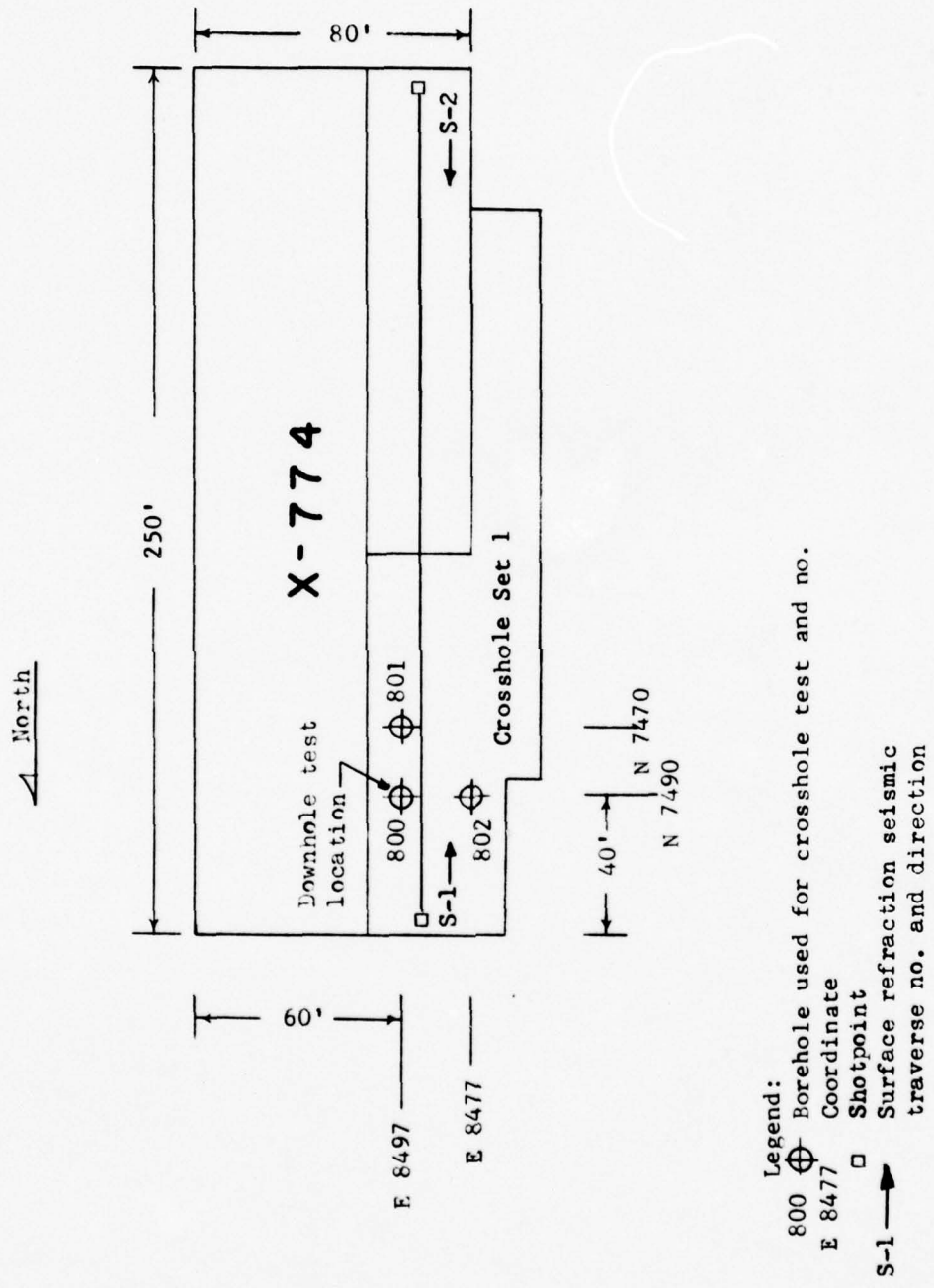
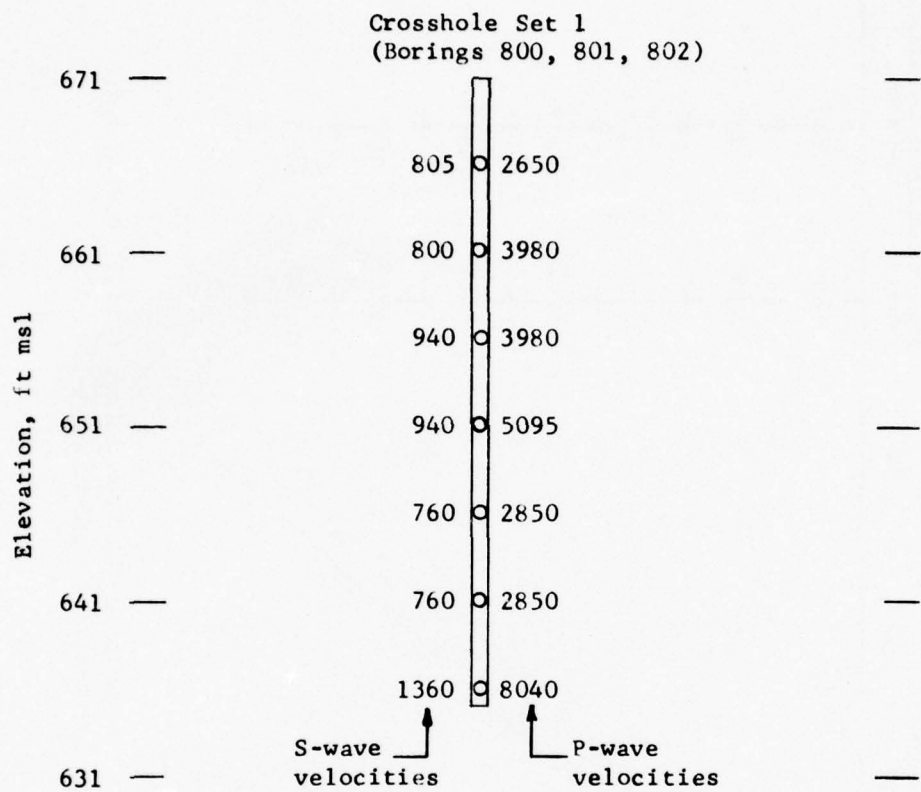


Figure A2. In situ seismic layout, proposed test loop location, X-774



Legend:

- Seismic source and geophone locations used for crosshole tests

Note: All velocities are fps.

Figure A3. P- and S-wave velocities determined from crosshole test, proposed test loop location X-774, hole set 1

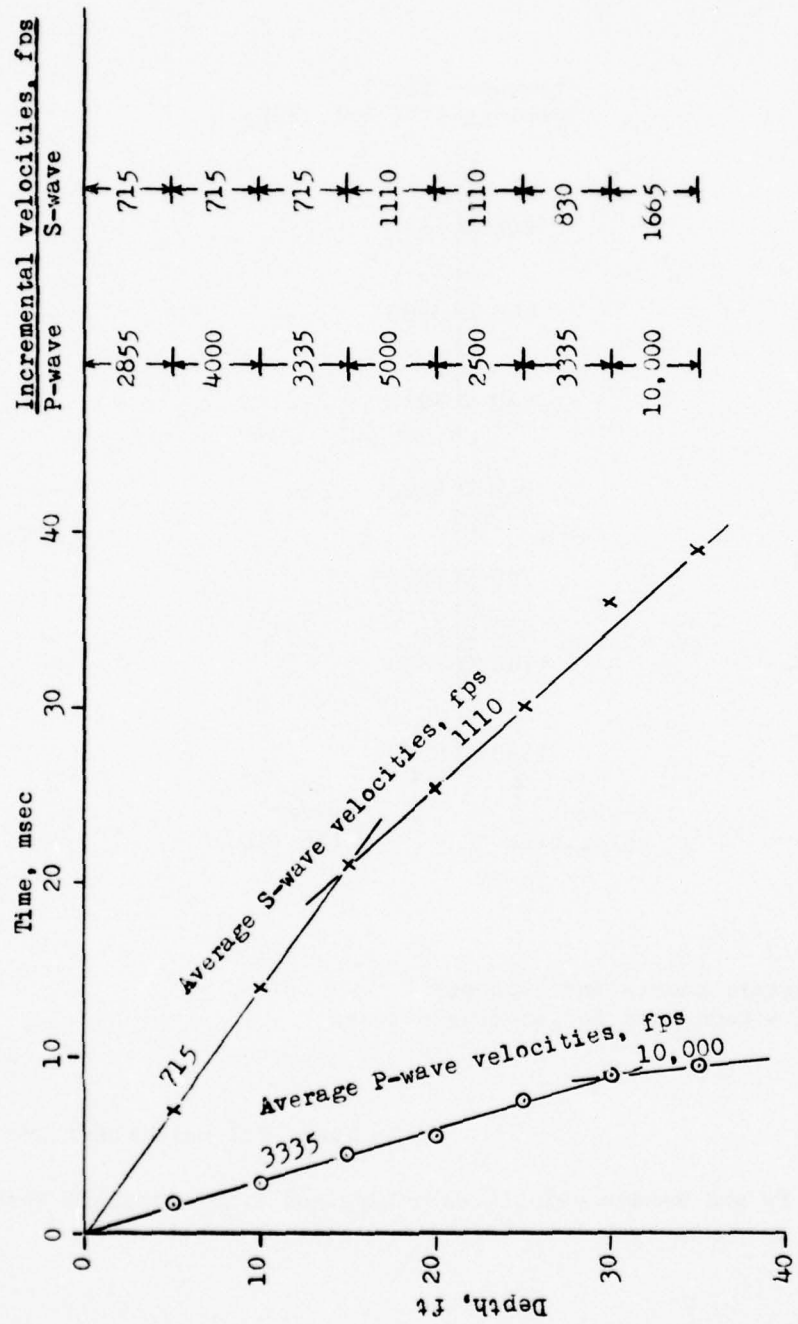


Figure A4. Arrival time versus depth from downhole test, boring 800,
proposed test loop location, X-774

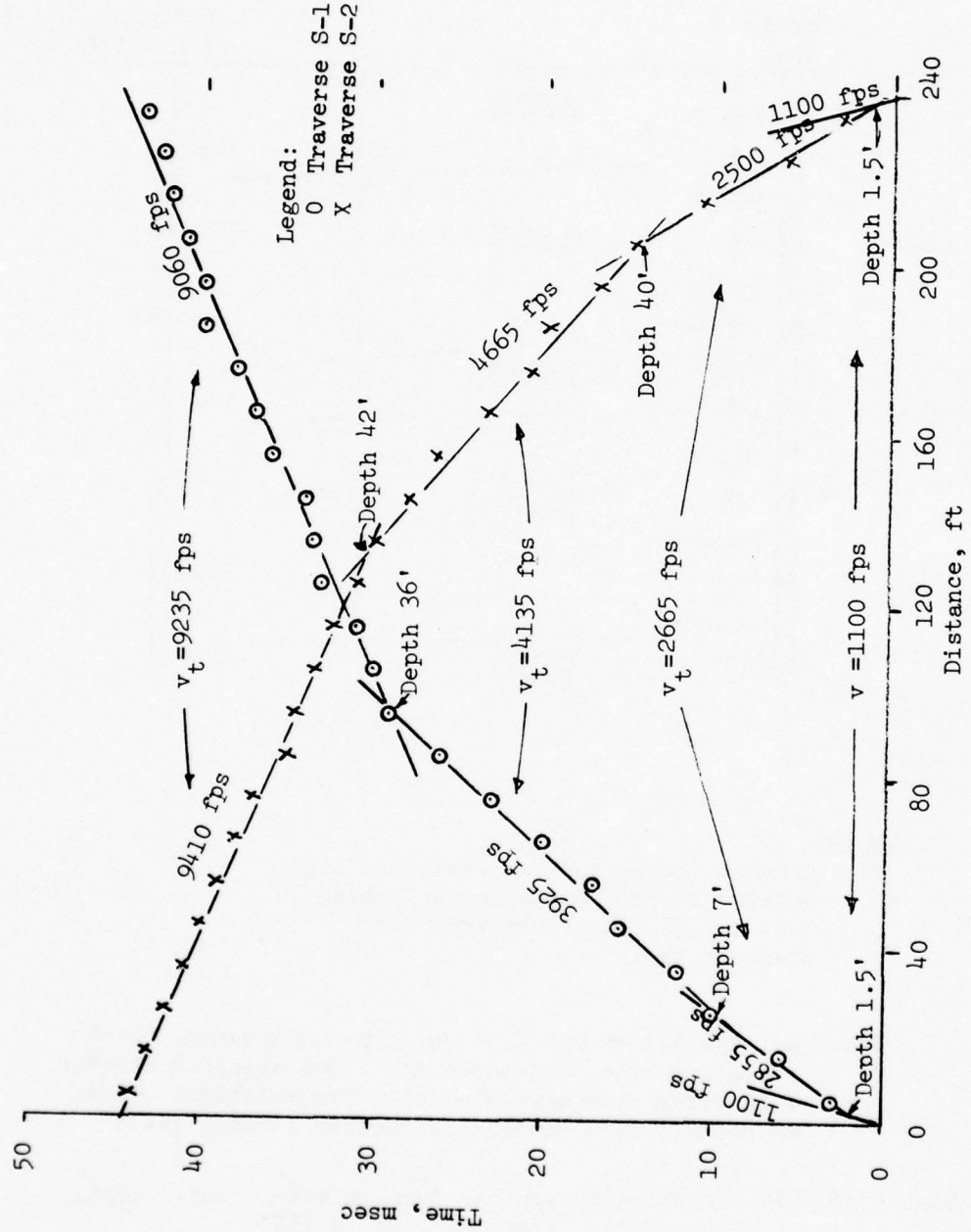
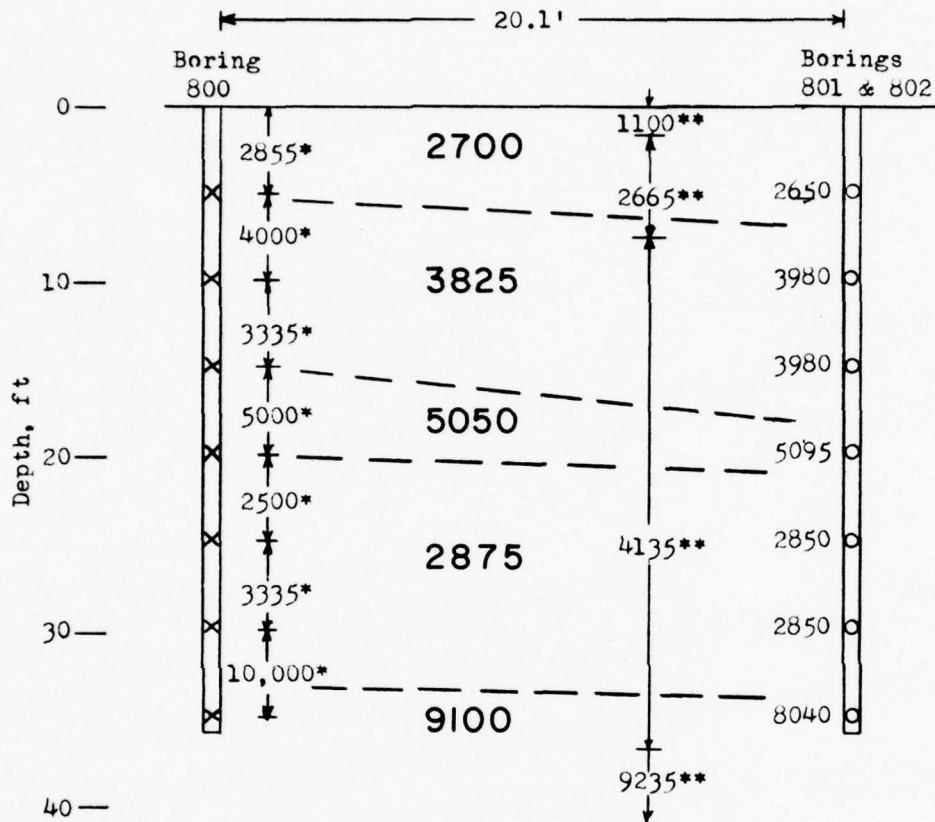


Figure A5. P-wave arrival time versus distance, proposed test loop location, X-774

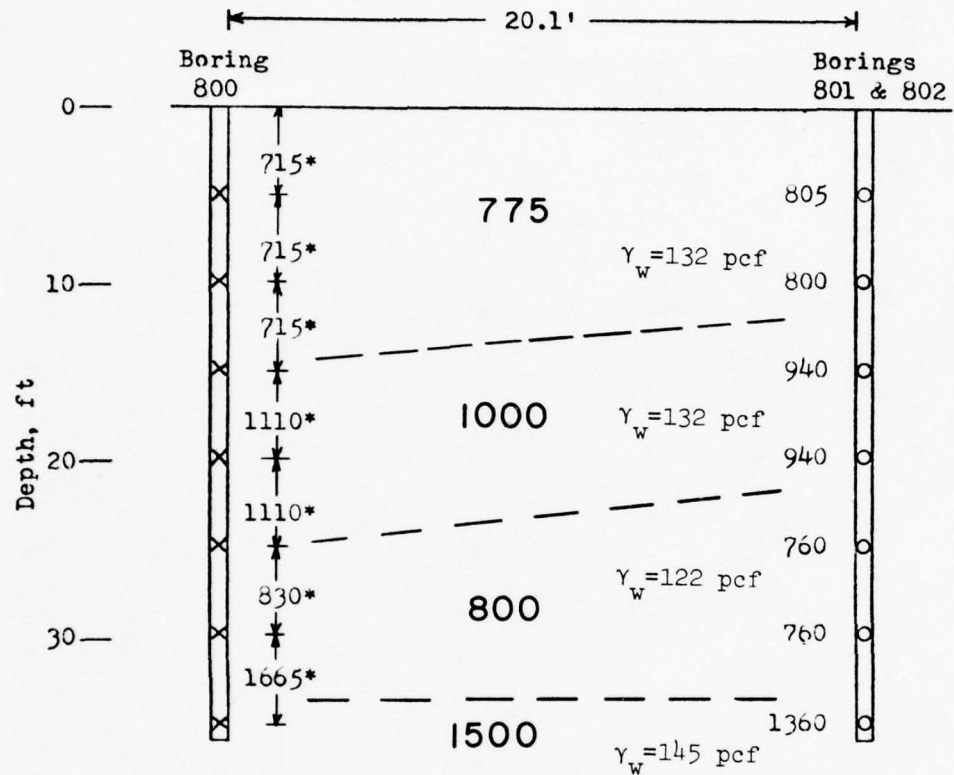


Legend:

- Geophone locations for crosshole test
- ✗ Seismic source locations for crosshole test and geophone locations for downhole test

Note: All velocities are fps. No asterisk denotes P-wave velocities from crosshole test. One asterisk denotes velocities from downhole test. Two asterisks denote velocities from surface refraction seismic test.

Figure A6. P-wave velocity profile from in situ seismic tests, proposed test loop location, X-774

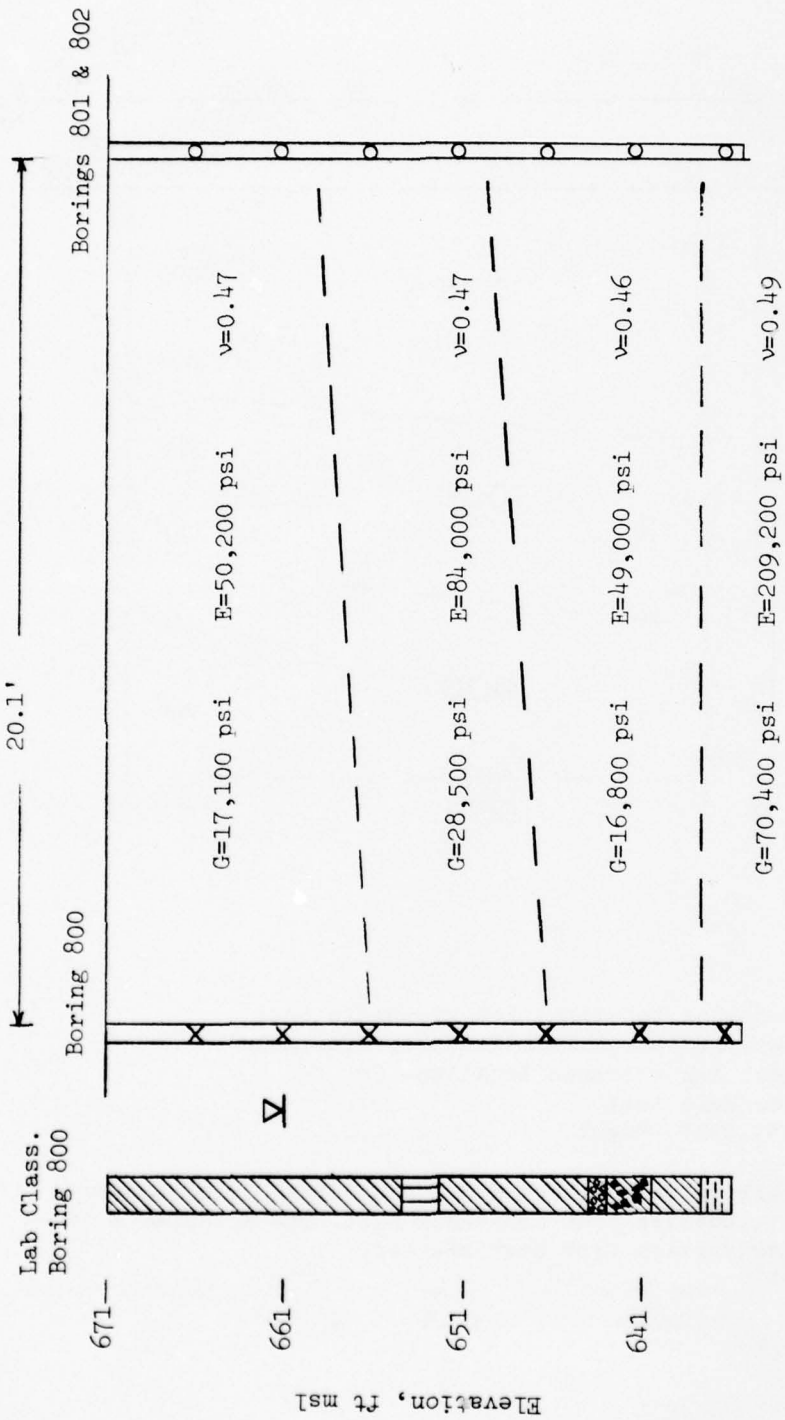


Legend:

- O Geophone locations for crosshole test
 X Seismic source locations for crosshole test and geophone locations for downhole test
 Y_w Wet unit weight

Note: All velocities are fps. No asterisk denotes S-wave velocities from crosshole test. One asterisk denotes velocities from downhole test.

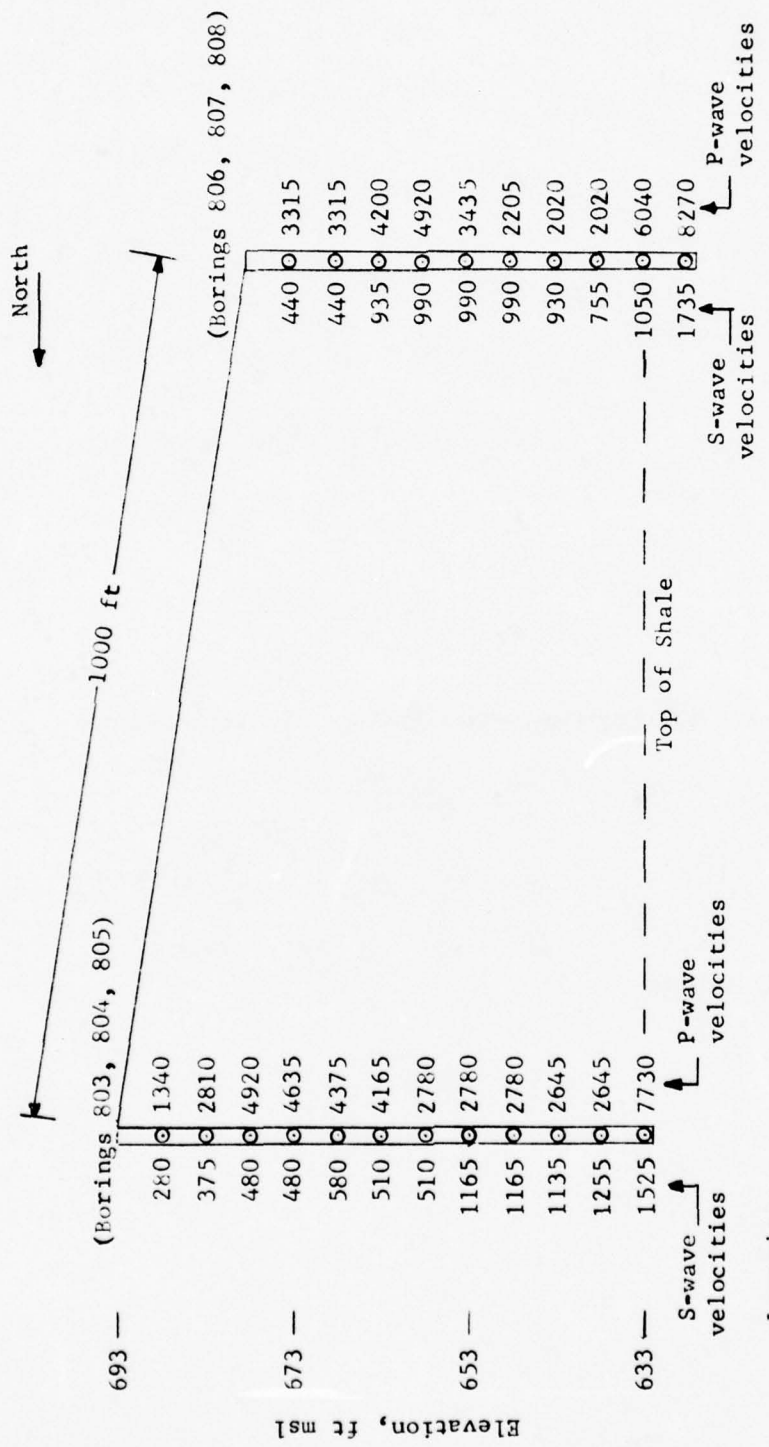
Figure A7. S-wave velocity profile from in situ seismic tests, proposed test loop location, X-774



Note: Explanation of graphic symbols for boring data are presented in Figure A1.

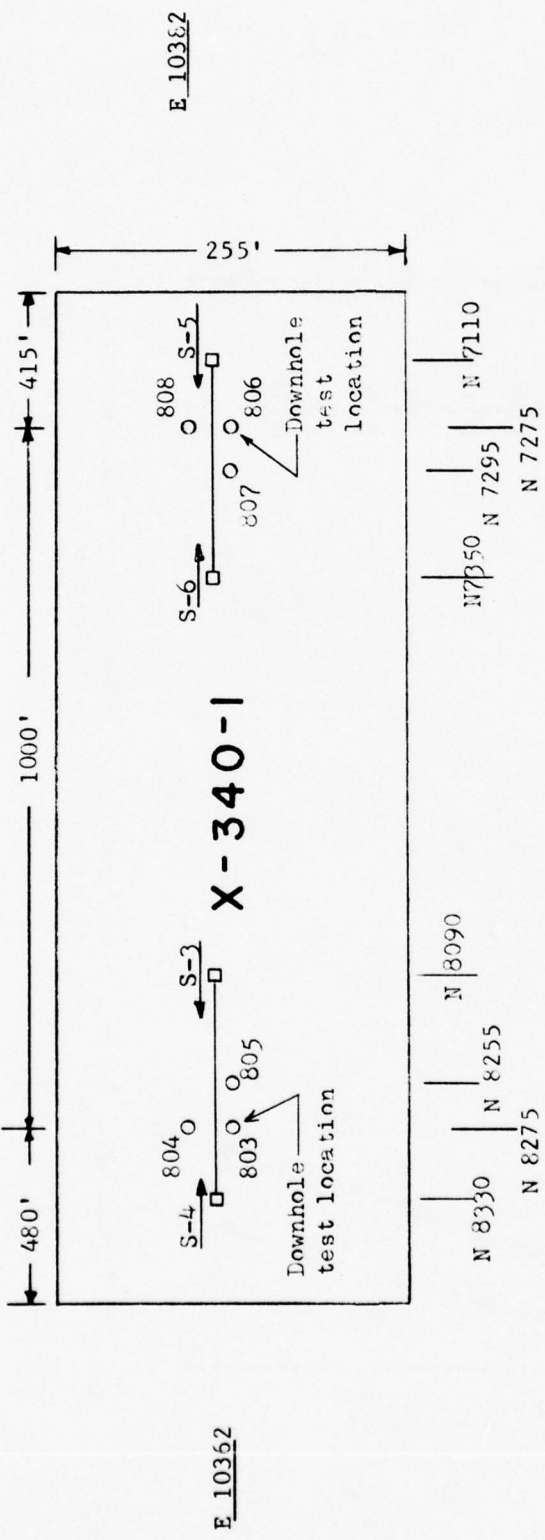
Figure A8. Shear and Young's moduli profile from in situ seismic tests, proposed test loop location, X-774

Figures A9-A17, Proposed Building X-340-1 Location



Legend:
 ○ Seismic source and geophone locations used for crosshole tests

Figure A9. In situ seismic test layout, proposed building X-340-1 location



Legend:

- 803 O** Borehole used for crosshole test and no.
- N 8275** Coordinate
- Shotpoint** □
- S-4** Surface refraction seismic traverse no. end direction
- E 10362**
- E 10382**
- 255'**
- 1000'**
- 480'**
- 415'**

Figure A10. P- and S-wave velocities determined from crosshole tests, proposed building X-340-1 location

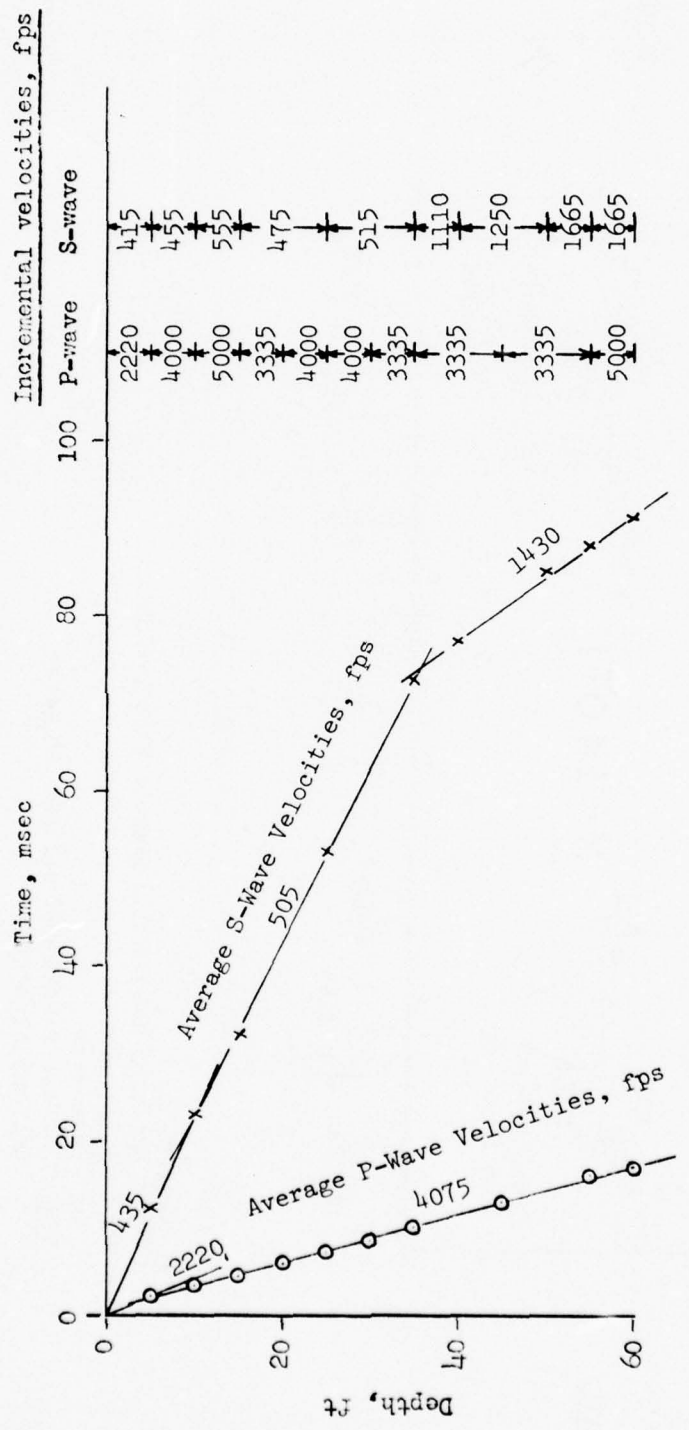


Figure All. Arrival time versus depth from downhole test, boring 803 proposed building X-340-1 location

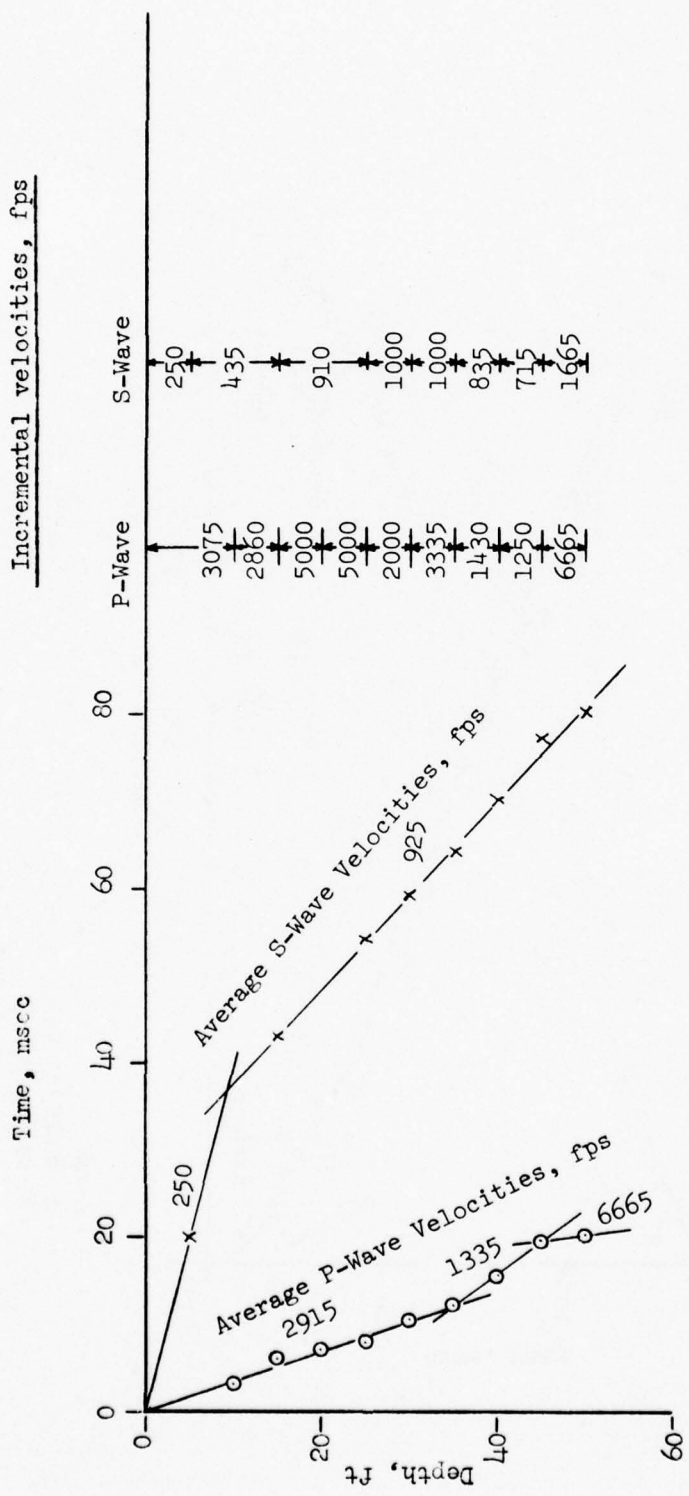


Figure A12. Arrival time versus depth from downhole test, boring 806, proposed building X-340-1 location

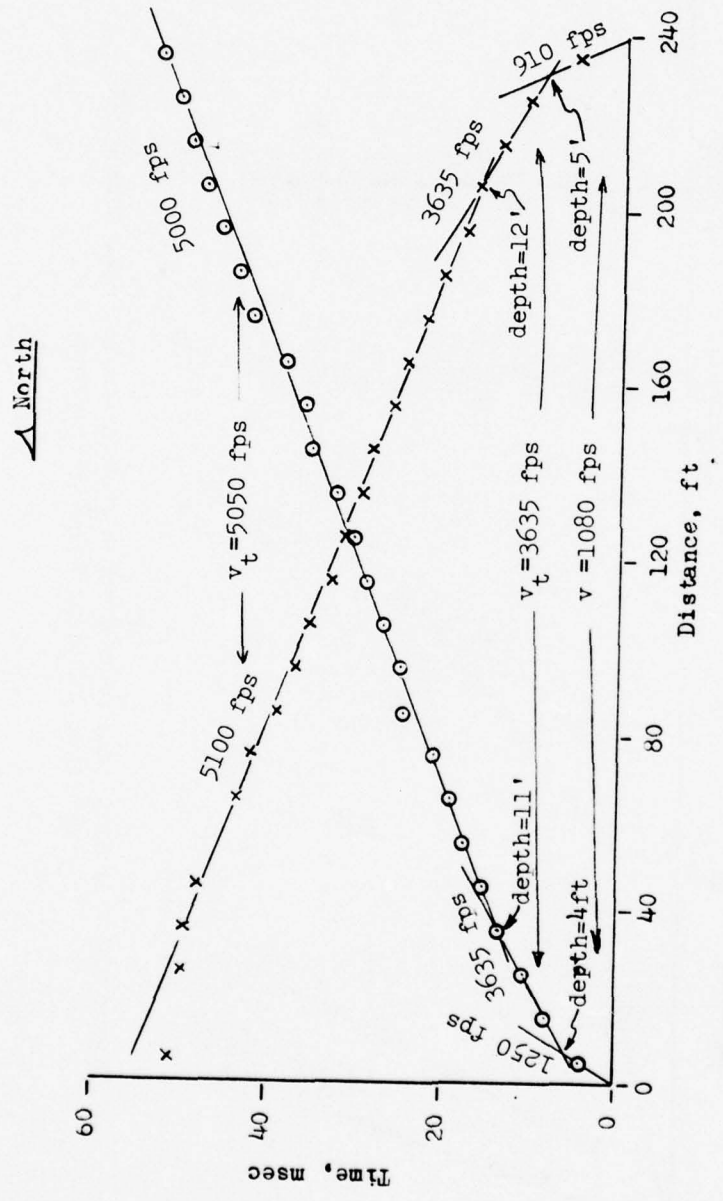


Figure A13. P-wave arrival time versus distance, proposed building X-340-1 location

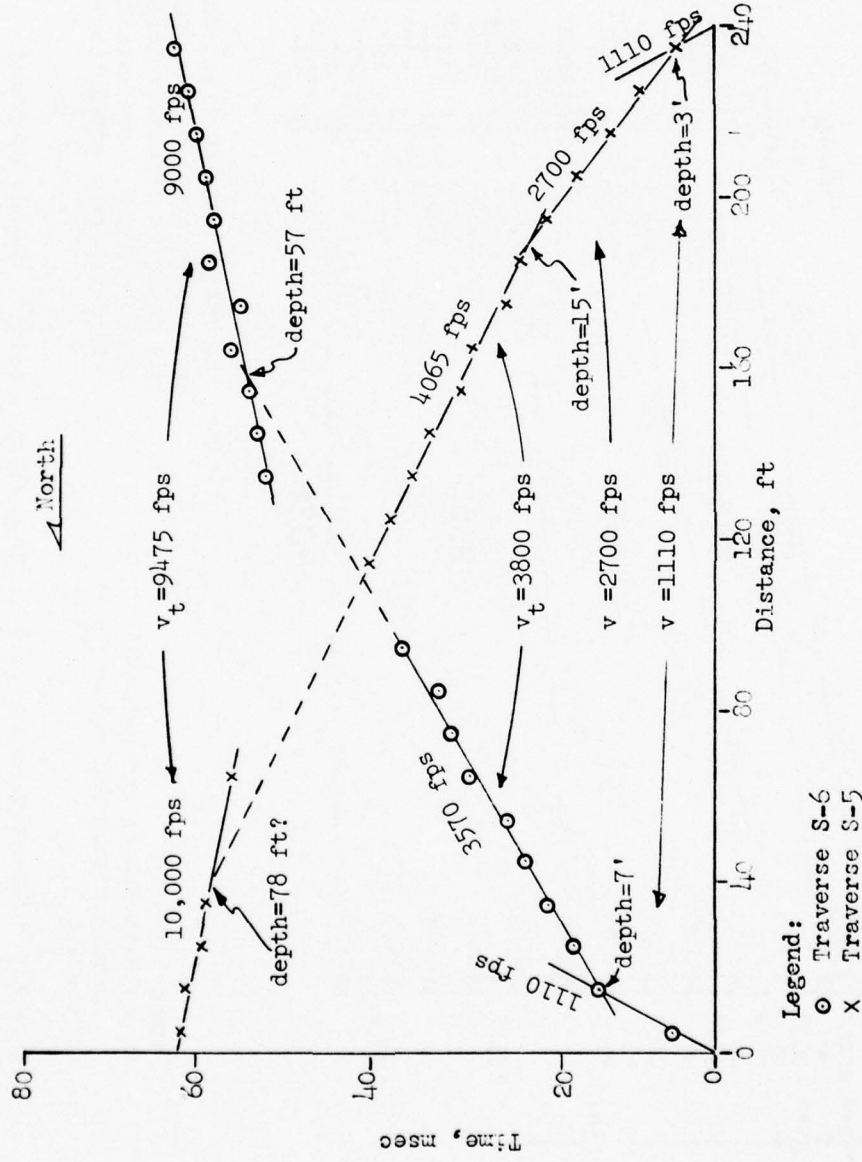
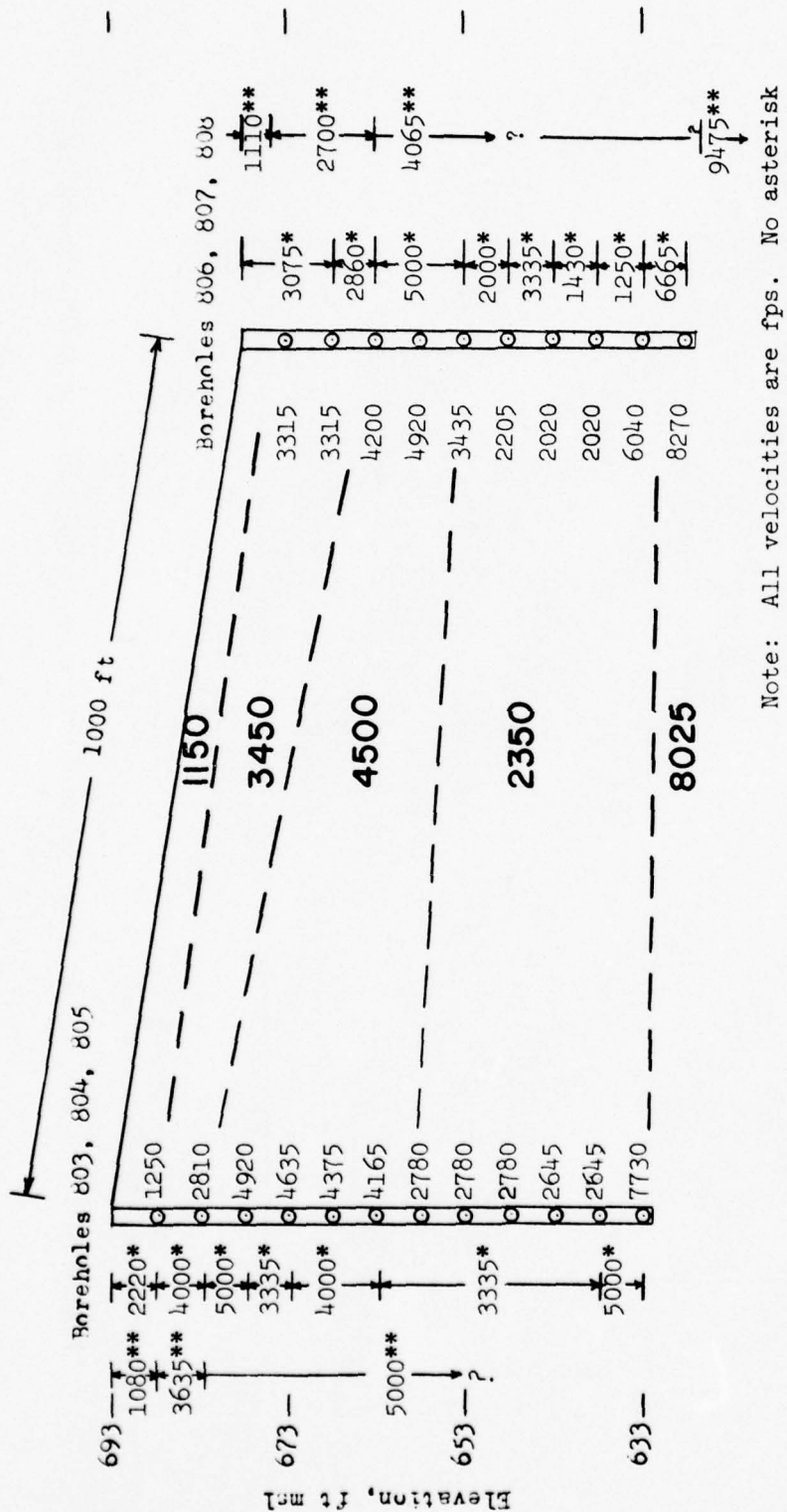
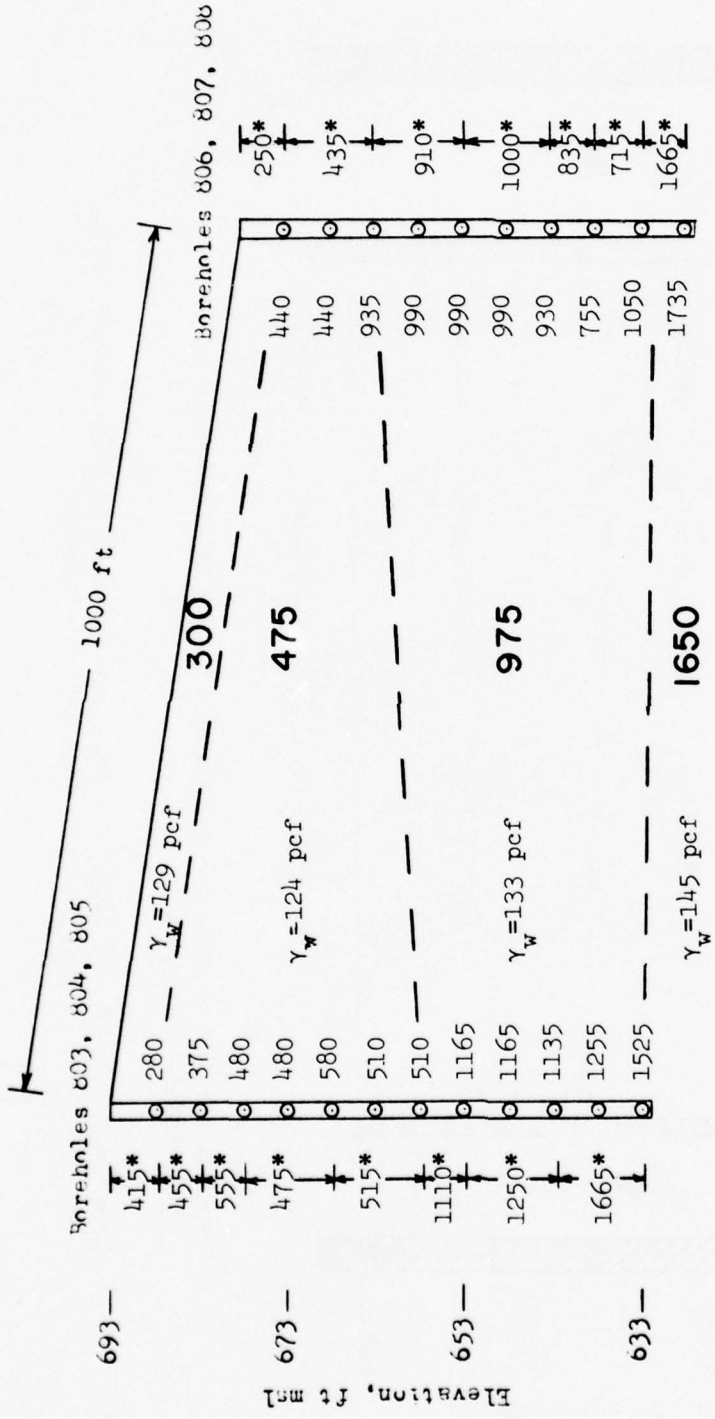


Figure A14. P-wave arrival time versus distance, proposed building X-340-1 location



Note: All velocities are fps. No asterisk denotes velocities from crosshole tests. One asterisk denotes velocities from downhole tests. Two asterisks denote velocities from refraction seismic tests.

Figure A15. P-wave velocity profile from in situ seismic tests, proposed building X-340-1 location



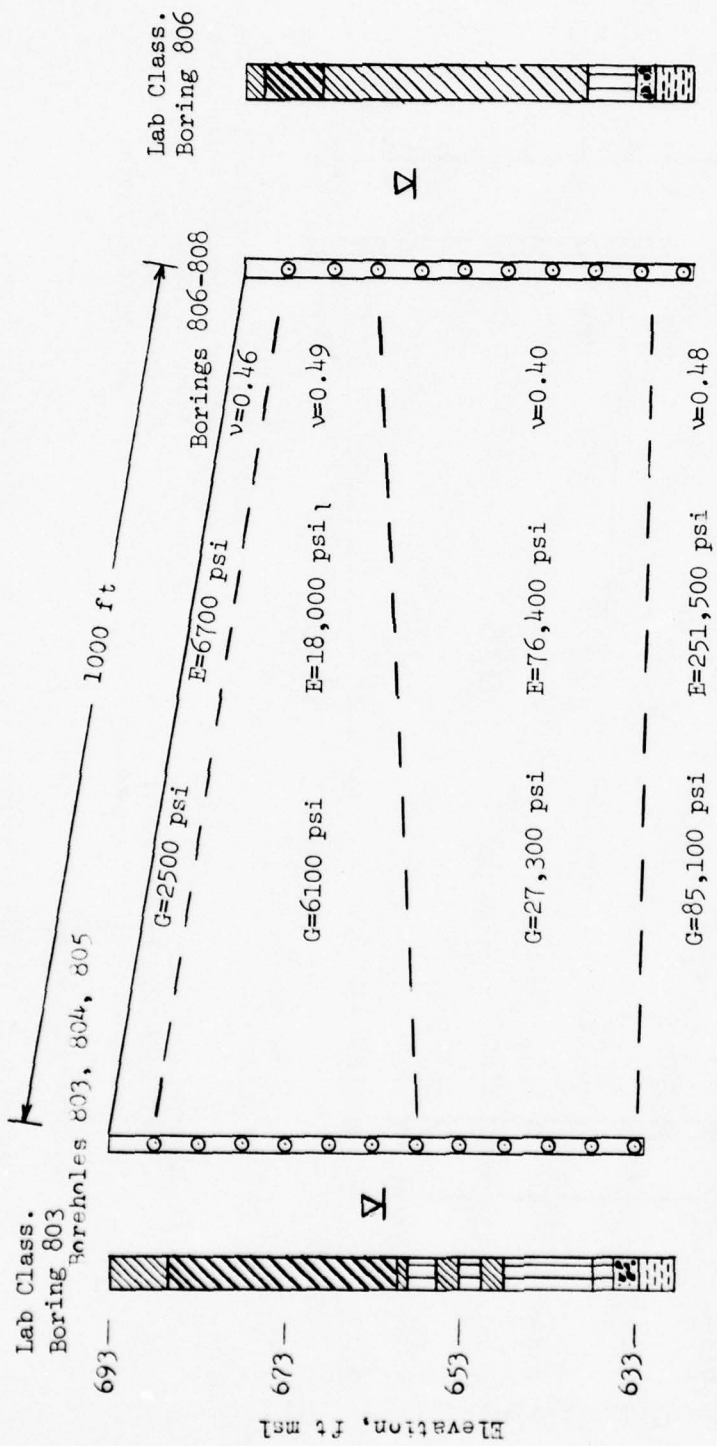
Note: All velocities are fps. No asterisk denotes velocities from crosshole tests. One asterisk denotes velocities from downhole tests.

Legend:

- Seismic source and geophone locations used for crosshole tests.

γ_w Wet unit weight

Figure A16. S-wave velocity profile from in situ seismic tests, proposed building X-340-1 location



Note: Explanation of graphic symbols for boring data are presented in Figure Al.

Figure A17. Shear and Young's moduli profile from in situ seismic tests, proposed building X-340-1 location

Figures A18-A26, Proposed Building X-340-2 Location

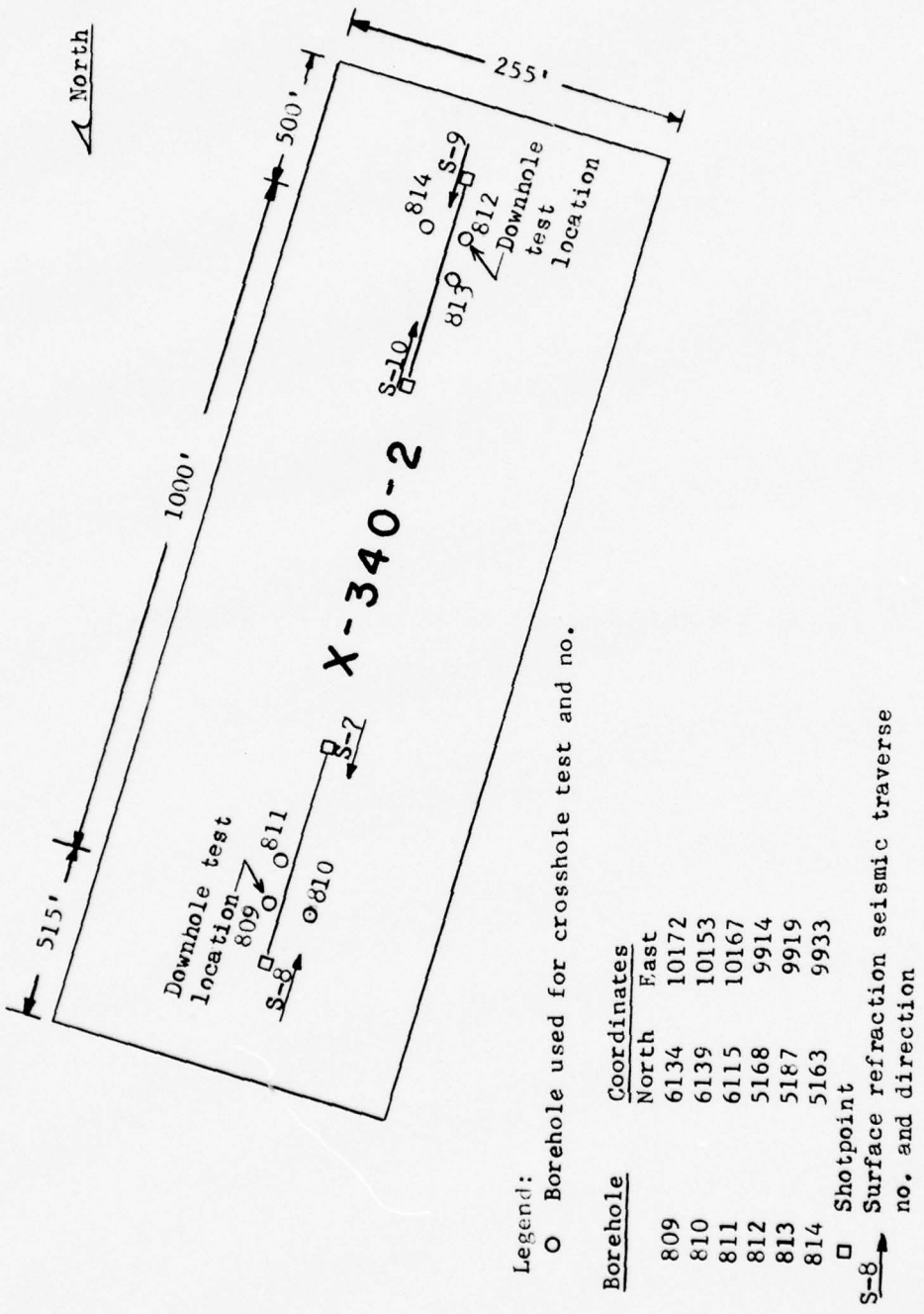
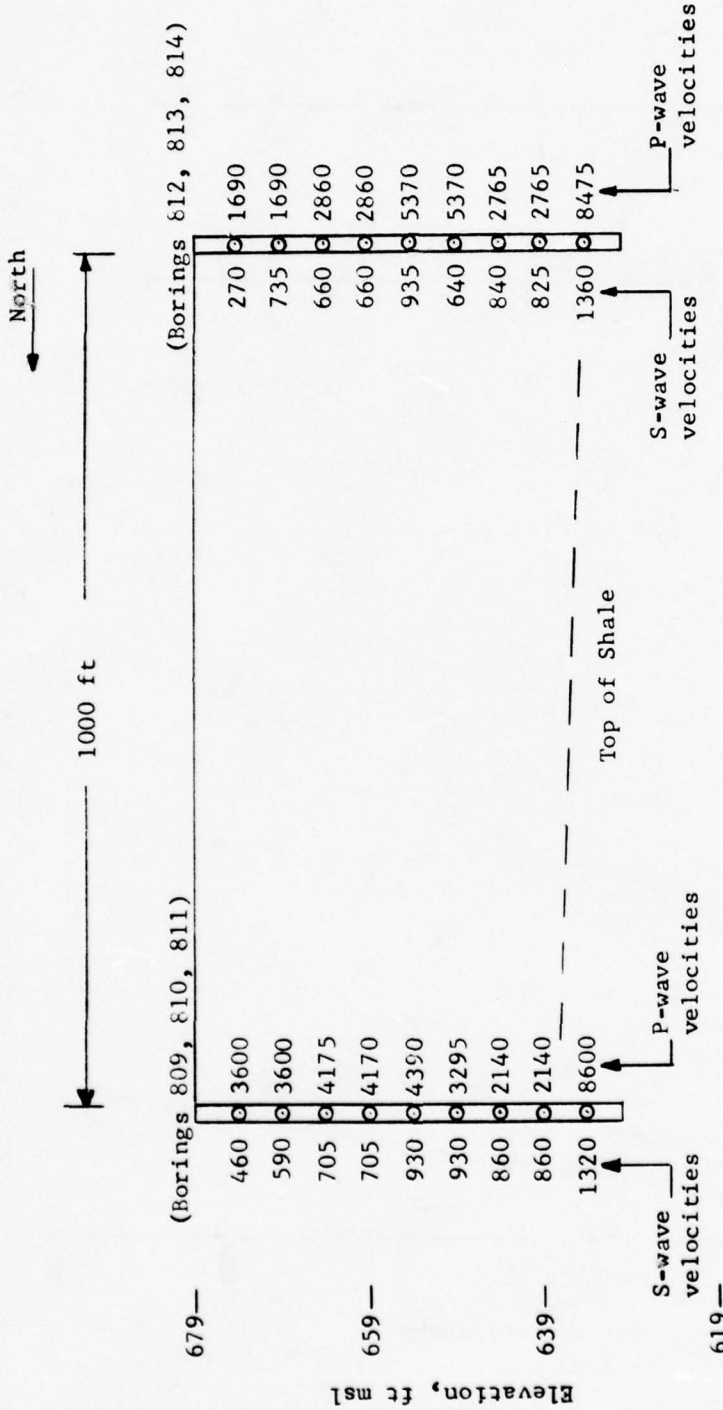


Figure A18. In situ seismic test layout, proposed building X-340-2 location



Note: All velocities are fps.

Figure A19. P- and S-wave velocities determined from crosshole tests, proposed building X-340-2 location

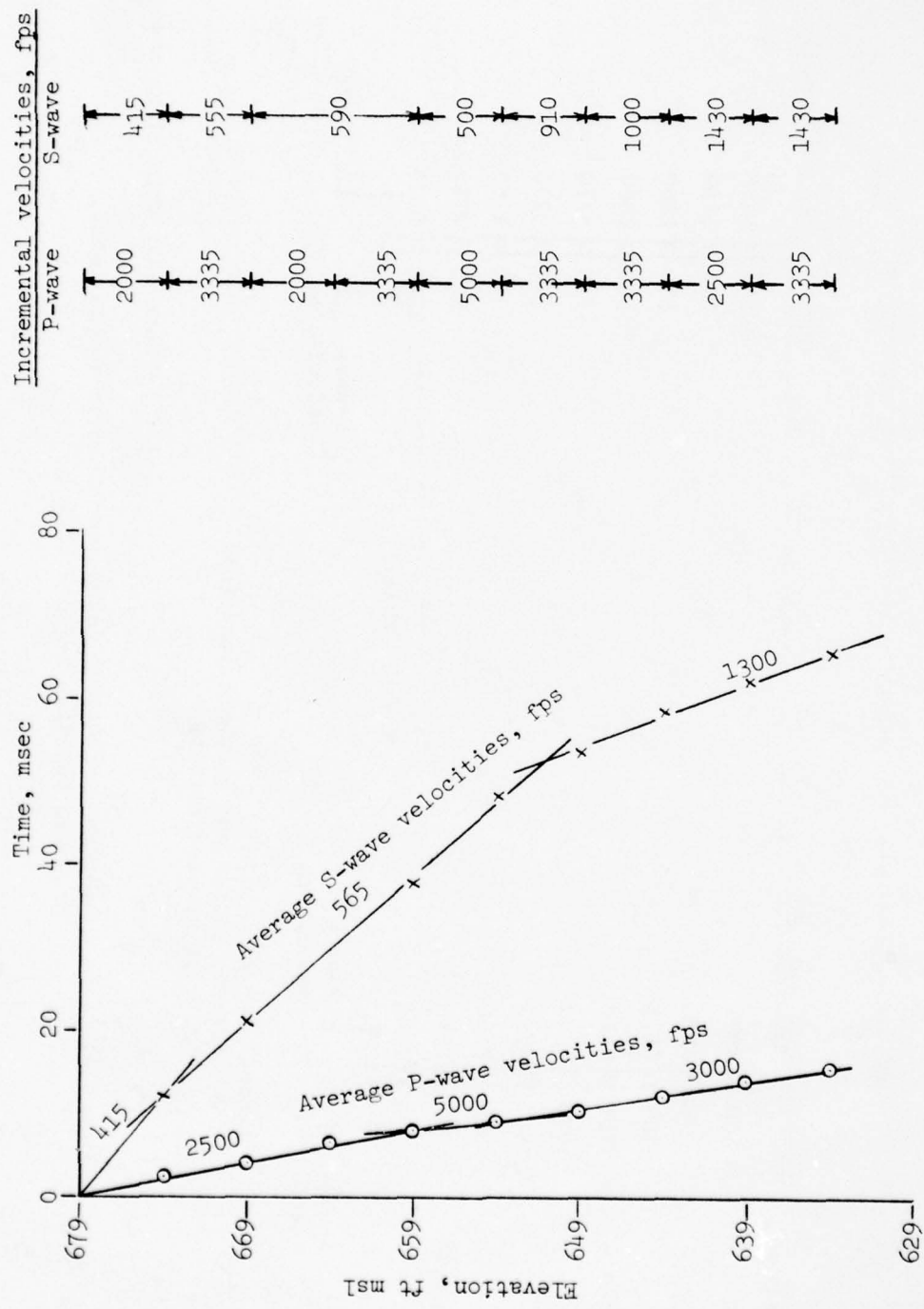


Figure A20. Arrival time versus depth from downhole test in boring 809, proposed building X-340-2 location

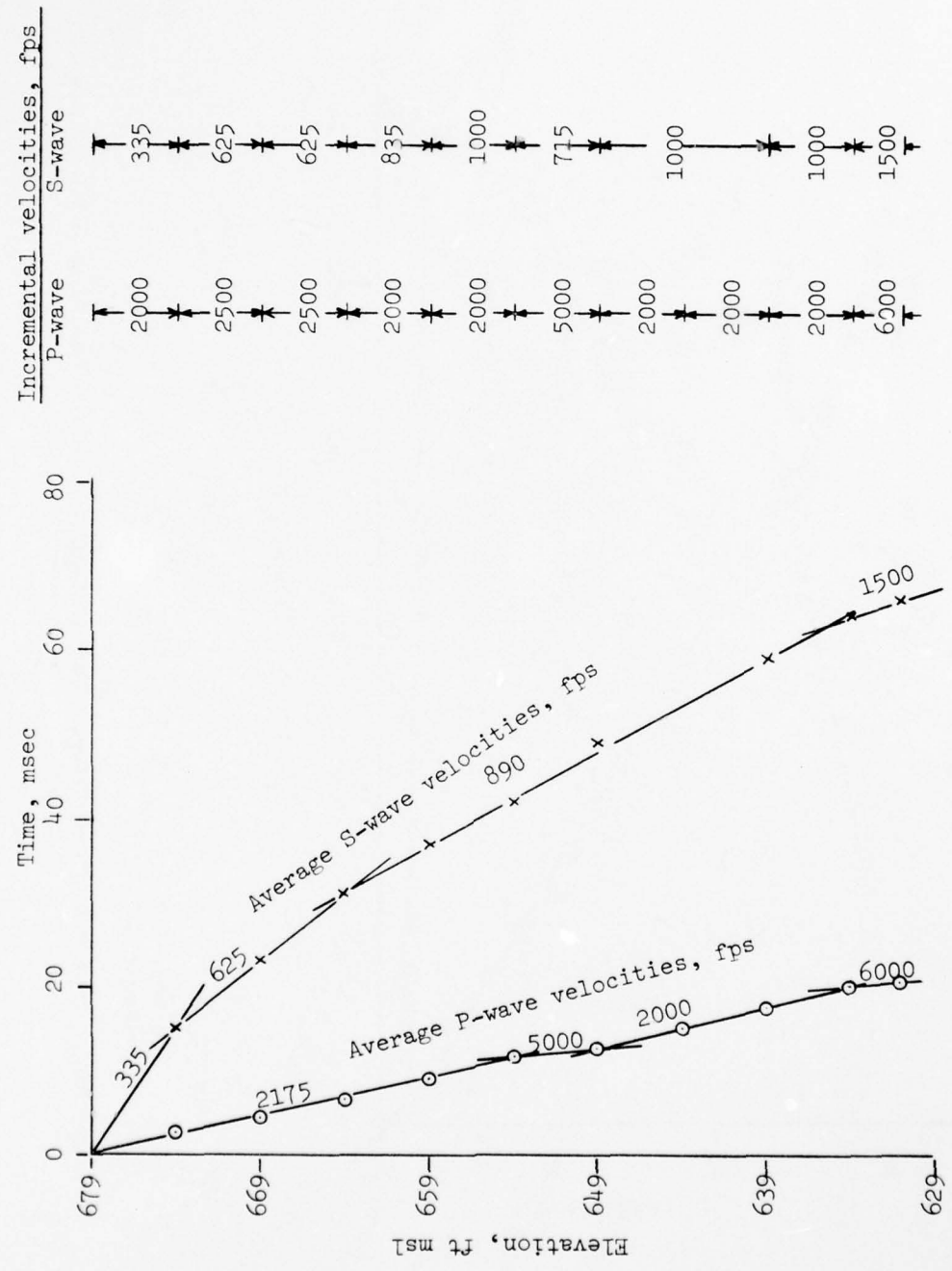


Figure A21. Arrival time versus depth from downhole test in boring 812, proposed building X-340-2 location

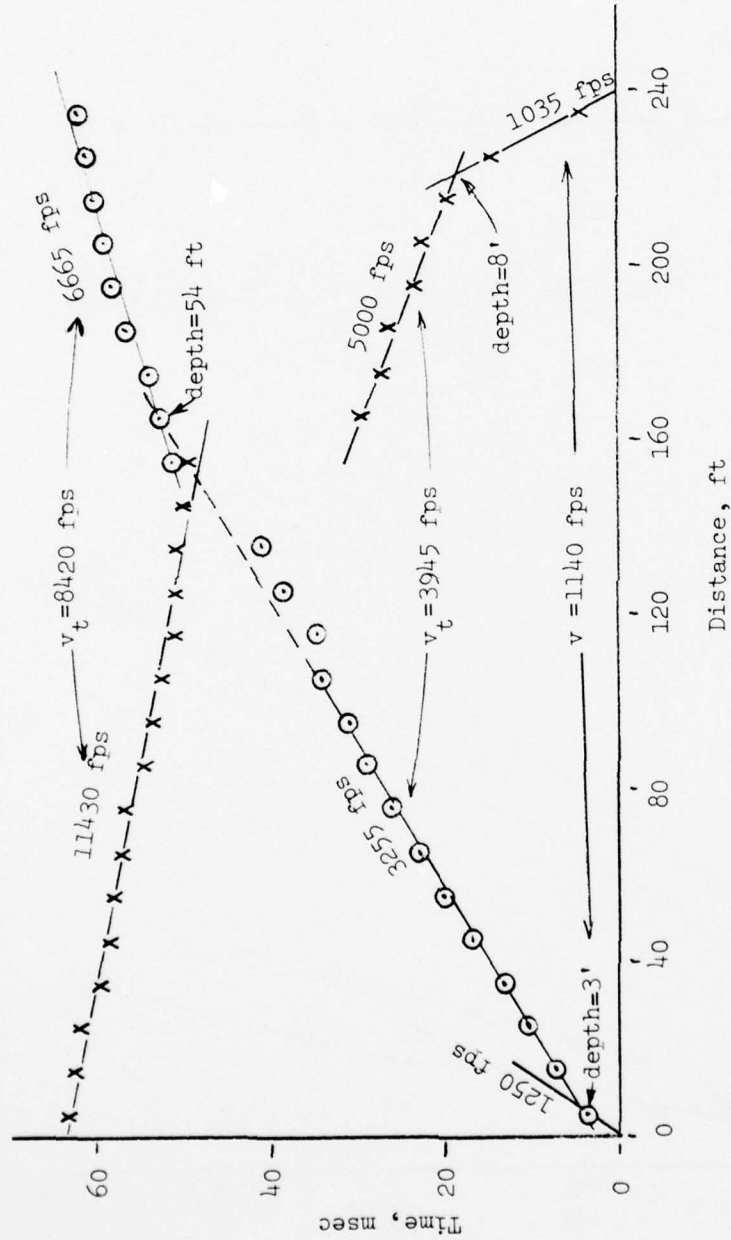


Figure A22. P-wave arrival time versus distance, proposed building X-340-2 location

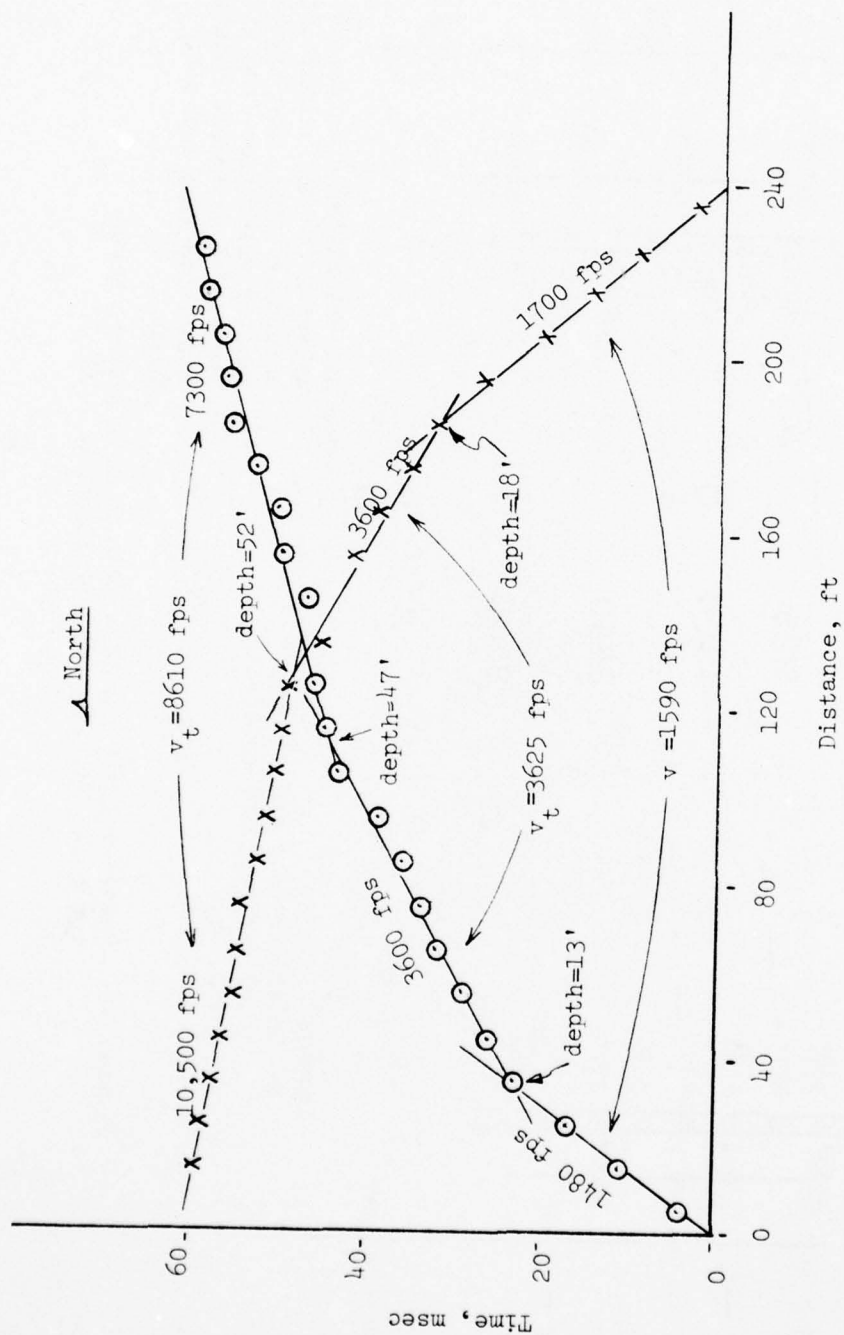


Figure A23. P-wave arrival time versus distance, proposed building X-340-2 location

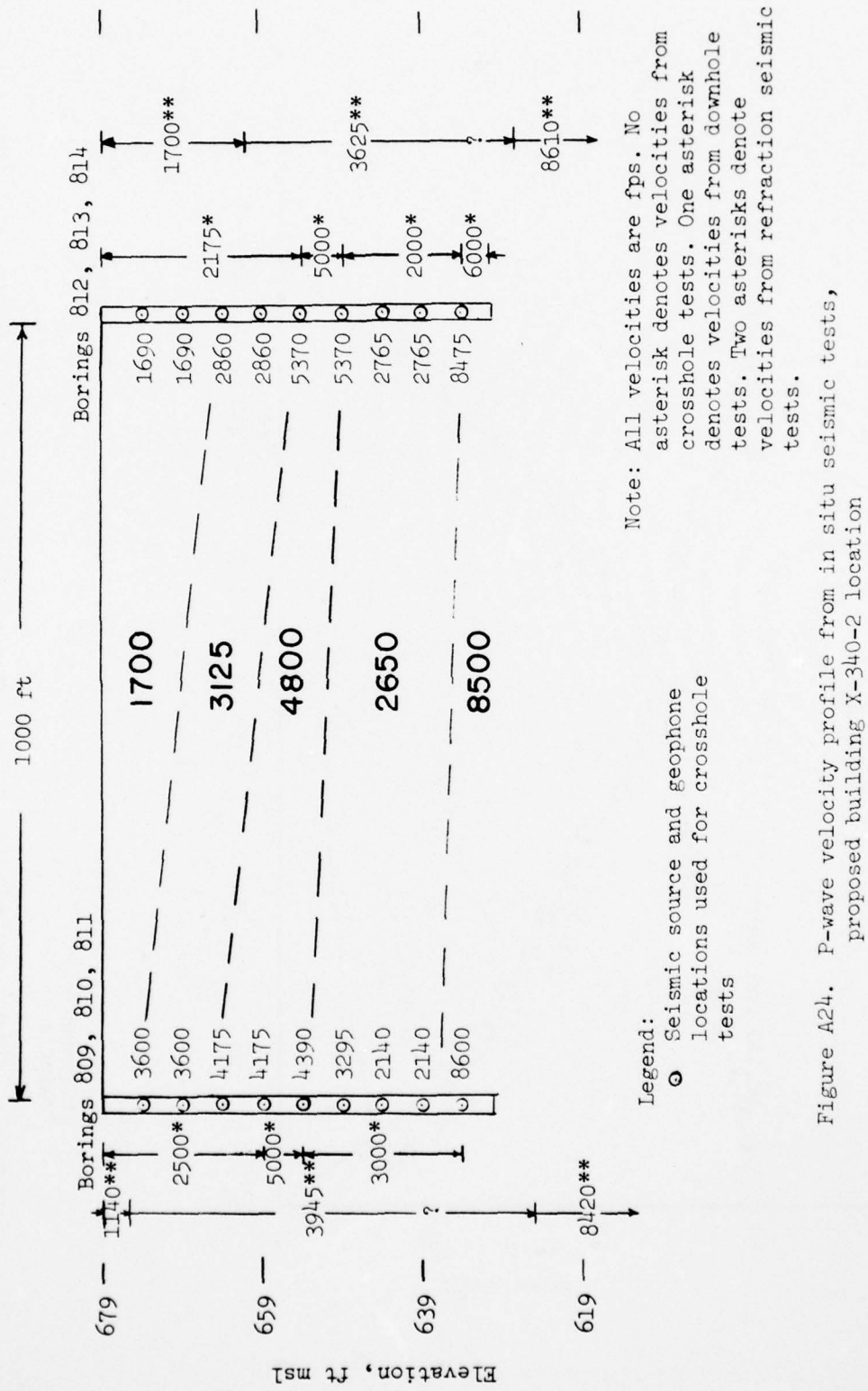
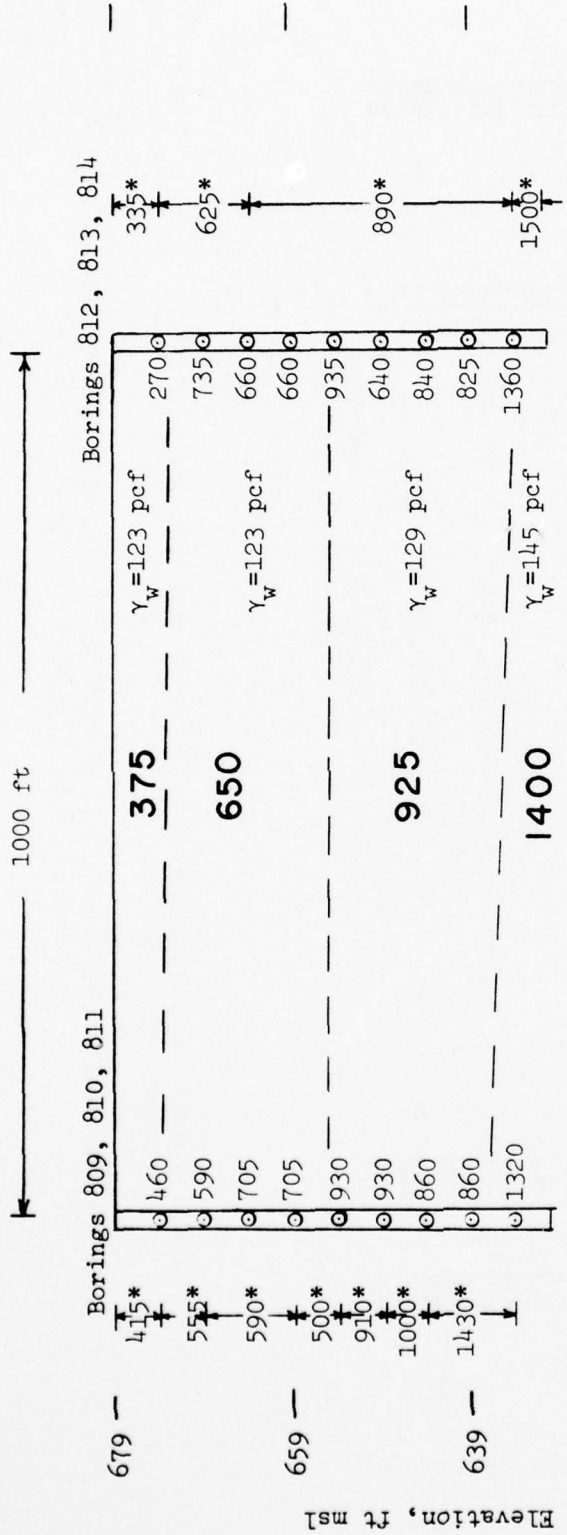
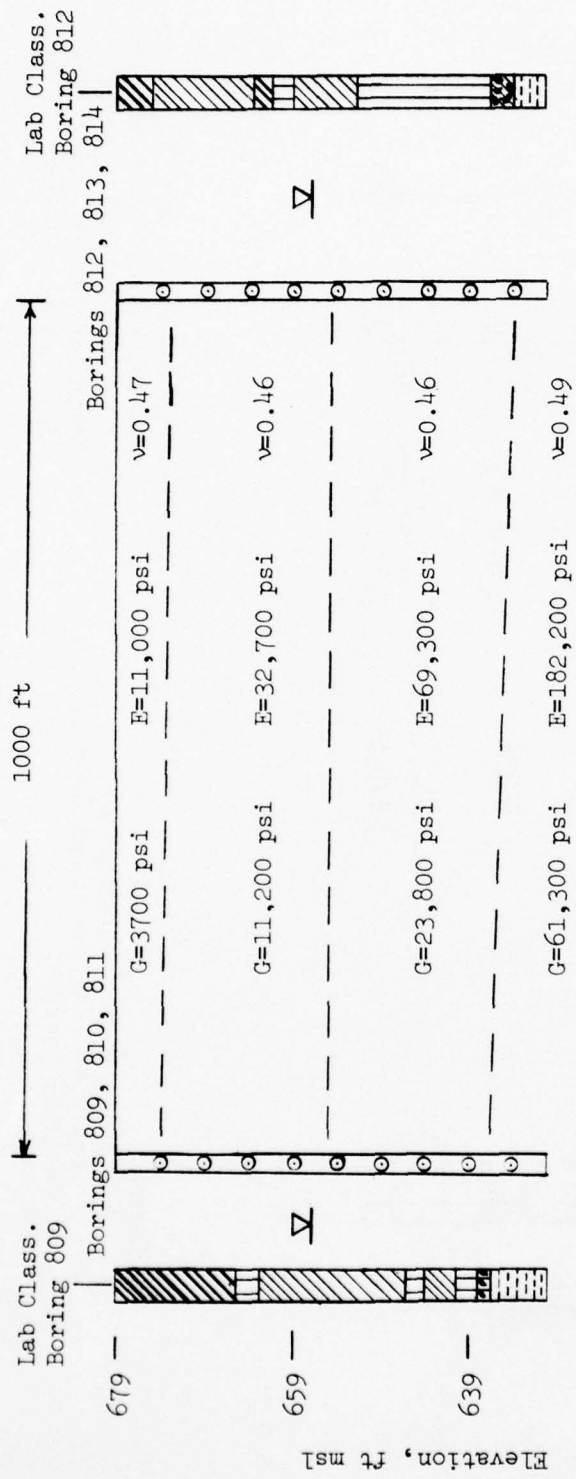


Figure A24. P-wave velocity profile from in situ seismic tests, proposed building X-340-2 location



Note: All velocities are fps.
 No asterisk denotes velocities from crosshole tests. One asterisk denotes velocities from downhole tests.

Figure A25. S-wave velocity profile from in situ seismic tests, proposed building X-340-2 location



Note: Explanation of graphic symbols for boring data are presented in Figure A1.

Figure A26. Shear and Young's moduli profile from in situ seismic tests, proposed building X-340-2 location

Figures A27-A35, Proposed Building X-340-3 Location

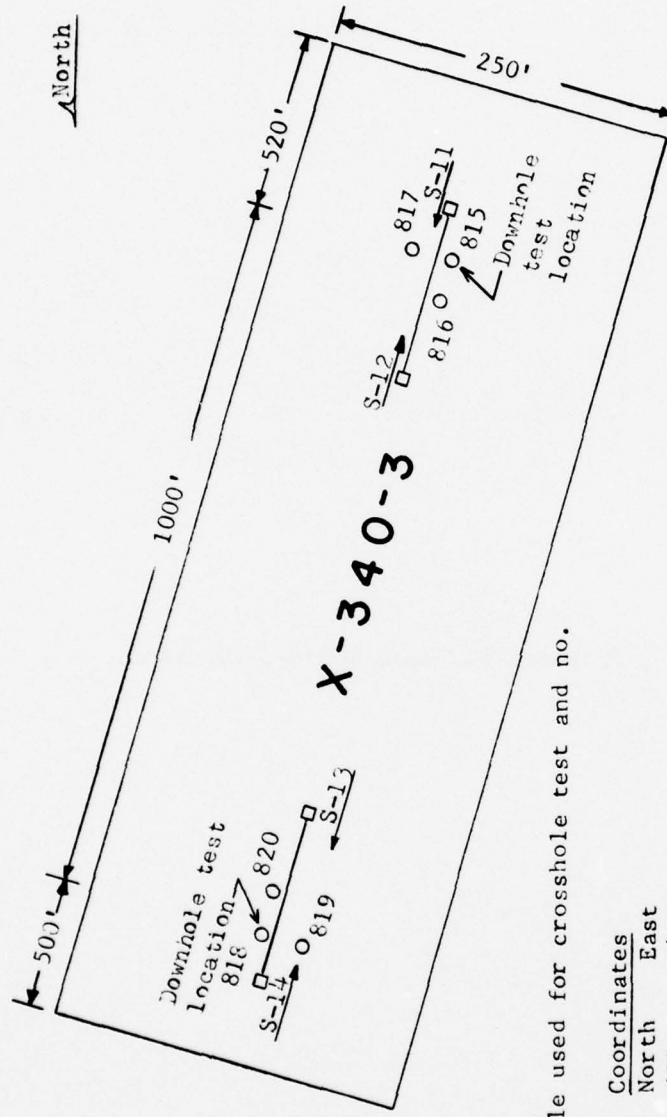


Figure A27. In situ seismic test layout, proposed building X-340-3 location

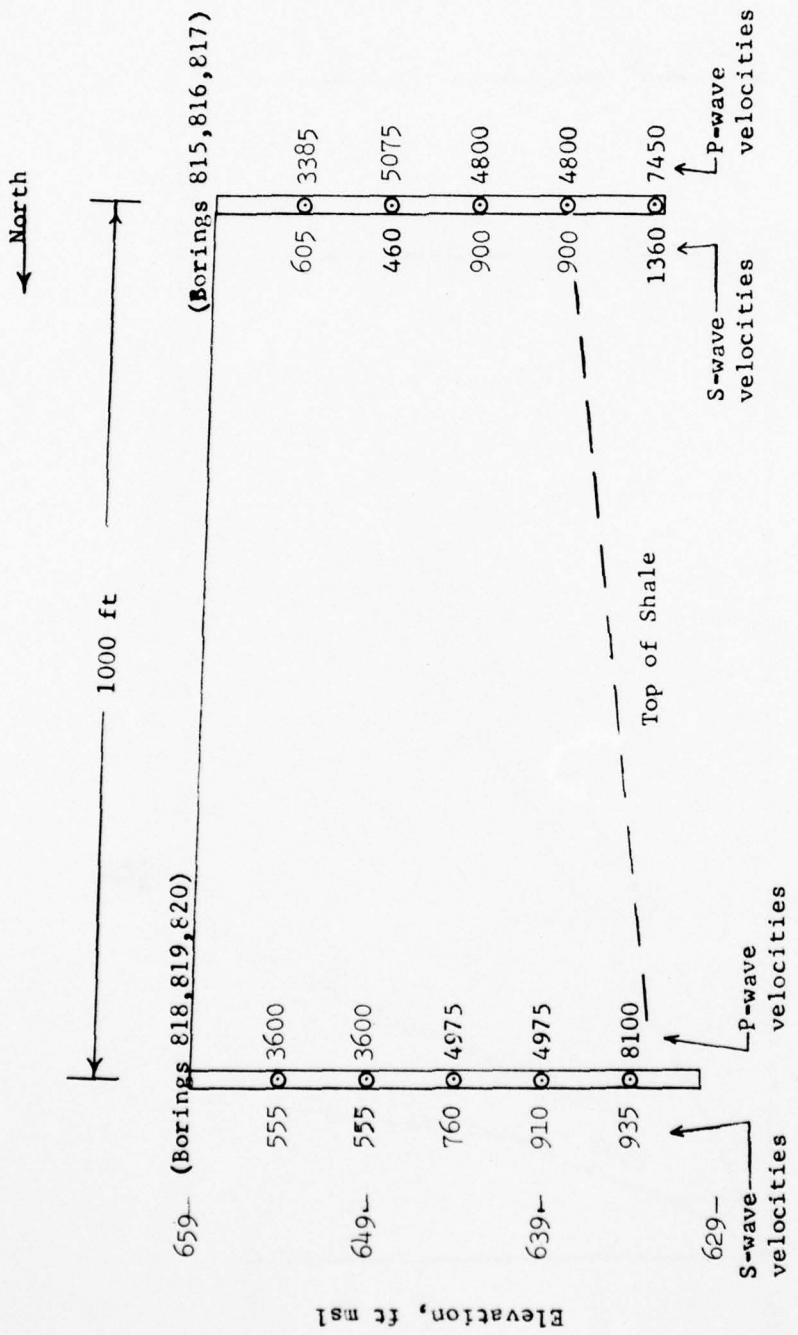


Figure A28. P- and S-wave velocities determined from crosshole tests, proposed building X-340-3

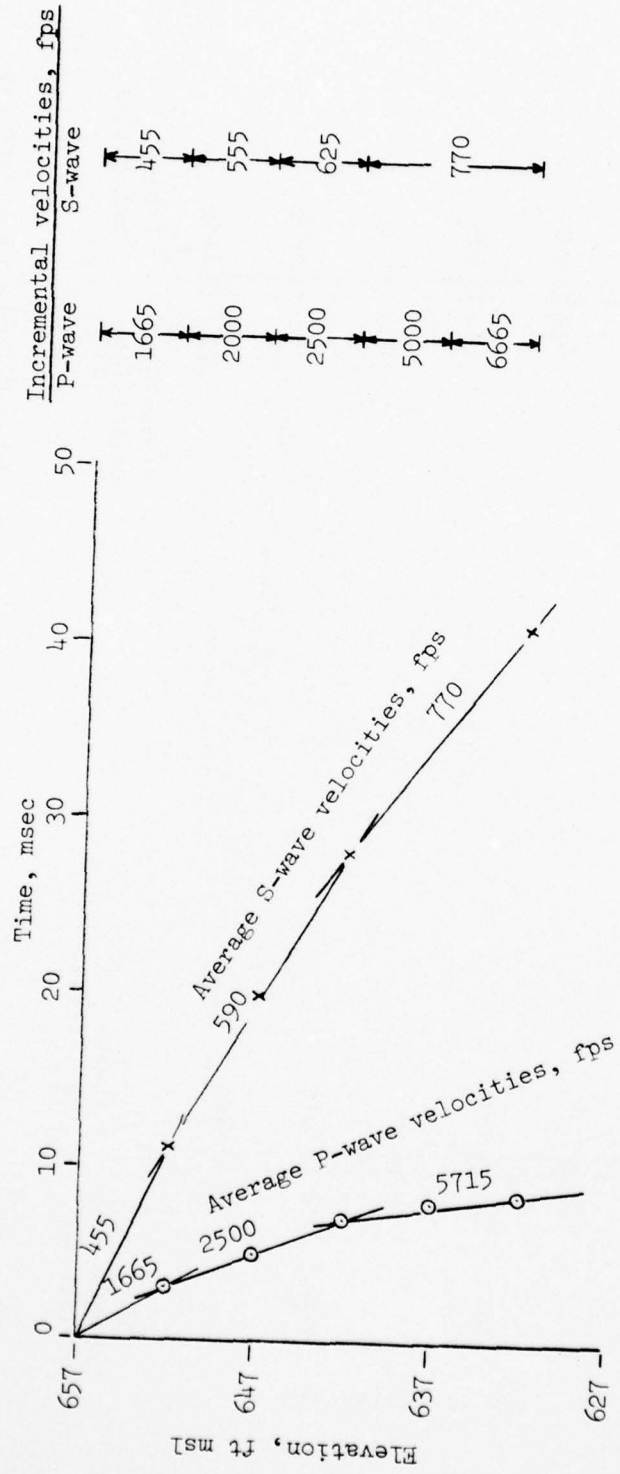


Figure A29. Arrival time versus depth from downhole test in boring 815,
proposed building X-340-3 location

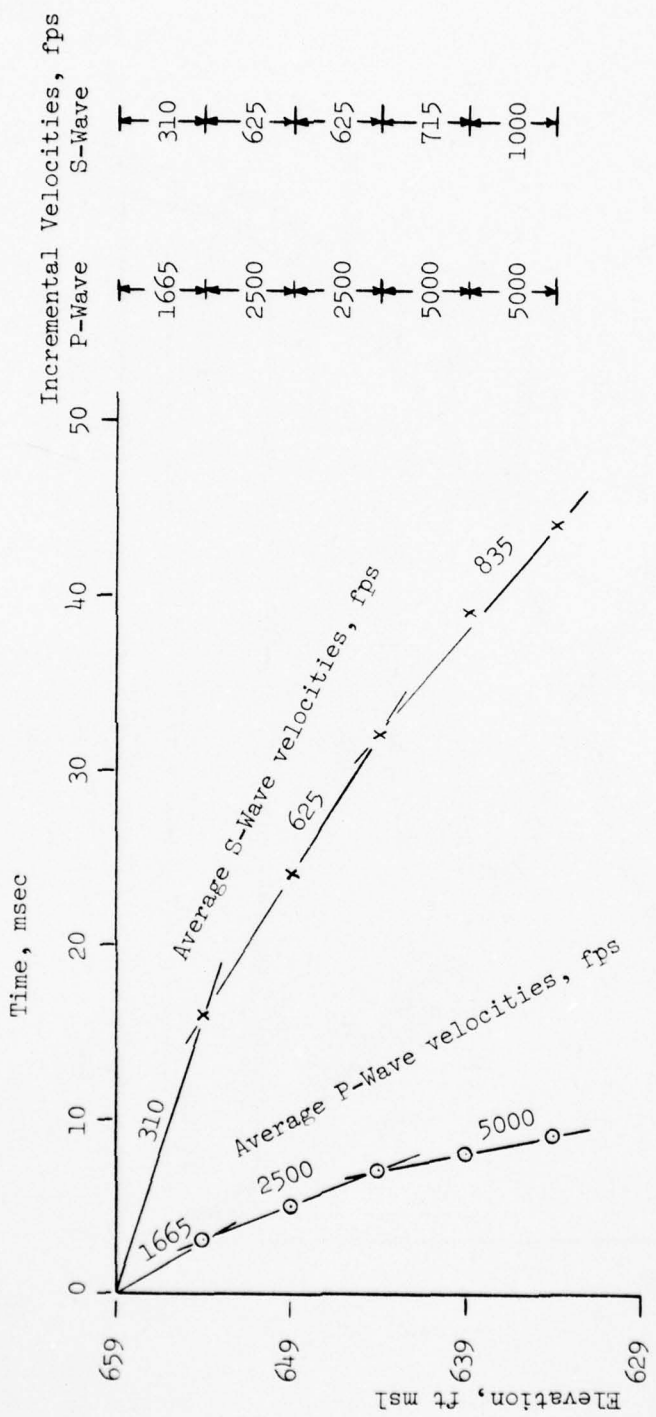
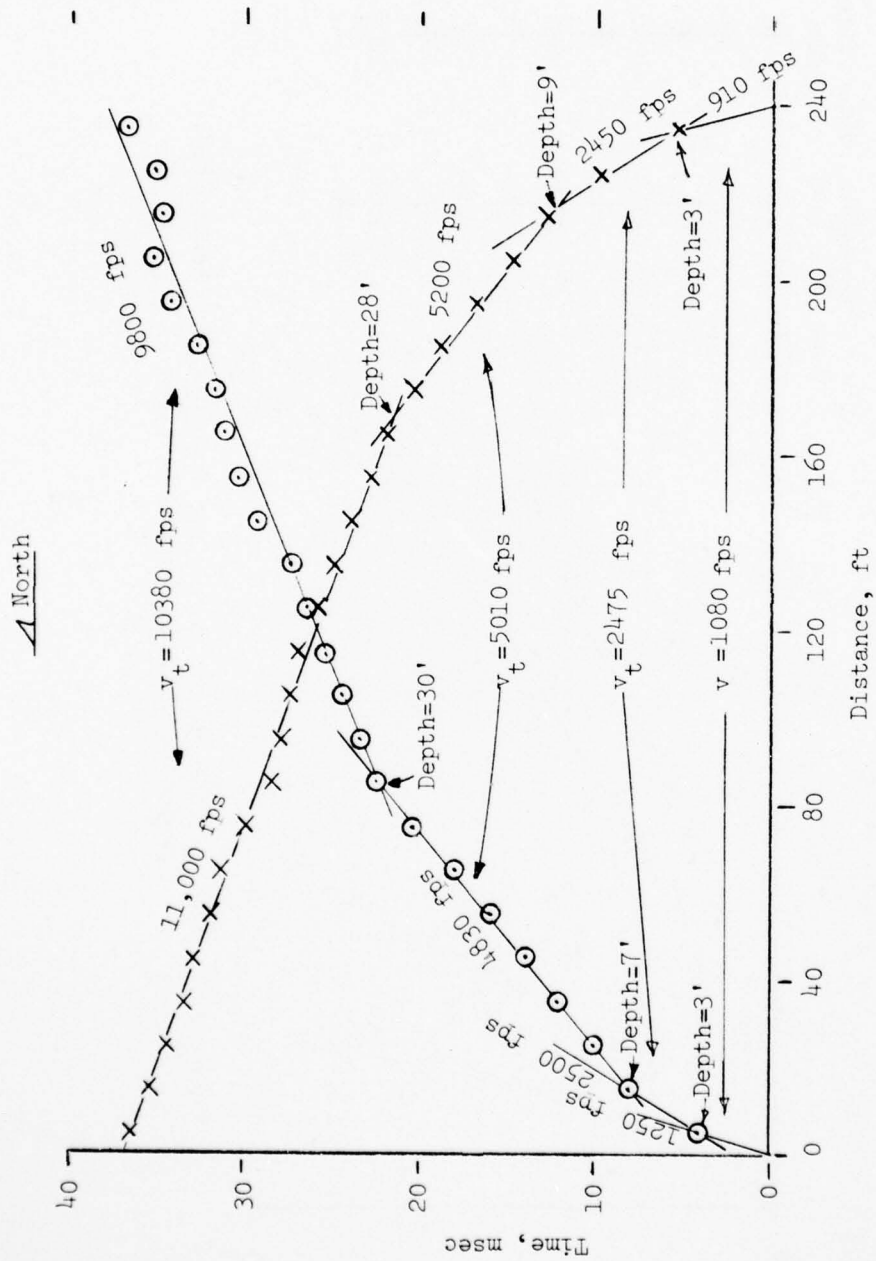


Figure A30. Arrival time versus depth from downhole test boring 818,
proposed building X-340-3 location

Figure A30. Arrival time versus depth from downhole test boring 818,

proposed building X-340-3 location

Figure A30.



Legend:

- 0 Traverse S-12
X Traverse S-11

Figure A31. P-wave arrival time versus distance, proposed building X-340-3 location

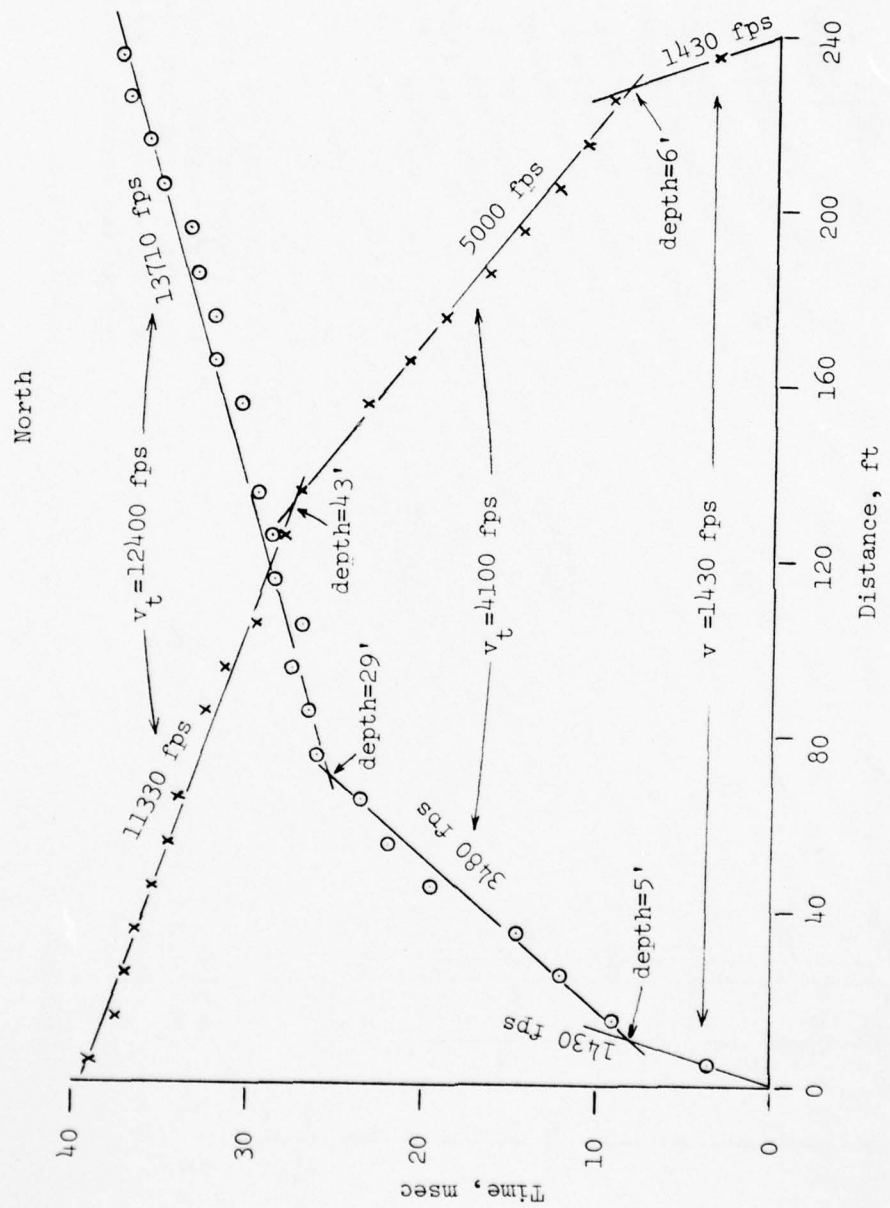
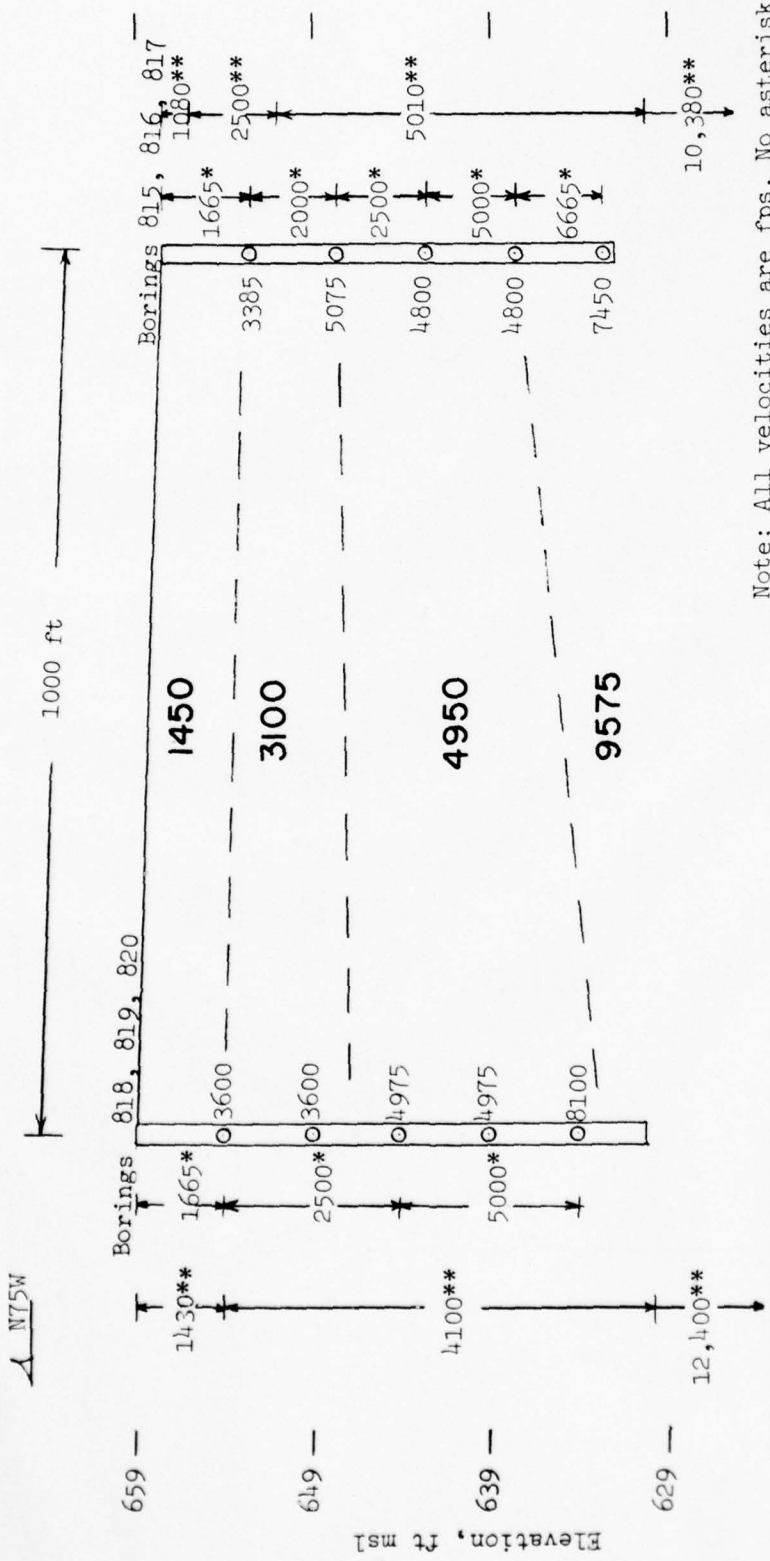


Figure A32. P-wave arrival time versus distance, proposed building X-340-3 location



Note: All velocities are fps. No asterisk denotes velocities from crosshole tests. One asterisk denotes velocities from downhole tests. Two asterisks denote velocities from refraction seismic tests.

Figure A33. P-wave velocity profile from in situ seismic tests, proposed building X-340-3 location

AD-A059 988

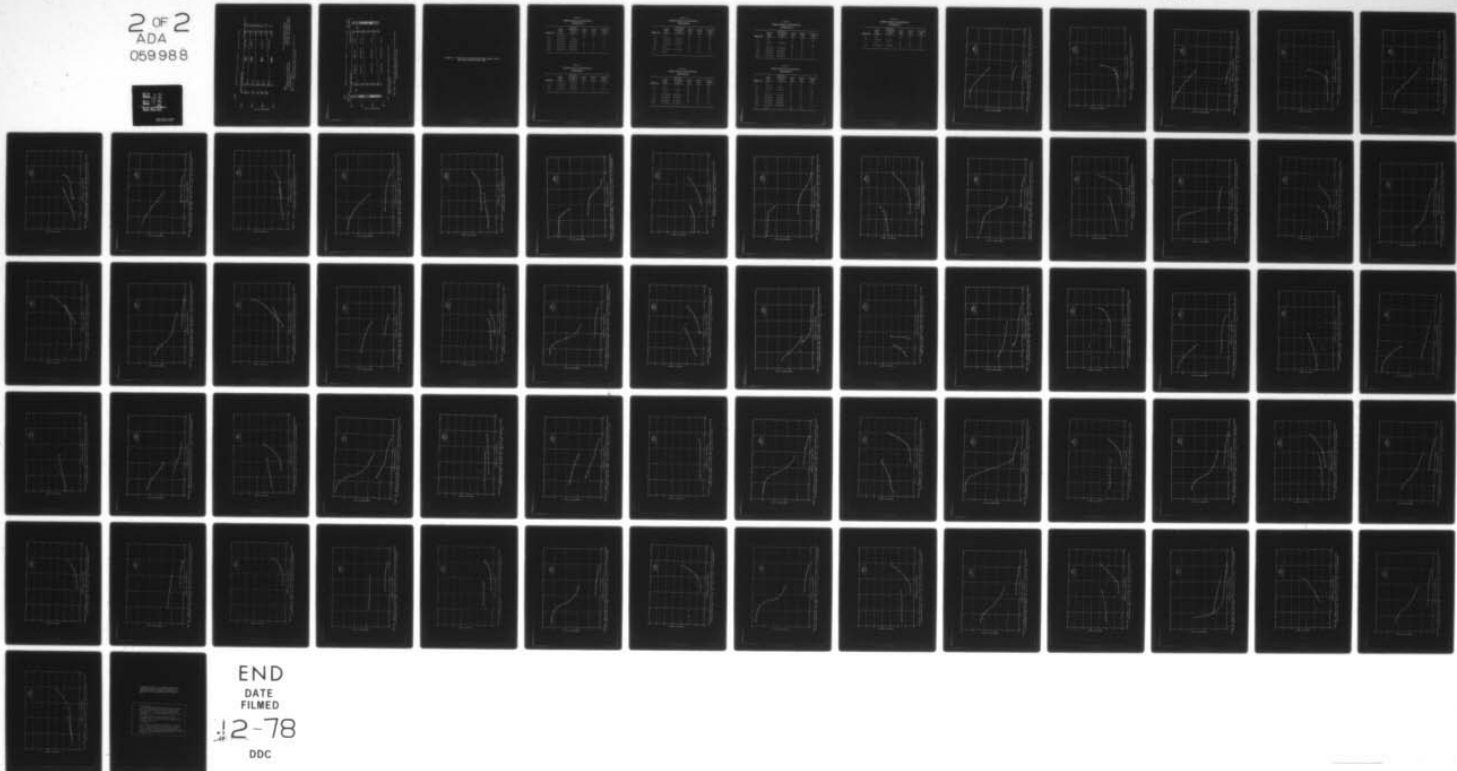
ARMY ENGINEER WATERWAYS EXPERIMENT STATION VICKSBURG MISS F/G 13/13
IN SITU AND LABORATORY DETERMINATIONS OF SHEAR AND YOUNG'S MODU--ETC(U)
AUG 78 J R CURRO, W F MARCUSON

UNCLASSIFIED

WES-MP-S-78-12

NL

2 OF 2
ADA
069988



END
DATE
FILED
12-78
DDC

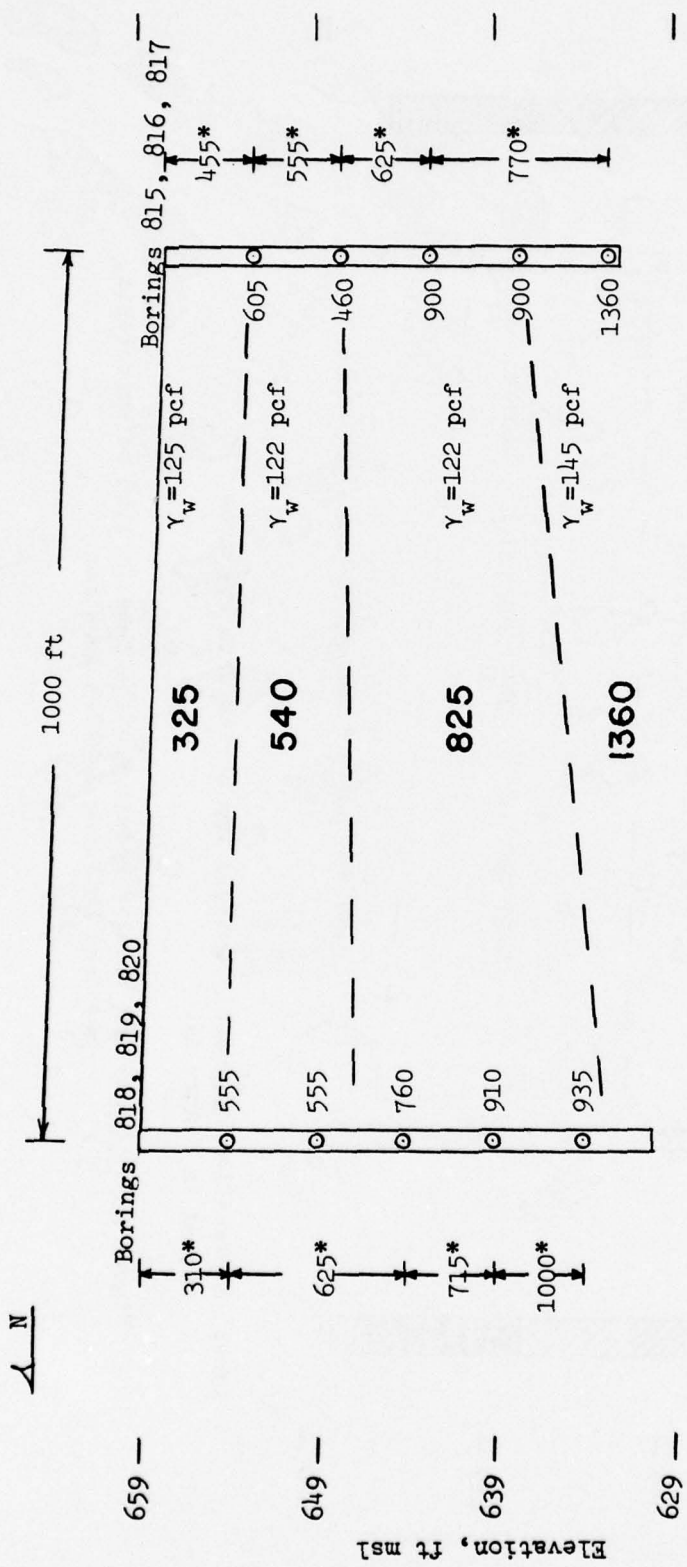
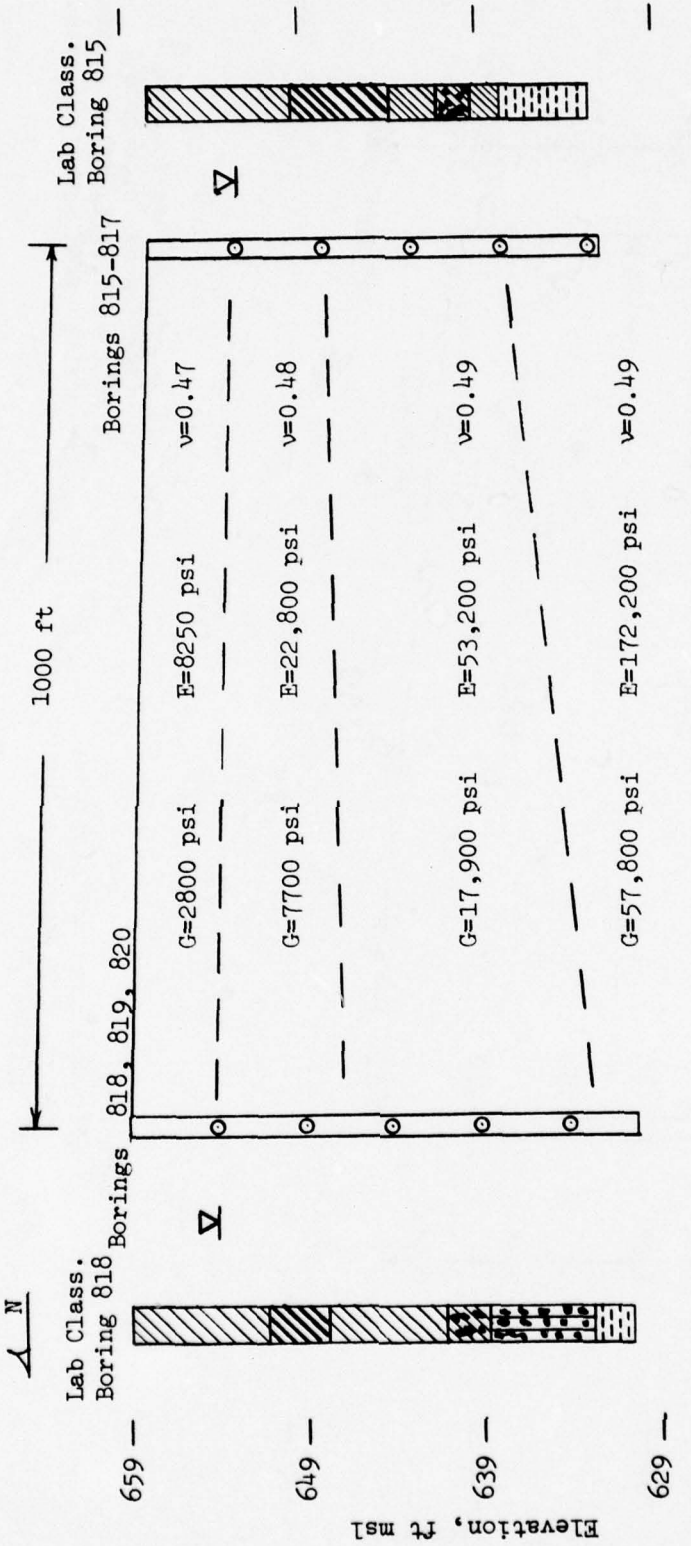


Figure A34. S-wave velocity profile from in situ seismic tests, proposed building X-340-3 location



Note: Explanation of graphic symbols for boring data are presented in Figure A1.

Figure A35. Shear and Young's moduli profile from in situ seismic tests, proposed building X-340-3 location

APPENDIX B: DYNAMIC MODULUS AND DAMPING VERSUS DYNAMIC STRAIN
AMPLITUDE, RESONANT COLUMN TESTS

Table B1
Samples Tested in the Laboratory
Boring 800 UD

<u>Sample No.</u>	<u>Sample Depth ft</u>	<u>Interval Represented by Sample ft</u>	<u>Liquid Limit %</u>	<u>Plastic Limit %</u>	<u>Plasticity Index %</u>
12	10.6-12.1	--	29	16	13
13-1	12.1-14.0	1.1-16.5	--	--	--
13-2	12.1-14.0	1.1-16.5	--	--	--
20-1	24.1-25.2	21.6-25.2	26	17	9
20-2	24.1-25.2	21.6-25.2	--	--	--
21-1	25.9-27.3	25.9-28.5	--	--	--

Table B2
Samples Tested in the Laboratory
Boring 803 UD

<u>Sample No.</u>	<u>Sample Depth ft</u>	<u>Interval Represented by Sample ft</u>	<u>Liquid Limit %</u>	<u>Plastic Limit %</u>	<u>Plasticity Index %</u>
3-1	5.0-06.6	3.9-08.2	44	21	23
3-2	5.0-06.6	3.9-08.2	--	--	--
9-2	22.2-24.6	8.4-32.6	51	25	26

Table B3
Samples Tested in the Laboratory
Boring 806 UD

<u>Sample No.</u>	<u>Sample Depth ft</u>	<u>Interval Represented by Sample ft</u>	<u>Liquid Limit %</u>	<u>Plastic Limit %</u>	<u>Plasticity Index %</u>
2	6.0	--	68	30	38
3-1	9.0-11.4	2.1-17.0	--	--	--
3-2	9.0-11.4	2.1-17.0	--	--	--
3-3	9.0-11.4	2.1-17.0	--	--	--
4	11.4	--	37	12	20
14-1	37.0-38.3	29.0-39.9	--	--	--
15	38.3	--	25	20	5

Table B4
Samples Tested in the Laboratory
Boring 809 UD

<u>Sample No.</u>	<u>Sample Depth ft</u>	<u>Interval Represented by Sample ft</u>	<u>Liquid Limit %</u>	<u>Plastic Limit %</u>	<u>Plasticity Index %</u>
1	2.0	--	62	28	34
2-1	2.8-5.4	0.0-13.5	--	--	--
3	7.9	--	65	27	38
7-1	16.3-18.8	13.8-21.3	28	17	11
7-2	16.3-18.8	13.8-21.3	--	--	--
11-1	26.1-28.3	21.5-36.7	28	17	11
11-2	26.1-28.3	21.5-36.7	--	--	--

Table B5
Samples Tested in the Laboratory
Boring 812 UD

<u>Sample No.</u>	<u>Sample Depth ft</u>	<u>Interval Represented by Sample ft</u>	<u>Liquid Limit %</u>	<u>Plastic Limit %</u>	<u>Plasticity Index %</u>
1	1.8	--	51	21	30
2-1	2.2-4.1	0.0-15.6	--	--	--
3	7.5	--	45	21	24
7-1	16.0-18.5	16.0-29.8	25	18	7
7-2	16.0-18.5	16.0-29.8	--	--	--
13-1	29.9-32.4	29.9-39.3	26	22	4
13-2	29.9-32.4	29.9-39.3	--	--	--

Table B6
Samples Tested in the Laboratory
Boring 815 UD

<u>Sample No.</u>	<u>Sample Depth ft</u>	<u>Interval Represented by Sample ft</u>	<u>Liquid Limit %</u>	<u>Plastic Limit %</u>	<u>Plasticity Index %</u>
1	2.0	--	41	21	20
2-1	1.0-2.0	1.0-7.5	--	--	--
2-2	1.0-2.0	1.0-7.5	--	--	--
3	4.7	--	36	18	18
7-1	11.9-13.6	8.1-13.6	45	15	30
7-2	11.9-13.6	8.1-13.6	--	--	--
8-1	14.1-16.3	13.8-18.3	--	--	--
8-2	14.1-16.3	13.8-18.3	--	--	--
8-3	14.1-16.3	13.8-18.3	--	--	--
9	19.8	--	28	19	9

Table B7
Samples Tested in the Laboratory
Boring 818 UD

<u>Sample No.</u>	<u>Sample Depth ft</u>	<u>Interval Represented by Sample ft</u>	<u>Liquid Limit %</u>	<u>Plastic Limit %</u>	<u>Plasticity Index %</u>
1	1.8	--	31	21	10
2-1	2.8-4.8	0.0-7.7	--	--	--
3	7.7	--	41	21	20
5-1	11.2-13.8	8.4-16.4	34	21	13

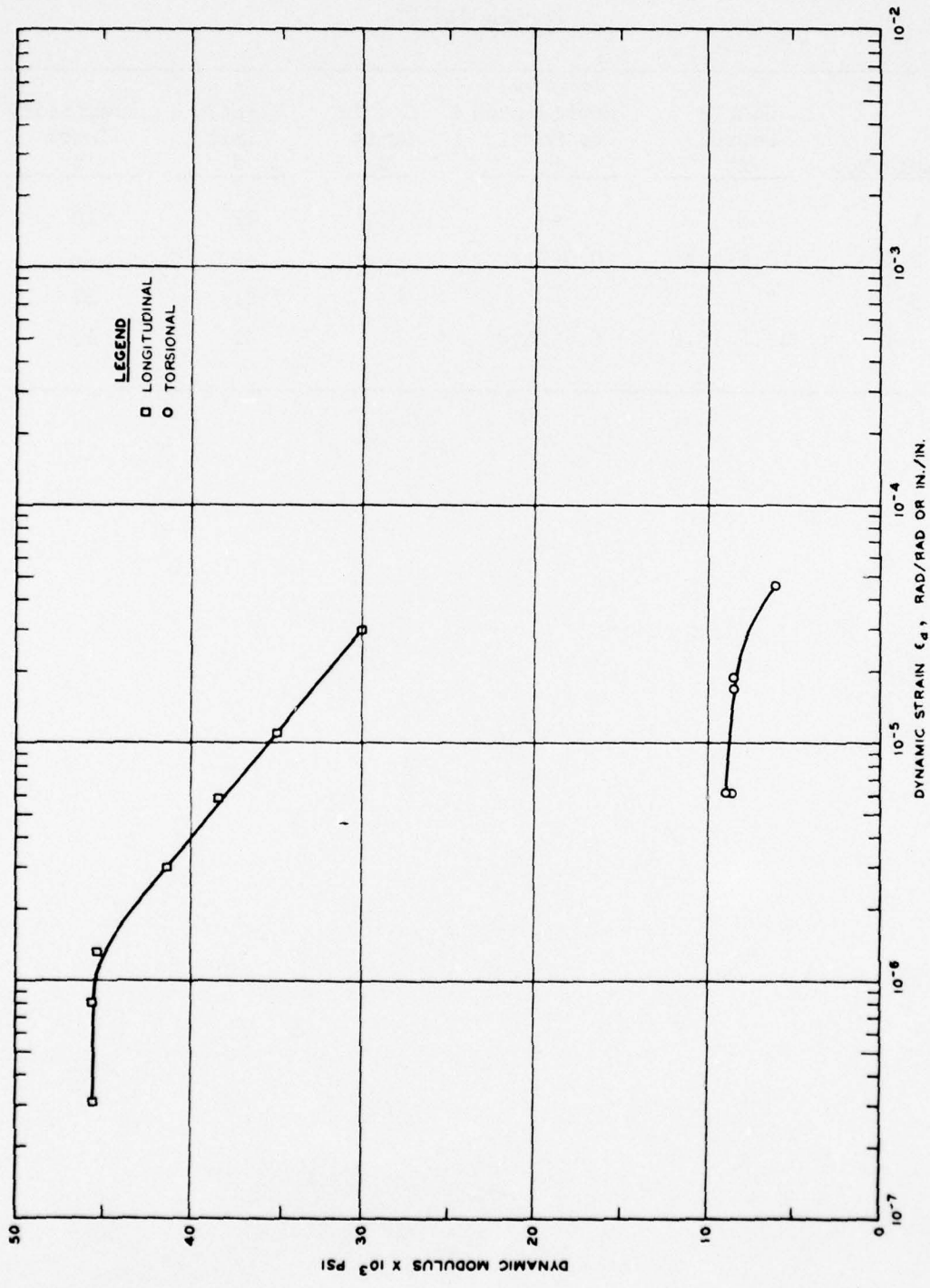


Figure B1. Dynamic shear and Young's moduli as a function of 0-peak strain amplitude as measured in the resonant column test, sample: 800 UD No. 13-1, $\bar{\sigma}_{\text{oct}} = 10 \text{ psi}$, $B = 0.92$

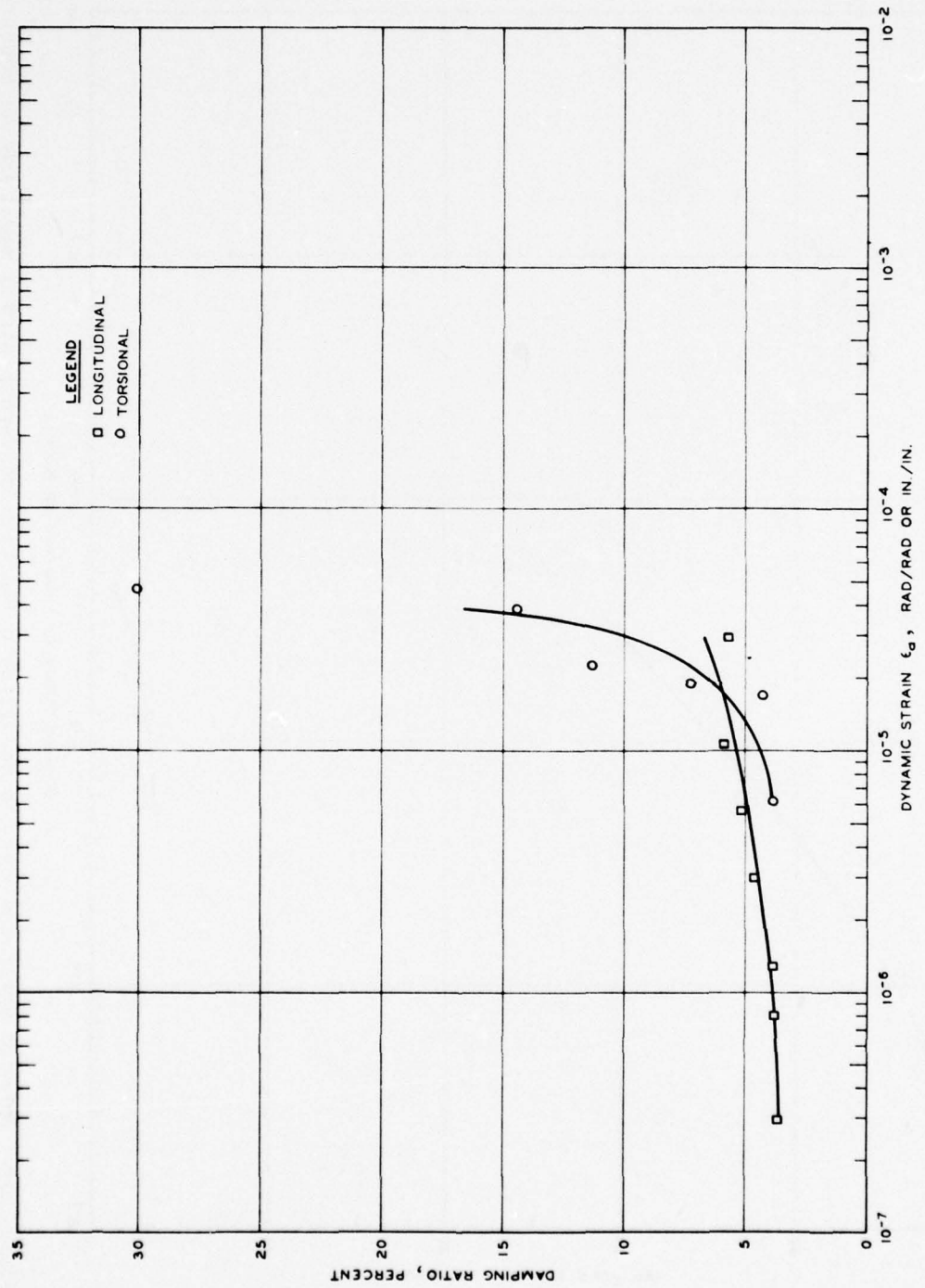


Figure B2. Damping as a function of 0-peak strain amplitude as determined by resonant column testing, sample: 800 UD No. 13-1

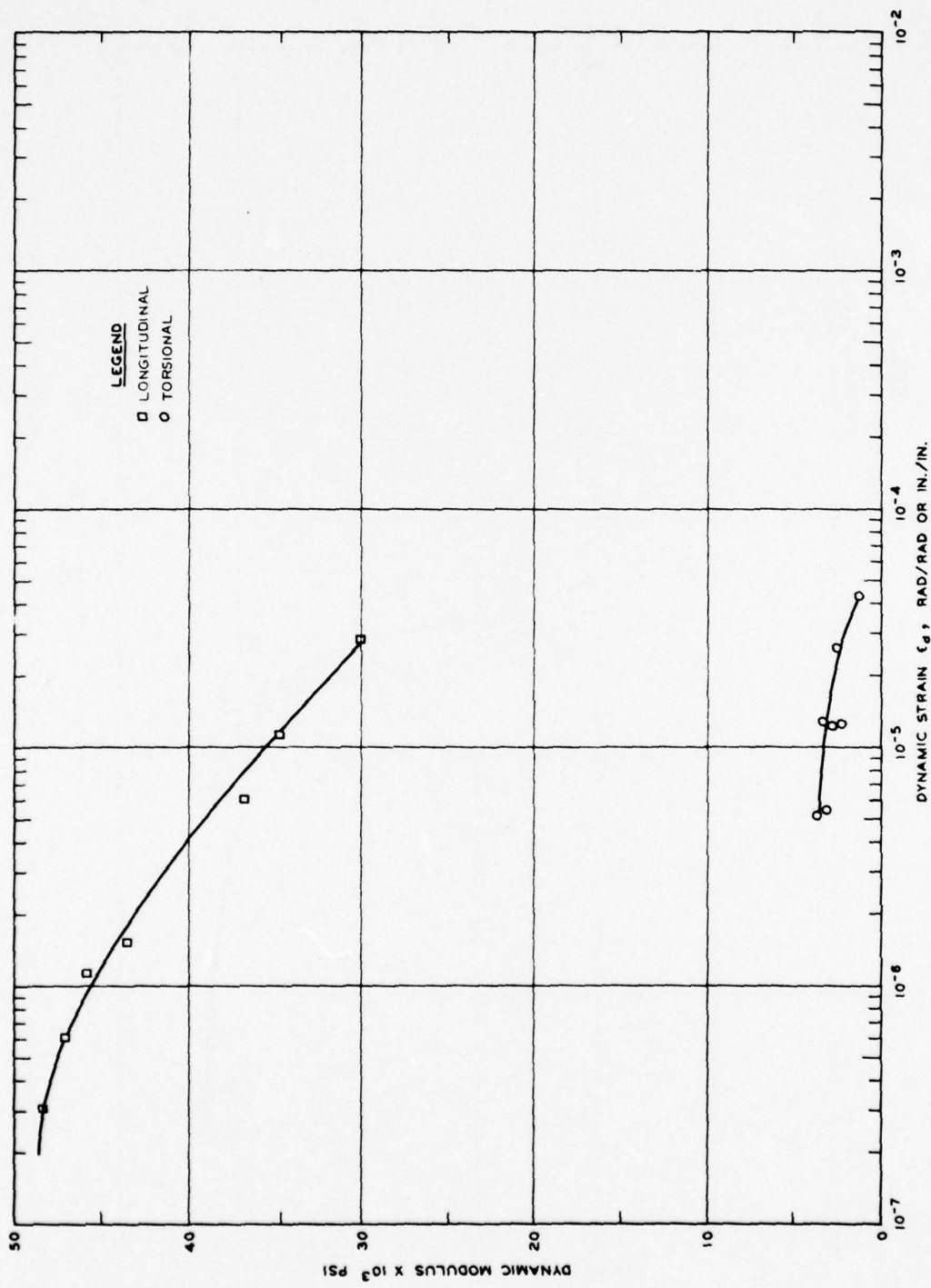


Figure B3. Dynamic shear and Young's moduli as a function of 0-peak strain amplitude as measured in the resonant column test, sample: 800 UD No. 13-2, $\bar{\sigma}_{oct} = 15$ psi, $B = 0.92$

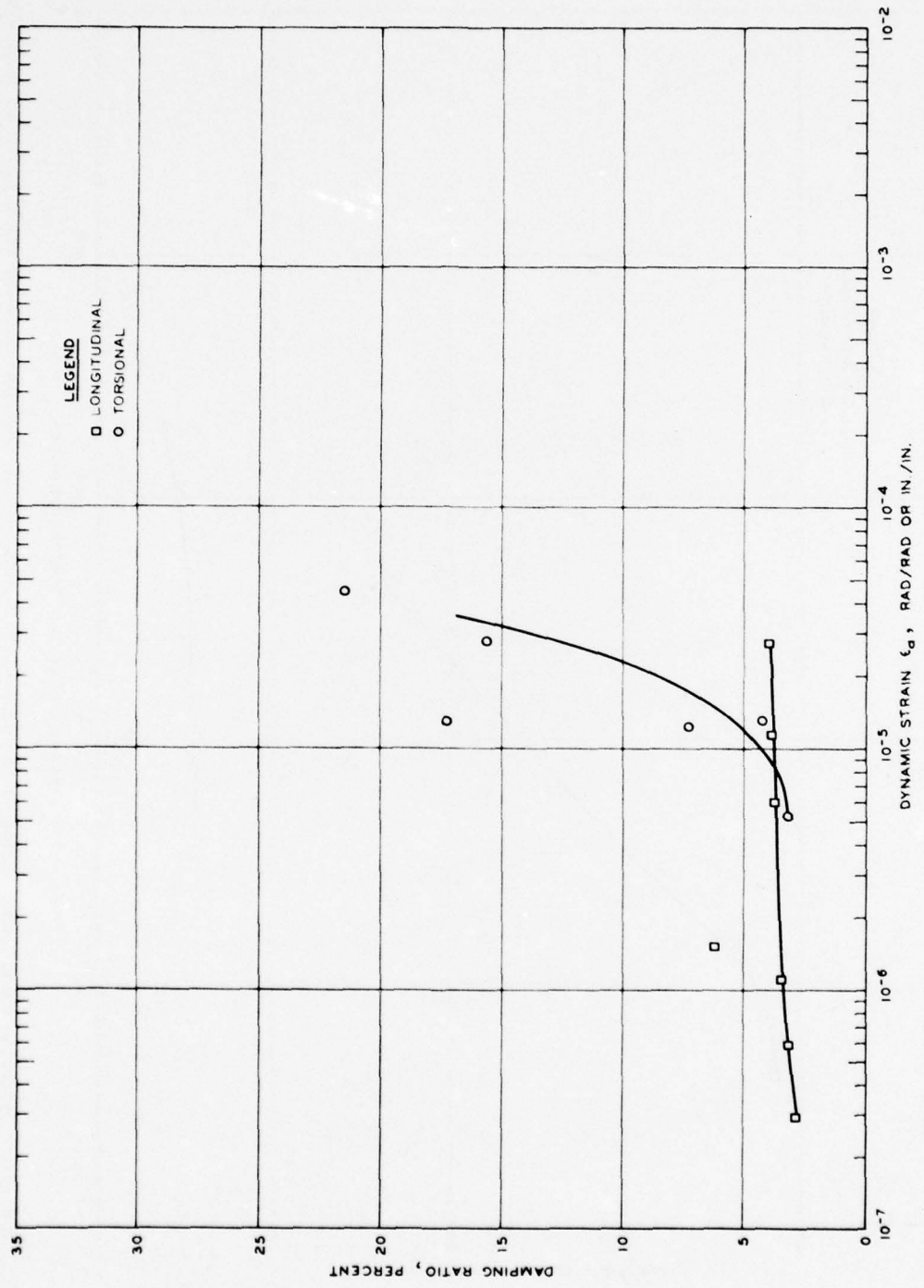


Figure B4. Damping as a function of 0-peak strain amplitude as determined by resonant column testing, sample: 800 UD No. 13-2

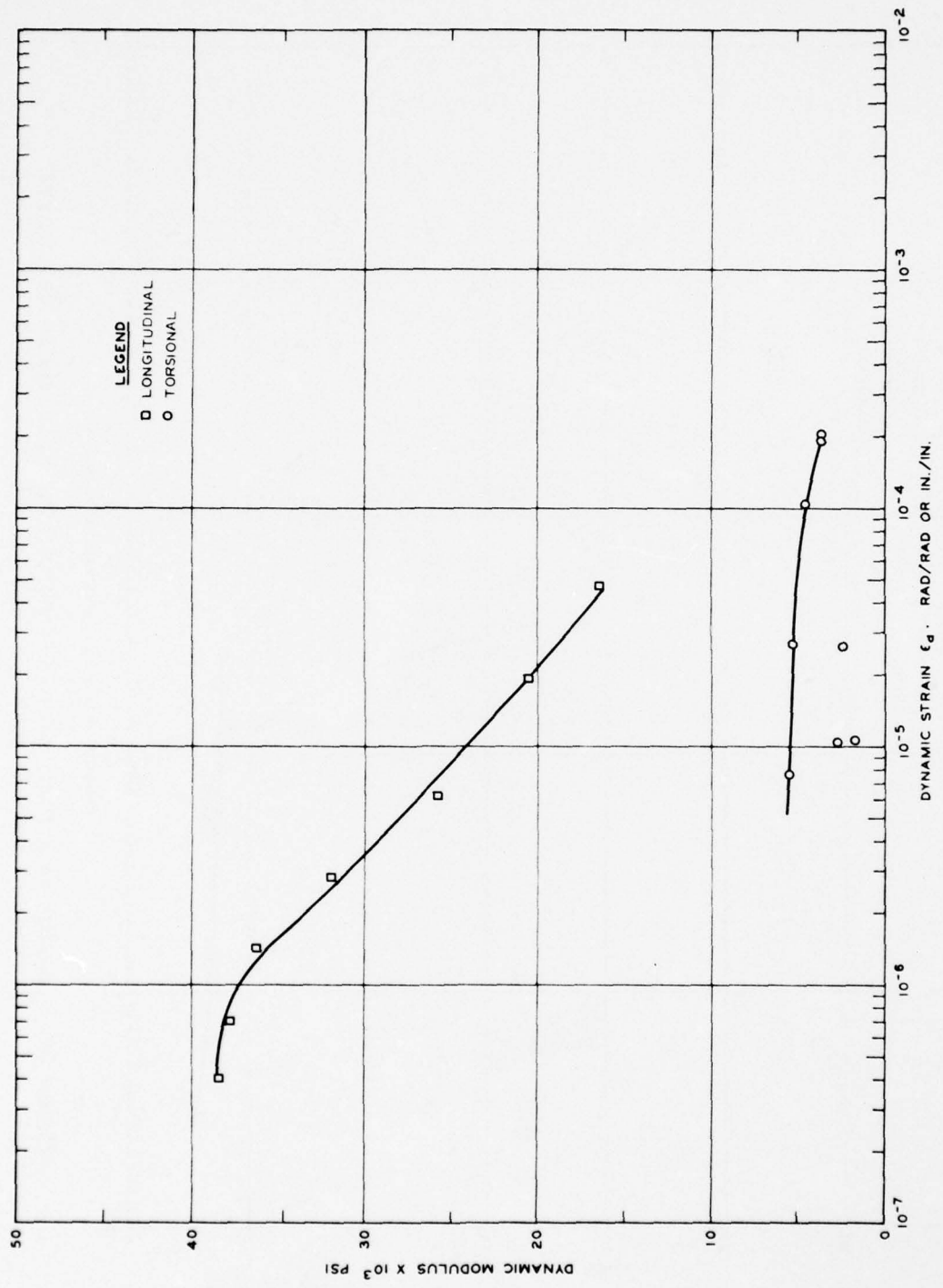


Figure B5. Dynamic shear and Young's moduli as a function of 0-peak strain amplitude as measured in the resonant column test, sample: 800 UD No. 20-1, $\bar{\sigma}_{oct} = 9.4$ psi, $B = 0.94$

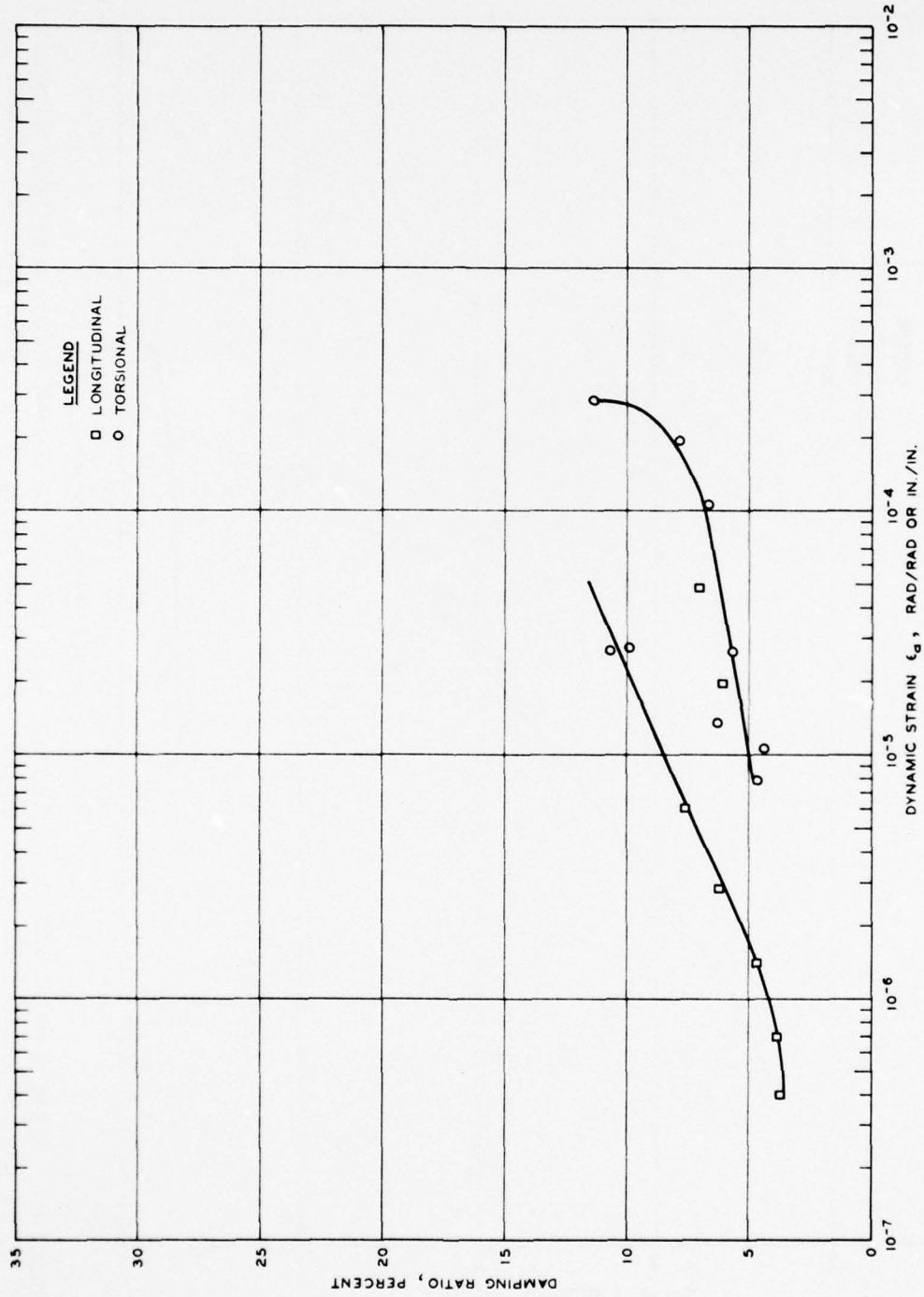


Figure B6. Damping as a function of 0-peak strain amplitude as determined by resonant column testing, sample: 800 UD No. 20-1, $\bar{\sigma}_{oct} = 9.4$ psi, $B = 0.94$

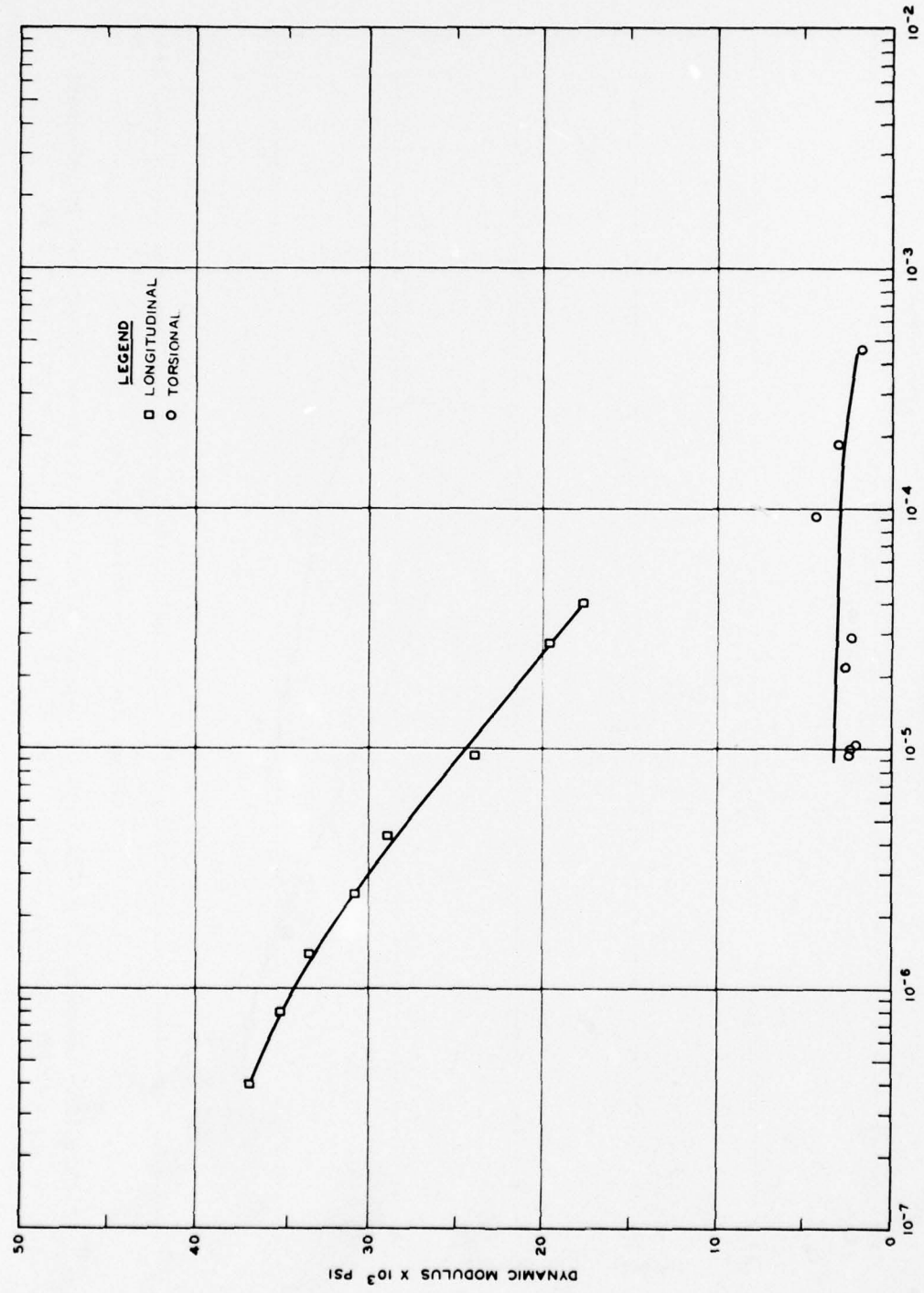


Figure B7. Dynamic shear and Young's moduli as a function of 0-peak strain amplitude as measured in the resonant column test, sample: 800 UD No. 20-2, $\bar{\sigma}_{oct} = 10.2$ psi, $B = 0.89$

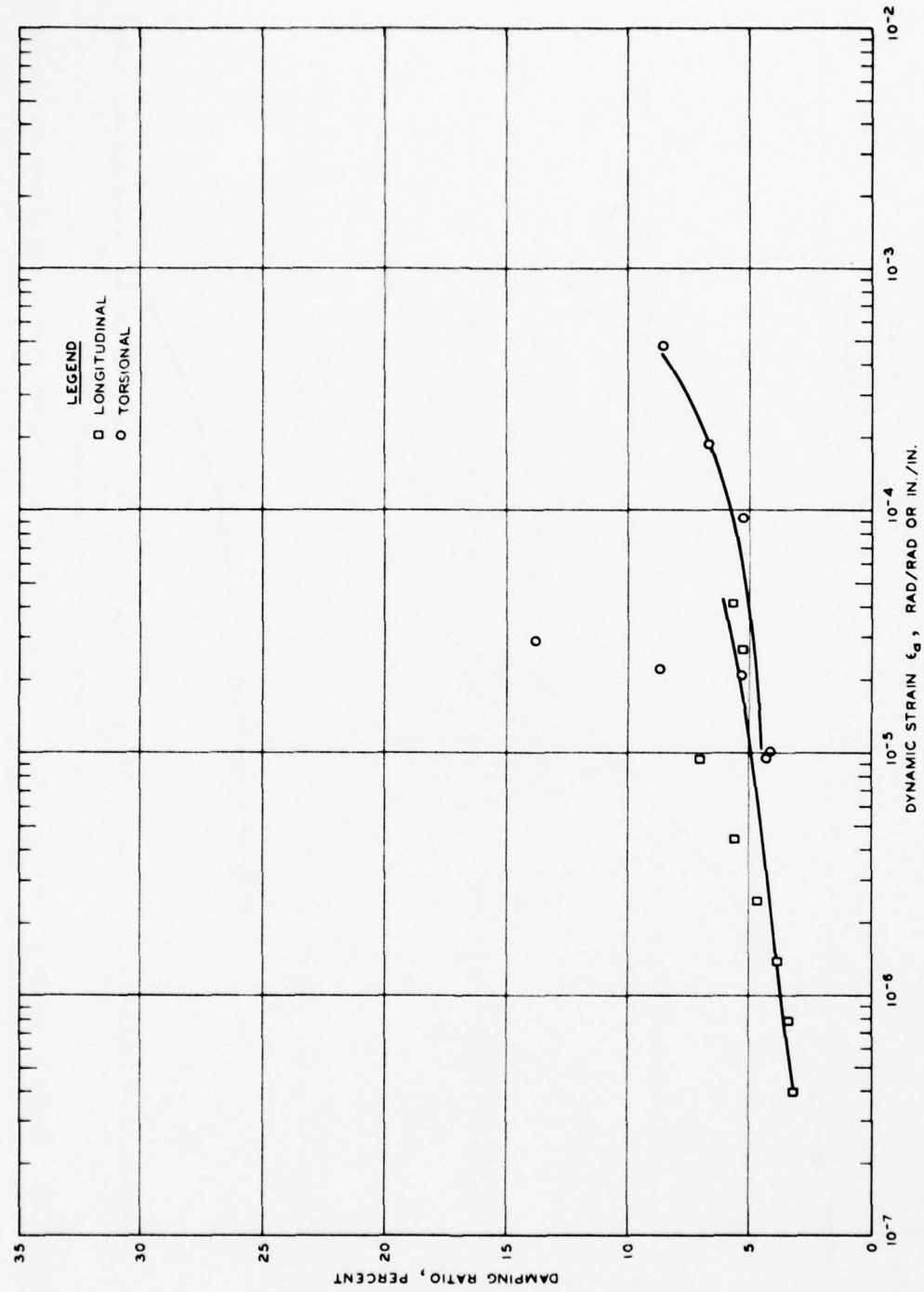


Figure B8. Damping as a function of 0-peak strain amplitude as determined by resonant column testing, sample: 800 UD No. 20-2

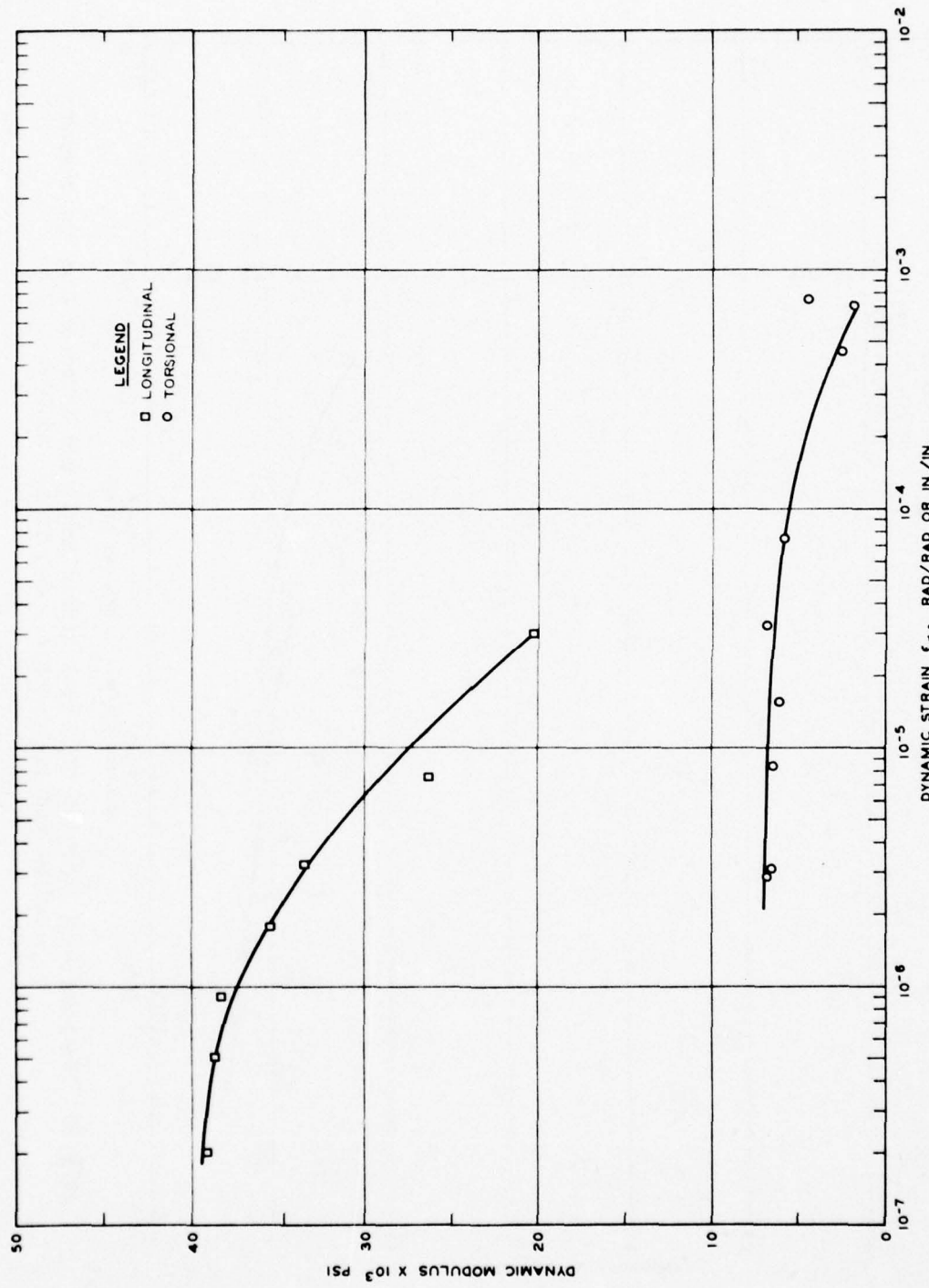


Figure B9. Dynamic shear and Young's moduli as a function of 0-peak strain amplitude as measured in the resonant column test, sample: 800 UD No. 21-1, $\bar{\sigma}_{\text{oct}} = 11 \text{ psi}$, $B = 0.94$

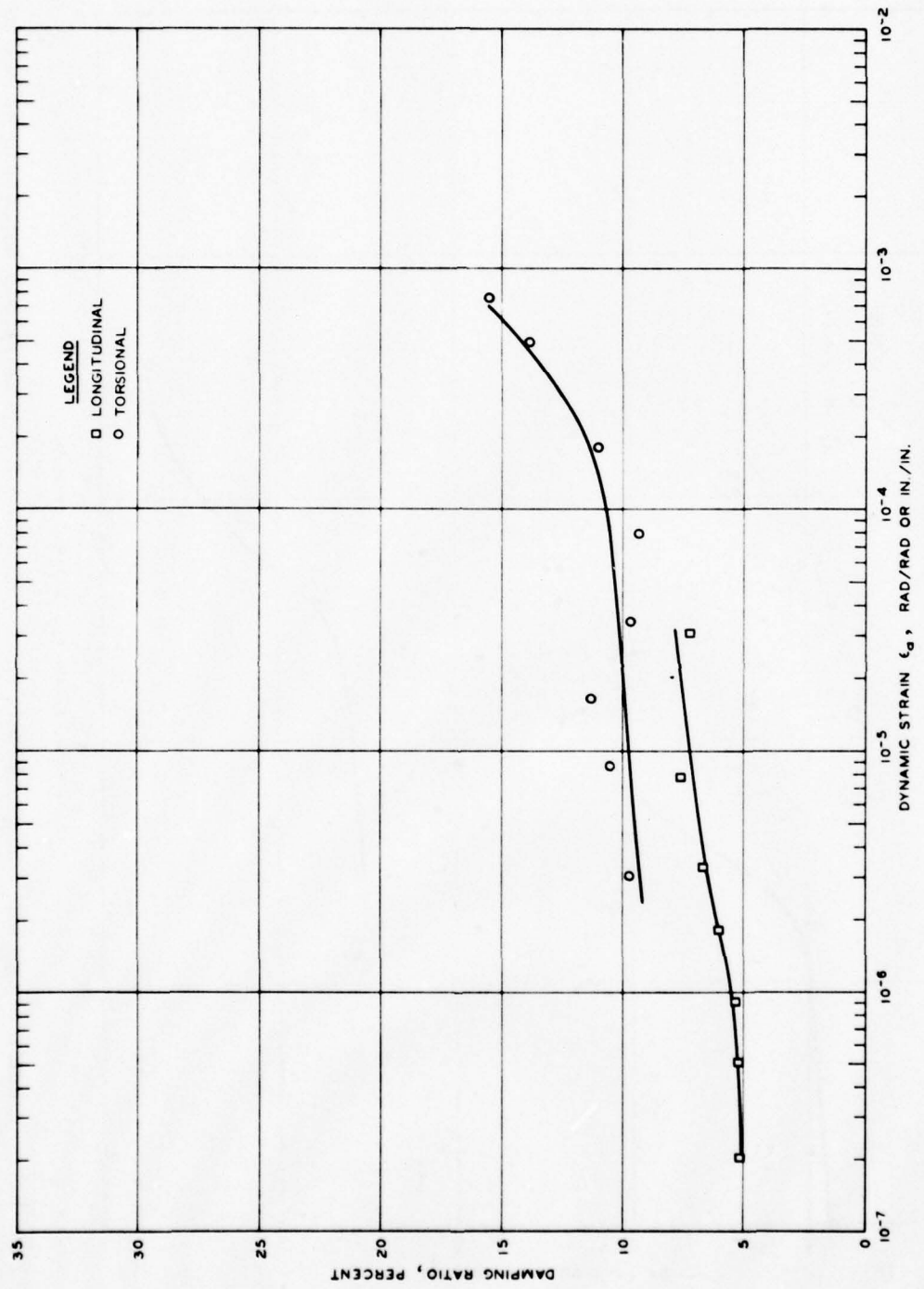


Figure B10. Damping as a function of 0-peak strain amplitude as determined by resonant column testing, sample: 800 UD No. 21-1

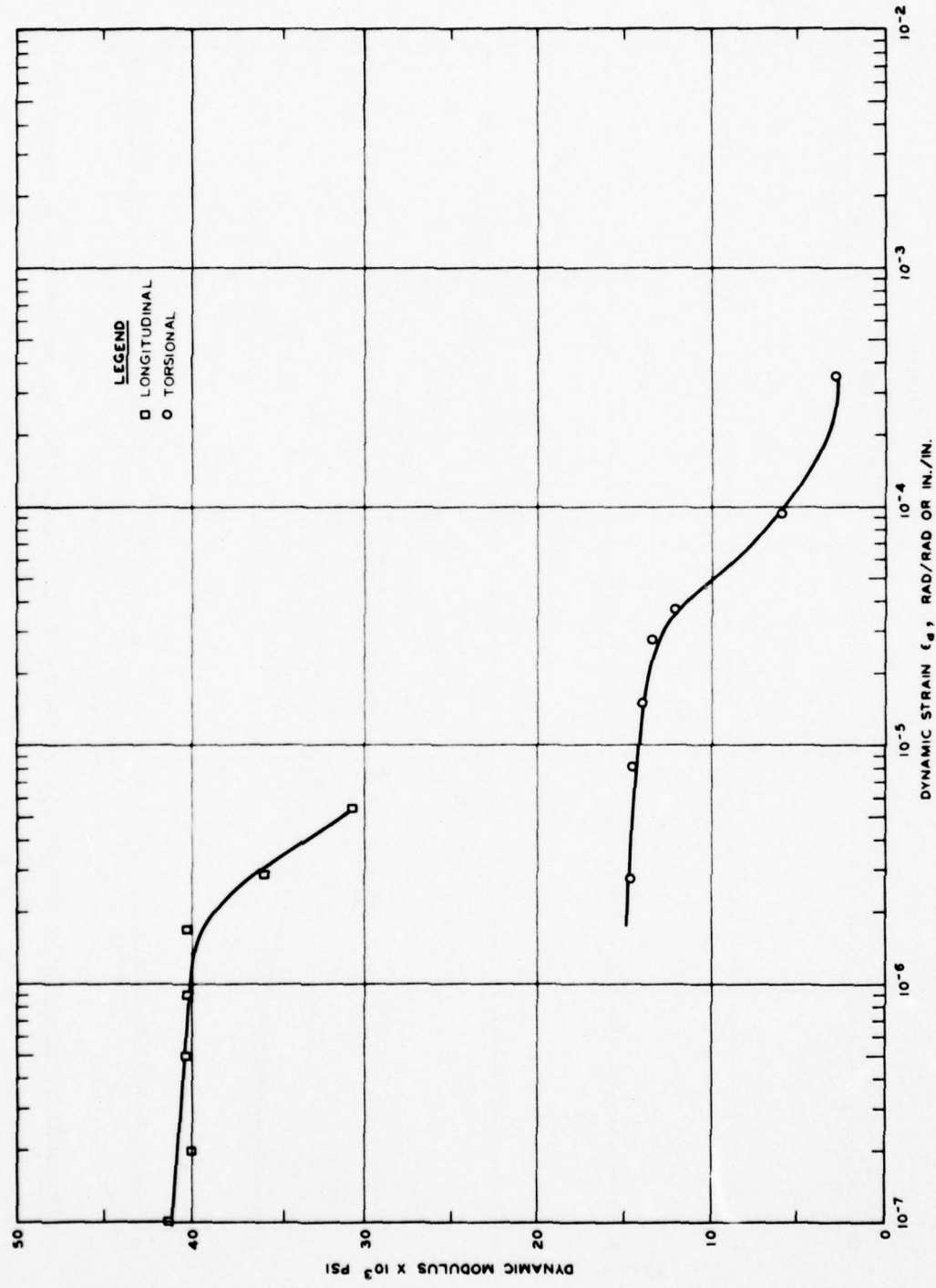


Figure B11. Dynamic shear and Young's moduli as a function of 0-peak strain amplitude as measured in the resonant column test, sample: 803 UD No. 3-1, $\bar{\sigma}_{oct} = 3$ psi, $B = ?$, nonsaturated

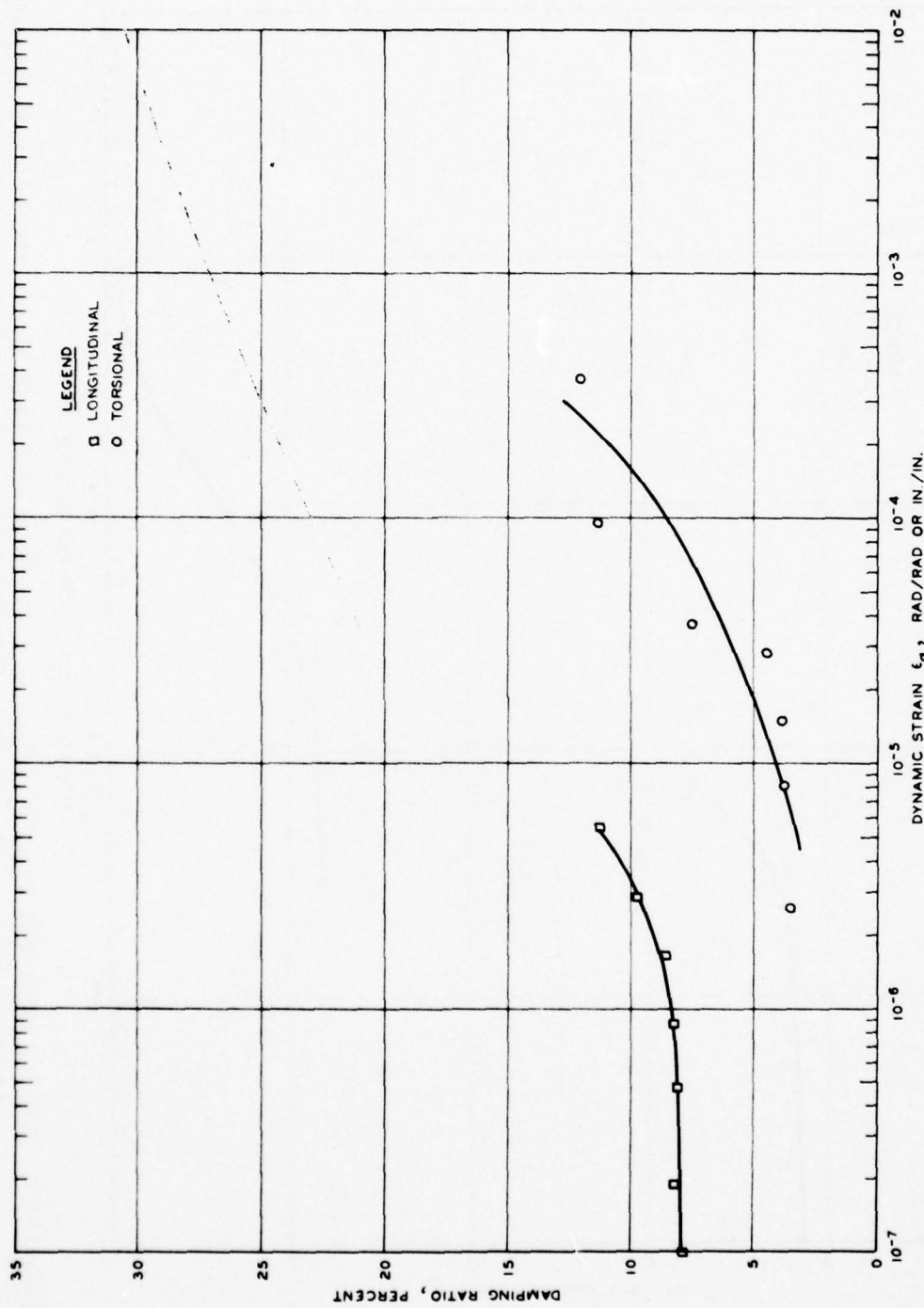


Figure B12. Damping as a function of 0-peak strain amplitude as determined by resonant column testing, sample: 803 UD No. 3-1

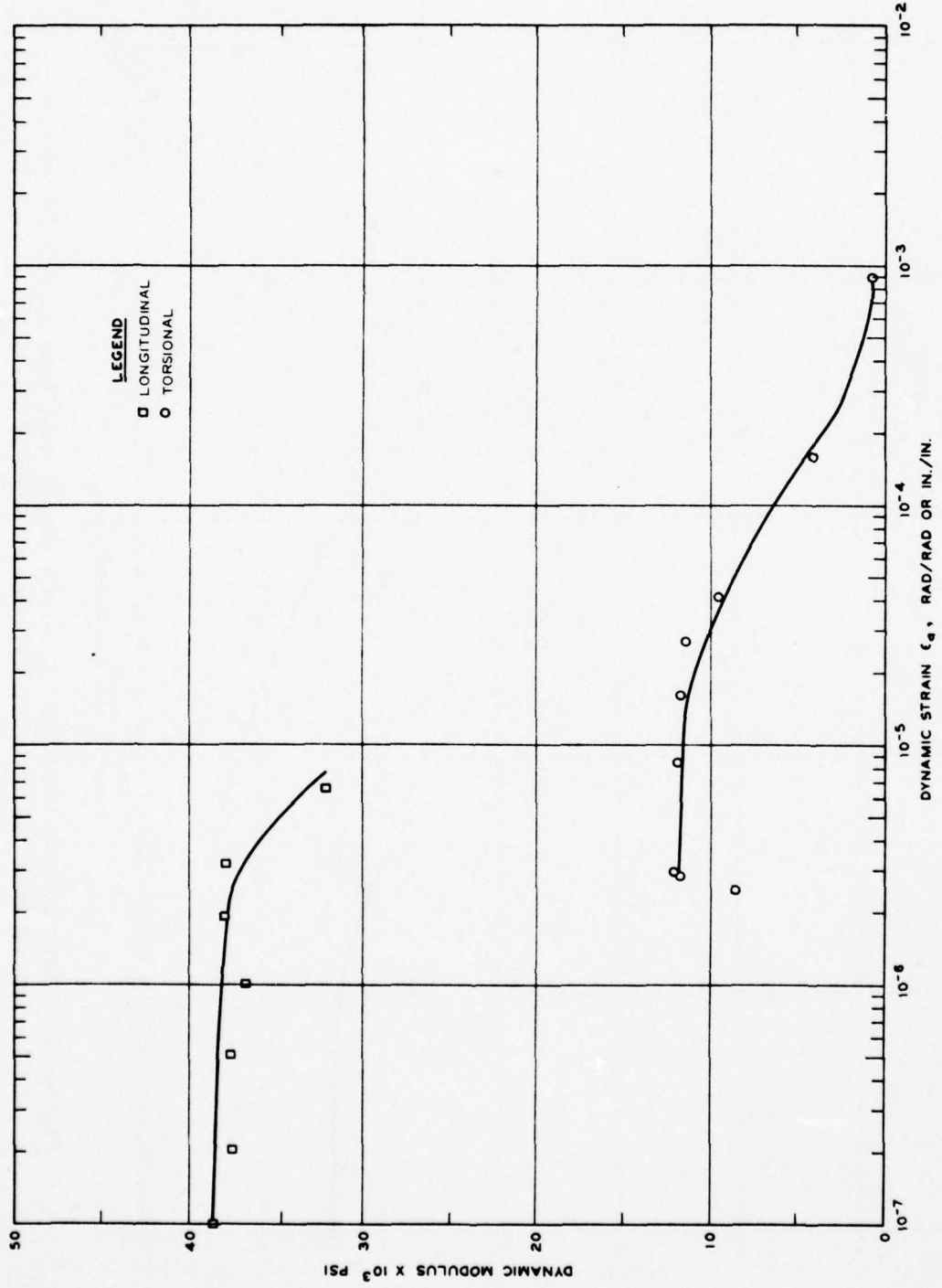


Figure B13. Dynamic shear and Young's moduli as a function of 0-peak strain amplitude as measured in the resonant column test, sample: 803 UD No. 3-2, $\frac{\sigma}{\sigma_{oct}} = 3$ psi, $B = 0.91$

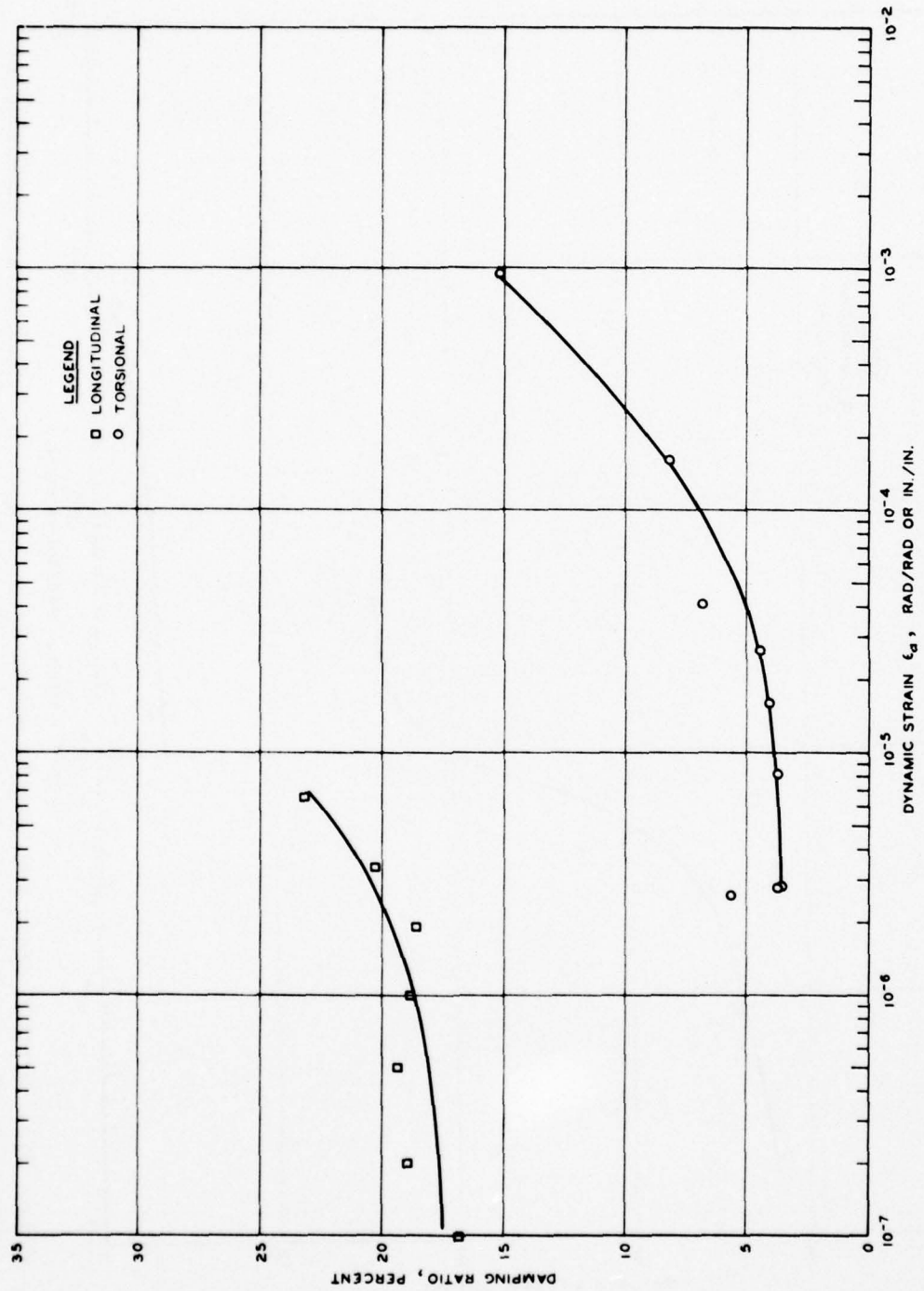


Figure Bl4. Damping as a function of 0-peak strain amplitude as determined by resonant column testing, sample: 803 UD No. 3-2

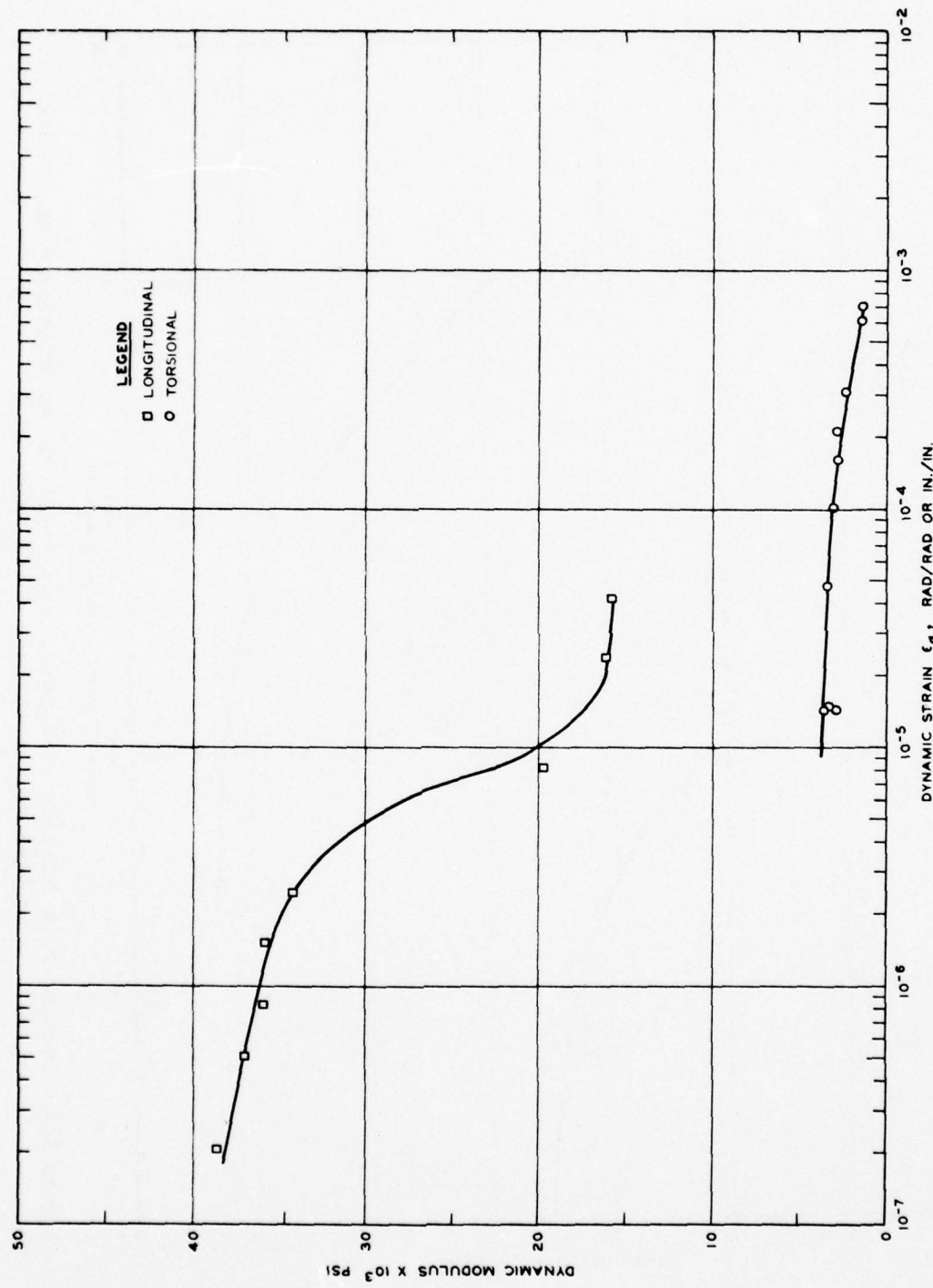


Figure B15. Dynamic shear and Young's moduli as a function of 0-peak strain amplitude as measured in the resonant column test, sample: 803 UD No. 9-2, $\bar{\sigma}_{oct} = 10.0$ psi, $B = 0.90$

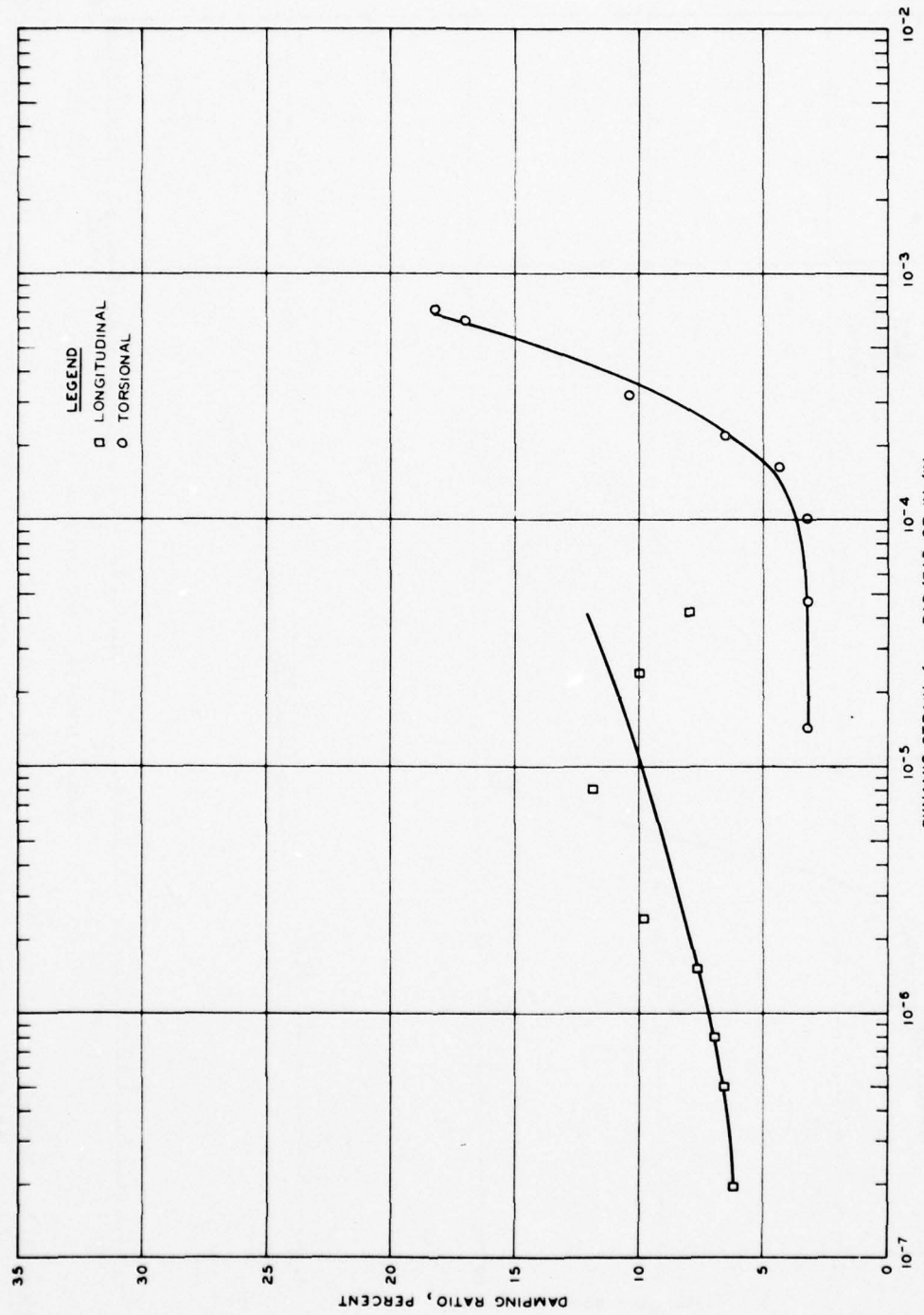


Figure B16. Damping as a function of 0-peak strain amplitude as determined by resonant column testing, sample: 803 UD No. 9-2

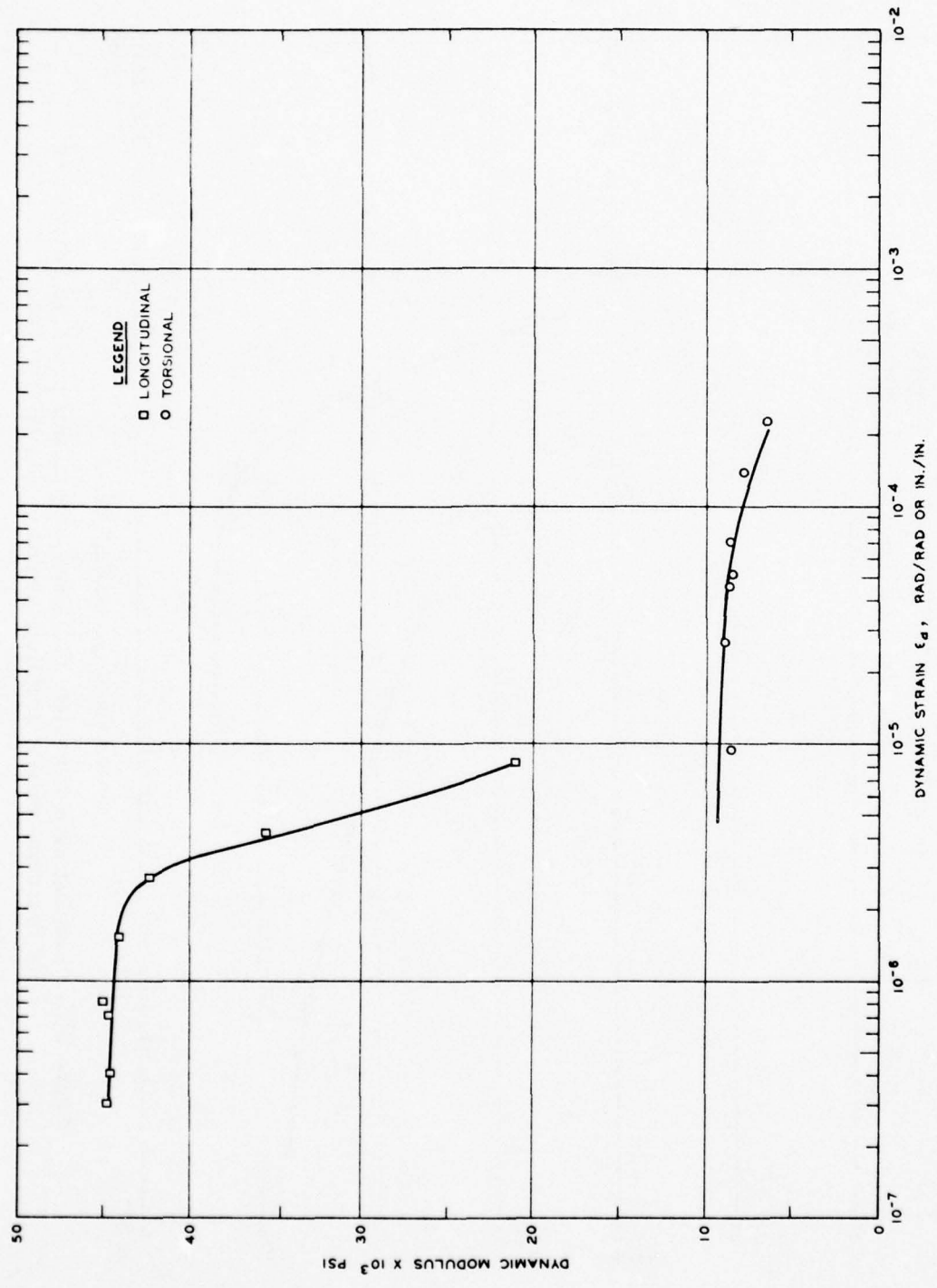


Figure B17. Dynamic shear and Young's moduli as a function of 0-peak strain amplitude as measured in the resonant column test, sample: 806 UD No. 3-1, $\bar{\sigma}_{oct} = 5.4$ psi, nonsaturated

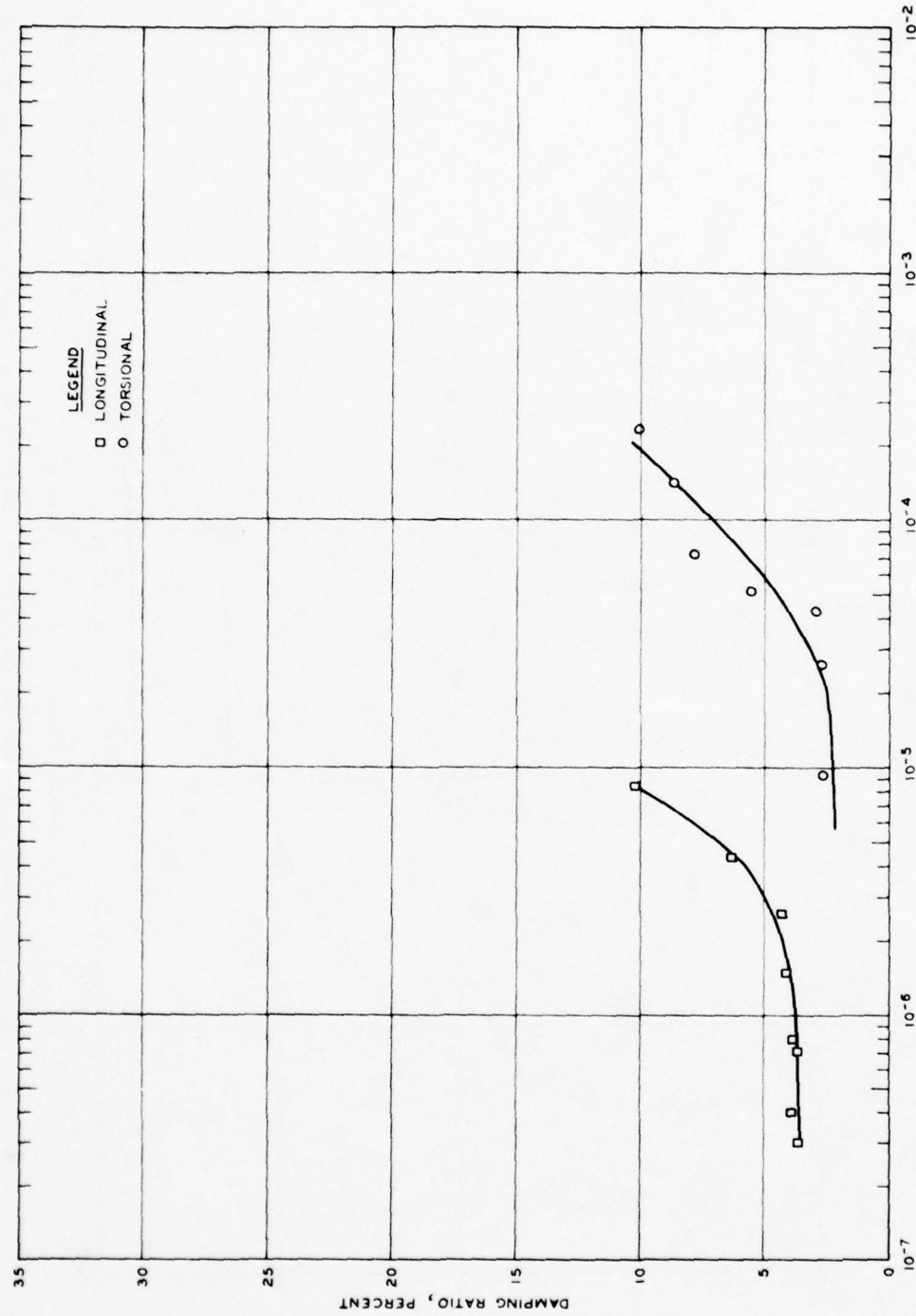


Figure B18. Damping as a function of 0-peak strain amplitude as determined by resonant column testing, sample: 806 UD No. 3-1, $\bar{\sigma}_{oct} = 5.4$ psi, nonsaturated

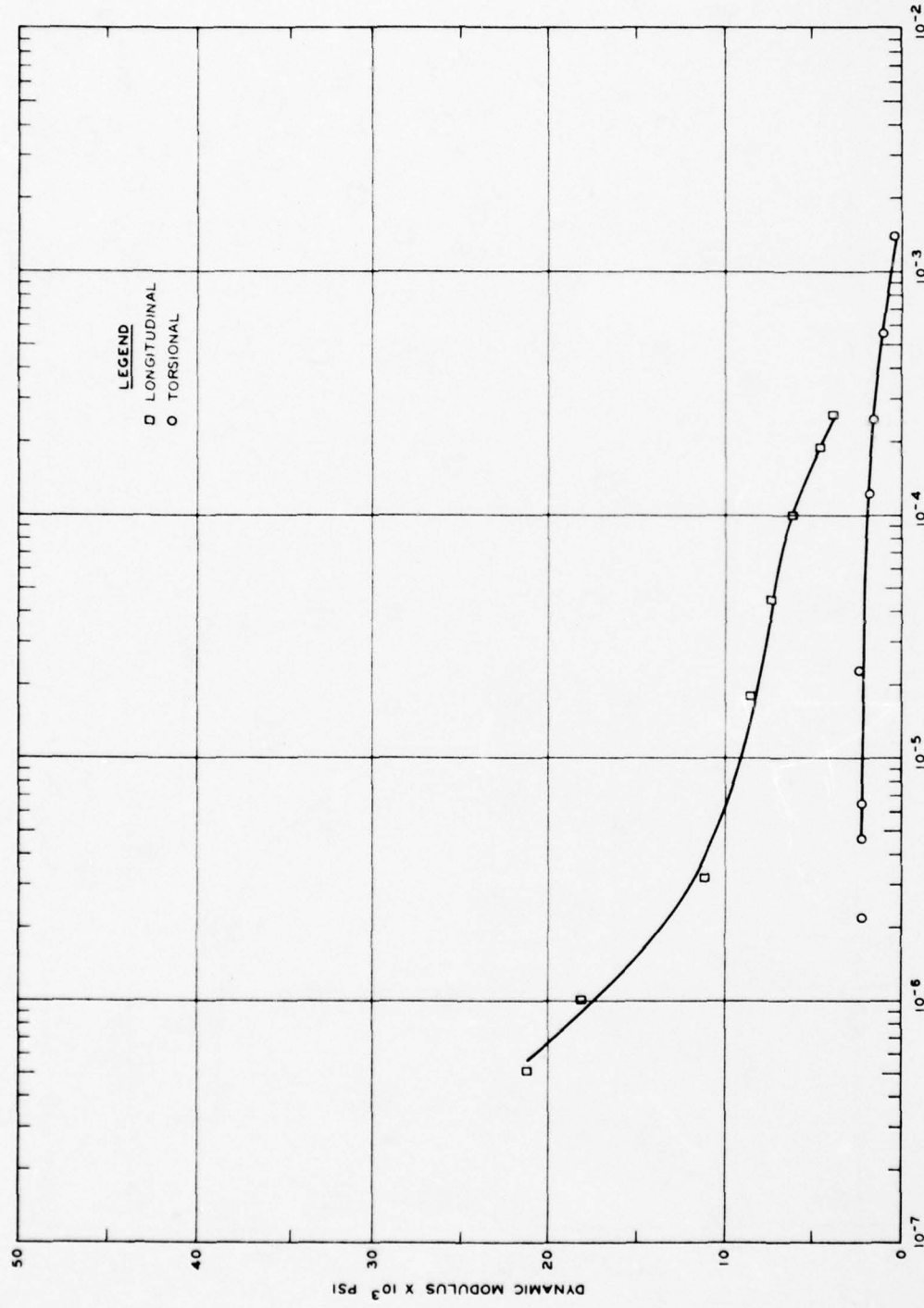


Figure B19. Dynamic shear and Young's moduli as a function of 0-peak strain amplitude as measured in the resonant column test, sample: 806 UD No. 3-2, $\bar{\sigma}_{\text{oct}} = 5.4$ psi, $B = 0.64$

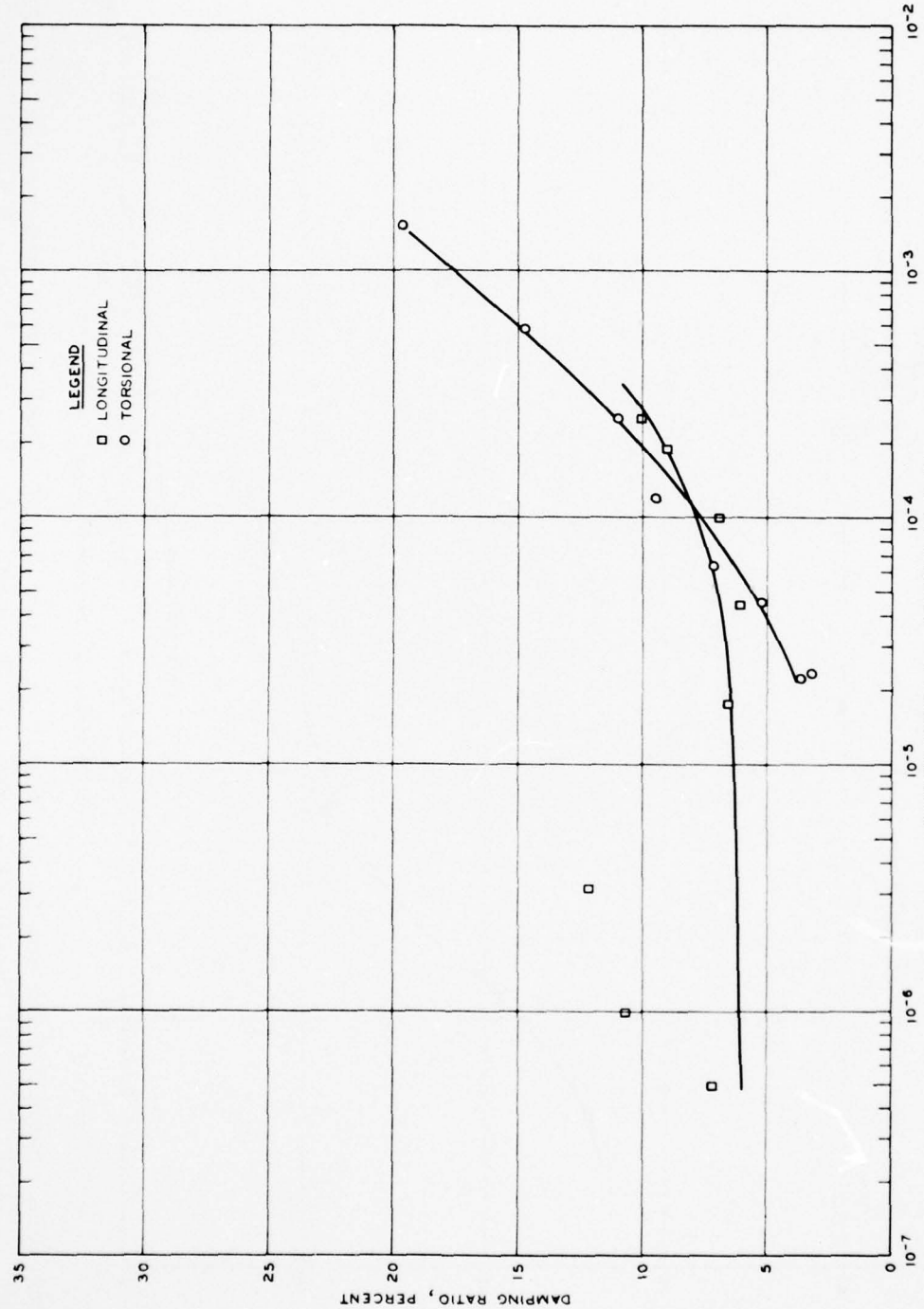


Figure B20. Damping as a function of 0-peak strain amplitude as determined by resonant column testing, sample: 806 UD No. 3-2, $\bar{\sigma}_{oct} = 5.4$ psi, $B = 0.64$

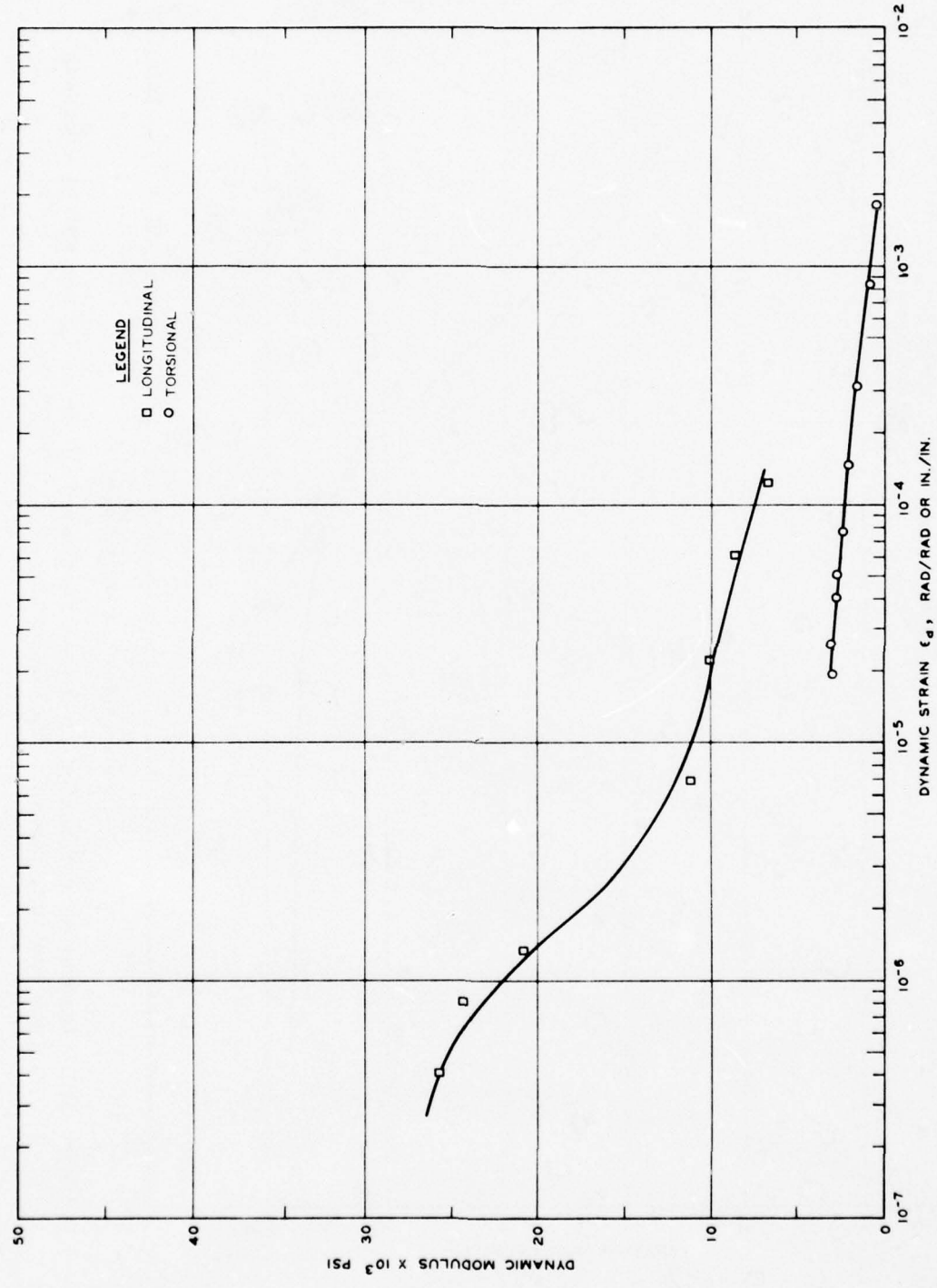


Figure B21. Dynamic shear and Young's moduli as a function of 0-peak strain amplitude as measured in the resonant column test, sample: 806 UD No. 3-3, $\bar{\sigma}_{oct} = 7.5$ psi, $B = 0.64$

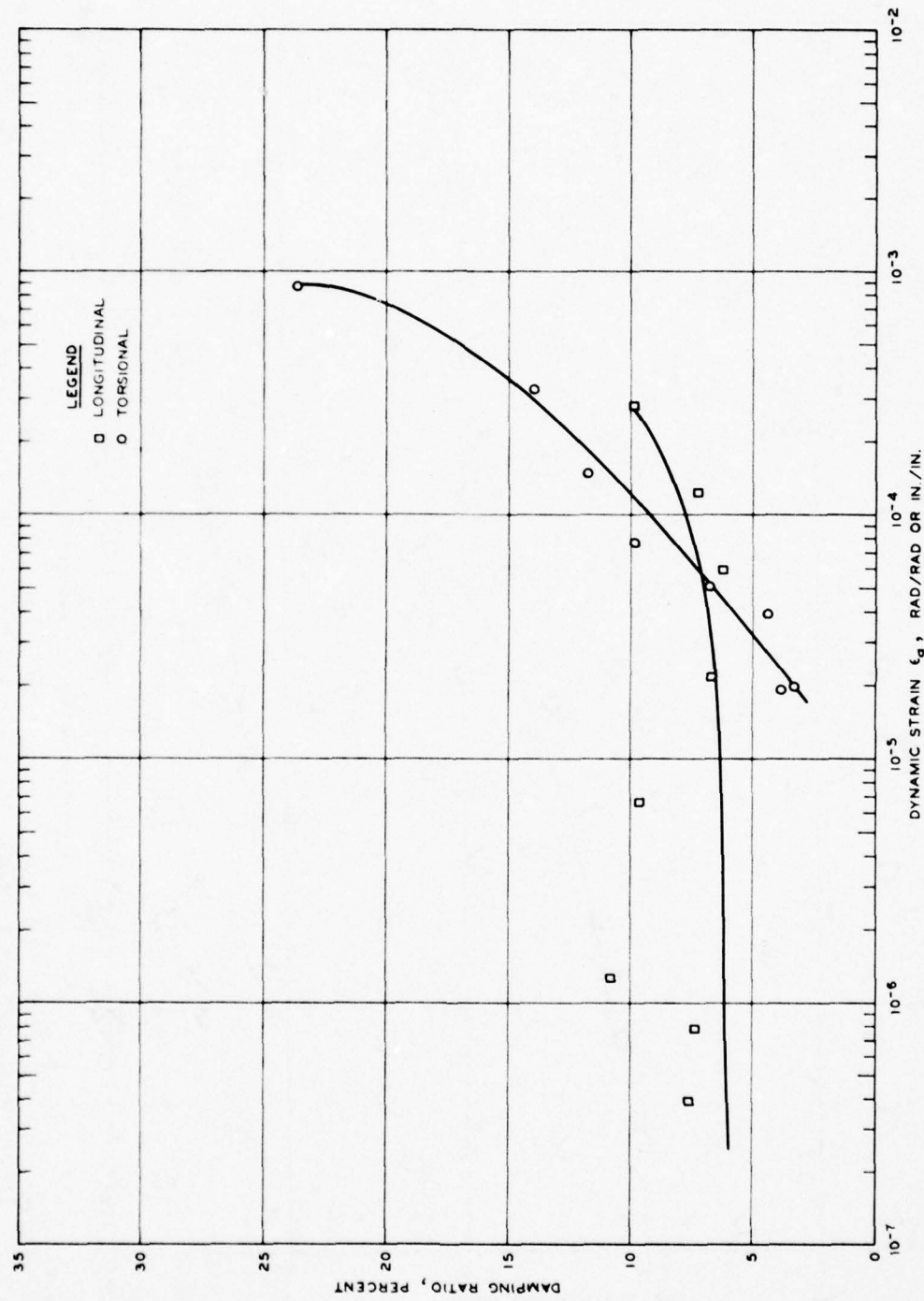


Figure B22. Damping as a function of 0-peak strain amplitude as determined by resonant column testing, sample: 806 UD No. 3-3, $\bar{\sigma}_{oct} = 7.5$ psi, $B = 0.64$

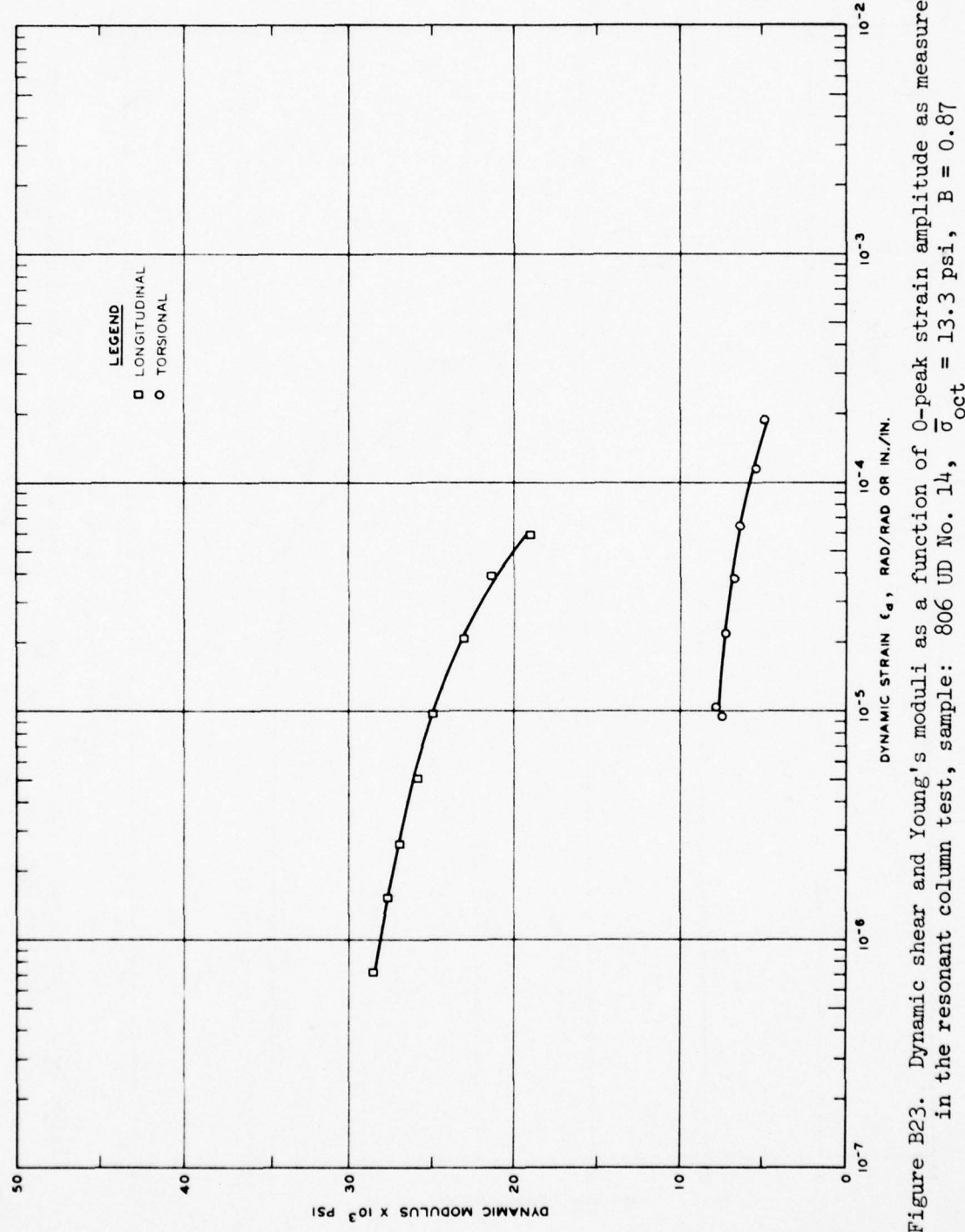


Figure B23. Dynamic shear and Young's moduli as a function of 0-peak strain amplitude as measured in the resonant column test, sample: 806 UD No. 14, $\bar{\sigma}_{oct} = 13.3$ psi, $B = 0.87$

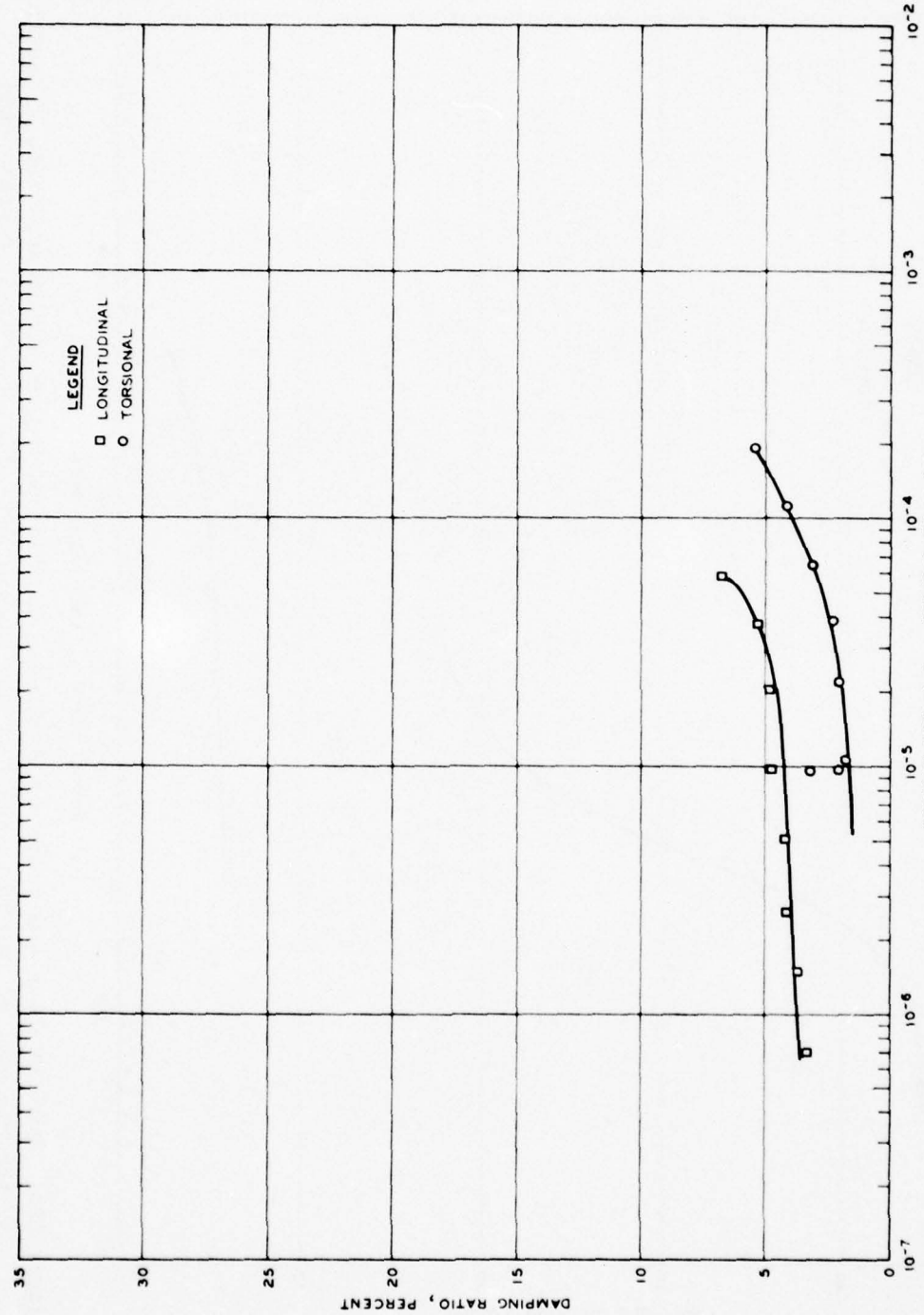


Figure B24. Damping as a function of 0-peak strain amplitude as determined by resonant column testing, sample: 806 UD No. 14, $\bar{\sigma}_{oct} = 13.3$ psi, $B = 0.87$

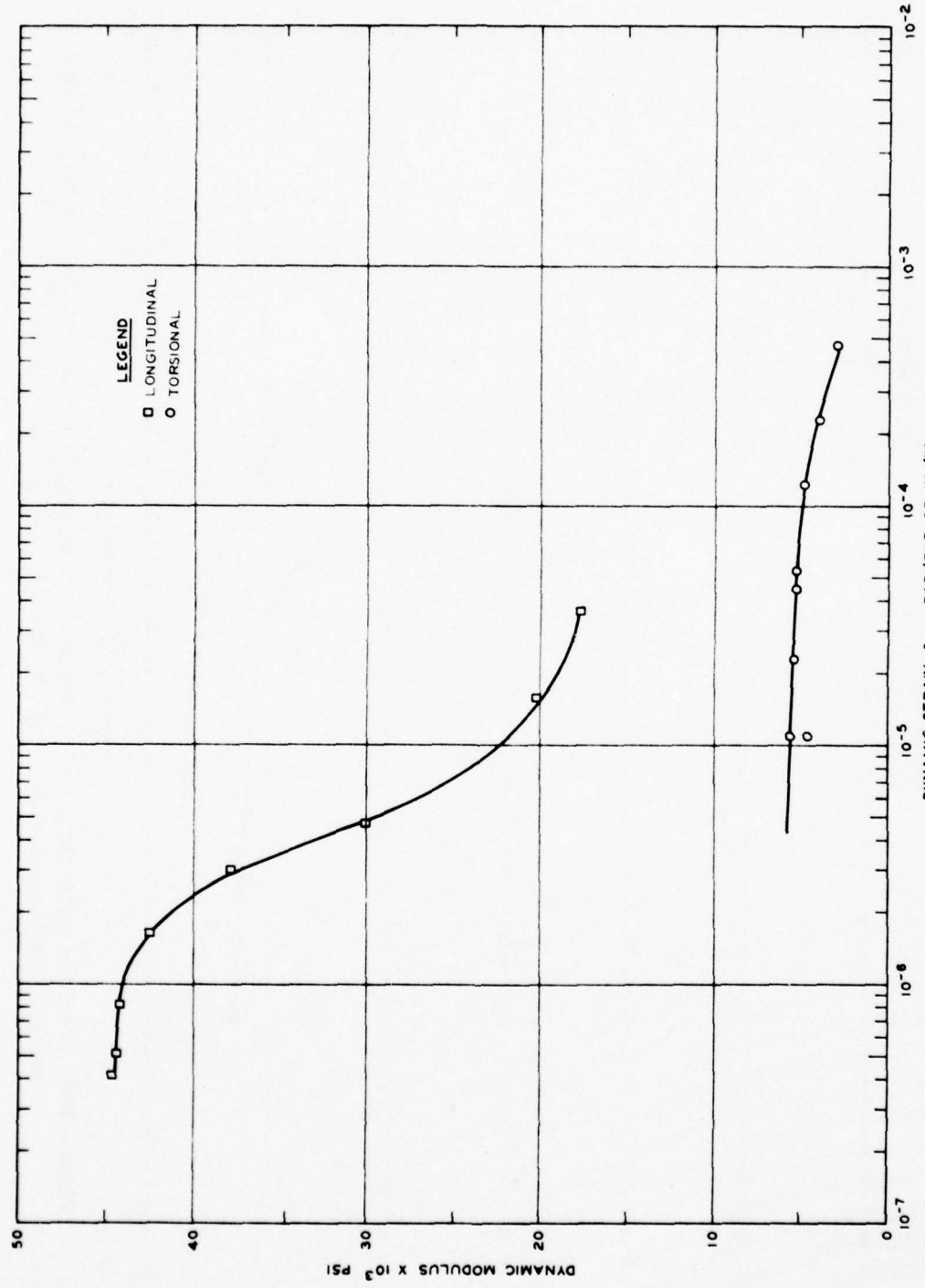


Figure B25. Dynamic shear and Young's moduli as a function of 0-peak strain amplitude as measured in the resonant column test, sample: 809 UD No. 2-1, $\bar{\sigma}_{oct} = 2.3$ psi, nonsaturated

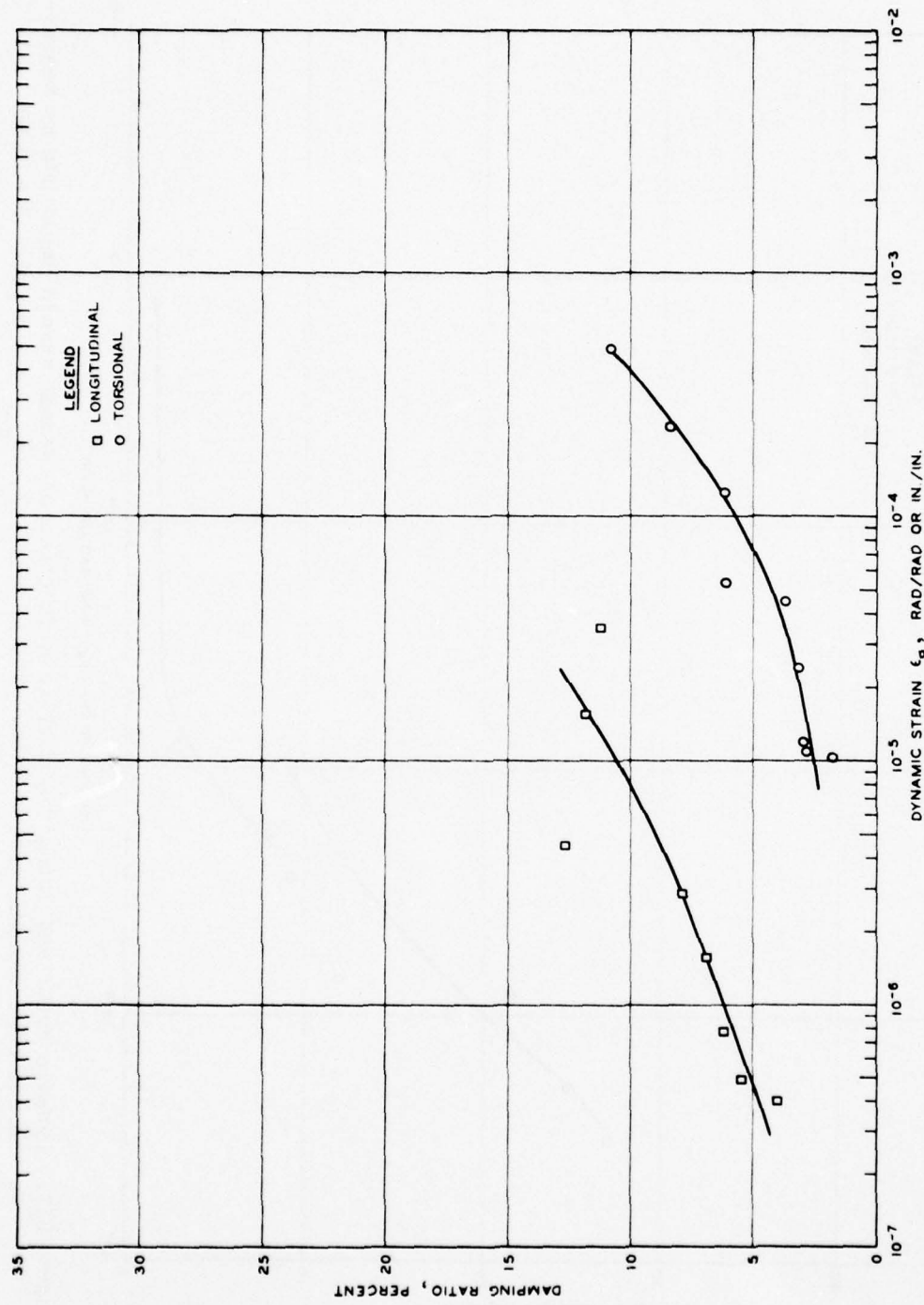


Figure B26. Damping as a function of 0-peak strain amplitude as determined by resonant column testing, sample: 809 UD No. 2-1, $\bar{\sigma}_{oct} = 2.3$ psi, nonsaturated

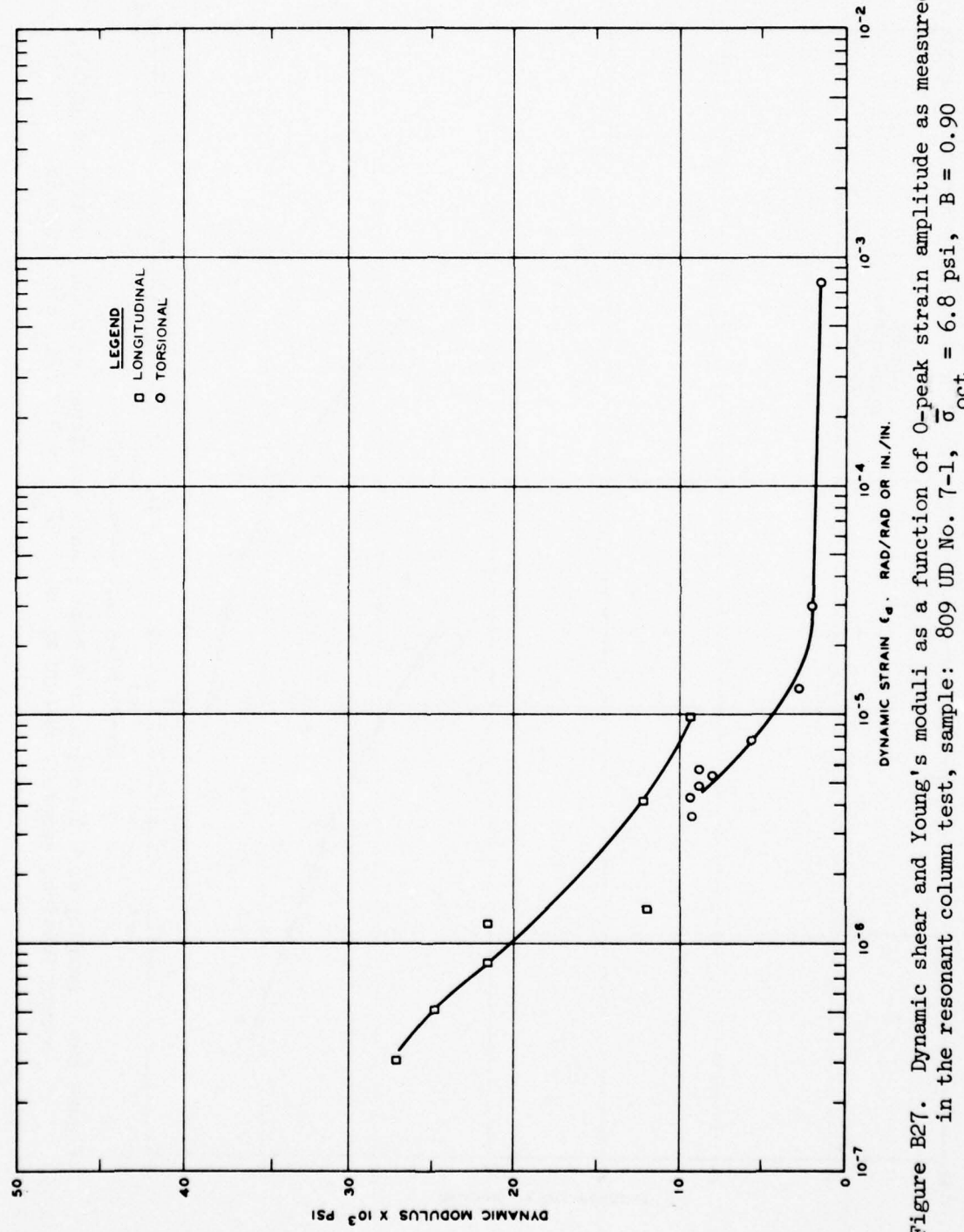


Figure B27. Dynamic shear and Young's moduli as a function of 0-peak strain amplitude as measured in the resonant column test, sample: 809 UD No. 7-1, $\bar{\sigma}_{oct} = 6.8$ psi, $B = 0.90$

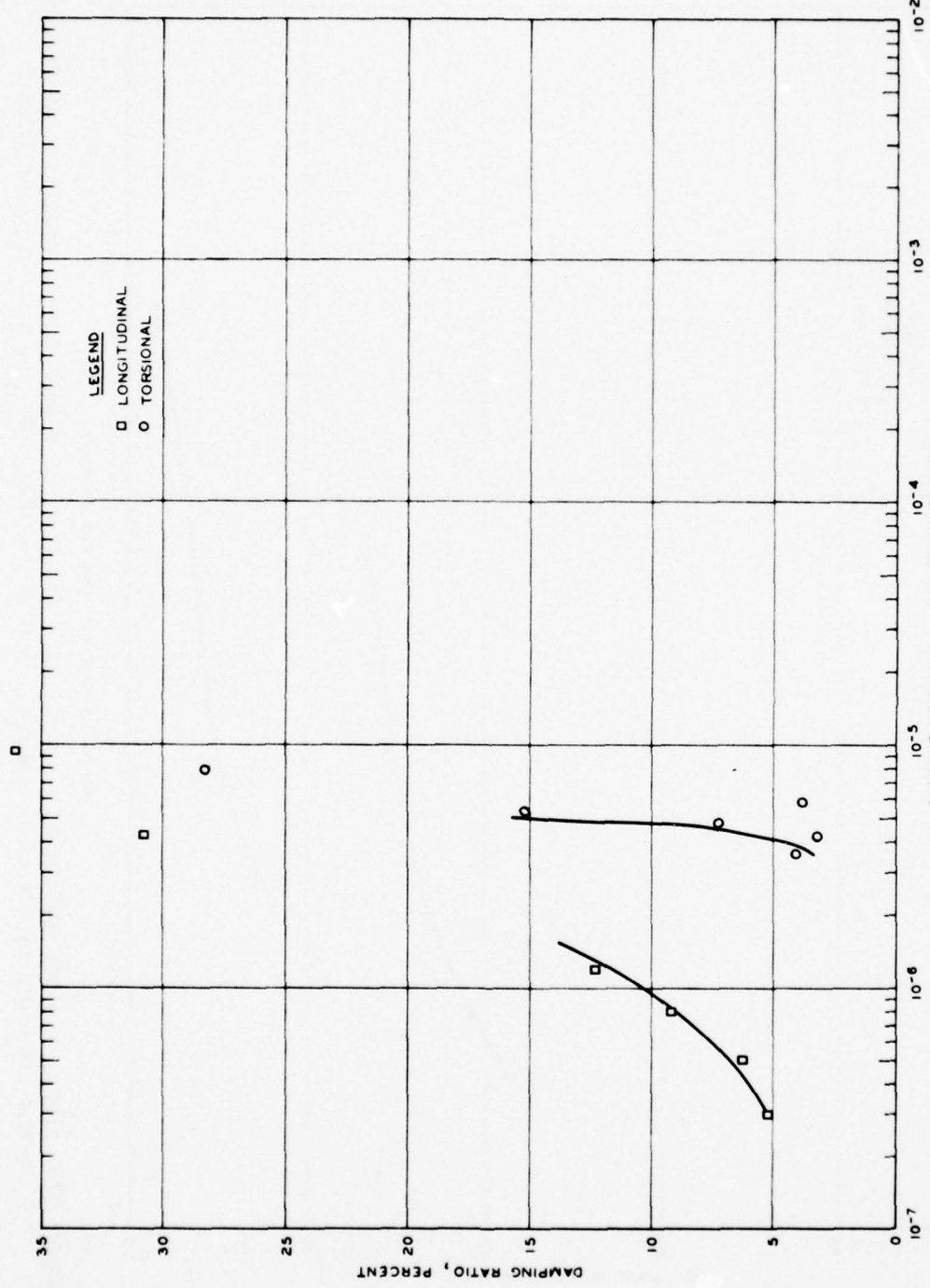


Figure B28. Damping as a function of 0-peak strain amplitude as determined by resonant column testing, sample: 809 UD No. 7-1, $\bar{\sigma}_{\text{oct}} = 6.8$ psi, $B = 0.90$

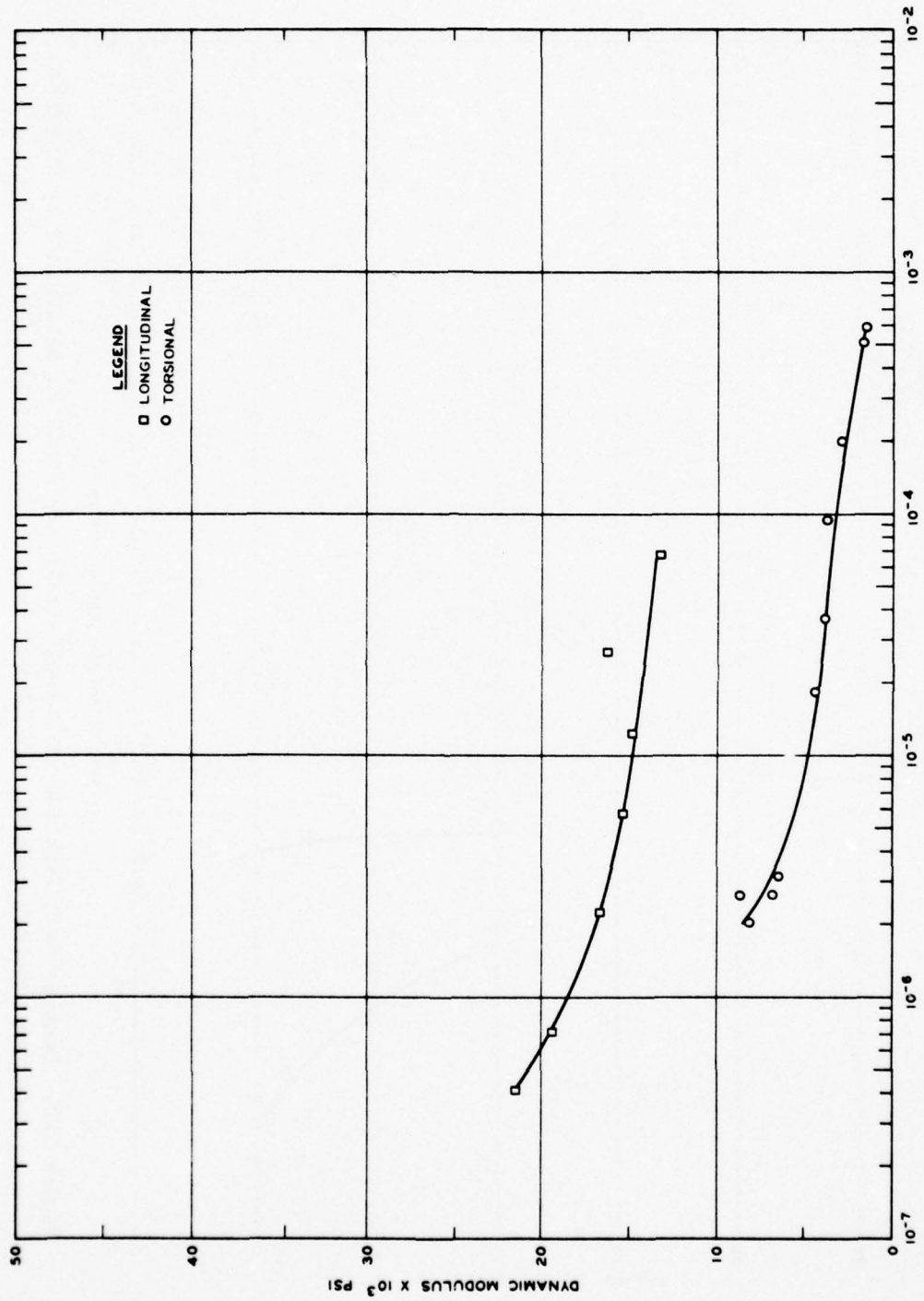


Figure B29. Dynamic shear and Young's moduli as a function of 0-peak strain amplitude as measured in the resonant column test, sample: 809 UD No. 7-2, $\bar{\sigma}_{oct} = 9.5$ psi, $B = 0.96$

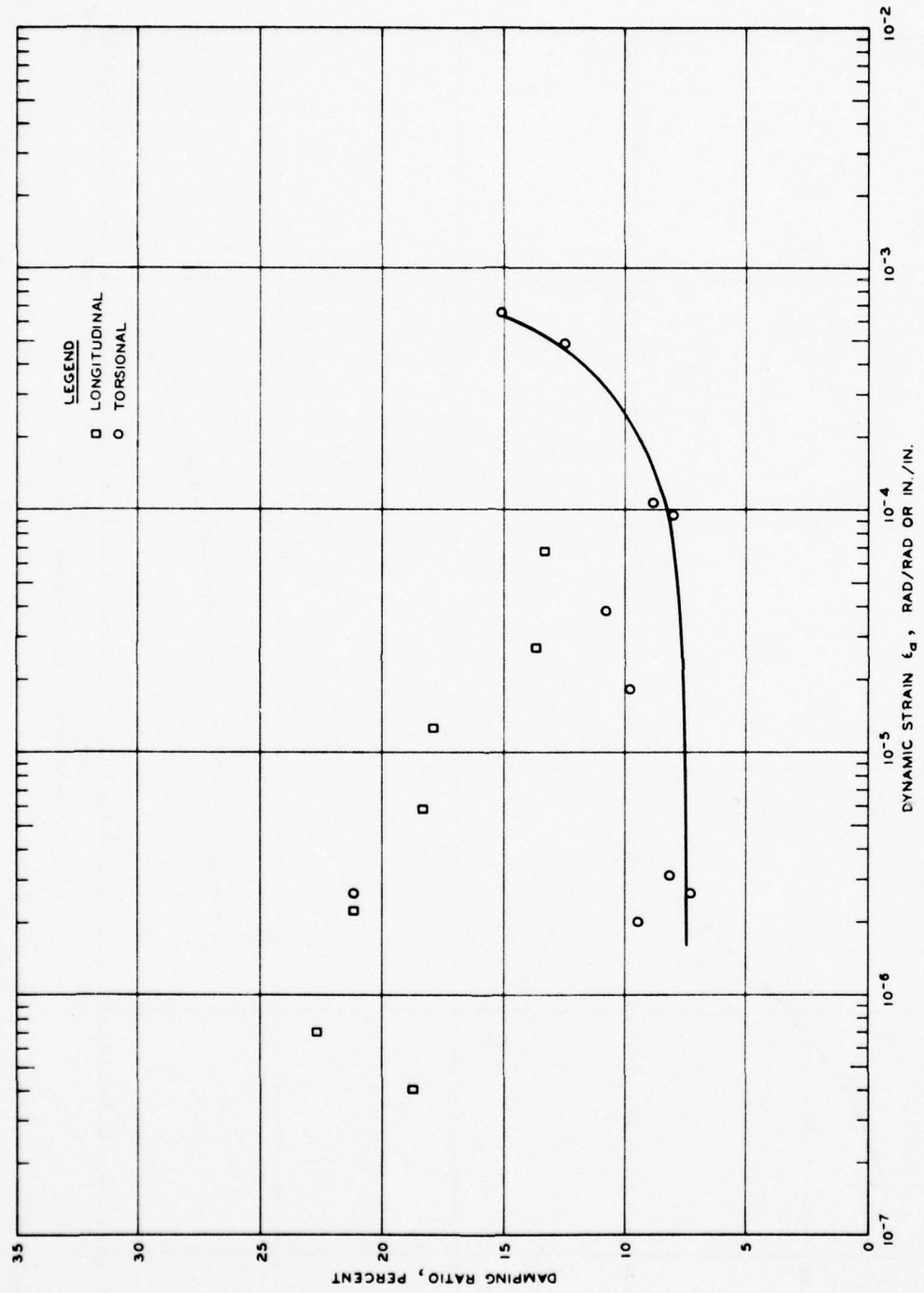


Figure B30. Damping as a function of 0-peak strain amplitude as determined by resonant column testing, sample: 809 UD No. 7-2, $\bar{\sigma}_{oct} = 9.5$ psi, $B = 0.96$

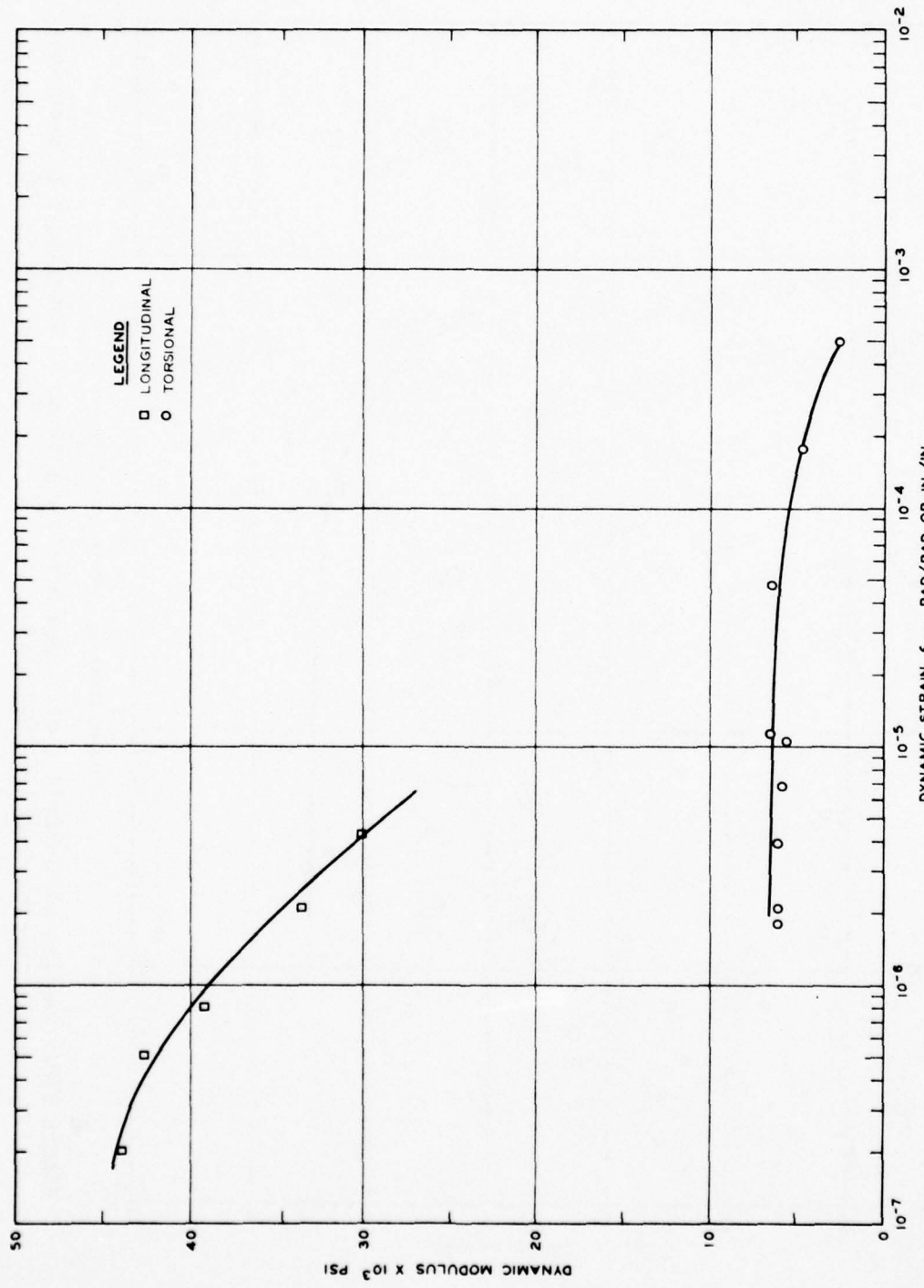


Figure B31. Dynamic shear and Young's moduli as a function of 0-peak strain amplitude as measured in the resonant column test, sample: 809 UD No. 11-1, $\bar{\sigma}_{oct} = 10.2$ psi, $B = 0.88$

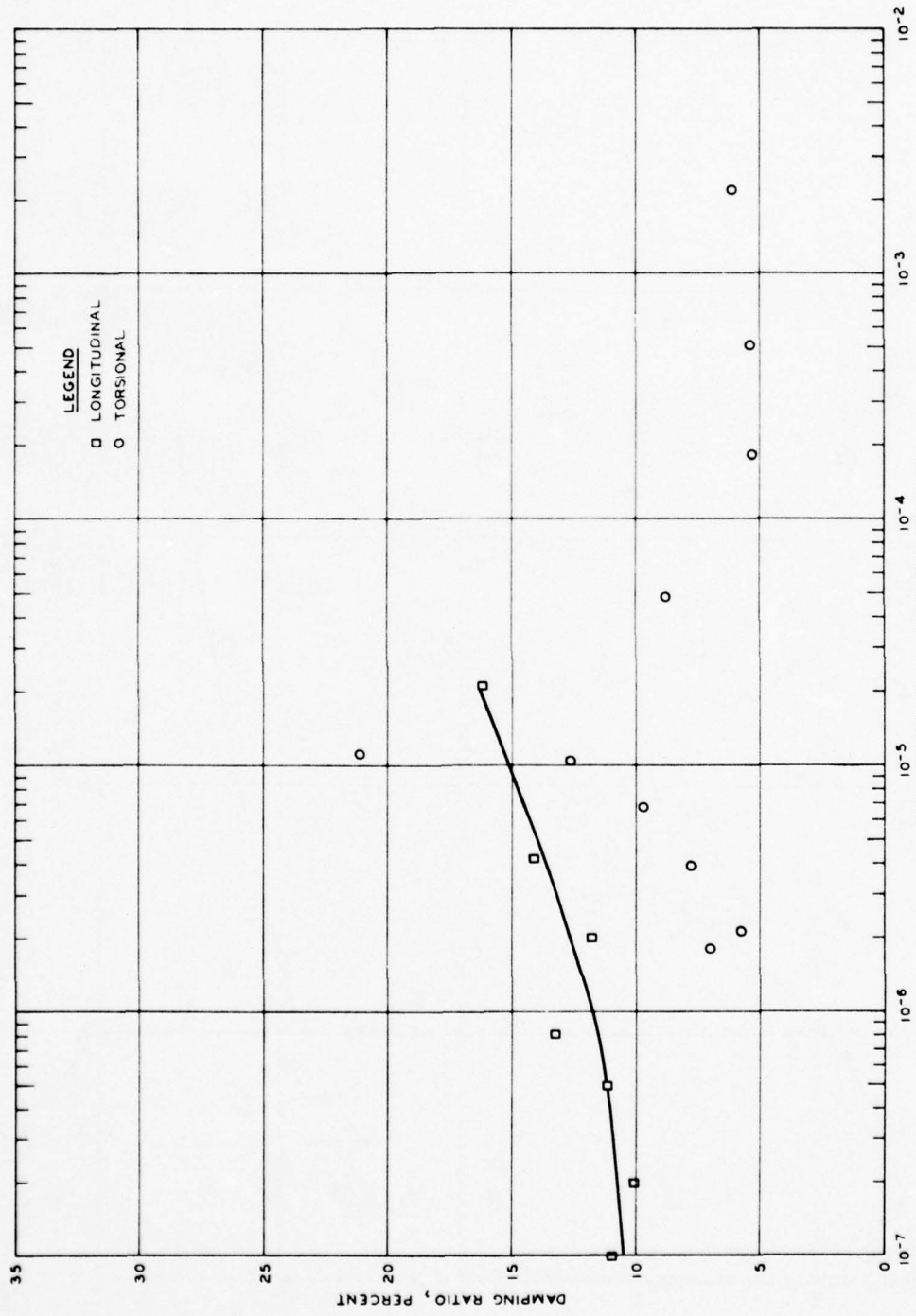


Figure B32. Damping as a function of 0-peak strain amplitude as determined by resonant column testing, sample: 809 UD No. 11-1, $\bar{\sigma}_{oct} = 10.2$ psi, $B = 0.88$

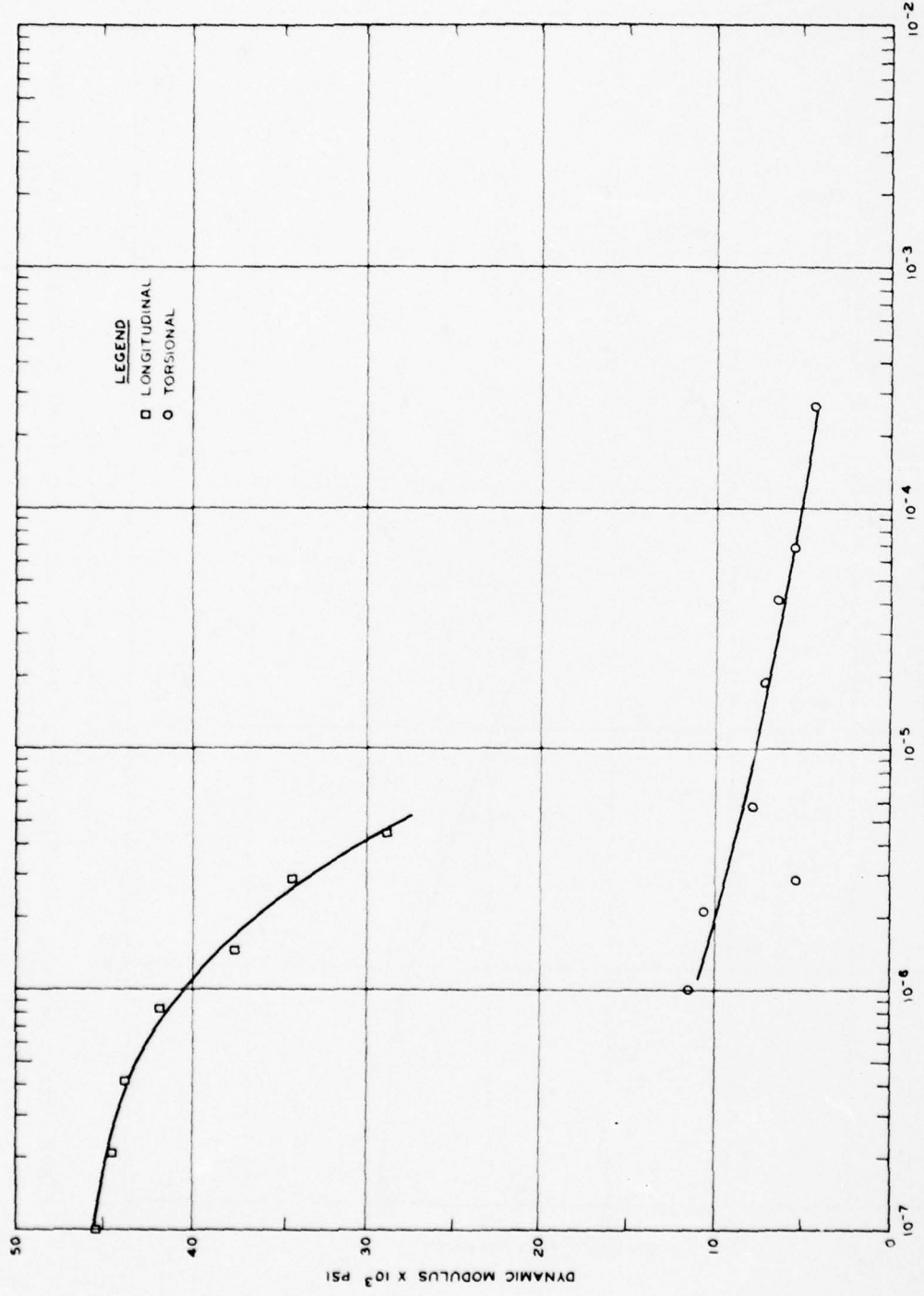


Figure B33. Dynamic shear and Young's moduli as a function of 0-peak strain amplitude measured in the resonant column test, sample: 809 UD No. 11-2, $\bar{\sigma}_{oct} = 12.6$ psi, $B = 0.5$

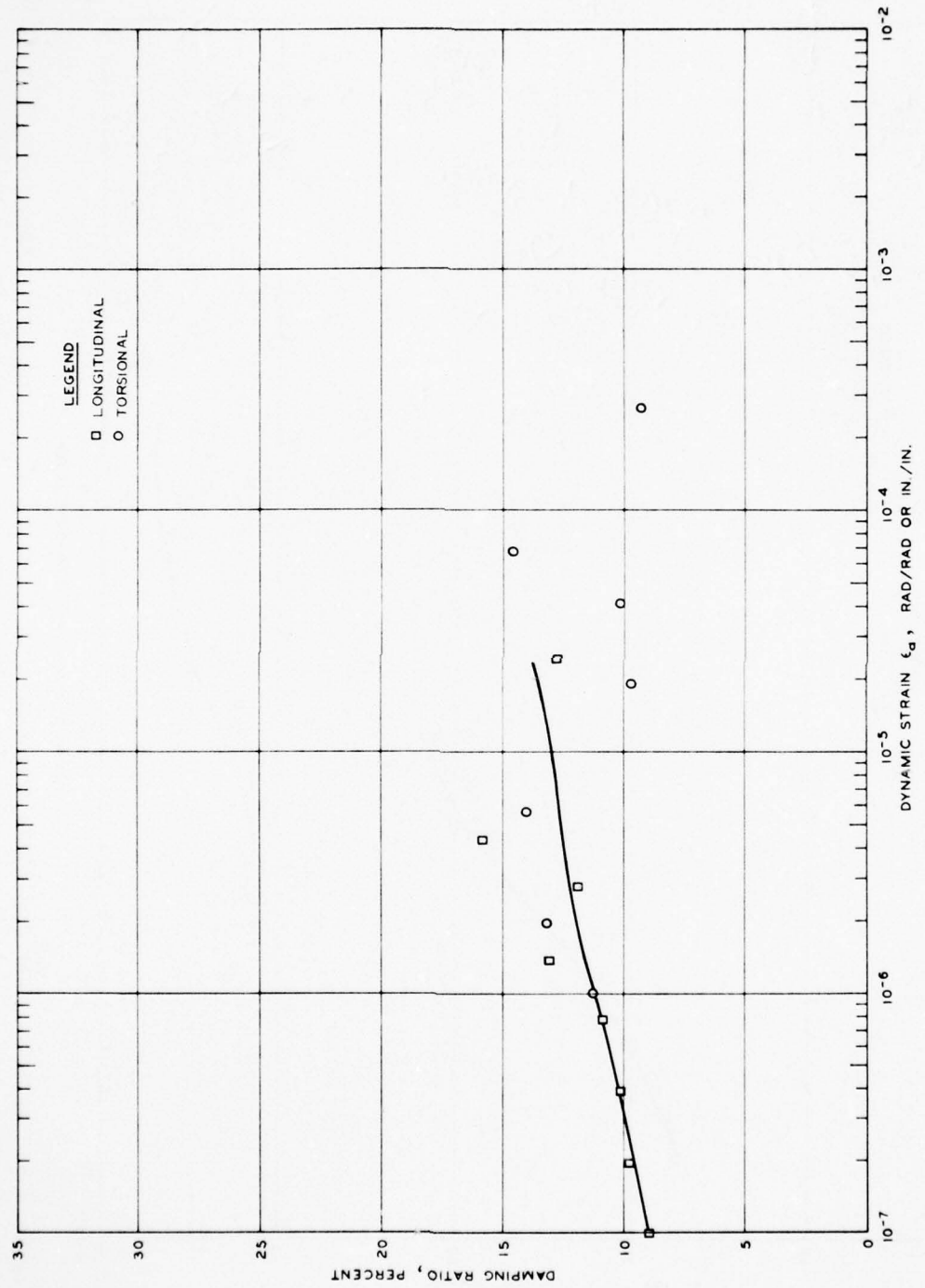


Figure B34. Damping as a function of 0-peak strain amplitude as determined by resonant column testing, sample: 809 UD No. 11-2, $\bar{\sigma}_{oct} = 12.6$ psi, $B = 0.88$

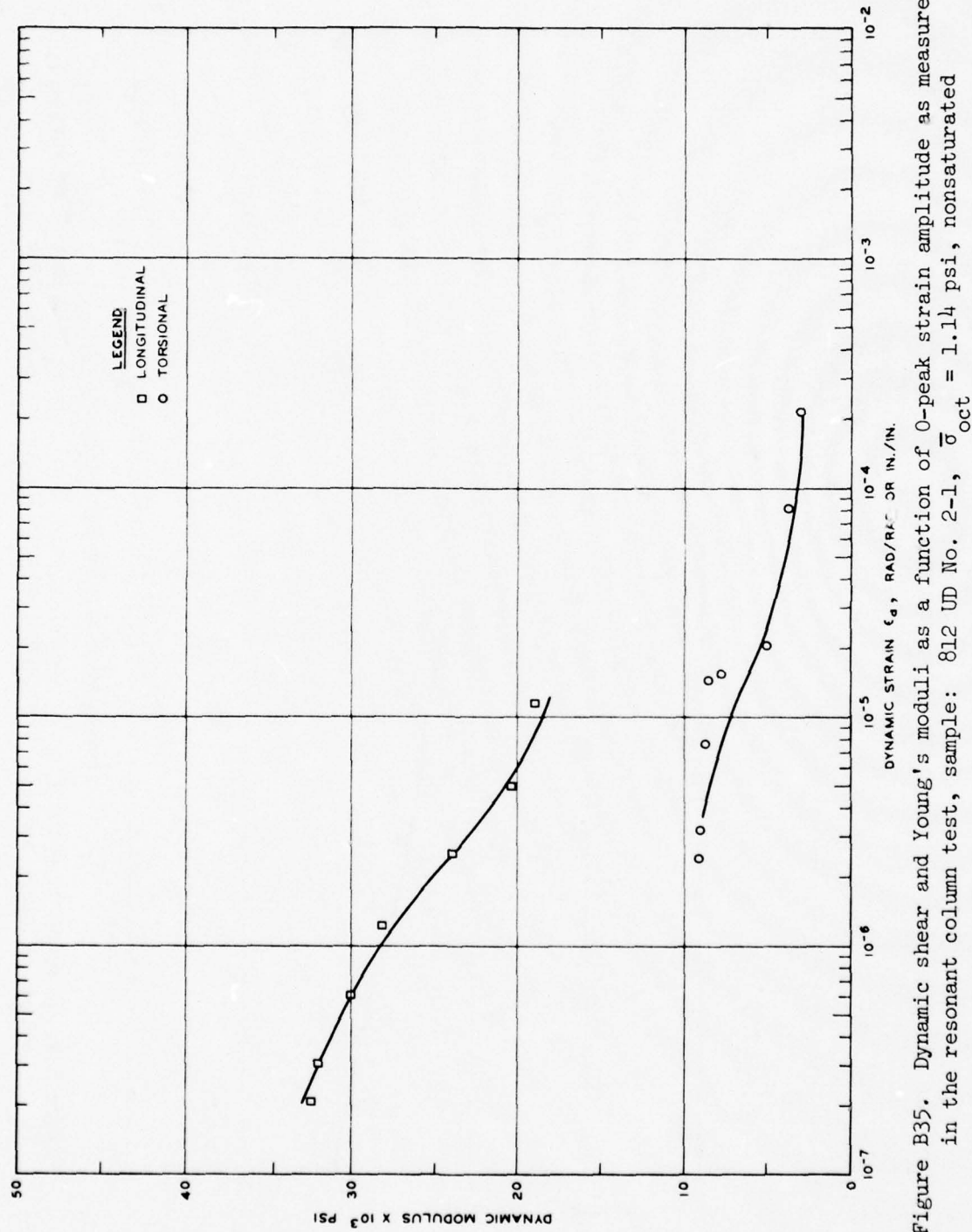


Figure B35. Dynamic shear and Young's moduli as a function of 0-peak strain amplitude as measured in the resonant column test, sample: 812 UD No. 2-1, $\bar{\sigma}_{oct} = 1.14$ psi, nonsaturated

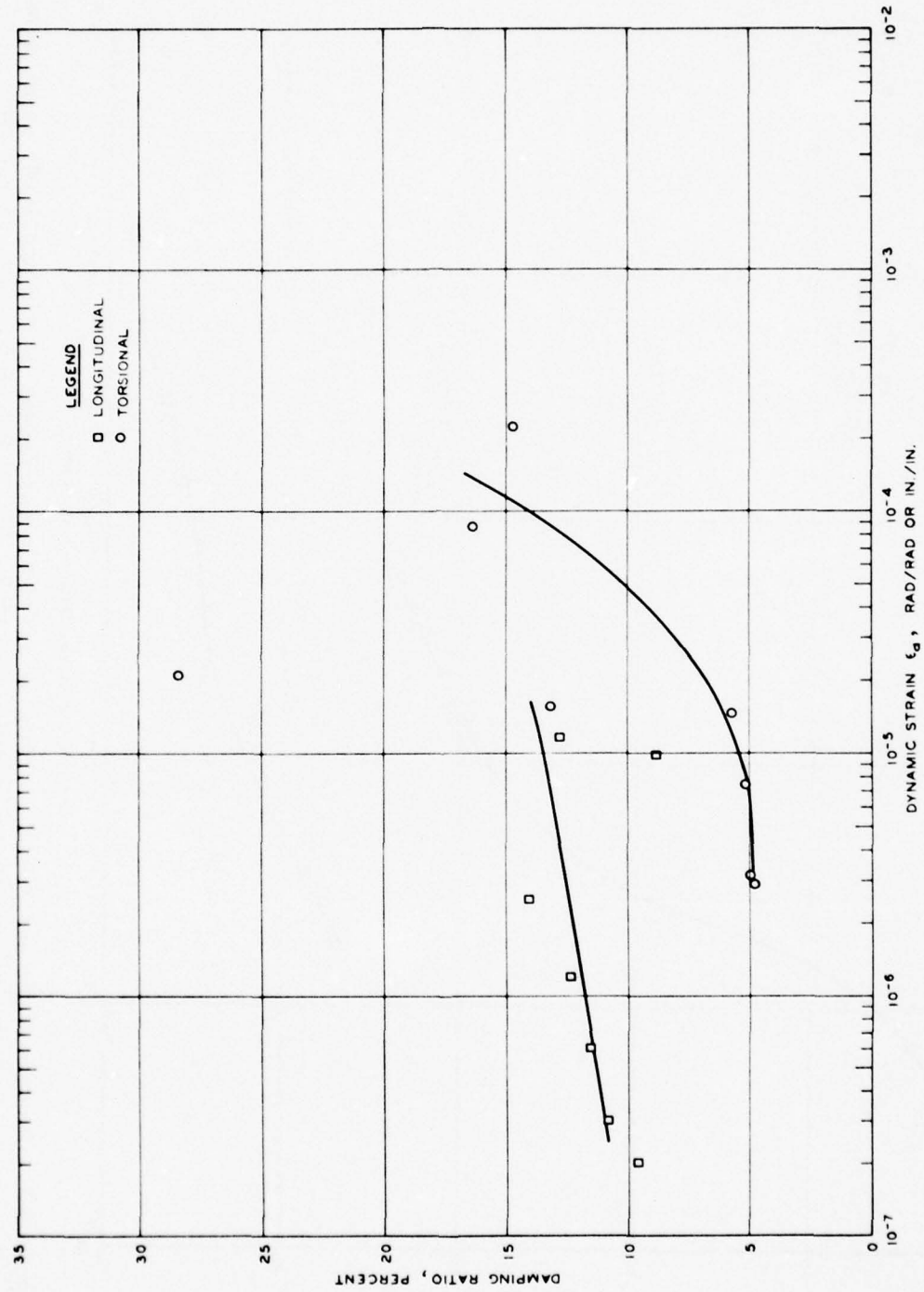


Figure B36. Damping as a function of 0-peak strain amplitude as determined by resonant column testing, sample: 812 UD No. 2-1, $\bar{\sigma}_{oct} = 1.14$ psi, nonsaturated

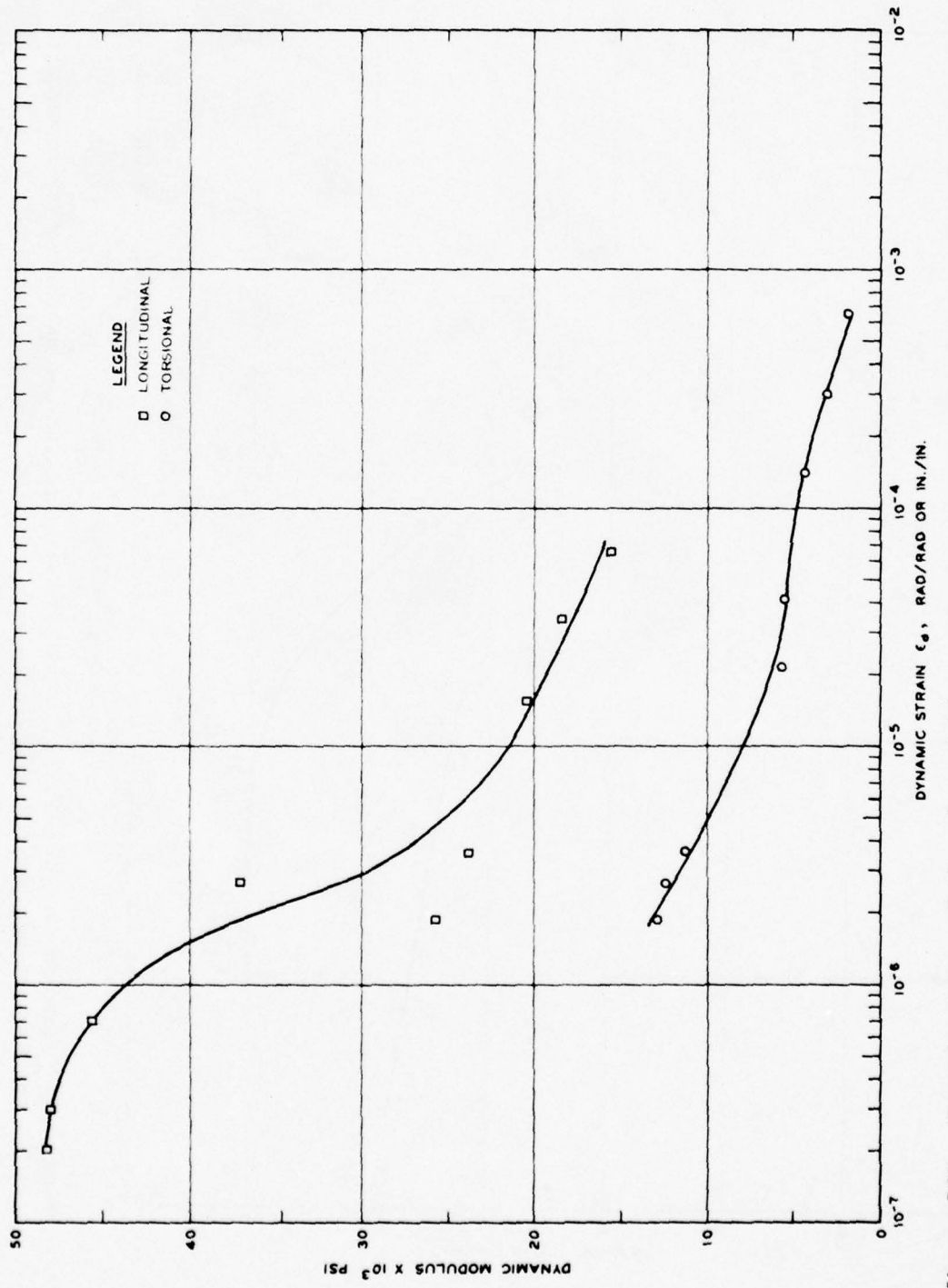


Figure B37. Dynamic shear and Young's moduli as a function of O-peak strain amplitude as measured in the resonant column test, sample: 812 UD No. 7-1, $\bar{\sigma}_{\text{oct}} = 7.4 \text{ psi}$, $B = 0.93$

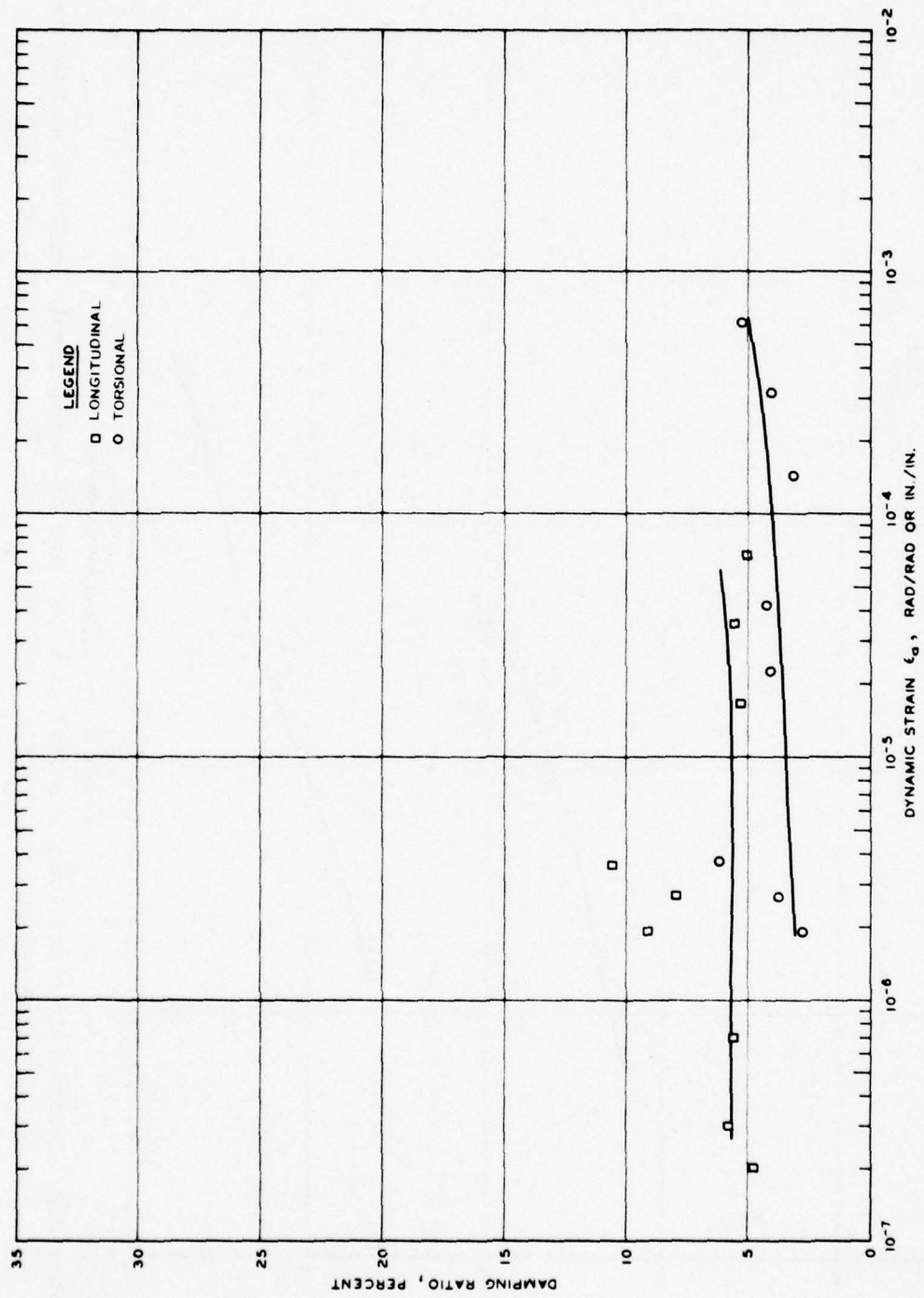


Figure B38. Damping as a function of 0-peak strain amplitude as determined by resonant column testing, sample: 812 UD No. 7-1, $\bar{\sigma}_{oct} = 7.4$ psi, $B = 0.93$

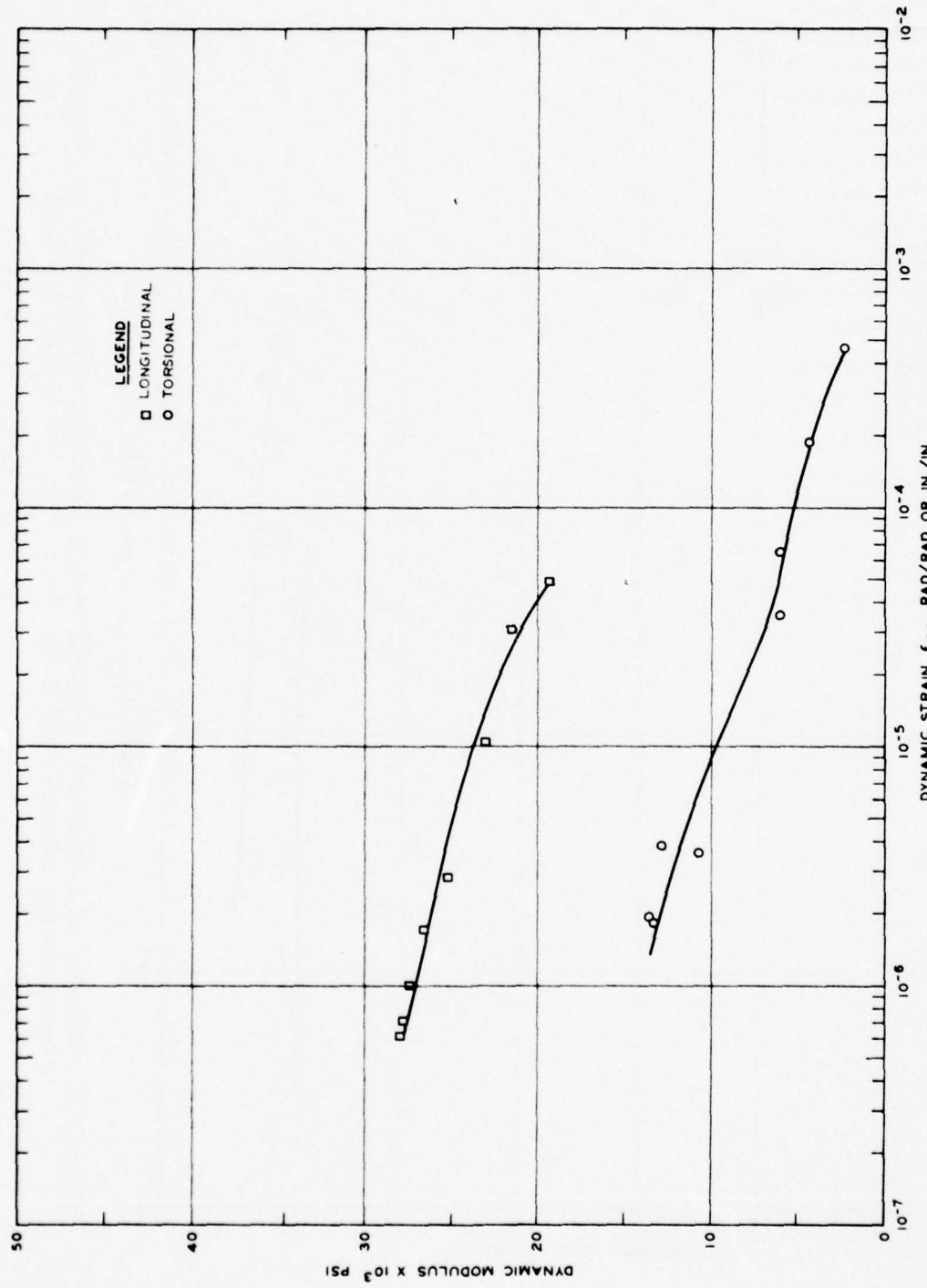


Figure B39. Dynamic shear and Young's moduli as a function of 0-peak strain amplitude as measured in the resonant column test, sample: 812 UD No. 7-2, $\bar{\sigma}_{oct} = 10$ psi, $B = 0.94$

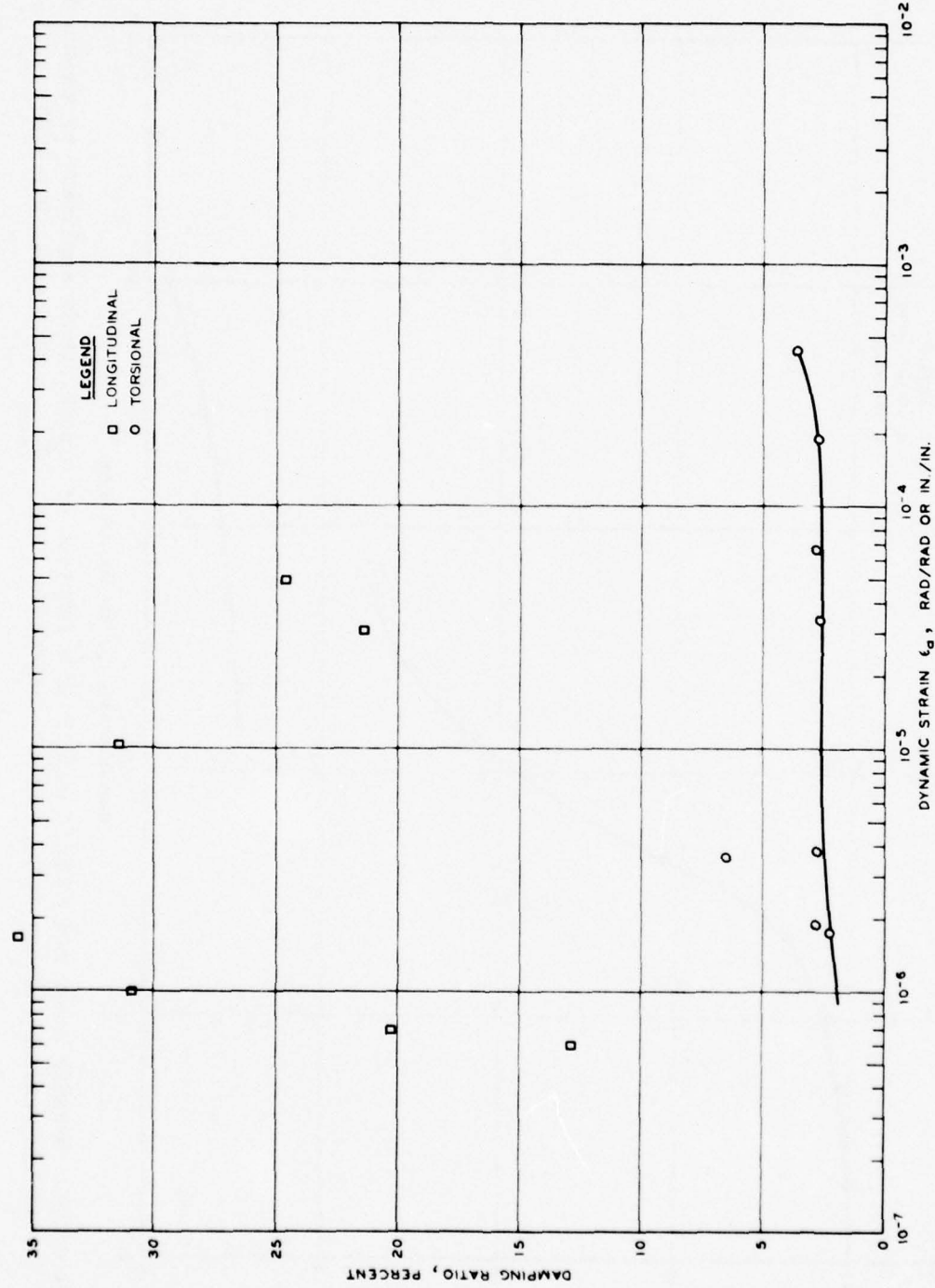


Figure B40. Damping as a function of 0-peak strain amplitude as determined by resonant column testing, sample: 812 UD No. 7-2, $\bar{G}_{oct} = 10$ psi, $B = 0.94$

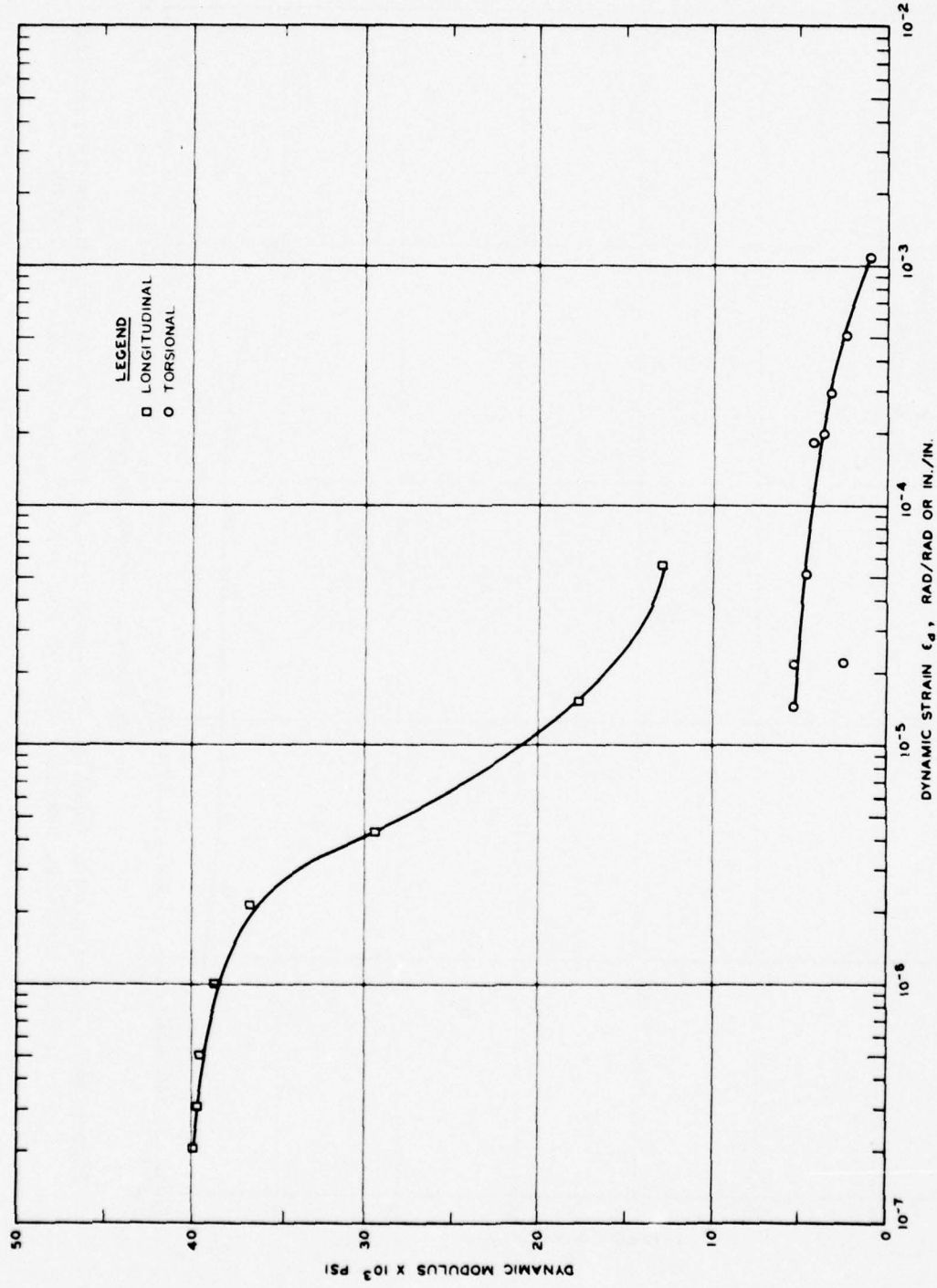


Figure B41. Dynamic shear and Young's moduli as a function of 0-peak strain amplitude as measured in the resonant column test, sample: 812 UD No. 13-1, $\bar{\sigma}_{oct} = 11.5$ psi, $B = 0.84$

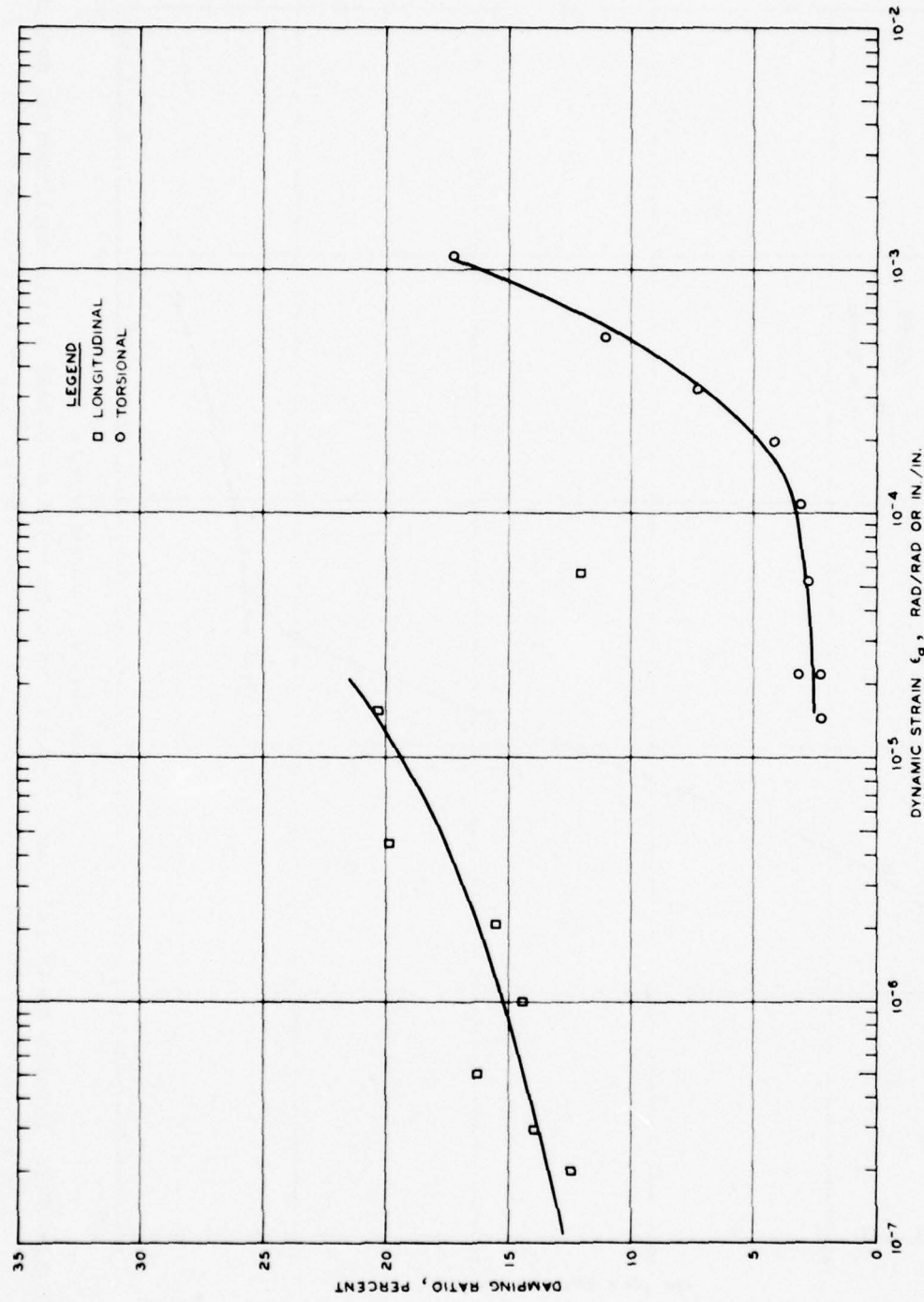


Figure B42. Damping as a function of 0-peak strain amplitude as determined by resonant column testing, sample: 812 UD No. 13-1, $\bar{\sigma}_{oct} = 11.5$ psi, $B = 0.84$

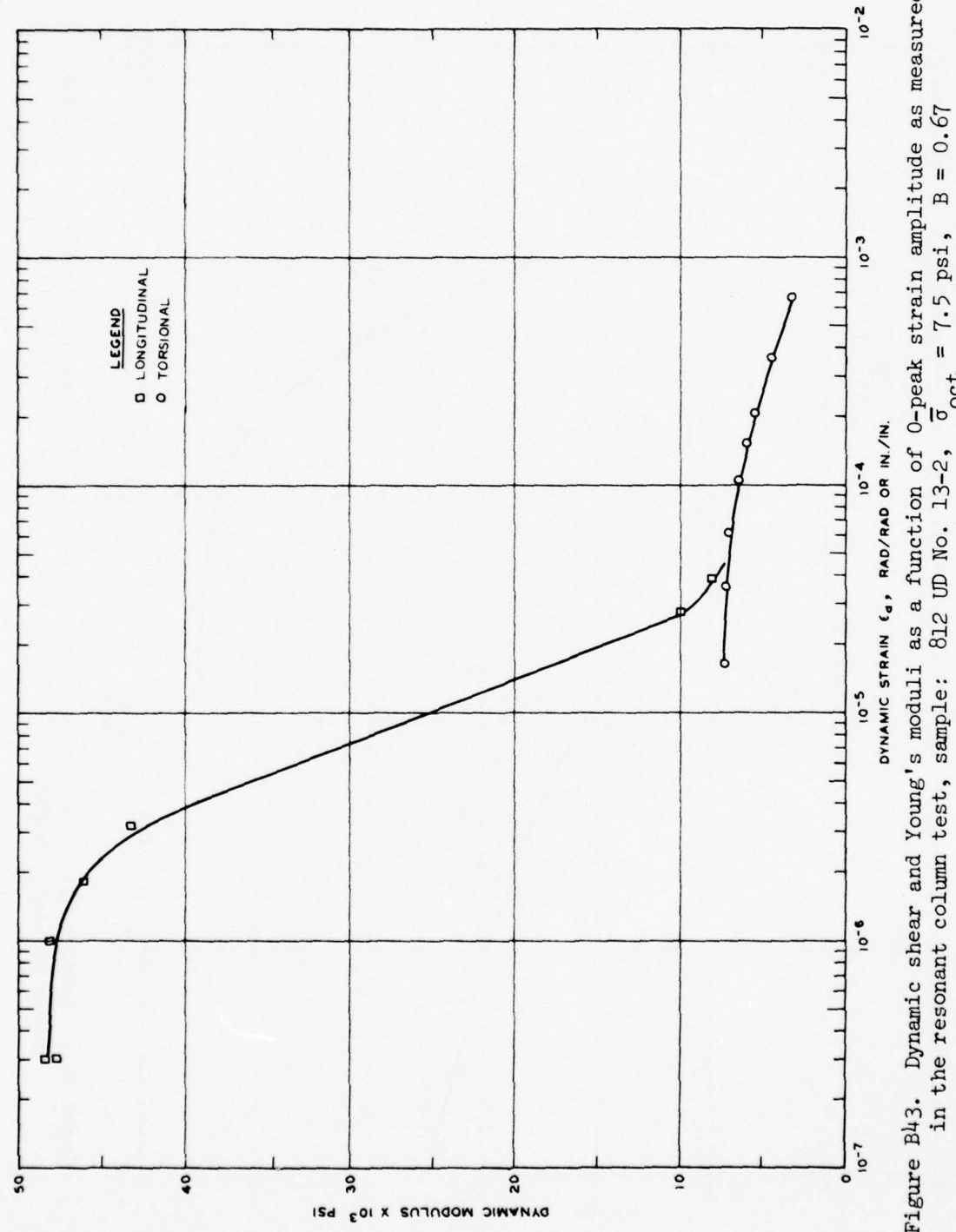


Figure B43. Dynamic shear and Young's moduli as a function of 0-peak strain amplitude as measured in the resonant column test, sample: 812 UD No. 13-2, $\bar{\sigma}_{oct} = 7.5$ psi, $B = 0.67$

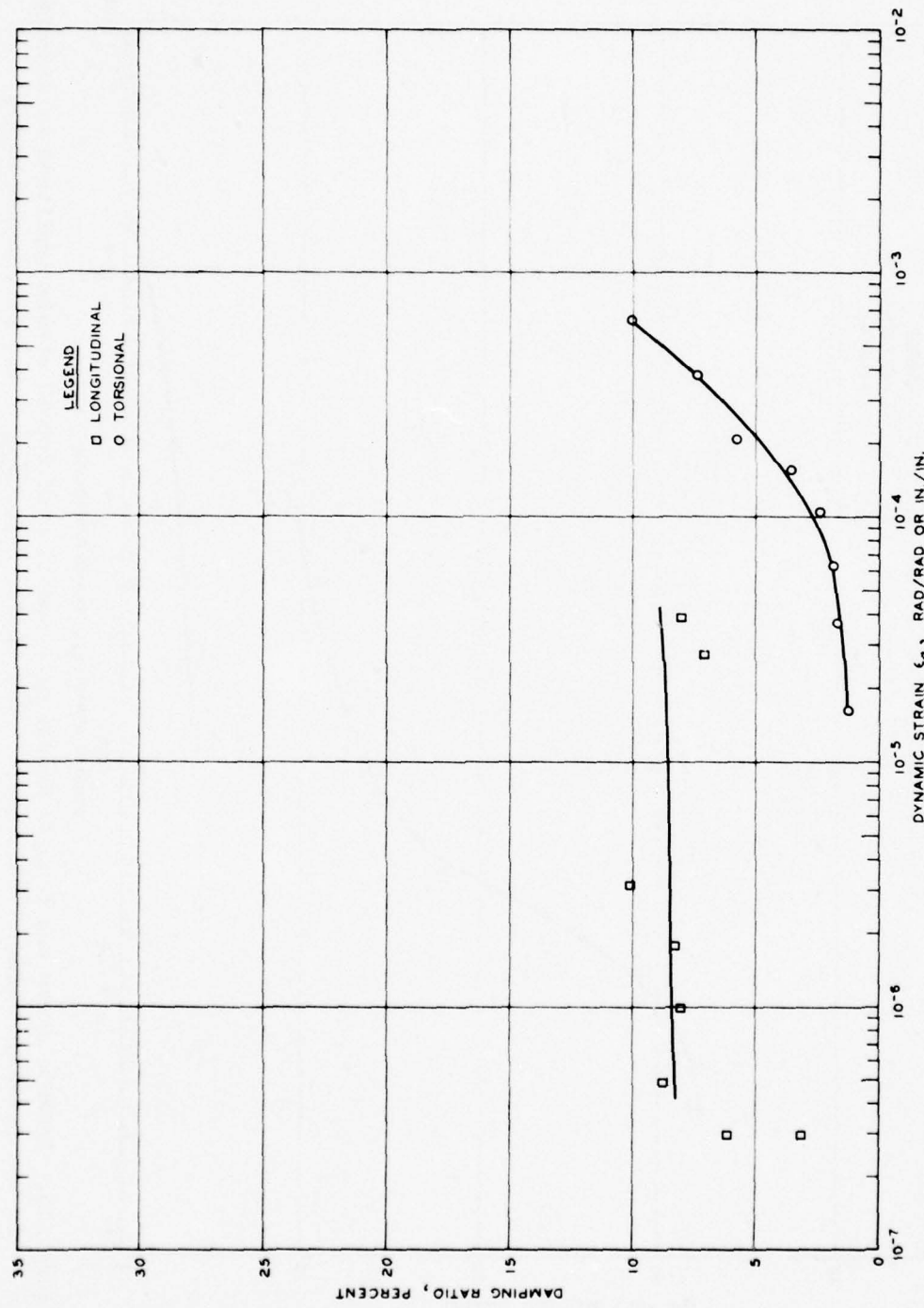


Figure B44. Damping as a function of 0-peak strain amplitude as determined by resonant column testing, sample: 812 UD No. 13-2, $\bar{\sigma}_{\text{oct}} = 7.5$ psi, $B = 0.67$

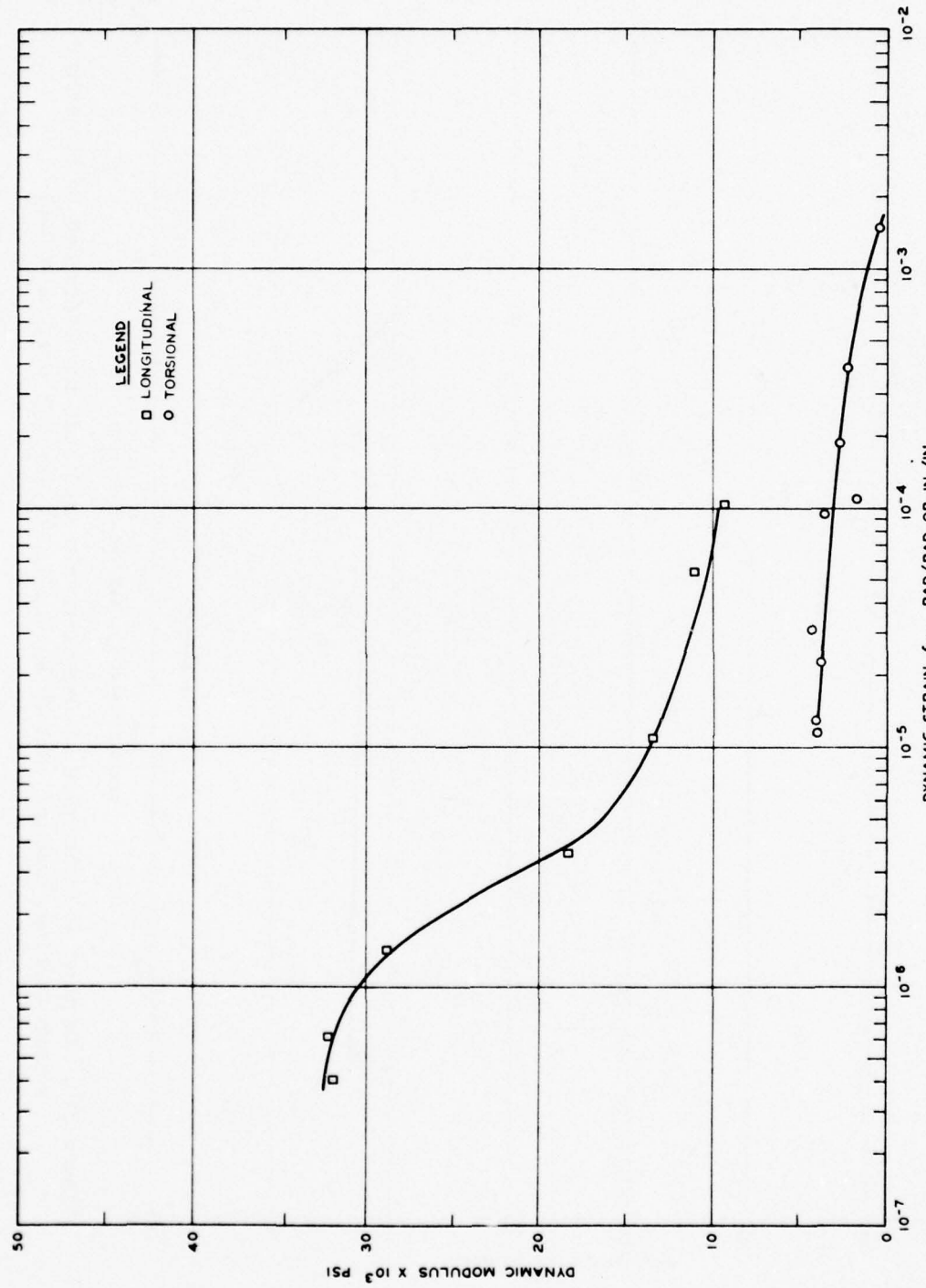


Figure B45. Dynamic shear and Young's moduli as a function of 0-peak strain amplitude as measured in the resonant column test, sample: 815 UD No. 2-1, $\bar{\sigma}_{oct} = 0.8$ psi, nonsaturated

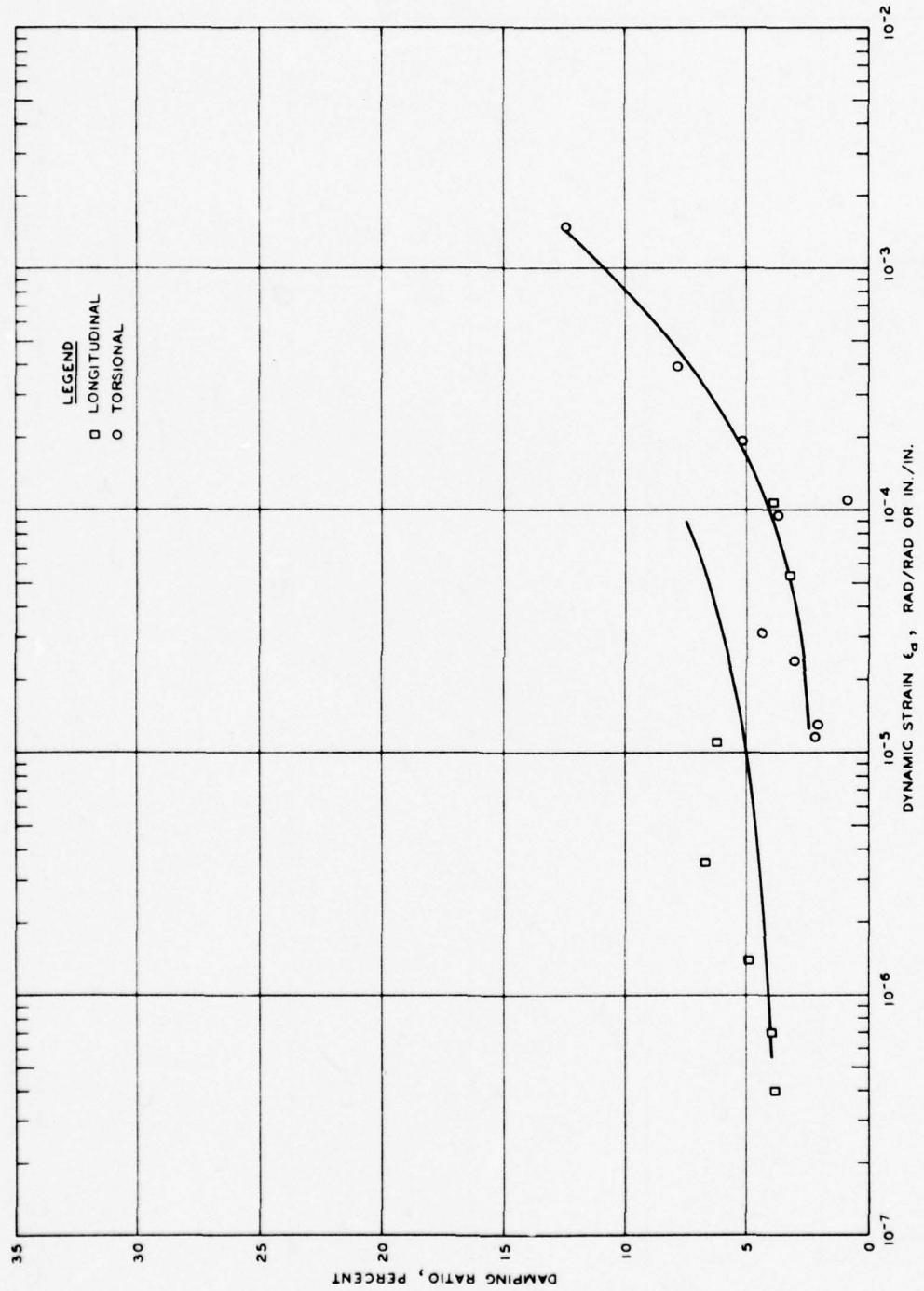


Figure B46. Damping as a function of 0-peak strain amplitude as determined by resonant column testing, sample: 815 UD No. 2-1, $\bar{\sigma}_{oct} = 0.8$ psi, nonsaturated

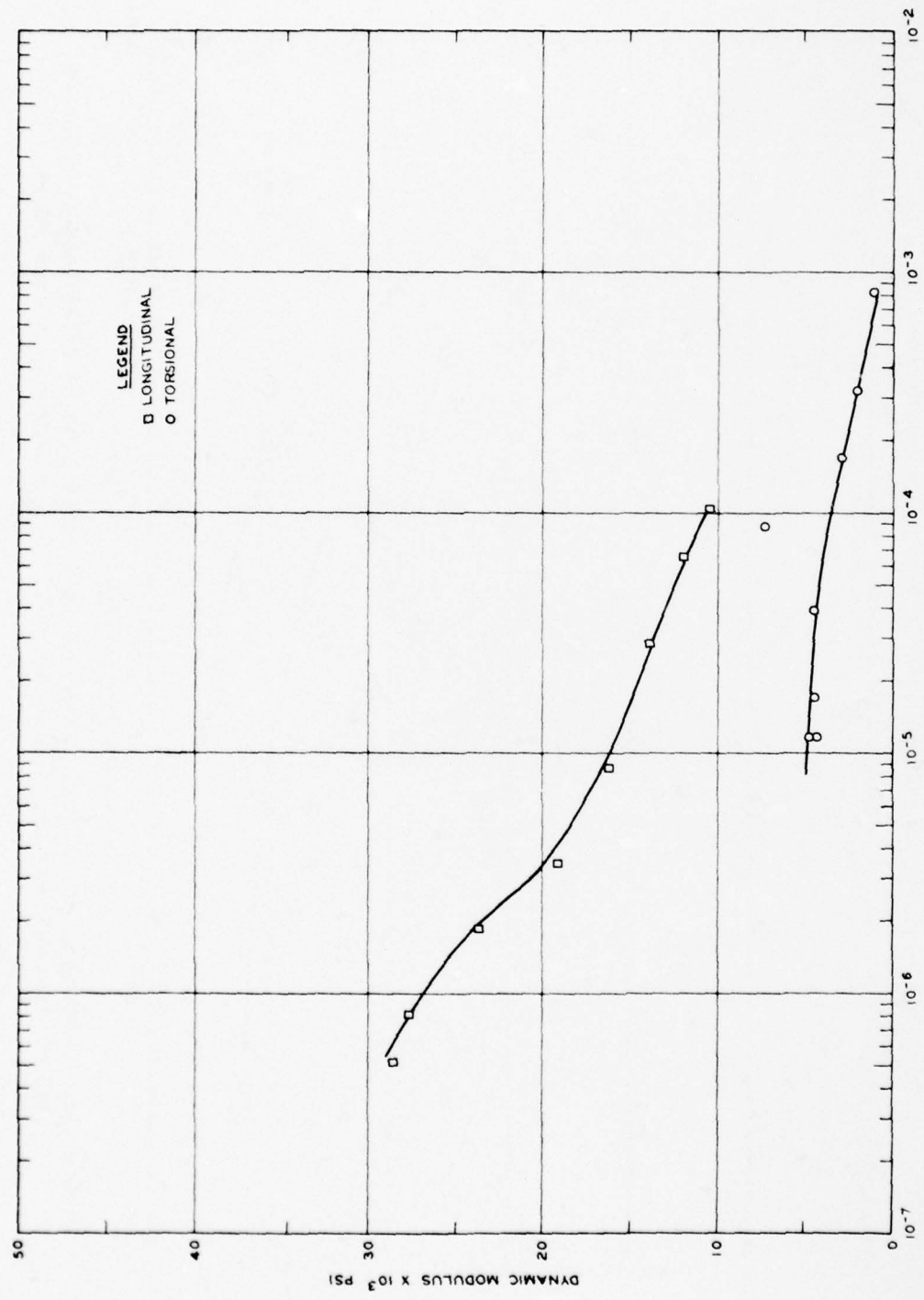


Figure B47. Dynamic shear and Young's moduli as a function of 0-peak strain amplitude as measured in the resonant column test, sample: 815 UD No. 2-2, $\bar{\sigma}_{oct} = 4.0$ psi, nonsaturated

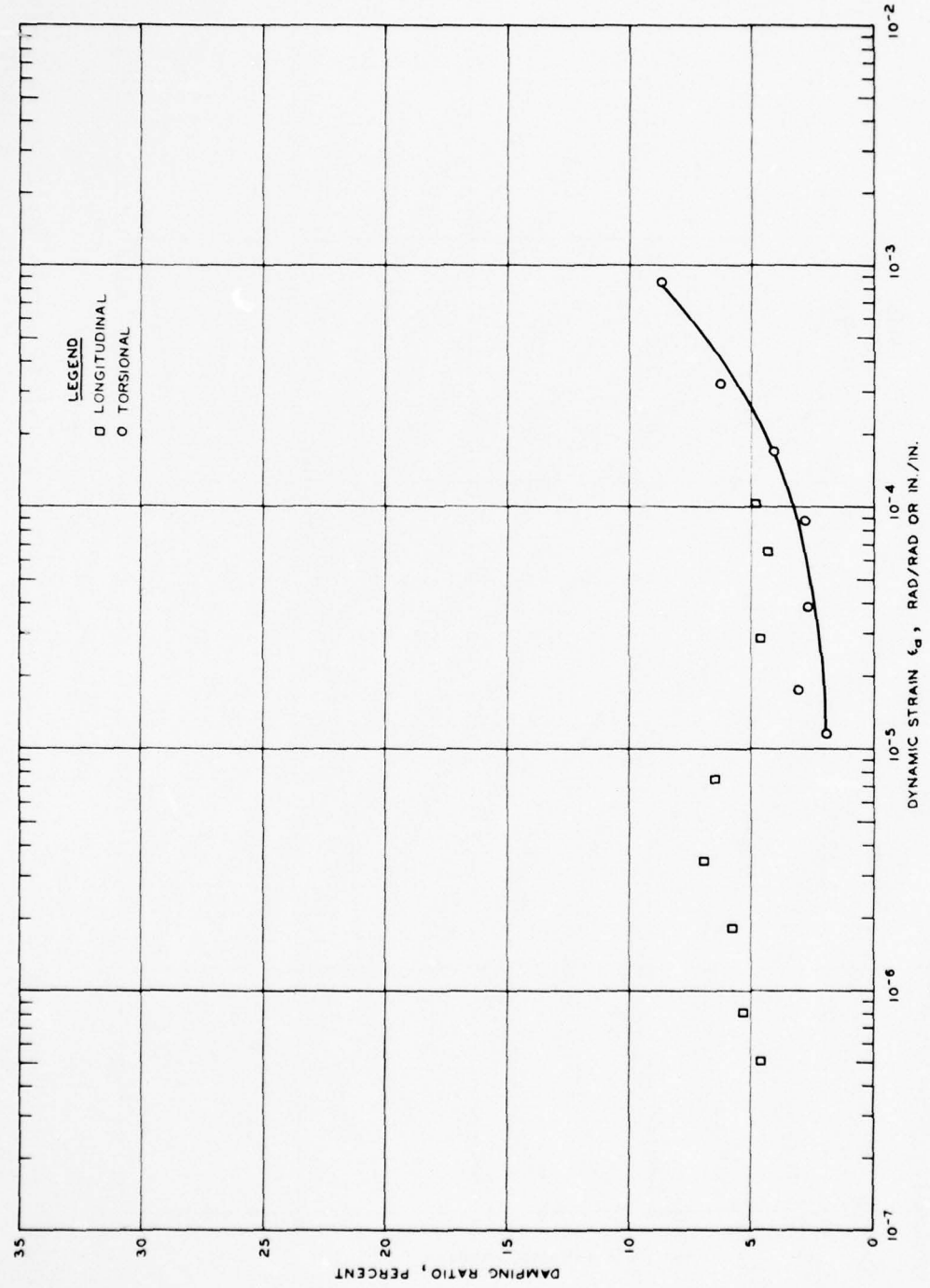


Figure B48. Damping as a function of 0-peak strain amplitude as determined by resonant column testing, sample: 815 UD No. 2-2, $\bar{\sigma}_{oct} = 4.0$ psi, nonsaturated

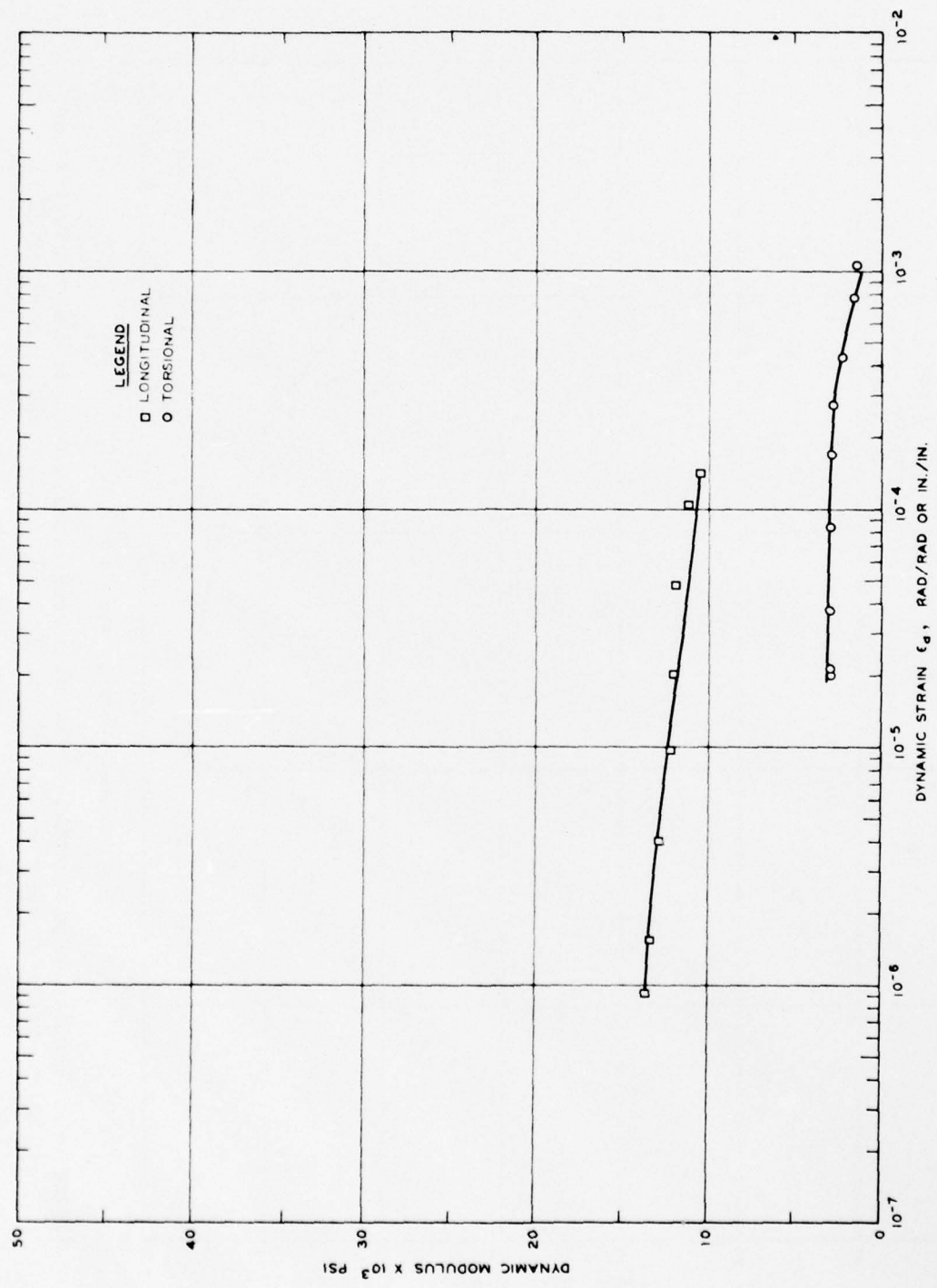


Figure B49. Dynamic shear and Young's moduli as a function of 0-peak strain amplitude as measured in the resonant column test, sample: 815 UD No. 7-1, $\bar{\sigma}_{oct} = 4.5$ psi, nonsaturated

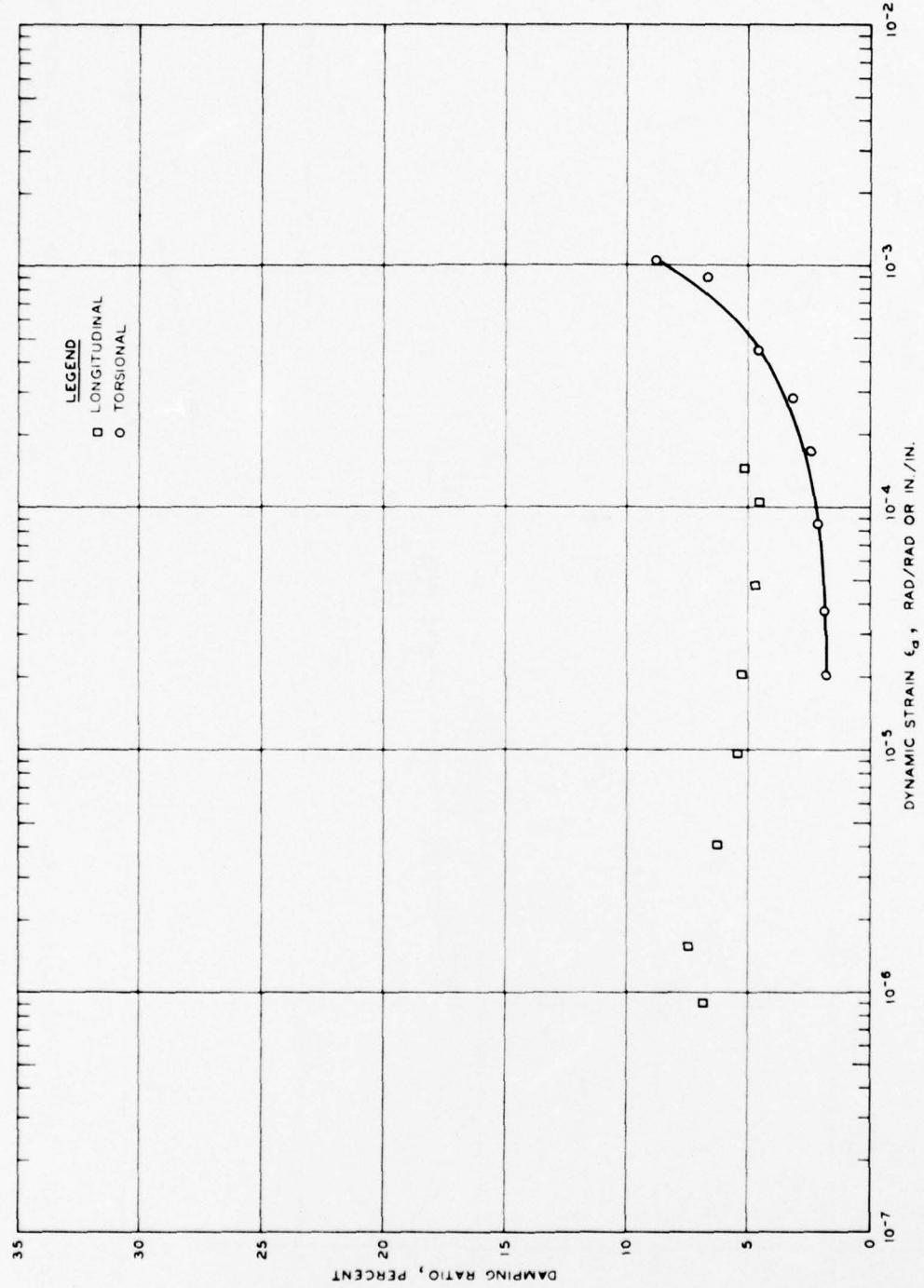


Figure B50. Damping as a function of 0-peak strain amplitude as determined by resonant column testing, sample: 815 UD No. 7-1, $\bar{\sigma}_{oct} = 4.5$ psi, nonsaturated

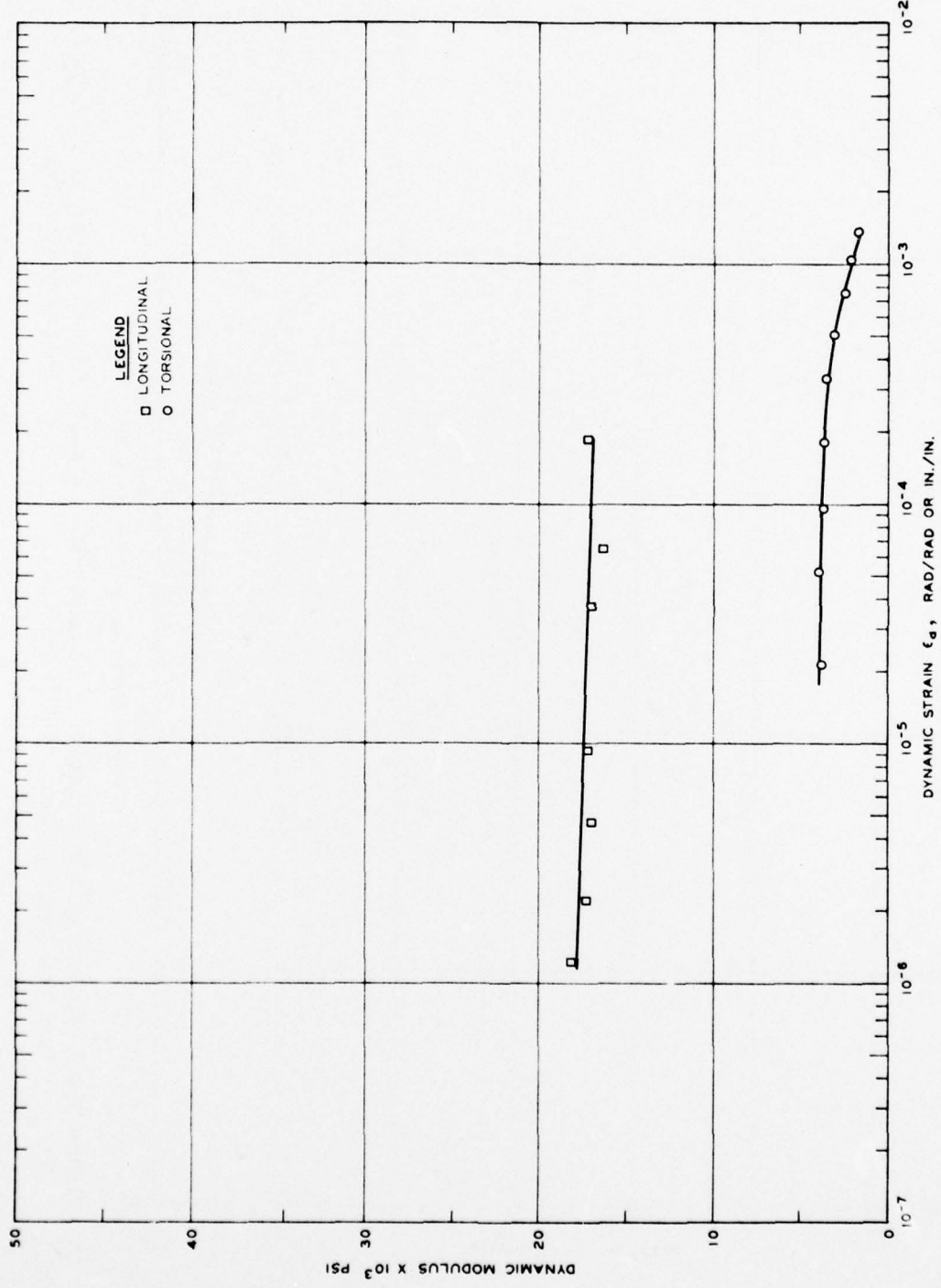


Figure B51. Dynamic shear and Young's moduli as a function of 0-peak strain amplitude as measured in the resonant column test, sample: 815 UD No. 7-2, $\bar{\sigma}_{oct} = 7.9$ psi, nonsaturated

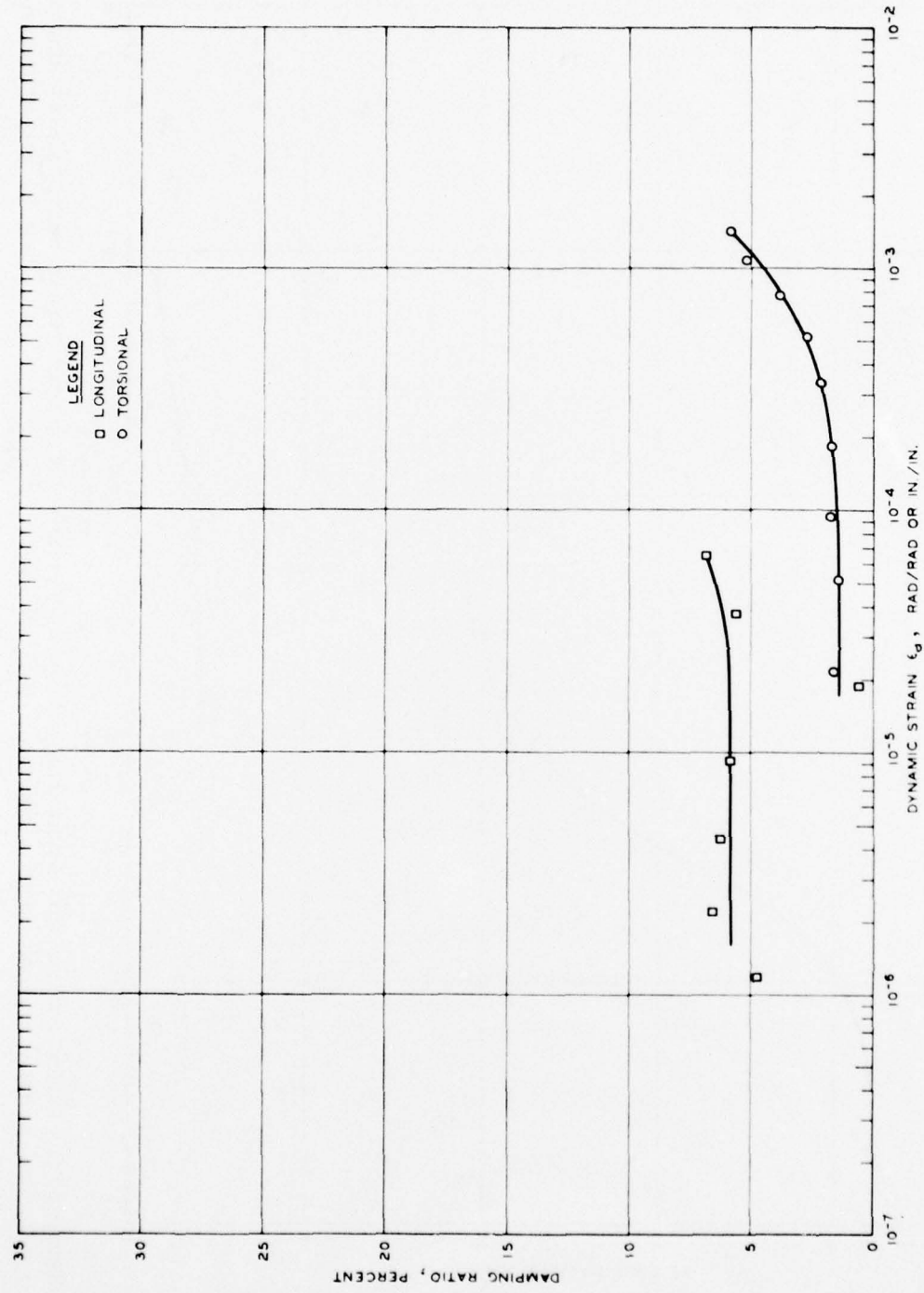


Figure B52. Damping as a function of 0-peak strain amplitude as determined by resonant column testing, sample: 815 UD No. 7-2, $\bar{\sigma}_{oct} = 7.9$ psi, nonsaturated

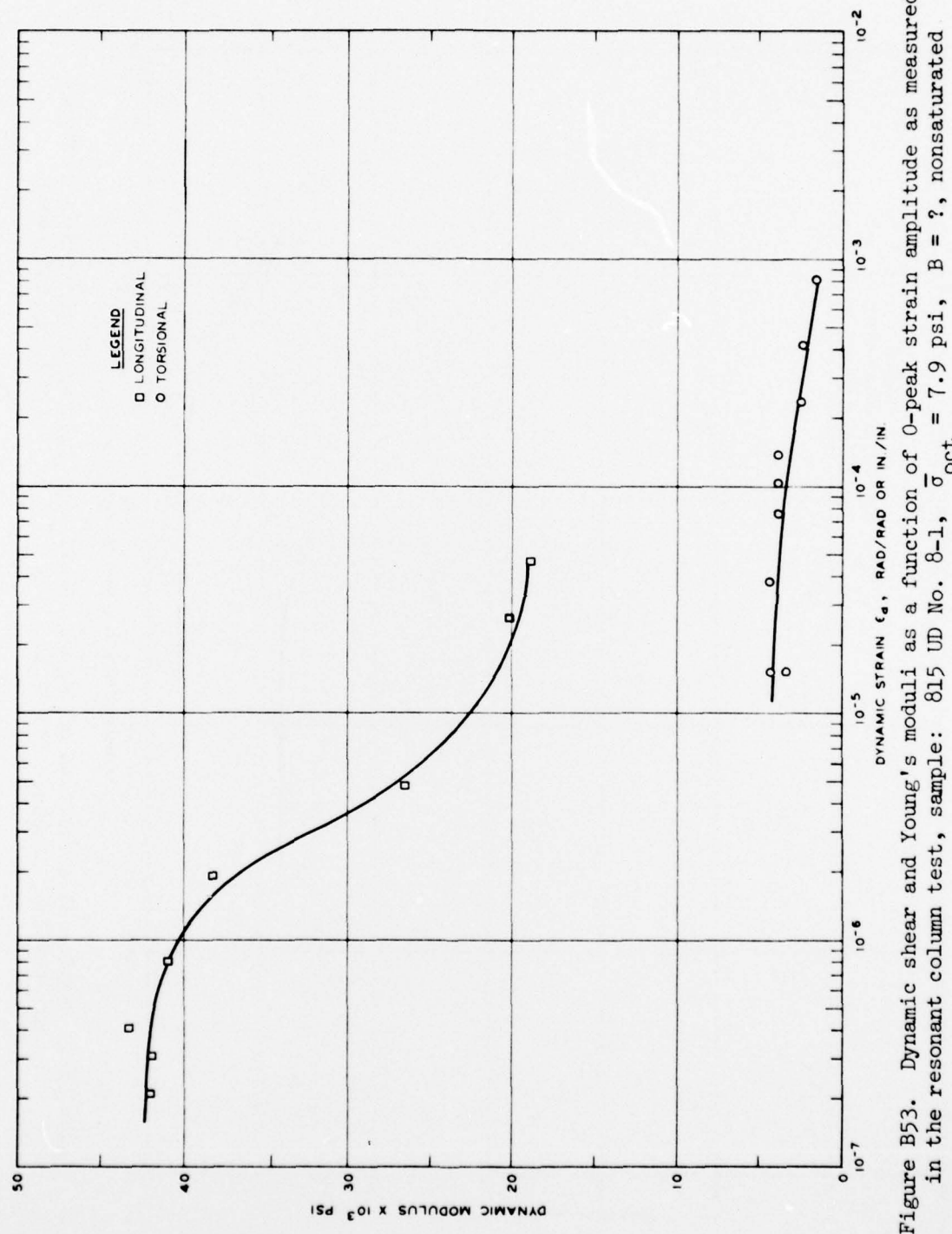


Figure B53. Dynamic shear and Young's moduli as a function of 0-peak strain amplitude as measured in the resonant column test, sample: 815 UD No. 8-1, $\bar{\sigma}_{oct} = 7.9$ psi, B = ?, nonsaturated

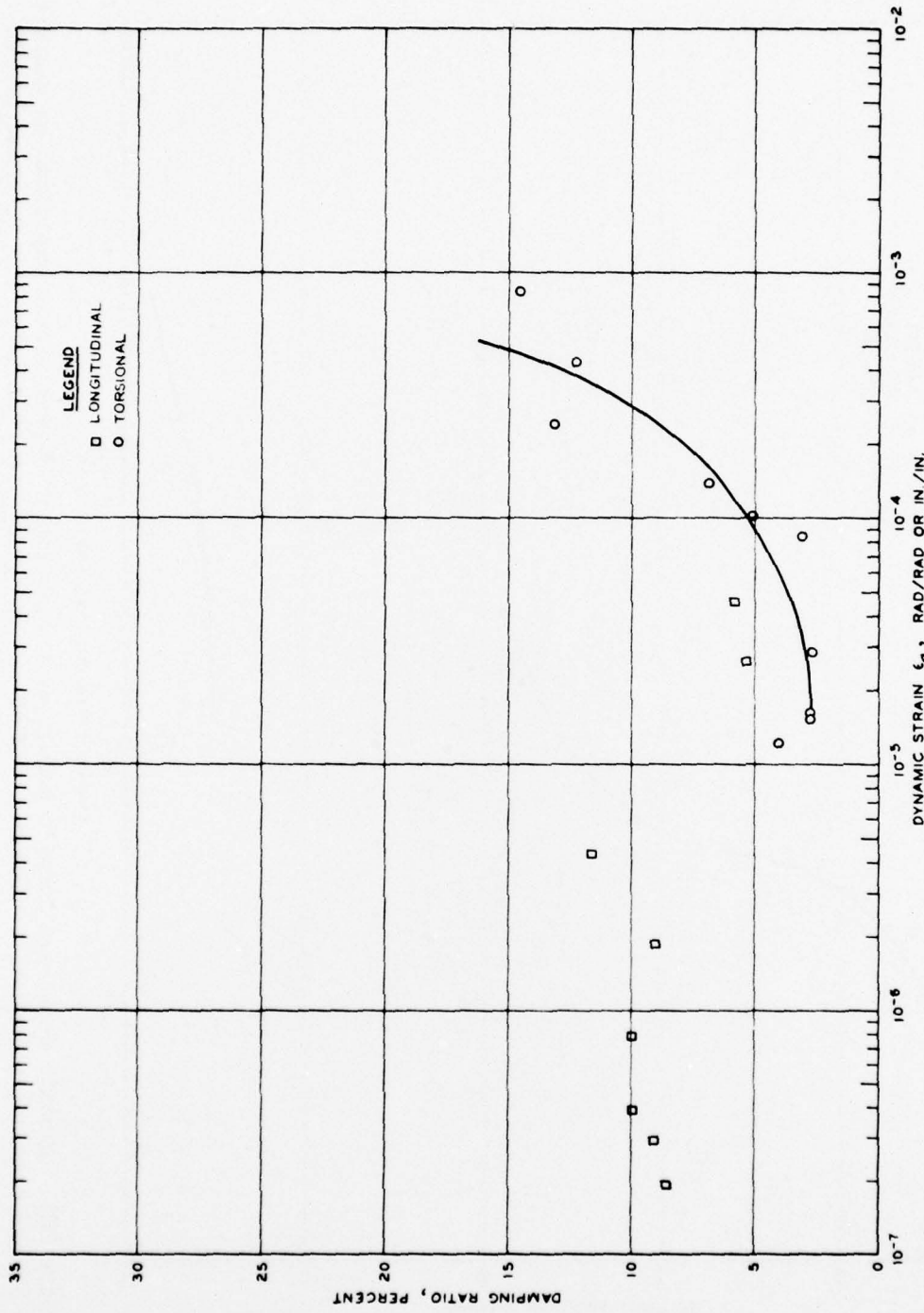


Figure B54. Damping as a function of 0-peak strain amplitude as determined by resonant column testing, sample: 815 UD No. 8-1, $\bar{\sigma}_{oct} = 7.9$ psi, B = ?, nonsaturated

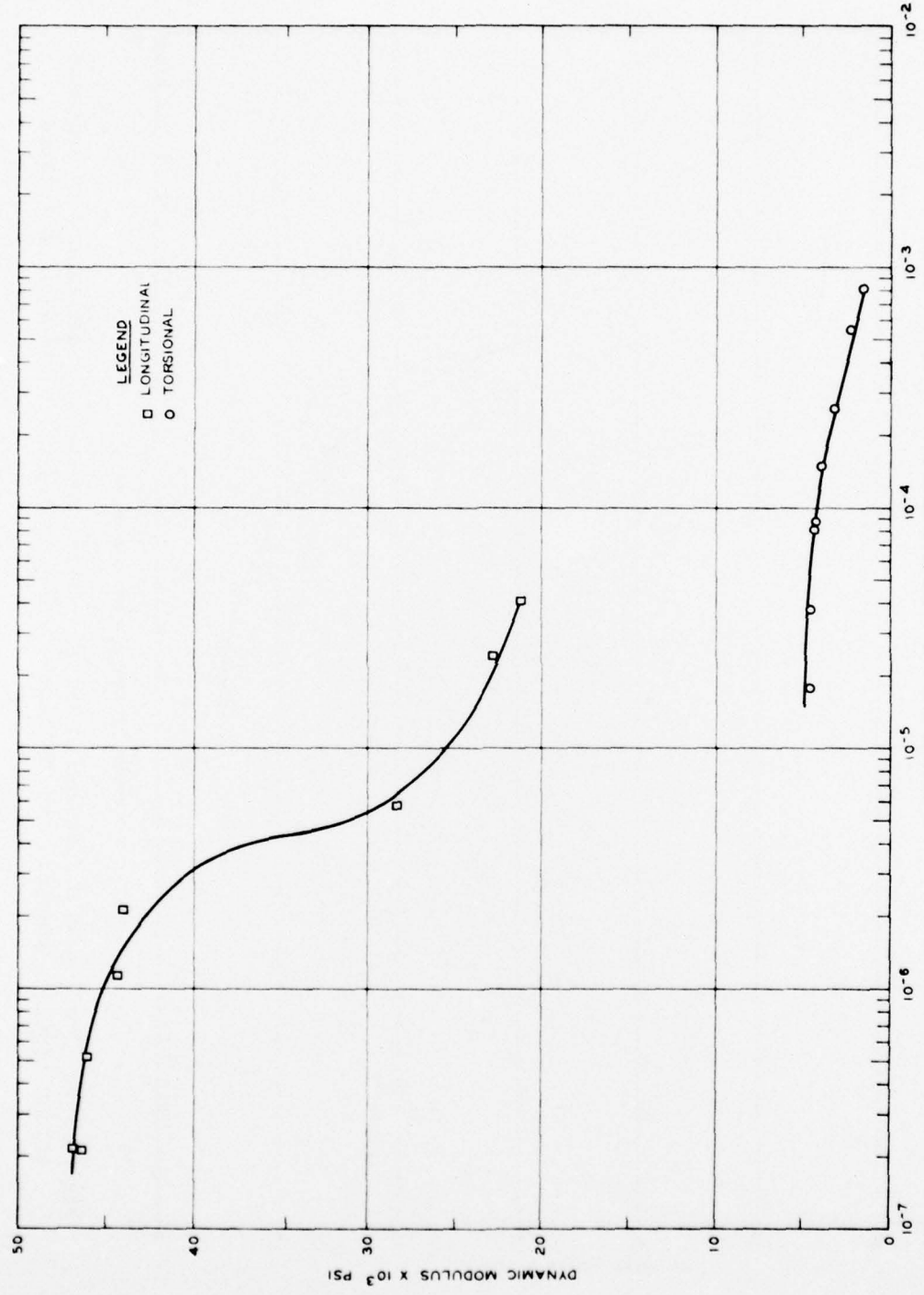


Figure B55. Dynamic shear and Young's moduli as a function of 0-peak strain amplitude as measured in the resonant column test, sample: 815 UD No. 8-2, $\bar{\sigma}_{oct} = 10.1$ psi, B = ?, nonsaturated

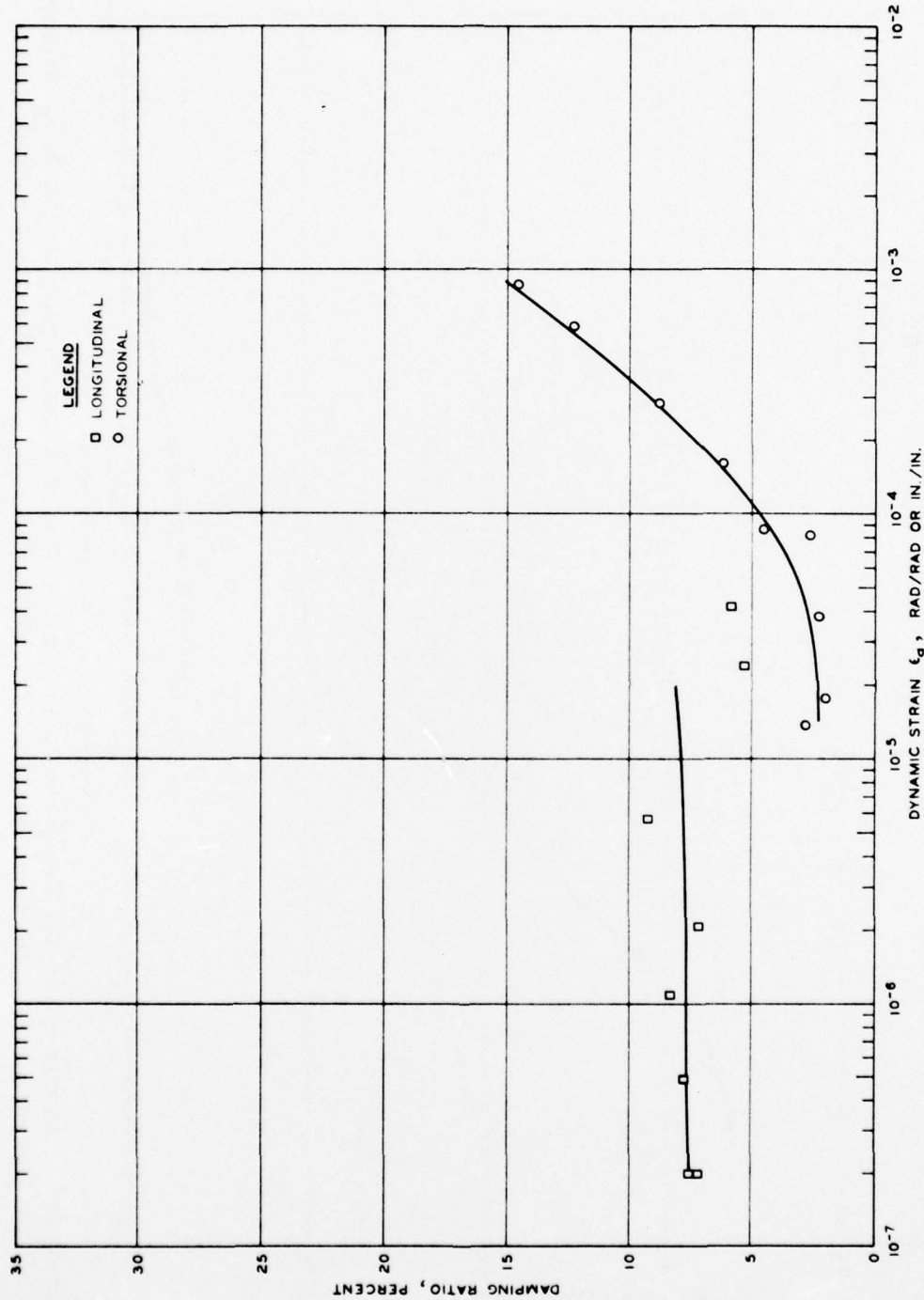


Figure B56. Damping as a function of 0-peak strain amplitude as determined by resonant column testing, sample: 815 UD No. 8-2, $\bar{\sigma}_{oct} = 10.1$ psi, $B = ?$, nonsaturated

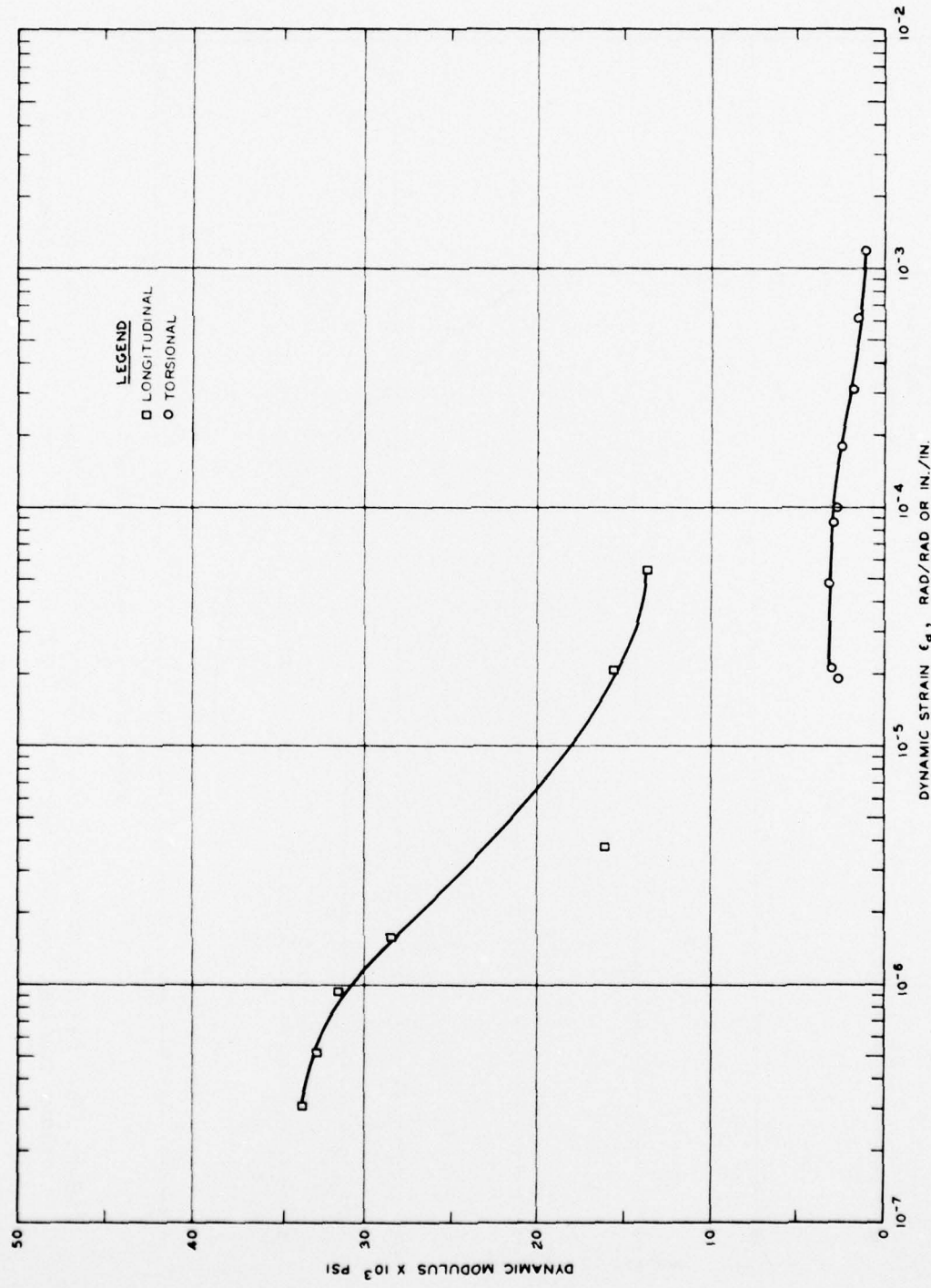


Figure B57. Dynamic shear and Young's moduli as a function of 0-peak strain amplitude as measured in the resonant column test, sample: 815 UD No. 8-3, $\bar{\sigma}_{oct} = 7.8$ psi, $B = 0.56$

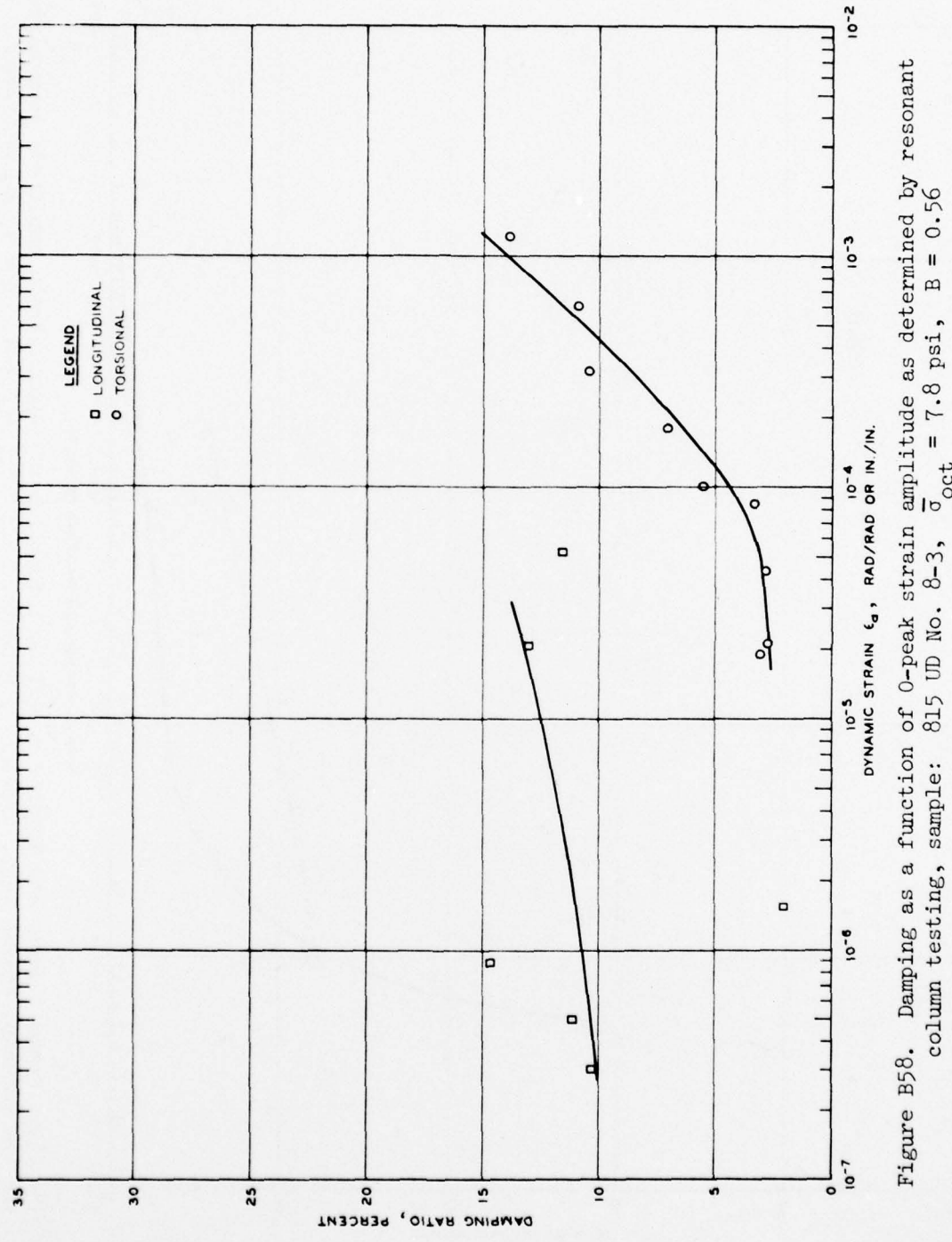


Figure B58. Damping as a function of 0-peak strain amplitude as determined by resonant column testing, sample: 815 UD No. 8-3, $\bar{\sigma}_{oct} = 7.8$ psi, $B = 0.56$

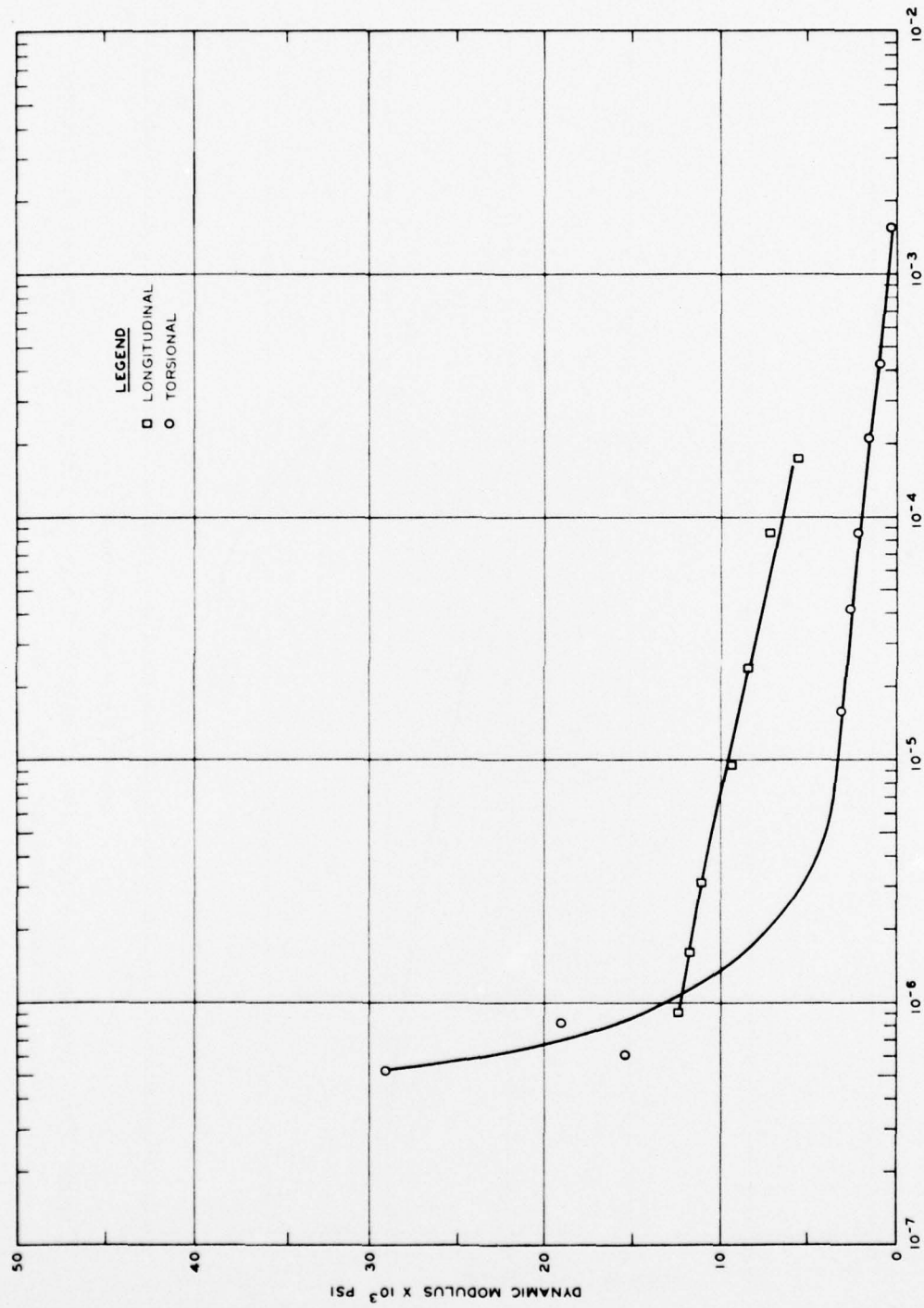


Figure B59. Dynamic shear and Young's moduli as a function of 0-peak strain amplitude as measured in the resonant column test, sample: 818 UD No. 2-1, $\bar{\sigma}_{oct} = 2$ psi, B = ?, nonsaturated

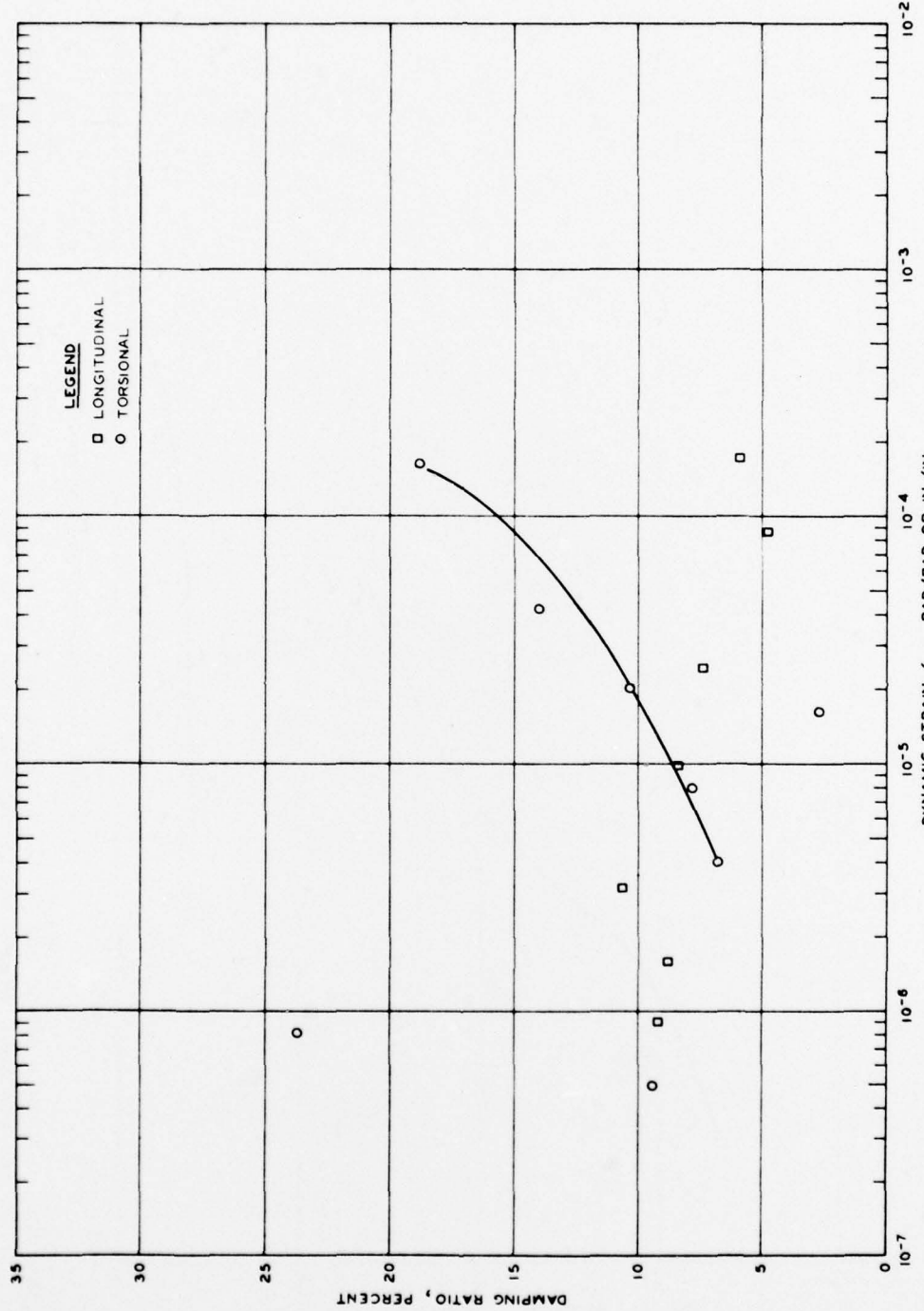


Figure B60. Damping as a function of 0-peak strain amplitude as determined by resonant column testing, sample: 818 UD No. 2-1, $\bar{\sigma}_{oct} = 2$ psi, B = ?, nonsaturated

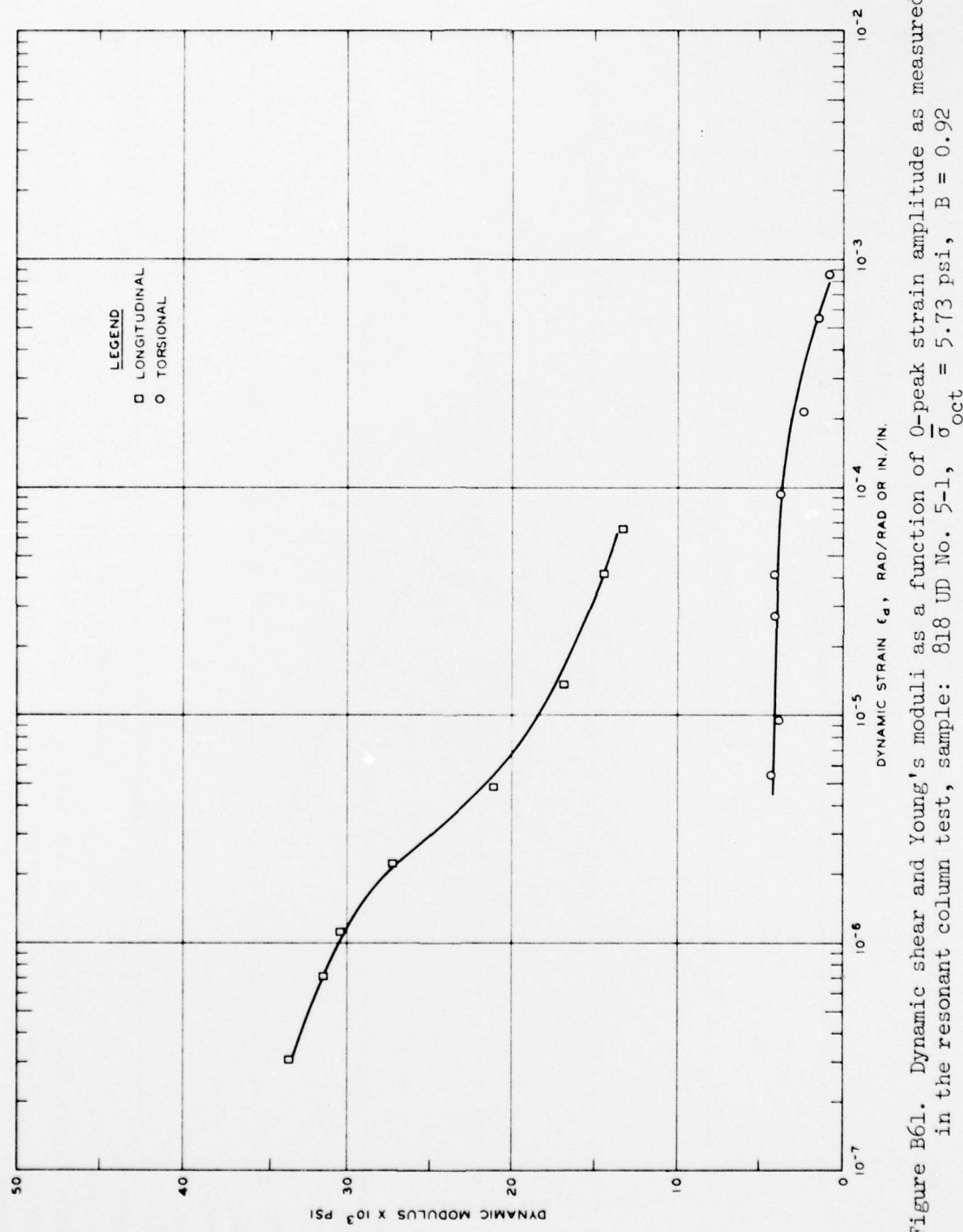


Figure B61. Dynamic shear and Young's moduli as a function of 0-peak strain amplitude as measured in the resonant column test, sample: 818 UD No. 5-1, $\bar{\sigma}_{oct} = 5.73$ psi, $B = 0.92$

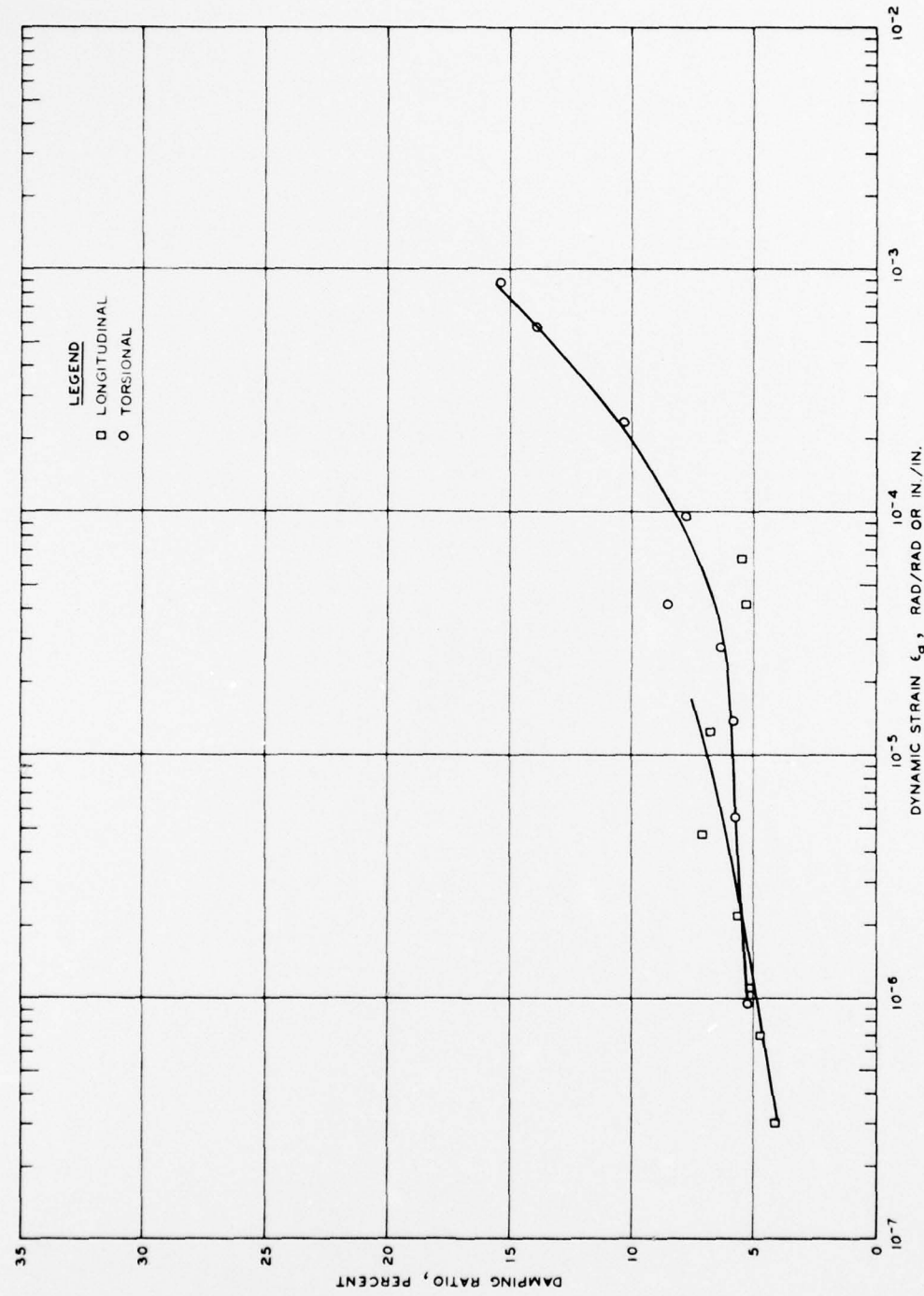


Figure B62. Damping as a function of 0-peak strain amplitude as determined by resonant column testing, sample: 818 UD No. 5-1, $\bar{\sigma}_{Oct} = 5.73$ psi, $B = 0.92$

In accordance with letter from DAEN-RDC, DAEN-ASI dated 22 July 1977, Subject: Facsimile Catalog Cards for Laboratory Technical Publications, a facsimile catalog card in Library of Congress MARC format is reproduced below.

Curro, Joseph R

In situ and laboratory determinations of shear and Young's moduli for the Portsmouth, Ohio, Gaseous Diffusion Add-on Site / by Joseph R. Curro, Jr., William F. Marcuson III. Vicksburg, Miss. : U. S. Waterways Experiment Station ; Springfield, Va. : available from National Technical Information Service, 1978.

31, [131] p. : ill. ; 27 cm. (Miscellaneous paper - U. S. Army Engineer Waterways Experiment Station ; S-78-12)

Prepared for U. S. Energy Research and Development Administration, Oak Ridge, Tenn.

References: p. 31.

1. Field tests. 2. Geophysical exploration. 3. Laboratory tests. 4. Shear properties. 5. Soil strength. 6. Young's modulus. I. Marcuson, William Frederick, joint author. II. United States. Energy Research and Development Administration. III. Series: United States. Waterways Experiment Station, Vicksburg, Miss. Miscellaneous paper ; S-78-12.
TA7.W34m no.S-78-12